Hybrid microscale analytical methods for environmental analysis

Josiane Pénélope Lafleur

Degree of

Department of Chemistry, Faculty of Graduate Studies

McGill University

Montreal, Quebec, Canada

July 30, 2009

A thesis submitted to McGill University in partial fulfillment of the requirements of

the degree of Doctor of Philosophy

Abstract

The contamination of natural resources by human activity can have severe socio-economical impacts. Environmental analytical chemistry plays an essential role in the solving of these environmental problems. However, conventional environmental analytical procedures are generally lengthy and necessitate several steps. Hybrid microscale analytical techniques have been developed with the objective of minimizing the number of sample preparation steps, avoiding the use of organic solvents and reducing the size of the samples required for an analysis as well as increasing the speed of analyses.

An Inductively Heated – Electrothermal Vaporizer (IH-ETV) was coupled to an Inductively Coupled Plasma Mass Spectrometer (ICP-MS) to vaporize mercury from single human hair strands without any prior sample preparation, such as the destruction of its matrix by digestion. The results were comparable to those obtained with a reference method.

For samples requiring chromatographic separation, sample handling was minimized by direct coupling of the chromatographic procedure to an ICP-MS through Laser Ablation (LA). Cr^{3+} and Cr^{6+} were separated on silica gel High Performance Thin Layer Chromatography plates (HPTLC) using aqueous mobile phases. LA was used to volatilize the chromium species directly from the

chromatographic stationary phase material for ICP-MS detection. This procedure allows for a rapid separation and quantification, and requires only 0.5 µL of sample.

The same procedure was used to couple miniature Solid Phase Extraction (SPE) columns implemented on centrifugal microfluidic discs to an ICP-MS to determine pre-concentrated metal chelates from drinking water. The miniature SPE devices require only 1 – 600 µL samples, allowing a reduction of three to four orders of magnitude in sample size compared to the conventional procedure, and the device requires no more than a simple motor to actuate fluid flow. The centrifugal microfluidic SPE discs can be used to perform up to eight extractions simultaneously and allow the easy storage of samples before transport to the laboratory for LA-ICP-MS analysis.

Finally, the centrifugal microfluidic SPE discs were modified to allow their coupling to absorption and fluorescence spectrometers. As well as the advantages listed above, this hyphenated system allows the *in-situ* screening of aquatic organic pollutants trapped on the SPE column directly in the field using simple and small light sources and detectors.

Abrégé

La contamination des ressources naturelles par l'activité humaine peut avoir des impacts socio-économiques graves pour les communautés qui en dépendent et la chimie analytique environnementale constitue un élément essentiel dans la résolution de ces problèmes environnementaux. Cependant, les procédés conventionnels d'analyse sont généralement longs et nécessitent plusieurs étapes. Plusieurs techniques hybrides ont été développées afin de: minimiser le nombre d'étapes nécessaires à la préparation d'un échantillon, éviter l'utilisation de solvants organiques, réduire la taille des échantillons, en plus de réduire le temps nécessaire pour compléter une analyse.

Un vaporisateur électrothermique à chauffage induit (IH-ETV) fut couplé à un plasma à couplage inductif avec détection par spectrométrie de masse (ICP-MS). Cette procédure permet de quantifier le mercure contenu dans un brin de cheveu sans aucune préparation préalable de l'échantillon, telle que la destruction de sa matrice par digestion. Les résultats obtenus sont comparables à ceux obtenus avec la méthode de référence.

Afin d'obtenir plus d'information sur la forme physico-chimiques de certains éléments, il est avantageux d'associer des techniques séparatives simples à l'ICP-MS. La chromatographie en couches minces (CCM) fut couplée directement à L'ICP-MS, à l'aide d'un système d'ablation laser (LA). Après leur

spéciation sur du gel de silice à l'aide d'un éluant à base d'eau, Cr^{3+} et Cr^{6+} ont étés prélevés directement sur la phase stationnaire par LA. Cette procédure à permis la spéciation et quantification rapide du chrome à partir d'un échantillon de 0.5 µL.

La méthode LA-ICP-MS fut également utilisée pour déterminer des complexes métal-8-hydroxyquinoline préconcentrés par adsorption sur des microcolonnes d'extraction en phase solide (SPE) incorporées à des plateformes microfluidiques centrifuges. Ces dispositifs miniatures de SPE nécessitent des échantillons de 1 – 600 µL, une réduction de trois à quatre ordres de grandeur, comparativement à la méthode conventionnelle, en plus d'éliminer l'élution du complexe chélaté à l'aide d'un solvant organique. Ce dispositif permet l'extraction simultanée de huit échantillons et peut aussi servir à entreposer les échantillons durant leur transport au laboratoire pour l'analyse par LA-ICP-MS.

Finalement, ces plateformes microfluidiques ont été modifiées pour permettre le couplage avec un spectromètre d'absorption ou d'émission. En plus des avantages susmentionnés, ce dispositif permet le contrôle de polluants organiques aquatiques directement sur le site d'échantillonnage par absorbance et fluorimétrie mesurées directement sur la microcolonne SPE.

Contributions to original knowledge

1. A simple method was developed for the quantification of mercury in a single human hair strand using Induction Heating - Electrothermal Vaporization Inductively Coupled Plasma - Mass Spectrometry (IH-ETV-ICP-MS).

2. A simple and rapid method was developed for the speciation of chromium by High Performance Thin Layer Chromatography (HPTLC) with only water as an eluent.

3. Using HPTLC plates, it was demonstrated that separated analytes could be detected and quantified by direct laser sampling on a silica gel sorbent using (Laser Ablation) LA-ICP-MS and furthermore that the silicon present in the stationary phase could be used as an internal standard to compensate for variations in laser energy.

4. A simple method for creating and retaining packed microcolumns on a centrifugal microfluidic polymeric platform was developed.

5. It was demonstrated that chelated metals can be extracted on Solid Phase Extraction (SPE) microcolumns under centrifugal action and that the extracted analytes could be preserved on the microfluidic platform prior to analysis.

6. It was demonstrated that analytes trapped on a microcolumn could be retrieved and quantified directly by LA-ICP-MS after laser ablation of the column's protective polycarbonate layer. It was also demonstrated that internal standards could be added to the sample in order to improve precision and accuracy for certain elements.

7. It was demonstrated that direct absorption and *in-situ* fluorescence spectrometry could be performed separately or simultaneously to detect organic analytes trapped on centrifugal microfluidic SPE columns for screening of aquatic pollutants directly in the field. The results obtained matched results predicted by theory.

Contributions of authors

All of the experimental work of this thesis was carried out by the author with some exceptions in Chapters 2 and 7. The experiments described in Chapter 2 were performed over the course of a full year. A fellow graduate student, Ms. Rebecca Lam, joined the author to perform the last set of experiments in the final month of experimentations and co-authored the resulting paper (Lafleur, J. P.; Lam, R.; Chan, H. M.; Salin, E. D. *JAAS* 2005, 20, 1315-1317).

In the case of Chapter 7, the author was fortunate enough to be given the opportunity to supervise two undergraduate Honours project during the course of her graduate studies. The two Honours students worked on a slight modification of the author'smain project. Direct detection of analytes trapped on centrifugal microfluidic chromatographic columns was performed by in-situ fluorescence (Andrien Rackov) and direct absorption (Scott McAuley) instead of LA-ICP-MS. Both students worked under the author's direct supervision using device designs, materials and protocols provided by the author. In some cases, the experiments were performed two by two (the author and a student or the two students together). The author indebted to both these students for their hard work in this project. The author performed all the data treatment and wrote the resulting paper (Lafleur, J. P.; Rackov, A. A.; McAuley, S.; Salin, E. D. *Talanta* 2009, Ms. Ref. No.: TAL-D-09-01648R01641).

Acknowledgments

Table of Contents

List of Figures

List of tables

Chapter 1 - Introduction

Hybrid techniques, in which a specialised sample introduction device, chromatographic separation, chromatographic enrichment procedure, etc., are coupled directly to various detection systems, play an important role in elemental and organic analyses. Several steps are normally necessary in order to transform a "natural" sample into a form that is suitable for introduction into an analytical instrument. These steps are very important as errors introduced before the actual analysis cannot be compensated for by even the most advanced methods and instrumentation.[1] The most common steps involved in a measurement process are *sampling*, *sample preservation*, *sample preparation* and finally, *analysis*.[2] Errors can occur during sampling due to the distribution or fractionation of an analyte in its natural matrix. Sample preservation can be an issue also as most analyses are not performed on-site, and therefore a delay is introduced between the sampling and the analysis when the sample is very susceptible to losses and contamination. The most important step, sample preparation, represents almost 60% of an analyst's time and contributes about 30% to the error in the global analysis of a sample.[3, 4] In comparison, only about 7% of the analysis time is spent on the actual measurement of the sample constituents,[4] the remainder of the time is used by sampling and data processing. Sample preparation includes steps such as homogenization, size reduction, extraction, concentration and

clean-up.[2] There are several ways of improving sample preparation methods for environmental analysis. A reduction in the number of sample preparation steps can minimize sample losses during transfers and reactions, contamination during handling as well as analysis time. Solvents can be eliminated to avoid dilution of the sample as well as the introduction of contaminants. The elimination of organic solvents is also desirable to reduce health hazards and comply with new government regulations and policies. Finally, a reduction in sample size can be beneficial to facilitate automation, sample acquisition, sample transport and on-site screening.

THESIS OUTLINE AND OBJECTIVES

The general objective of the project was to develop new hybrid microscale analytical methods that minimises sample preparation for the environmental analytical chemist's toolbox. Most of the work focused on elemental analysis although the last chapter presents an exploration of the applicability of these methods to organic analyses as well.

In the first paper (Chapter 2), sample preparation steps are eliminated completely as hair strands are introduced directly into an Inductively Heated Electrothermal Vaporizer (IH-ETV) coupled to an Inductively Coupled Plasma Mass Spectrometer (ICP-MS) for mercury analysis without any sample pre-treatment such as digestion. Provided the instrument is on-site, one can obtain total mercury results in less than a minute after sample collection.

Some attempts have been made (Appendix A) at using the IH-ETV for the thermal speciation of methylmercury from inorganic mercury in the hair samples from Chapter 2. Speciation is important since the toxicity of metals and their potential for bio-accumulation in human subjects depends on their chemical form. The following paper (Chapter 3) therefore focused on Chromium speciation. In this Chapter, the use of noxious organic solvents is completely eliminated. The separation is carried out with water as the sole eluent. Messy sample scraping from the plate followed by extraction and dilution is avoided by coupling High

Performance Thin Layer Chromatography (HPTLC) to an ICP-MS through Laser Ablation (LA). The ultra-violet laser is used to sample separated chromium species directly on an HPTLC plate so that contamination possibilities and analysis time are greatly reduced.

The following chapters all build upon the ideas introduced in Chapter 3, where analytes are determined directly on a chromatographic bed to minimize sample handling. Instead of TLC, these papers are based on Solid Phase Extraction (SPE), which is a sample preparation step widely used in environmental analyses. An important novelty introduced in Chapter 4 is the miniaturization of the process through the use of centrifugal microfluidic devices. The miniaturization allows the processing of many samples in parallel, has a very high potential for automation and greatly facilitates on-site extraction and detection. Chapter 4 describes in detail the fabrication procedure used to create these miniature centrifugal chromatographic devices. Chapter 5 presents results for the extraction of lead on several models of the centrifugal chromatographic devices followed by the paper reproduced in Chapter 6 which presents the multi-element pre-concentration of trace metals on centrifugal microfluidic discs. In both these chapters, miniature SPE devices are coupled to an ICP-MS directly through LA.

Chapters 2 to 6 focus on the coupling of electrothermal and chromatographic methods to a relatively large and expensive analytical instrument, the Inductively Coupled Plasma Mass Spectrometer (ICP-MS), to perform the analysis step of the experimental procedure. In these methods, the sample preparation steps can be performed in the field; but samples still need to be brought back to the laboratory for analysis, creating delays in result delivery. In appendix B, we explored how the IH-ETV could be used in conjunction with absorption spectrometry instead of the ICP-MS in order to increase portability. A similar type of study was conducted in Chapter 7, where the miniature centrifugal SPE devices are coupled to absorbance and fluorescence spectrometers to allow rapid on-site screening of organic pollutants.

THEORETICAL CONCEPTS AND LITERATURE REVIEW: FROM CONVENTIONAL CHROMATOGRAPHY TO MICROFLUIDIC DEVICES

Chromatographic separations of metal ions

The analysis of complex environmental samples can sometimes be enhanced by the use of hybrid methods. Inductively Coupled Plasma Mass Spectrometry (ICP-MS), the main detection system used in this project, is widely used for the determination of trace amounts of metals, but it provides information only on the elemental and isotopic composition of the sample. Since the toxicity of metals depends on their chemical form, it is of considerable importance to be able to distinguish species. Coupling chromatographic methods with mass spectrometry can therefore increase the information content available.

Chromatography is one of the most widely used means of performing analytical separations. Chromatography (from the Greek *chroma* meaning *colour* and *graphein* meaning *to write*) has received considerable interest since it was first discovered at the beginning of the 20th century.[5] This general term is applied to a vast array of separation techniques that rely on the partition of the sample between a mobile phase and a stationary phase. The mobile phase can either be a gas (gas chromatography) or a liquid (liquid chromatography). We will focus our discussion on methods that can be used to separate metal ions.

General chromatography theory

In elution chromatography, a sample containing a mixture is injected as a finite slug on a chromatographic bed. As the mobile phase is fed continuously on the stationary phase, the extent of retention of the different analytes on the chromatographic bed will vary. The analytes will therefore be separated based upon the amount of time they spend in the stationary phase. In partition chromatography, the chromatographic bed can either be polar (normal phase chromatography) or non-polar (reversed phase chromatography). Other types of chromatographic methods can be used to separate molecules according to their size (size exclusion chromatography or gel permeation chromatography) or according to their net charge (ion exchange chromatography, capillary electrophoresis, ion pair chromatography, ion exclusion chromatography) or according to specific interactive forces (affinity chromatography).

Van Deemter developed a rate model for column efficiency in 1956.[6] This expression accurately describes chromatographic peak shapes based on column variables listed in Table 1-1. For historical reasons, the efficiency of the column is described in terms of plate height, H, and number of plates. Martin and Synge[7] introduced this terminology in 1941, in an attempt to account for the Gaussian shape of chromatographic peaks and their rate of movement down a column. According to this theory, a chromatographic column is analogous to a system

made of multiple contiguous layers, called theoretical plates, resulting in a stepwise transfer of the mobile phase, from one plate to the other, after equilibration.

Table 1-1. Column variables that determine peak shape

Variable	Symbol
Linear velocity of the mobile phase	υ
Diffusion coefficient in mobile phase	D_M
Diffusion coefficient in stationary phase	D_S
Capacity factor (mass distribution coefficient of the analyte between the stationary and mobile phases)	k'
Diameter of packing particles	d_p
Thickness of the stationary phase	d_f
The obstruction factor	γ
Quality factor	λ

The Van Deemter equation is generally expressed in term of A, B and C, the coefficients for eddy diffusion, longitudinal diffusion and resistance to mass transfer, respectively. Maximum efficiencies are achieved when the plate height is minimal, or conversely, the number of plates is the highest.

Equation 1-1 $$H = A + \frac{B}{\upsilon} + C\upsilon$$

Equation 1-2 $$A = 2\lambda d_p$$

Equation 1-3 $\qquad B = 2\gamma D_M$

Equation 1-4 $\qquad C = C_s + C_M = \dfrac{f_1(k')d_p^2}{D_M} + \dfrac{f_2(k')d_f^2}{D_S}$

Equation 1-5 $\qquad C = \left(\dfrac{1 + 6k' + 11k'^2}{24(1+k')^2} \dfrac{d_p^2}{D_M} + \dfrac{8k'}{\pi^2(1+k')^2} \dfrac{d_f^2}{D_s} \right)$

These equations were used to predict column efficiencies for the centrifugal chromatographic microfluidic devices used in Chapters 4 - 7. Detailed calculations and Van Deemter plots can be found in Appendix F.

Thin layer chromatography

Thin layer chromatography (TLC) is a relatively simple and inexpensive technique, routinely used in many laboratories to assess compound purity. In this method, the stationary phase is generally coated on a glass or aluminum plate. A small aliquot of the sample is "spotted" close to one extremity of the plate, generally by contact transfer. The plate is then introduced into a vessel containing the mobile phase, called a developing chamber as illustrated in Figure 1-1.Capillary forces induce the transfer of the mobile phase through the thin

layer. Even though the Van Deemter equation was originally introduced to describe efficiency in column chromatography, it can also be applied to TLC. [8]
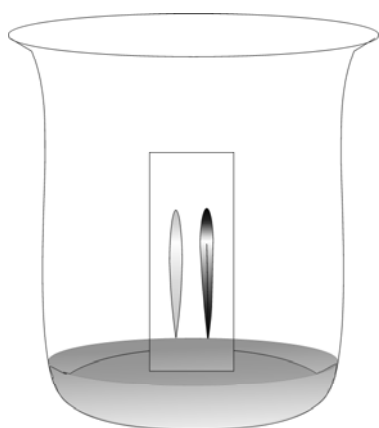
Figure 1-1. A simple beaker covered with a watch glass can be used as a developing chamber for TLC.

The efficiency of the chromatographic plate can be expressed in terms of Z, the migration distance of the analyte, and $W_{1/2}$, the spot width at half height.

Equation 1-6 $\qquad N = 5.545(Z/W_{1/2})^2$

Equation 1-7 $\qquad H = \dfrac{Z}{N}$

Although more commonly used for the separation of organic compounds, procedures for the separation of environmentally important heavy metals, such

as Cr(III) and Cr(VI), by TLC have been developed[9] (also see Chapter 3 for an example). Extensive reviews have been written by Mohammad *et al.* [10-14] on the separation of inorganic ions by TLC.

Solid Phase Extraction (SPE)

SPE is a special case of liquid chromatography where the capacity factors of the sample components are very high, so that the sample components will be retained as a single band often occupying 50% or more of the column length.[15] After a rinse to wash-off concomitant species, the extracted analytes can be eluted in a small amount of solvent. The elution is generally followed by High Performance Liquid Chromatography (HPLC) or Gas Chromatography (GC). Camel reviewed the SPE of trace elements in a 2003 article.[16] Other reviews[17, 18] focus on new sorbent materials for the SPE of trace metals.

Octadecylsilane silica phases are commonly used for the SPE of organic compounds from water (see Chapter 7 for an example) but can also be used in the pre-concentration of metal ions (Chapters 5 and 6). In this technique, 8-hydroxyquinoline (8-HQ) is used to form chelates with the metal ions to be extracted. 8-HQ is a bidentate monoprotic chelating agent which can form water soluble uncharged chelates with at least 60 elements.[19, 20] Metals are bound to 8-HQ through the ring nitrogen and phenolate oxygen as shown in Figure 1-2. Addition of excess 8-HQ to a metal ion in solution produces a neutral metal-8-HQ

chelate which can then be sorbed onto a reversed phase sorbent such as octadecylsilane silica. Ion exchange chromatography, described below, can also be used for the SPE of metal ions.
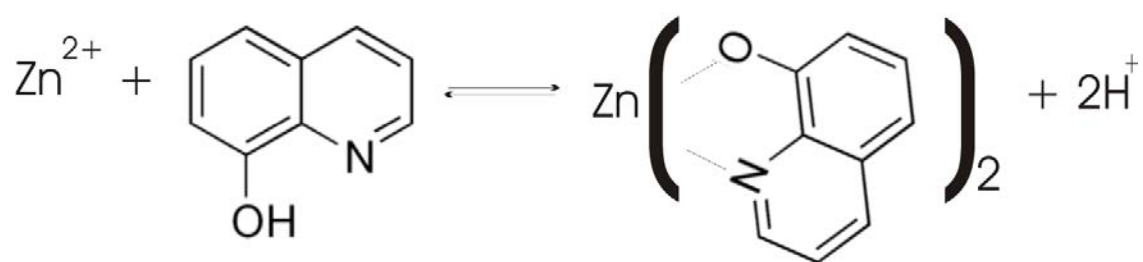
Figure 1-2. Formation of a neutral metal-8-HQ chelate

Ion chromatography - Ion exchange chromatography

In ion exchange chromatography, the analytes are separated or concentrated on a stationary phase containing ionic sites called an ion exchange resin. The analyte ions are exchanged reversibly between the two phases leading to an equilibrium that is dependent on the affinity of the analyte ions for the functional groups of the stationary phase. Although electrostatic interactions dominate, non-ionic interactions with the stationary phase can also occur. For example, adsorption can occur, as well as π-π interactions between ions with aromatic or olefinic carbons and the aromatic backbone resin. The sample is first injected onto the column, where it will exchange with ions already present on the

packing. The sample is then eluted from the column using a buffered aqueous solution containing a counter ion of the same charge as the analyte. The extent of analyte retention is dependent on their affinity for the ion exchange sites. Solution parameters such as pH, ionic strength and counter ion type can affect selectivity. Lucy and Haddad have written extensive reviews on the evolution of ion exchange chromatography.[21, 22]

Although ion exchange chromatography is most commonly used to separate proteins according to their charge, it can also be used for the determination of heavy and transition metals. Weiss gives several examples of separations of metals on ion exchange resins with either conductometric or spectrophotometric detection.[23] Steiner *et al.*[24] developed a colorimetric solid-phase extraction (CSPE) method for the rapid concentration and speciation of Cr(III) and Cr(VI) in water samples. The apparatus is simple and consists of two small, ion exchange disks placed on top of each other in a plastic holder. As an aqueous sample is forced through the disks, Cr(VI) is retained on the top anion-exchange disk while Cr(III) is extracted by the second cation-exchange disk. Measurements by diffuse reflectance spectroscopy allow determination of the chromium species at low ppm levels.

Ion chromatography - Ion pair chromatography

In ion pair chromatography, pairing ions, sometimes called hetaerons, are added to the mobile phase. The ionic analytes can then be separated as an ion pair on a conventional reversed-phase column. The ion-pairing agent is usually a large hydrophobic ion with a charge opposite to that of the analyte. For example, the negatively charged alkyl sulfonates are often used to determine cations and positively charged long chain quaternary ammonium salts can be used to determine anions. Less commonly, ion pairing can also be used in normal phase chromatography. In this case, the hetaeron is loaded on the sorbent and a non-aqueous mobile phase is employed. The basis of the retention mechanism in ion pair chromatography is still not fully understood and several models have been proposed over the years.[25, 26]

Ion pair chromatography has often been used as a fast and simple means of separating heavy metals by conventional reversed phase HPLC. Speciation of Cr(III) and Cr(VI) by ion pair chromatography has been used in conjunction with inductively coupled plasma atomic emission spectroscopy (HPLC-ICP-AES)[27], with postcolumn derivatization and spectrophotometric detection,[28] and with hydraulic high pressure nebulization inductively coupled plasma mass spectrometry (HPLC-HHPN-ICP-MS). [29]

Capillary electrophoresis

Separation by electrophoresis relies on the differential migration rate of charged species in an electrical field. Electrophoresis on slab gels (gel electrophoresis) is performed routinely in biochemical laboratories. Capillary electrophoresis (CE), a technique in which analytical electrophoresis is performed on a microscale in capillary columns of great length (50 to 100 cm) and small cross sectional area (25 - 100 µm I.D.), appeared in the 1980s.[5] The advantages of CE are numerous. Several factors, such as the flat electroosmotic flow (EOF) profile and the efficient heat dissipation attributable to the high surface to volume ratio of the capillaries contribute to the minimization of band broadening, so that efficiencies of several thousand plates are achievable.[30]

In electrophoresis, the migration velocity of an analyte, υ, is dependent upon its electrophoretic mobility, µ, as well as on the applied electric field, E, as shown in Equation 1-8.

Equation 1-8 $\qquad \upsilon = \mu E$

Faster separations can therefore be obtained by increasing the magnitude of the applied electric field. However, an increase in the electric field will also result in an increase in Joule heating. As Joule heating occurs, a temperature

gradient, ΔT, is created between the warmer center of the capillary and its walls, which can dissipate the heat more efficiently. Equation 1-9 illustrates the dependence of the temperature gradient on the magnitude of the applied electric field.

Equation 1-9 $\Delta T \approx E^2 k r^2$

This can result in unwanted band broadening due to thermally driven convective mixing. Equation 1-10 demonstrates that the conductivity of the solution, k, as well as the column radius, r, should be small in order to use high fields and low currents, I.[30]

Equation 1-10 $I = E r^2 k$

Capillary electrophoresis on microfluidic devices

Since the concept of micro-Total Analysis System (μTAS) was introduced in the 1990s, several lab-on-a-chip devices based on CE were commercialized for applications in the life sciences. The application of microfluidic systems in environmental analysis has attracted considerable attention and has been the object of a recent review.[31] However, the separation of inorganic ions on

microfluidic devices has received little attention. Most of the published work in this area involves isotachophoresis (ITP) or ITP hyphenated with capillary zone electrophoresis (ITP-CZE).[32]

These two modes of capillary electrophoresis, ITP and CZE, which are specialized modes of CE used for the analysis of small ions, are briefly described below.

Capillary zone electrophoresis (CZE)

The most commonly used type of CE due to its simplicity and versatility, CZE, is also referred to as free solution CE (FSCE). In CZE, the sample is introduced in a capillary filled with an appropriate buffer of desired pH. An electric field up to 1 kV/cm is applied to the system and separation results from the different electrophoretic mobility of the solutes in the capillary.
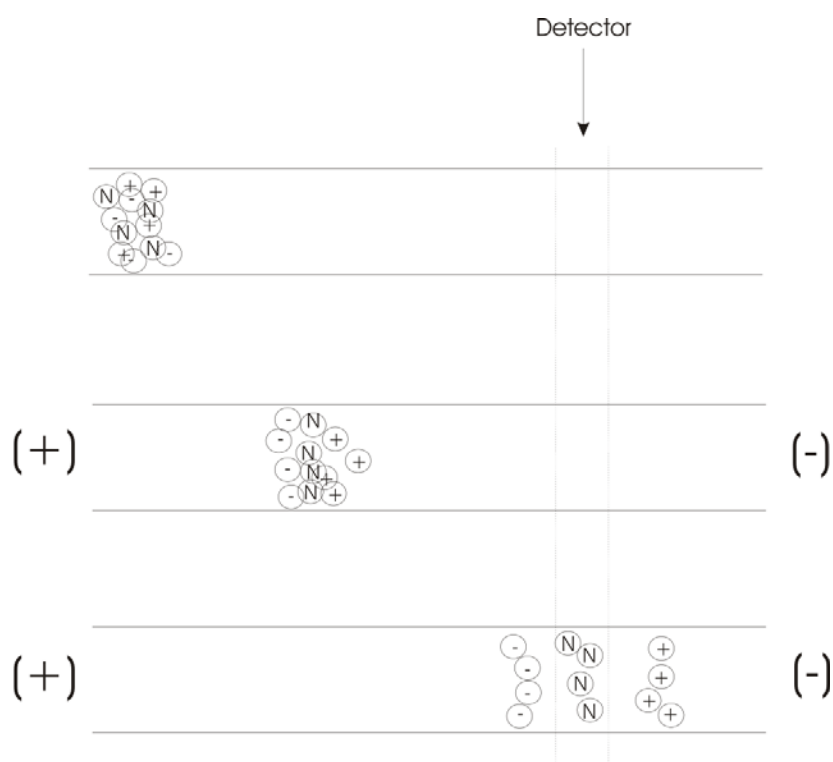
Figure 1-3. Movement of analytes during CZE, from injection (top) to separation (bottom).

Even though it seems that in an applied field, only the cationic analytes, attracted to the negative electrode, would pass the detector, Figure 1-3 illustrates that under appropriate conditions, all species will pass the detector. This is due to the presence of an electroosmotic flow (EOF) that drags the bulk buffer solution towards the negative electrode. However, neutral analytes migrate with the speed of the EOF and are therefore not separated by CZE.

It is the presence of ionized silanol groups (SiO^-) on the inner walls of the capillary that is responsible for the net movement of the bulk solution towards the

negative electrode. Under these conditions, buffer cations pair with the silanol ions to form a static double layer (Inner Helmoltz layer or Stern layer) close to the inner capillary walls. The formation of this double layer of ions creates a potential difference that decreases linearly with distance in the compact fixed layer and exponentially with distance in the diffuse layer. The zeta potential, ζ, is the potential at the interface between the static and diffuse layers. The remaining mobile buffer cations form a distal layer (Outer Helmoltz plane) that will, under an applied field, move towards the negative electrode carrying the bulk solution behind them.[33] The process is illustrated in Figure 1-4. The extent of bulk flow, under fixed conditions, depends on the charge of the capillary wall.[30] Modifying the electric field, altering the pH of the buffer or its concentration or modifying the capillary wall coatings can be used to control the EOF and optimize separations. An EOF which is too strong would not allow the components to separate according to their electrophoretic mobility while a weak EOF would result in band broadening due to diffusion.
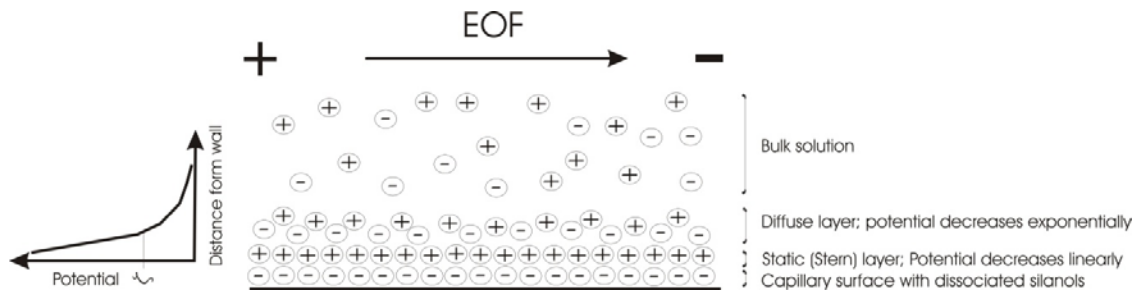
Figure 1-4. Double ionic layer formed at a silica capillary/solution interface (adapted form Karger[30] and Oda and Landers[33])

Isotachophoresis (ITC)

Two carefully chosen buffer systems are necessary to perform an ITC separation, a leading electrolyte (LE) and a tailing electrolyte (TE). In the case where a separation of cations is desired, the cations from the LE should have a higher mobility than those of the analytes while the cations from the TE should migrate more slowly in an electric field. When an electric field is applied, the analytes will separate into zones determined by their respective mobility, with the fastest moving cations following the LE. The separation process is illustrated in Figure 1-5.
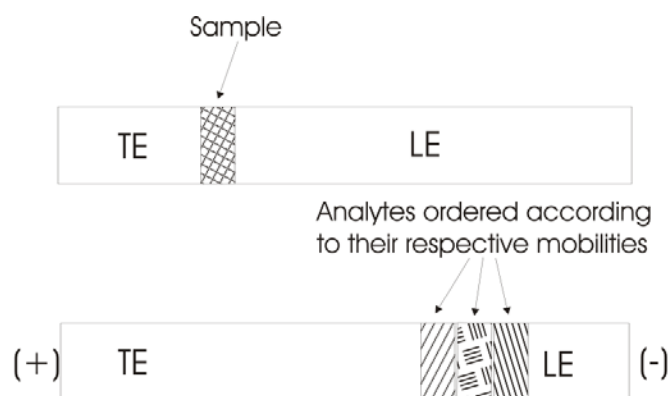
Figure 1-5. Separation of cations by isotachophoresis. (Top) the EOF is suppressed while the analyte is injected in between the leading and tailing electrolyte. Separation occurs when a voltage is applied (Bottom). (Adapted from Camilleri[34])

Hyphenated and cyclic methods

Some variations on the two methods presented above have been described in the literature. Briefly, both methods have disadvantages and the analyst can benefit from a synergistic combination of the two techniques. In ITP, a narrow analyte zone can be difficult to quantify accurately while in CZE, matrix ions can often mask analyte peaks. In the hyphenated method, ITP is used first to separate the analytes from undesirable components of the sample matrix. Careful switching of the voltages is then used to redirect only the analyte zones to the CZE channel where they can separate into sharp peaks according to their mobility. The extensive review by Evenhuis *et al.* [32] provides more details.

Cyclic methods have also been used to overcome the voltage limitations in CE. As mentioned above, Joule heating can still be a problem in CE and as a result, some analytes with very similar electrophoretic mobilities can remain unresolved due to these voltage limitations. In synchronized cyclic CE (SCCE), a triangular or square channel structure is employed. The voltage application points are switched in a circular fashion around the polygonal channel structure with a result analogous to column switching in conventional liquid chromatography. A review on cyclic separations was published by Eijkel *et al.*[35]

An alternative to electrokinetic pumping: centrifugal force

Electrokinetic pumping in microfluidic devices can require voltages up to 30 kV to force the flow of conducting liquids. While the high surface-to-volume ratio of capillaries allows for a very efficient dissipation of heat energy generated in the separation processes compared to conventional electrophoresis on gel slabs, Joule heating remains problematic for liquids with high ionic strength.[33] Microfluidic devices that use centrifugal force to drive the flow of liquids have been developed[36-44] and are the object of recent reviews.[45, 46] These have certain advantages over the more conventional electrokinetic pumping described above that is dependent on pH and ionic strength. A flow of liquid accelerated by centrifugal force is relatively insensitive to those physicochemical properties and careful design of the channels allows one to work in a wide range of flow rates.

Centrifugal microfluidic devices

Fundamentals of fluid flow in Capillaries

Macroscale fluid flow

The Hagen-Poiseuille law describes the volumetric flow rate of an incompressible fluid through a circular capillary. By analogy to Ohm's law for electrical circuits, the volumetric flow rate Q in a capillary of radius r can be expressed as a function of the pressure drop ΔP over the length, l, and the fluid resistance to flow, R. The dimensions are illustrated in Figure 1-6.

Equation 1-11 $$Q = \frac{\Delta P}{R}$$
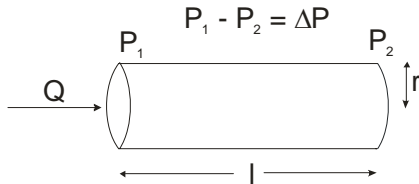
Figure 1-6. Macroscale fluid flow.

The resistance to flow is related to the fluid viscosity η and the capillary dimensions. For a circular channel,

Equation 1-12 $$R = \frac{8\eta l}{\pi r^4}$$

Equation 1-13 $$Q = \frac{\pi r^4 \Delta P}{8\eta l}$$

For a rectangular channel of width w and height h:

Equation 1-14 $$R = \frac{12\eta l}{wh^3}$$

Equation 1-15 $$Q = \frac{wh^3 \Delta P}{12\eta l}$$

From Equation 1-13 and Equation 1-15, we can conclude that larger flow rates can be obtained with larger tubes, and that it will reduce as the 4th power of the radius of the capillary, thus high pressures are required in microsystems. The average linear velocity, U, is also often used and is obtained by dividing the volumetric flow rate by the cross-sectional area of the channel, A.

Equation 1-16 $$U = \frac{Q}{A}$$

It is important to note that the flow is laminar in microfluidic devices, a fact that has important consequences for mixing solutions. Reynolds (Re) numbers are usually used to classify the flow of a fluid as laminar (Re < 2100) or turbulent (Re > 4000). Reynolds numbers are dependent on the fluid density, ρ, and

viscosity, as well as on the average linear fluid velocity. For a capillary, the characteristic length L is its diameter since it is far more important in determining the nature of the flow than the length.[47]

Equation 1-17 $\qquad \text{Re} = \dfrac{\rho U L}{\eta}$

Liquid flow in open microchannels achieved through centrifugally induced pressure

In the case of CD-like microfluidic devices, the centrifugal force, G, drives the flow of liquid through the micro-channels. The magnitude of the centrifugal force experienced by a particle on the CD will be dependent on the angular velocity, ω, of the platform as well as on the distance, r, of the particle from the centre of rotation.

Equation 1-18 $\qquad G = \omega r^{2}$

The flow rate of aqueous solutions in fluidic CD structures as been characterized experimentally by Duffy *et al.*[43] and the results compared to centrifuge theory. The average velocity of the liquid U from centrifugal theory is given by:

Equation 1-19 $$U = \frac{D_h^2 \rho \omega^2 \bar{r} \Delta r}{32 \eta L}$$

The quantities $\bar{r}$ and Δr represent the average distance of the liquid in the channels to the centre of the disk and the radial extent of the fluid, respectively. They both can be expressed in terms of r_0 and r_1, the inner and outer radii of the flowing liquid, and H, the head of the liquid being pumped through the micro-channel. L is the length of the liquid in the microchannel.

Equation 1-20 $$\bar{r} = \frac{(r_1 + (r_0 - H))}{2}$$

Equation 1-21 $$\Delta r = r_1 - (r_0 - H)$$

A graphic illustration of these dimensions is given in Figure 1-7. Care should be taken to note the difference in the definitions between the three papers listed in Figure 1-7. The definition by Penrose et al., [38] is the only one that relates to packed microchannels. Definitions by Duffy et al.,[43] and Zoval et al.[48] refer to the flow of liquids in open rather than packed microchannels.

The hydraulic diameter, D_h is a term used to account for the shape as well as the size of a non-circular conduit. It is defined as four times the ratio of the

26

cross-sectional area, A, to the wetted perimeter, P_W, of the cross section. The hydraulic radius, R_h, is defined as the ratio of the cross-sectional area to the wetted perimeter of the cross section.[49]

Equation 1-22 $$R_h = \frac{A}{P_w}$$

Equation 1-23 $$D_h = \frac{4A}{P_W}$$

Experiments by Duffy *et al.*[43] showed no systematic deviations for the experimental flow rates compared to the theory and therefore concluded that Equation 1-19 adequately describes the flow of aqueous solutions under centrifugal pumping. However, later studies by Maruyama and Maeuchi[50] showed that the increase in frictional loss due to the Coriolis force could not be neglected at high rotational rates. Therefore, when only the centrifugal force is taken into account to predict volumetric flow rates, measured flow rates will be lower than the predicted at high revolution speeds.

A) Penrose, A., et al., Analyst, 2004. **129**(8): p. 704-9.

r_0

r_1

CD Center

H   L

$$U = \frac{(2R_{Hpached})^2 \rho \omega^2 \bar{r} \Delta r}{32 \eta L_{eff}}$$

⬡ Column Packing   ⬤ Liquid

L: length of micro-channel
$\bar{r}$: average distance of the liquid in the channel from the disk center
Δr: radial extent of fluid subjected to centrifugal force
H: head of liquid being pumped through the packed channel
r_0: inner radii of the flowing liquid
r_1: outer radii of the flowing liquid

B) Duffy, D.C., et al., Analytical Chemistry, 1999. **71**(20): p. 4669-4678.

CD Center

r_0

r_1

H

L

$$U = \frac{D_h^2 \rho \omega^2 \bar{r} \Delta r}{32 \eta L}$$

L: length of micro-channel
$\bar{r}$: average distance of the liquid in the channel from the disk center
Δr: radial extent of fluid subjected to centrifugal force
H: head of the liquid in the reservoir that feeds the channel
r_0: inner radii of the flowing liquid
r_1: outer radii of the flowing liquid

C) Zoval, J.V. and M.J. Madou, Proceedings of the IEEE, 2004. **92**(1): p. 140-153.

⬤ CD Center

$\bar{r}$

L Δr

$$U = \frac{D_h^2 \rho \omega^2 \bar{r} \Delta r}{32 \eta L}$$

L: length of the liquid in the capillary channel
$\bar{r}$: average distance of the liquid in the channel from the disk center
Δr: radial extent of fluid subjected to centrifugal force

Figure 1-7. Summary of the different parameter definitions found in the literature on the flow of liquid on microfluidic disks. A) Packed micro-channel, B) and C) open micro-channels.

Liquid flow in packed microchannels achieved through centrifugally induced

pressure

Modifications have to be made to Equation 1-19 in order to adequately describe flow rates through packed micro-channels. First, it can be re-written as a function of the hydraulic radius using the above definitions.[1]

Equation 1-24 $$U = \frac{(4R_h)^2 \rho \omega^2 \bar{r} \Delta r}{32 \eta L}$$

In order to apply this equation to a packed channel, Penrose *et al.*[38] used the hydraulic radius theory to calculate a corrected hydraulic radius, $R_{Hpacked}$. The premises of this theory are:[51]

---

[1] Note that we follow closely the derivation found in the paper by Penrose *et al.*[38] but that our expression

differs by a factor of 4 as they defined the linear flow velocity as $U = \frac{(2R_h)^2 \rho \omega^2 \bar{r} \Delta r}{32 \eta L}$. Although for a

circular conduit, the hydraulic diameter is effectively equal to the diameter D: $D_h = \frac{4A}{P_w} = \frac{\frac{4\pi D^2}{4}}{\pi D} = D$,

the hydraulic diameter is *not* twice the hydraulic radius as shown by Equation 1-22 and Equation 1-23:

$R_h = \frac{A}{P_w} = \frac{\frac{\pi D^2}{4}}{\pi D} = \frac{D}{4}$.

- No pores are sealed off;

- The pores are distributed at random;

- The pores are reasonably uniform in size;

- The porosity is not too high;

- Diffusion phenomena are absent;

- Fluid motion occurs like motion through a batch of capillaries.

The hydraulic radius for a porous medium is defined as the ratio of the volume open to flow to the wetted surface area. For a granular, or porous medium, a specific surface area, a_v, which is an intrinsic property of the medium, is defined:

Equation 1-25 $$a_V = \frac{wetted\ surface\ area}{solid\ volume}$$

Using the definitions of specific surface area and hydraulic radius, the latter can be expressed as:

Equation 1-26 $$R_{Hpacked} = \frac{\varepsilon}{a_v(1-\varepsilon)}$$

Where ε is a porosity factor representing the fractional void volume in the column. In the case of a pack of uniform spheres of diameter D_p:

Equation 1-27
$$a_v = \frac{area\ of\ spheres}{volume\ of\ spheres} = \frac{\pi D_p^2}{\frac{\pi}{6} D_p^3} = \frac{6}{D_p}$$

Equation 1-28
$$R_{Hpacked} = \frac{\varepsilon D_p}{6(1-\varepsilon)}$$

A tortuosity factor, T, is also introduced to account for the longer effective packed bed length, L_{eff}. With these adjustments, the liquid flow through packed micro-channels achieved through centrifugally induced pressure can be described by Equation 1-29.

Equation 1-29
$$Q = \left(\frac{(4R_{Hpached})^2 \rho \omega^2 \bar{r} \Delta r}{32 \eta L_{eff}} \right) hw\varepsilon$$

Where h and w are the height and width of the channel respectively. Appendix F provides an example of the application of Equation 1-29 to model the volumetric flow rates in the centrifugal microfluidic systems used in Chapters 4-7.

Gating of the flow of liquids in microfluidic devices

For a microfluidic system to be useful, pumps and valves must control the flow of liquids. Valves that require external energy to function are classified as "active" whereas those that use the energy from the flow are termed "passive". The ideal characteristics of a valve include: [52]

- No leakage;

- No power consumption;

- No dead volume;

- Infinite differential pressure capability;

- No delays;

- Insensitivity to particulate contamination;

- Ability to operate with any fluid.

Gating of the fluid flow in conventional microfluidic devices

Many active valves have been designed for different microfluidic applications. The actuation principles are various and include: [52]

- Pneumatic (using compressed air);

- Thermopneumatic (using heated/cooled fluid);

- Piezoelectric (using materials that expand under the application of a voltage);

- Electrostatic (using electrical attraction/repulsion);

- Shape memory alloy (metals that can revert to their original shape after a temperature activated change);

- Electromagnetic.

Many single-use passive valves have also been developed. They can usually be used only once because their functioning depends on an air-liquid interface, which is only present when first filling the chip [52]. Thin strips of silicon in a cantilever arrangement have been used as simple passive valves as well as valves based on changes in the volume of hydrogels when subjected to a physical or chemical stimulus.

Gating of the fluid flow in centrifugal microfluidic devices

Two types of passive valves are commonly used to gate the flow of fluid in centrifugal microfluidic platforms: hydrophobic breaks and capillary burst valves. Both valves work by preventing the flow of liquids at low enough rotational speed. When the rotational speed attains a critical frequency, the liquid bursts through the valve.

Hydrophobic valves

Hydrophobic breaks can be made by a constriction in a chamber made of hydrophobic material or by applying hydrophobic material to a zone in the channel. [48] The required pressure, ΔP, to overcome a sudden narrowing in a rectangular hydrophobic channel is given by: [48]

Equation 1-30 $$\Delta P = 2\gamma \cos(\theta_c) \left[\left(\frac{1}{w_1} \right) + \left(\frac{1}{h_1} \right) \right] - \left[\left(\frac{1}{w_2} \right) + \left(\frac{1}{h_2} \right) \right]$$

Where γ is the liquid's surface tension, θ_c, is the contact angle, w_1 and h_1 are the width and height of the channel before the restriction and w_2 and h_2 are the channel dimensions after the restriction. This type of valve is used to gate the flow of fluids on commercially available CD-like microfluidic platforms for simultaneous multiple immunoassays (Bioaffy CD, Gyros AB, Uppsala, Sweden).

Capillary burst valves

When liquid flows through a channel that exits into a chamber, the liquid will be pinned at the discontinuity in the fluidic network due to the surface tension that develops when the cross section of the capillary expands abruptly. For the pinned liquid to enter the chamber, the centripetal force has to exceed the capillary barrier pressure. The rotational frequency at which this occurs is called the burst frequency. An exact solution to determine the burst frequency of a capillary valve would be complex as factors such as surface roughness and the specific geometries of each channel would have to be taken into account, but a simple model based on capillary forces and empirical measurements of burst frequencies was developed by Duffy *et al.* [43] According to this model, the centrifugal pressure at the meniscus of the capillary, P_m, can be written as:

Equation 1-31
$$P_m = \rho \omega^2 \bar{r} \Delta r$$

While the capillary barrier pressure, P_{cb}, can be written as:

Equation 1-32
$$P_{cb} = a\left(\frac{4\gamma}{D_h}\right) + b$$

Where a and b are empirical constants that are determined by the shape of the droplet, the geometry of the chamber and the wettability of the walls of the chamber. By balancing Equation 1-31 and Equation 1-32, a simplified expression for the angular burst velocity, ω_c, is obtained: [43, 44, 48, 53]

Equation 1-33
$$\rho \omega_c^2 \bar{r} \Delta r = a\left(\frac{4\gamma}{D_h}\right) + b$$

Equation 1-34
$$\omega_c \geq \left(\frac{a(4\gamma / D_h) + b}{\rho \bar{r} \Delta r}\right)$$

Other expressions for the capillary barrier pressure can also be found in the literature.[39, 40, 54] The capillary force due to interfacial tension can also more conveniently be defined as:

Equation 1-35 $\qquad P_{ch} = \dfrac{\gamma Cos\theta_c P_w}{A}$

In this case, the burst frequency ($f_c = \omega_c/2\pi$) can be defined as:

Equation 1-36 $\qquad f_c \geq \left(\dfrac{\gamma \cos\theta_c P_w}{\pi^2 \rho \bar{r} \Delta r 4A} \right) \geq \left(\dfrac{\gamma \cos\theta_c}{\pi^2 \rho \bar{r} \Delta r D_h} \right)$

This type of valve has been used for elaborate fluid handling on centrifugal microfluidic platforms.[37, 39-41, 43, 44] Since the precision in gating provided by these valves is determined by the quality of the microfluidic channels, the greater surface roughness of channels produced by machining compared to those produced by photolithography leads to a larger error.[43] Johnson *et al.* [41] found that a spacing of ~ 200 rpm in burst frequencies is sufficient to prevent premature release of undesired fluids. This spacing allows for microfabrication tolerances of 10% and roughness of a few micrometers, which are common for machined features.

As seen from Equation 1-33, the use of capillary burst valves for liquids with low surface tension could pose a problem. Indeed, solutions of surfactants will tend to flow directly out of the capillary into the chamber when the channel diameters exceed 100 µm. However, at smaller diameters (<100 µm), this type of

valve has been used successfully to gate the flow of solutions of surfactant (0.1% Triton X-100).[43]

Mixing in centrifugal microfluidic devices

Duffy *et al.*[43] calculated that in their largest microfabricated channel, the Reynolds Number was below 100, well below values associated with turbulent flow. Due to the laminar flow characteristic of microfluidic devices, special features need to be incorporated in the devices to facilitate mixing.

Mixing by diffusion

An approach to mixing solutions in centrifugal microfluidic devices is to rely on diffusion. In this technique, the two solutions are combined into a single, long, meandering channel. By carefully adjusting the length of the channels as well as the reservoir size, Duffy *et al.*[43] obtained stochiometric reactions by diffusional mixing. The rates of rotation were set such that the solutions were in the mixing channels for about 2 s. Calculations based on diffusion across a rectangular 100 μm diameter channel indicated that the solutions were 90% mixed after this time.

Mixing by chaotic advection

During chaotic advection, the interfacial area where diffusion occurs is increased, thereby enhancing the diffusion process. Emptying two narrow

streams into a common chamber can create turbulence and mixing as the streams violently splash against the chamber walls. [48]

Batch-mode mixing

It was demonstrated by Grumann *et al.*[55] that mixing on centrifugal microfluidic devices can be accelerated from 7 minutes using diffusion to less than five seconds using two different strategies. In the first case, advection is induced when magnetic beads pre-filled in the mixing chamber are periodically deflected by a set of fixed permanent magnets. In the second strategy, the liquids are stirred by periodically changing the sense of rotation of the disk. It was also demonstrated that when both strategies are combined, mixing time could be reduced to less than a second.

Dual-Pumping microfluidic devices

To date, only one example is found in the literature where the advantages of electrokinetic and centrifugal pumping are combined in a single device. Experimental results obtained by Wang *et al.* [36] show that the EOF effect can be effectively reduced when the electric field force and the centrifugal force are in the opposite direction, allowing for longer separations in shorter channels as well as a diminution of Joule heating.

Detection of inorganic ions on microfluidic devices

Electrochemical detection methods

Although amperometry and potentiometry could potentially be used as detection methods, of all the electrochemical methods, conductometric detection has received the most attention for the determination of inorganic ions.[32] In conductometry, the electrical conductivity of the solution is measured using electrodes. The electrodes can be in direct contact with the test solution (contact mode) or not (contactless mode).[56] However, these methods are not easily applied to moving platforms, such as centrifugal microfluidic devices, therefore focus will be placed on detection methods that require no contact with the microfluidic device. Several reviews report recent advances in electrochemical detection on microfluidic devices.[32, 57, 58]

Chemiluminescence

Chemiluminescence is an attractive detection scheme for microfluidic devices. It requires no excitation source and a simple photomultiplier tube (PMT) can be used to detect the emitted light. Many metal cations catalyze the oxidation of luminol in basic aqueous solution to form a chemiluminescent emitter, and this reaction can therefore be used to quantify metal cations.
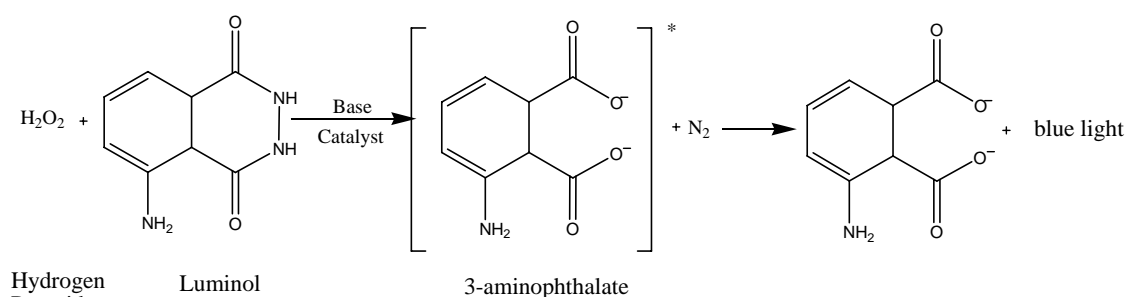
Figure 1-8. Metal catalyzed chemiluminescent reaction of luminol.

Chromium(III) was detected at a concentration of 10^{-7} M using this chemiluminescent reaction in a micromachined mixer/reactor.[59] Liu *et al.*[60] also used the metal ion-catalyzed luminol-peroxide chemiluminescent reaction successfully to detect Cr(III), Co(II) and Cu(II) on a microchip capillary electrophoretic system.

Ion-Selective Optodes

Ion-selective optodes membranes, composed of a selective ionophore, a pH-sensitive chromoionophore, and a lipophilic additive embedded within a plasticized poly(vinylchloride) (PVC) were developed by Johnson *et al.*[41] for the measurement of potassium ions on centrifugal microfluidic devices. The standards are allowed to flow sequentially into the measuring reservoir by the use of capillary burst valves, where they are allowed to equilibrate with the potassium selective membrane. Absorption measurements are carried out at 650 nm, the wavelength of maximum absorption of the protonated form of the

chromoionophore by means of a filter and photomultiplier tube (PMT). Detection

limits and linear dynamic range were later improved by Badr *et al.*[44] who used

fluorescence rather than absorption detection.

Inductively Coupled Plasma Mass Spectrometry (ICP-MS)

Several groups have reported the successful interfacing of microfluidic

capillary electrophoresis with ICP-MS through the use of micro-flow nebulizers

and volatile species generation.[61-66] However, the technique described in

Chapters 5 and 6 is the first instance of the use of Laser Ablation (LA) to couple

microfluidic devices directly to an ICP-MS.

REFERENCES

(1)   Pawliszyn, J. Journal of High Resolution Chromatography **1993**, 16, 565.

(2)   Mitra, S.; Brukh, R. In Sample preparation techniques in analytical chemistry; Mitra, S., Ed.; John Wiley & Sons, Inc.: Hoboken, New Jersey, 2003, pp 1-36.

(3)   Papadoyannis, I. N.; Samanidou, V. F. In Encyclopedia of chromatography; Cazes, J., Ed.; CRC: Boca Raton, Fl, 2004, pp 250-266.

(4)   Pipkin, W. American Laboratory **1990**.

(5)   Skoog, D. A.; Leary, J. J. Principles of instrumental analysis, 4 ed.; Saunders College Publishers: Philadelphia, 1992.

(6)   van Deemter, J. J.; Zuiderweg, F. J.; Klinkenberg, A. Chemical Engineering Science **1956**, 5, 271-289.

(7)   Martin, A. J. P.; Synge, R. L. M. Biochemical journal **1941**, 35, 1358.

(8)   Kowalska, T.; Kaczmarski, K.; Prus, W. In Handbook of Thin-Layer Chromatography, 3rd edition, revised and expanded, 3rd ed.; Sherma, J., Fried, B., Eds.; Marcel Dekker, Inc.: New York, 2003, pp 47-80.

(9)   Mohammad, A.; Sirwal, Y. H. Acta Chromatographica **2003**, 13, 117-134.

(10)   Mohammad, A. Journal of Planar Chromatography--Modern TLC **1997**, 10, 48-54.

(11)   Mohammad, A. Chemical & Environmental Research **1994**, 3, 275-282.

(12) Mohammad, A.; Tiwari, S.; Yusuf, R.; Chahar, J. P. S. Chemical & Environmental Research **1998**, 7, 3-46.

(13) Mohammad, A.; Khan, M. A. M. Chemical & Environmental Research **1992**, 1, 3-31.

(14) Mohammad, A.; Fatima, N.; Ahmad, J.; Khan, M. A. M. Journal of Chromatography **1993**, 642, 445-453.

(15) Fritz, J. S. Analytical Solid Phase Extraction; Wiley-VCH: New York, 1999.

(16) Camel, V. Spectrochimica Acta - Part B Atomic Spectroscopy **2003**, 58, 1177-1233.

(17) Lemos, V. A.; Teixeira, L. S. G.; Bezerra, M. d. A.; Spinola Costa, A. C.; Castro, J. T.; Cardoso, L. A. M.; de Jesus, D. S.; Santos, E. S.; Baliza, P. X.; Santos, L. N. Applied Spectroscopy Reviews **2008**, 43, 303-334.

(18) Turker, A. R. Clean - Soil, Air, Water **2007**, 35, 548-557.

(19) Sandell, E. B.; Onishi, H. Photometric determination of traces of metals : general aspects; Wiley: New York, 1978 pp. 422-425.

(20) Minczewski, J.; Chwastowska, J.; Dybczyński , R. Separation and preconcentration methods in inorganic trace analysis; Halsted Press: New York, 1982, p. 197.

(21) Lucy, C. A. Journal of Chromatography A **2003**, 1000, 711-724.

(22) Haddad, P. R. Analytical Chemistry **2001**, 73, 266A-273A.

(23) Weiss, J. In Ion chromatography, 2nd ed.; VCH publishers, Inc.: New York, 1995, pp 190-204.

(24) Steiner, S. A.; Porter, M. D.; Fritz, J. S. Journal of Chromatography A **2006**, In Press, Corrected Proof, Available online 14 February 2006.

(25) Walton, H. F.; Rocklin, R., D. In Ion exchange in analytical chemistry; CRC Press, Inc.: Boca Raton, 1990, pp 99-119.

(26) Weiss, J. In Ion Chromatography; VCH Publishers, Inc.: New York, 1995, pp 239-290.

(27) Krull, I. S.; Bushee, D.; Savage, R. N.; Schleicher, R. G.; Smith, S. B., Jr. Analytical Letters **1982**, 15, 267-281.

(28) Trojanowicz, M.; Pobozy, E.; Worsfold, P. J. Analytical Letters **1992**, 25, 1373-1387.

(29) Jakubowski, N.; Jepkens, B.; Stuewer, D.; Berndt, H. Journal of Analytical Atomic Spectrometry **1994**, 9, 193-198.

(30) Karger, B. L. In High-Performance Capillary Electrophoresis. Theory, Techniques, And Applications; Khaledi, M. G., Ed.; John Wiley & Sons, Inc.: New York, 1998; Vol. 146, pp 3-23.

(31) Li, H.-F.; Lin, J.-M. Analytical and Bioanalytical Chemistry **2009**, 393, 555-567.

(32) Evenhuis, C. J.; Guijt, R. M.; Macka, M.; Haddad, P. R. Electrophoresis **2004**, 25, 3602-3624.

(33) Oda, R. P.; Landers, J. P. In Handbook of capillary electrophoresis; Landers, J. P., Ed.; CRC Press: Boca Raton, 1997, pp 2-42.

(34) Camilleri, P. Capillary Electrophoresis - Theory and Practice, 2 ed.; CRC Press: Boca Raton, Fl, 1998.

(35) Eijkel, J. C. T.; van den Berg, A.; Manz, A. Electrophoresis **2004**, 25, 243-252.

(36) Wang, G.-J.; Hsu, W.-H.; Chang, Y.-Z.; Yang, H. Biomedical Microdevices **2004**, 6, 47-53.

(37) Puckett, L. G.; Dikici, E.; Lai, S.; Madou, M.; Bachas, L. G.; Daunert, S. Analytical Chemistry **2004**, 76, 7263-7268.

(38) Penrose, A.; Myers, P.; Bartle, K.; McCrossen, S. Analyst **2004**, 129, 704-709.

(39) Madou, M. J.; Lee, L. J.; Daunert, S.; Lai, S.; Shih, C.-H. Biomedical Microdevices **2001**, 3, 245-254.

(40) Lai, S.; Wang, S.; Luo, J.; Lee, L. J.; Yang, S.-T.; Madou, M. J. Analytical Chemistry **2004**, 76, 1832-1837.

(41) Johnson, R. D.; Badr, I. H. A.; Barrett, G.; Lai, S.; Lu, Y.; Madou, M. J.; Bachas, L. G. Analytical Chemistry **2001**, 73, 3940-3946.

(42) Honda, N.; Lindberg, U.; Andersson, P.; Hoffmann, S.; Takei, H. Clinical Chemistry (Washington, DC, United States) **2005**, 51, 1955-1961.

(43) Duffy, D. C.; Gillis, H. L.; Lin, J.; Sheppard, N. F., Jr.; Kellogg, G. J. Analytical Chemistry **1999**, 71, 4669-4678.

(44) Badr, I. H. A.; Johnson, R. D.; Madou, M. J.; Bachas, L. G. Analytical Chemistry **2002**, 74, 5569-5575.

(45) Madou, M.; Zoval, J.; Jia, G.; Kido, H.; Kim, J.; Kim, N. In Annual Review of Biomedical Engineering, 2006; Vol. 8, pp 601-628.

(46) Haeberle, S.; Zengerle, R. Lab on a chip **2007**, 7, 1094-1110.

(47) Madou, M. J. Fundamentals of microfabrication, 2nd ed.; CRC Press Boca Raton, Florida, 2002.

(48) Zoval, J. V.; Madou, M. J. Proceedings of the IEEE **2004**, 92, 140-153.

(49) Basu, D., K., Ed. Dictionary of material science and high energy physics; CRC Press, 2001.

(50) Maruyama, T.; Maeuchi, T. Chemical Engineering Science **2008**, 63, 153-156.

(51) Scheidegger, A. E. In The physics of flow through porous media, 3rd edition ed.; University of Toronto Press, 1974, pp 136.

(52) Kutter, J. P.; Mogensen, K. B.; Klank, H.; Geschke, O. In Microsystem engineering of lab-on-a-chip devices; Geschke, O., Klank, H., Tellemann, P., Eds.; Wiley-VCH Velag GmbH & Co. KGaA: Weinheim, 2004, pp 39-76.

(53) Johnson, R. D.; Badr, I. H.; Barrett, G.; Lai, S.; Lu, Y.; Madou, M. J.; Bachas, L. G. Analytical chemistry **2001**, 73, 3940-3946.

(54) Madou, M. J. Fundamentals of microfabriacation, 2nd ed.; CRC Press Boca Raton, Florida, 2002.

(55) Grumann, M.; Geipel, A.; Riegger, L.; Zengerle, R.; Ducree, J. Lab on a Chip **2005**, 5, 560-565.

(56) Schoning, M. J.; Gluck, O.; Thust, M. In The measurement, instrumentation, and sensors handbook; Webster, J. G., Ed.; CRC Press: Boca Raton, Florida, 1999, pp Chapter 70.71.

(57) Auroux, P.-A.; Iossifidis, D.; Reyes, D. R.; Manz, A. Analytical Chemistry **2002**, 74, 2637-2652.

(58) Vilkner, T.; Janasek, D.; Manz, A. Analytical Chemistry **2004**, 76, 3373-3386.

(59) Xu, Y.; Bessoth, F. G.; Eijkel, J. C. T.; Manz, A. Analyst (Cambridge, United Kingdom) **2000**, 125, 677-683.

(60) Liu, B.-F.; Ozaki, M.; Utsumi, Y.; Hattori, T.; Terabe, S. Analytical Chemistry **2003**, 75, 36-41.

(61) Hui, A. Y. N.; Wang, G.; Lin, B.; Chan, W. T. Journal of Analytical Atomic Spectrometry **2006**, 21, 134-140.

(62) Alvarez-Llamas, G.; Fernandez De La Campa, M. R.; Sanz-Medel, A. Analytica Chimica Acta **2005**, 546, 236-243.

(63) Alvarez-Llamas, G.; Fernandez De LaCampa, M. D. R.; Sanz-Medel, A. TrAC - Trends in Analytical Chemistry **2005**, 24, 28-36.

(64) Pearson, G.; Greenway, G. Journal of Analytical Atomic Spectrometry **2007**, 22, 657-662.

(65) Song, Q. J.; Greenway, G. M.; McCreedy, T. Journal of Analytical Atomic Spectrometry **2003**, 18, 1-3.

(66) Song, Q. J.; Greenway, G. M.; McCreedy, T. Journal of Analytical Atomic Spectrometry **2004**, 19, 883-887.

Chapter 2 - Induction heating-electrothermal vaporization for direct mercury analysis of a single human hair strand by inductively coupled plasma mass spectrometry

In this chapter, a solid sample introduction device, the Induction Heating Electrothermal Vaporizer (IH-ETV), is coupled to an Inductively Coupled Plasma Mass Spectrometer (ICP-MS) for the rapid detection of mercury in a single human hair strand. Although the IH-ETV is solely used as a sample introduction device in this chapter, Appendix A demonstrates that it could also potentially be used to perform thermal online speciation of mercury. Unlike all subsequent chapters in this thesis, Chapter 2 deals with the analysis of a solid sample, human hair, rather than pollutants in aquatic samples. The hair strands analysed in this chapter were collected from women in the Brazilian Amazon, where fish is a dietary staple. A mercury amalgamation process is used in gold mining in South America and especially Brazil, the continent's largest gold producer.[1] As mercury gets converted to methylmercury in aquatic environments, it bioaccumulates in fish and in humans who feed from them. In contaminated areas, predatory fish can reach mercury levels as high as 6 ppm, compared to 0.2 ppm in pristine areas.[1]

South-American populations are not the only ones impacted by mercury contaminations in their lakes and rivers. In Quebec, the James Bay hydroelectric

49

mega projects had severe impacts on the health of subarctic Cree Indians. Boreal hydroelectric developments generally involve the flooding of substantial quantities of organic biomass, which predisposes these reservoirs to high production rates of methylmercury through microbial methylation of naturally occurring mercury.[2] After the Government of Quebec's La Grande Rivière hydroelectric project in 1971, fish consumption had to be severely restricted, and even prohibited in certain stretches of the river, to reduce mercury exposure in the Cree Indians.[3] The results presented in this chapter were originally published as:

Lafleur, J. P.; Lam, R.; Chan, H. M.; Salin, E. D. *Journal of Analytical Atomic Spectrometry* **2005**, *20*, 1315-1317.

Information on the temperature calibration of the IH-ETV can be found in Appendix A and preliminary work on the hyphenation of the IH-ETV with an absorbance spectrometer for rapid on-site monitoring can be found in Appendix B.

(1)   Malm, O. *Environmental Research* **1998**, *77*, 73-78.
(2)   Bodaly, R. A.; Beaty, K. G.; Hendzel, L. H.; Majewski, A. R.; Paterson, M. J.; Rolfhus, K. R.; Penn, A. F.; St. Louis, V. L.; Hall, B. D.; Matthews, C. J. D.; Cherewyk, K. A.; Mailman, M.; Hurley, J. P.; Schiff, S. L.; Venkiteswaran, J. J. *Environmental Science and Technology* **2004**, *38*.
(3)   Sala, O. E.; Meyerson, L. A.; Parmesan, C. In *Biodiversity change and human health - From ecosystem services to spread of disease,* 2 ed.; Island Press: Washington D.C., 2009, pp 66-67.

ABSTRACT

It was demonstrated that a single human hair strand can be analyzed for total mercury using an induction heating-electrothermal vaporizer with ICP-MS detection, achieving a detection limit of 20 pg or 30 ng g^{-1} (based on a 0.6 mg sample).

INTRODUCTION

There is a growing concern about mercury from environmental and dietary sources and its effects on human health. For example, populations where fish is a dietary staple may be at risk due to mercury levels present in fish tissue. In many epidemiological studies, hair has been used as a biomarker because the mercury in the bloodstream is incorporated into the hair structure as it grows. Natural mercury concentrations in hair range from 0.3 to 1.0 µg g^{-1} for typical North American populations.[1] Since hair grows at roughly one cm per month, it is possible to track mercury exposure along the length of the hair. Hair samples are also more convenient to collect and store when compared to blood samples.

The most widely used methods of determining mercury in hair involve a digestion protocol followed by detection using either cold-vapor atomic absorption (CV-AAS), cold-vapor fluorescence spectroscopy (CV-AFS), or inductively coupled plasma mass spectrometry (ICP-MS).[2] However, a digestion step is time consuming (typically hours) and may result in sample contamination

or analyte loss. These methods also require about 5–10 mg of hair; 100 hair strands may be needed to achieve this amount.

X-ray fluorescence,[3] particle induced X-ray emission spectroscopy, [4] and laser ablation-ICP-MS[5] have been used to directly analyze human hair strands for mercury. While there is little sample preparation required, X-ray fluorescence has relatively high detection limits, particle induced X-ray spectrometry is expensive and LA-ICP-MS often has calibration problems. Recently, commercial mercury analyzers have been used for direct analysis of solid hair samples. These instruments integrate a methodology called combustion-gold amalgamation-atomic absorption spectroscopy (C-G-AAS) that uses sample combustion with a catalyst, mercury collection with gold amalgamation, then detection by CV-AAS. This technique has been successfully applied to the analysis of powdered human hair, horse fur, and single human hair strands.[6, 7] However, some sample preparation can still be required, as the addition of modifiers to the hair sample may be needed to absorb combustion by-products.

We report an alternate method using an induction heating-electrothermal vaporizer (IH-ETV) that requires only simple, direct sample vaporization followed by detection. In an IH-ETV, a graphite cup containing the sample is inductively heated at a user-set temperature. The vaporized analyte is transported to a detector (an ICP-MS in our case) by a carrier gas. An advantage of this set-up is

the reduction of the risk of contamination due to the non-contact heating environment and the ability to interchange the graphite sample cup. Furthermore, no sample preparation is required. There is also the potential for multi-elemental analysis and excellent detection limits with ICP-MS, the vaporization temperature is easily controlled, and the inexpensive graphite cups can be customized in shape and size to suit a particular sample. In previous work, the IH-ETV has been used to vaporize soil slurries and cellulose filters.[8, 9] Our objective in this project is to show that IH-ETV-ICP-MS can be used to rapidly determine mercury in a single hair strand.

EXPERIMENTAL

Instrumentation

The IH-ETV system used in this study, a modified LECO Model 521 induction furnace (LECO, St. Joseph, MI, USA), has been previously described in detail.[10-12] To eliminate the risk of arcing, the glass sample chamber was replaced with one made of quartz and the argon carrier gas was passed through a sparger containing distilled deionized water.[13] Commercially available graphite cups along with boiler caps were used (type S-16 and BC-1, Bay Carbon Inc., Bay City, MI, USA). The vaporized samples were carried in the argon stream to a Perkin-Elmer SCIEX Elan 6000 ICP-MS system (SCIEX, Concord, ON, Canada)

through PTFE tubing at a flow rate of 0.5 l min^{-1}. Typical operating values were used for the other parameters of the ICP-MS.

Samples and standards

The hair samples came from women living in the village of Brasilia Legal, Brazil. Details of this population and hair collection procedures are described elsewhere.[14] For this study, hair strands collected from four individuals were cut to a 12-cm length from the root end and weighed to the nearest 0.01 mg. As part of two other interdisciplinary projects, the mercury concentrations of 12-cm segments of these hair strands were previously determined by CV-AAS and C-GA-AAS. [7, 14]

Calibration using the external standards methodology was undertaken with Hg standard solutions and with a hair certified reference material (CRM). Mercury calibration solutions were prepared in a 1% HNO$_3$ matrix from a 1000 μg g^{-1} Hg stock solution (SCP Science, Baie D'Urfé, QC, Canada) on the same day of analysis. The CRM, BCR 397 (IRMM, Belgium), was composed of powdered human hair. The samples or standards (one coiled hair strand, 10 μl of solution, or up to 1 mg of CRM) were placed inside a graphite cup, then covered with a boiler cap and heated to approximately 800°C. A boiler cap is a graphite lid that fits over the sample cup. The cap prevents the unvaporized sample from

escaping from the cup when the carrier gas and heating is applied, while a small hole at the top of the cap allows the vaporized sample to exit.

The same graphite cup and boiler cap were used for all samples in a given day, and then changed daily. Blanks (empty graphite cup) were checked routinely. No problems with sample carryover were seen. The ^{197}Au isotope was also monitored as a background signal. Total analysis time for a sample was less than two minutes.

RESULTS AND DISCUSSION

Typical ^{202}Hg transient profiles from a hair strand, powdered hair CRM and a mercury calibration solution with approximately the same peak area are overlaid in Figure 2-1. The graphite cup was heated for 40 seconds (data acquisition started 10 s before the beginning of the heating step). The hair strand and the powdered hair CRM show similar peak shapes, though a minor distinction can be made between the steepness of the leading edges. This is probably due to different heating rates between the hair strand and the powdered hair. The entire hair strand touched the walls of the cup and was vaporized quickly, while the some of the hair rested on other hair and was momentarily insulated. The slight differences in peak heights show that height is not useful for accurate quantification. However, the peak areas are the same, indicating that

powdered hair is a suitable calibration material for hair strands if peak areas are used.
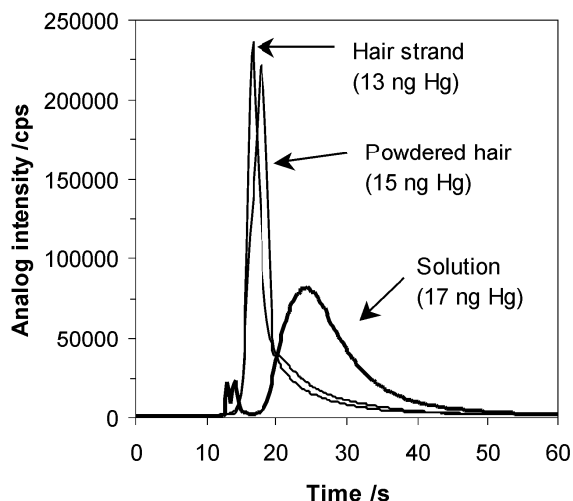
Figure 2-1. Transient profiles of ^{202}Hg for various types of samples

In contrast to the hair matrices, the transient profile of the mercury solution shows two distinct sets of peaks for ^{202}Hg. Infrared measurements have shown that it takes roughly 10 s after power has been applied to the induction coil for the cup to reach 80% of its final temperature setting. Therefore when the cup was heated, the water in the solution immediately vaporized. The water probably carried some of the mercury, resulting in the small peak at the beginning of the profile, while the rest of the mercury came off as a broad peak afterwards. There may be two possible reasons for the broad peak shape of the solution when

compared to the peaks for the hair. First, it was observed that the solution permeated into the graphite cup, and it may have taken longer for it to be released when heated. Second, it may be due to different thermal properties of the forms of mercury present in the samples (organic mercury bound to sulfur in the hair matrices versus inorganic mercury in the solution). One last observation can be made about the liquid calibration peak area - it was less than that of the hair strand and the powdered hair. The peak areas for mercury solutions were consistently low when cups containing mercury solution were not immediately analyzed. Experiments show that the loss of mercury is time-dependent and reheating of the cup at higher temperatures did not result in further mercury release. This indicates that there was some analyte loss, probably due to evaporation. Therefore mercury solutions are unsuitable for external standards calibration of hair strands.

An external standards calibration plot was constructed using the peak areas of the transient signals for the blank, and roughly 0.5 mg and 1 mg of the CRM. Using a linear least squares regression, R^2 greater than 0.999 were routinely achieved. In Table 2-1, the total mercury concentrations determined for the hair strands by external standards using the powdered CRM are compared with an estimate previously determined by CV-AAS using the protocol described by Farant *et al.* [15] When the concentrations of the four hair strand samples (11

total replicates) from IH-ETV-ICP-MS were plotted against the concentrations estimated by CV-AAS, a slope of 1.03 and R^2 of 0.95 were obtained. At less than 4% relative standard deviation (RSD), precision for hair strand analysis was comparable to that of C-G-AAS and CV-AAS methods.[6, 15] On average, the percent recovery was 110%.

Table 2-1. Determination of mercury concentrations in hair strands

Sample ID	Hg by CV-AAS ($\mu g\ g^{-1}$)	Mean Hg by IH-ETV-ICP-MS ($\mu g\ g^{-1} \pm$ SD)*	% RSD	% Recovery
BL529	3.9	3.94 ± 0.03	0.8	101
BL565	8.2	10.5 ± 0.3	2	128
BL591	13.8	13.6 ± 0.3	4	99
BL442	13.9	15.51 ± 0.08	0.5	112

*n = 3, except n = 2 for BL529

The detection limit (3σ) achieved by this method was 20 pg of Hg, or the equivalent of 30 ng g^{-1} for a 12 cm strand of hair (0.6 mg, 1 cm of hair = 0.05 mg). This detection limit also means that only 0.4 cm (corresponding to about two weeks of growth) or roughly 0.02 mg of hair is needed to detect a natural mercury level of 1 $\mu g\ g^{-1}$. As a consequence, just one hair strand is sufficient to estimate mercury levels in an individual – much less hair than the 100 strands that may be required for traditional methods with a digestion step.

We have demonstrated that IH-ETV-ICP-MS can easily determine mercury concentrations in a single hair strand, using external standards calibration with powdered hair CRMs. The results were comparable to that of CV-AAS, but were obtained more quickly and required a smaller sample size – making IH-ETV-ICP-MS a possibility for routine hair analysis for mercury. In the future, with the controllable temperature of the IH-ETV and the multi-element capability of the ICP-MS, we hope to determine other elements in human hair.

ACKNOWLEDGMENTS

REFERENCES

(1) (USNRC), U. S. N. R. C. *Toxicological Effects of Methylmercury*; National Academy Press: Washington, D.C., 2000.

(2) Gill, U. S.; Schwartz, H. M.; Bigras, L. *Archives of Environmental Contamination and Toxicology* **2002**, *43*, 466-472.

(3) Toribara, T. Y.; Jackson, D. A. *Analytical Chemistry* **1982**, *54*, 1844-1849.

(4) Valkovic, V.; Miljanic, D.; Wheeler, R. M.; Liebert, R. B.; Zabel, T.; Phillips, G. C. *Nature* **1973**, *111*, 251-252.

(5) Legrand, M.; Lam, R.; Jensen-Fontaine, M.; Salin, E. D.; Chan, H. M. *Journal of Analytical Atomic Spectrometry* **2004**, *19*, 1287-1288.

(6) Cizdziel, J. V.; Gerstenberger, S. *Talanta* **2004**, *64*, 918-921.

(7) Legrand, M.; Passos, C. J. S.; Mergler, D.; Chan, H. M. *Environmental Science and Technology* **2005**, *39*, 4594-4598.

(8) Rybak, M. E.; Salin, E. D. *Applied Spectroscopy* **2001**, *55*, 816-821.

(9) Salin, E. D.; Ren, J. M. *Journal of Analytical Atomic Spectrometry* **2003**, *18*, 953-954.

(10) Goltz, D. M.; Skinner, C. D.; Salin, E. D. *Spectrochimica Acta, Part B: Atomic Spectroscopy* **1998**, *53B*, 1139-1147.

(11) Goltz, D. M.; Salin, E. D. *Journal of Analytical Atomic Spectrometry* **1997**, *12*, 1175-1180.

(12) Rybak, M. E.; Salin, E. D. *Spectrochimica Acta, Part B: Atomic Spectroscopy* **2001**, *56B*, 289-307.

(13) Ren, J. M.; Rybak, M. E.; Salin, E. D. *Journal of Analytical Atomic Spectrometry* **2003**, *18*, 485-486.

(14) Passos, C. J.; Mergler, D.; Gaspar, E.; Morais, S.; Lucotte, M.; Larribe, F.; Davidson, R.; de Grosbois, S. *Environmental Research* **2003**, *93*, 123-130.

(15) Farant, J. P.; Brissette, D.; Moncion, L.; Bigras, L.; Chartrand, A. *Journal of Analytical Toxicology* **1981**, *5*, 47-51.

Chapter 3 - Rapid speciation of chromium by high performance thin layer chromatography with direct determination by laser ablation inductively coupled plasma mass spectrometry

In Chapter 2, total mercury in single hair strands was determined by ICP-MS. However, the ICP-MS instrument does not provide the ability to distinguish between metallic species, such as organic and inorganic mercury. This chapter, demonstrates that Thin Layer Chromatography can be directly interfaced to an ICP-MS instrument through laser ablation in order to rapidly obtain information on the chemical form of a sample. The work presented in this chapter was originally published as:

Lafleur, J. P.; Salin, E. D. *Analytical Chemistry* **2008**, *80*, 6821-6823.

The detailed procedure for the signal-to-noise ratio optimization of the laser ablation parameters for the analysis of thin layer chromatographic plates can be found in Appendix C. Analyte pre-concentration and internal standardization studies as well as calibration curves for the results presented in Chapter 3 can be found in Appendix D.

ABSTRACT

It is of considerable importance to be able to distinguish metallic species because their toxicity depends on their chemical form. Therefore the analysis of

environmental samples can be enhanced by the combination of High Performance Thin-Layer Chromatography (HPTLC) with Laser Ablation Inductively Coupled Plasma Mass Spectrometry (LA-ICP-MS). In this study, Cr^{3+} and Cr^{6+} were separated on silica gel HPTLC plates using aqueous mobile phases. Separation was achieved in seconds with retardation factors (R_f) of 0 and 1 for Cr^{3+} and Cr^{6+} respectively. LA was used to volatilize the chromium species directly from the chromatographic material prior to ICP-MS detection. A linear calibration was obtained and detection limits (3σ) of 6 ng for Cr^{6+} and 0.4 ng for Cr^{3+} were achieved with precision ranging from 3 to 40% at the 95% confidence level. The silicon present in the stationary phase was used as an internal standard. This procedure allows for a rapid separation and quantification, requires only 0.5 µL of sample and lower detection limits can be achieved through pre-concentration.

INTRODUCTION

Chromium is present naturally in the earth crust, but its use in industrial processes has caused increased contamination of soil and water. While Cr^{3+} is an essential nutrient for normal mammalian metabolism, Cr^{6+} is considered a toxic substance and the Maximum Contaminant Level (MCL) for total Cr in drinking water has been set to 100 µg L^{-1} by the USEPA. Chromium speciation studies are often complicated by the fact that the toxic Cr^{6+} reduces to the more

stable Cr^{3+} over time, making transport and storage of samples a potential source of error.

ICP-MS is widely used for the determination of trace amounts of metals, but it provides information only on the elemental composition of the sample and can therefore benefit from being coupled to chromatographic methods in speciation analyses. Speciation of Cr by the coupling of ICP-MS and chromatographic methods (primarily ion chromatography) is an active area of research.[1, 2] HPTLC is a relatively simple and inexpensive separation technique, routinely used in many laboratories to assess compound purity. Although more commonly used for the separation of organic compounds, procedures for the separation of Cr^{6+} and Cr^{3+} on silica gel plates have been developed using a mixture of methanol, dimethylamine and formic acid, but only semi-quantitative determination was achieved through spot area measurements.[3] Other heavy metal cations (Ni^{2+}-Pb^{2+}, Cd^{2+}-Cu^{2+}, Ni^{2+}-Zn^{2+}, Co^{2+}-Fe^{3+}, Ni^{2+}-Bi^{3+} and more) have also been separated on TLC plates with aqueous mobile phases containing the non-ionic surfactant Triton X-100 (Tx-100).[4]

Several groups have explored the direct coupling of TLC with MS, mainly for the analysis of organic compounds by Matrix Assisted Laser Desorption Ionization-Mass Spectrometry (MALDI-MS), but the process is complicated by the necessity of adding a matrix layer to the TLC plate.[5-7] The use of a Nd-YAG

laser was also investigated for the qualitative analysis of lubricating oil additives by Laser Microprobe Mass Spectrometry (TLC-LMMS).[8] The use of the laser to desorb and ionize organic samples has certain disadvantages as the laser power needs to be optimized for each analysis.[8] Recently direct detection of As species on cellulose TLC plates by LA-ICP-MS has been achieved,[9] but the researchers obtained poor correlation between analyte concentration and signal. The present paper demonstrates that it is indeed possible to obtain linear calibration curves and adequate detection limits with this technique by scoring separation channels in the sorbent layer and using an appropriate internal standard.

EXPERIMENTAL SECTION

Instrumentation

A Q-switched Nd:YAG laser, frequency quadrupled to 266 nm LA system (LSX-200, CETAC technologies, Omaha, NE, USA) coupled to a Perkin-Elmer Elan 6000 ICP-MS system (SCIEX, Concord, ON, Canada) was used.

Instrumental parameter optimization

The ICP-MS operating parameters were optimized using the standard procedure for solution nebulization. It has been demonstrated that extensive optimization of the ICP-MS operational parameters is unnecessary when an internal standard is used in LA.[10] The LA system was operated in the single line scan mode, in which the sample cell moved horizontally at a constant speed

while the laser was firing repetitively. The laser defocus (50 μm), energy level (10 on a scale of 1-20), pulse repetition rate (10 Hz) and scanning speed (100 μm s^{-1}) were all optimized for the ablation of silica gel HPTLC plates. The largest spot size available (300 μm) was used in order to maximize the amount of material ablated.

Standards and reagents

Triton X-100 (AccuSpec), Cr^{3+} and Cr^{6+} (custom standards, 1000 μg/ml in 4% HNO$_3$ and distilled deionized water respectively) were obtained from SCP Science (Baie d'Urfé, QC, Canada). Separations were performed on 150 μm thick HPTLC plates (Hard Layer Silica Gel GHL Uniplates, Analtech, Newark, DE, USA). Conventional TLC plates with gypsum binder (Silica gel 60F, 250 μm, Silicycle, Quebec City, QC, Canada) were used for comparative purposes.

Analytical Procedure

The HPTLC plates (2.5 cm x 4 cm) were prepared by scoring five 3 mm wide chromatographic channels in the sorbent using a 2 mm wide HPTLC scraper. Disposable 0.5 μL pipettes (Drummond microcaps, Drummond Scientific Company, Broomal, PA) were used to spot the aqueous standards on the sorbent stationary phase. The scored plates could contain 5 replicates of a sample without risk of cross-contamination. Four different concentrations of standards were prepared, each spotted on 3-15 different chromatographic

channels to obtain replicates, resulting in applied samples of 6 ng-20 ng Cr^{3+} and 50-100 ng Cr^{6+}. For the mobile phase optimization conditions, single analyte solutions were used to determine retardation factors (R_f). For final speciation experiments, mixtures of different concentrations of both analytes were used. Blanks (7 replicates) were spotted with 0.5 µl distilled deionised water (DDW) and treated like the standards. Spotted plates were allowed to dry prior to development in a saturated chamber with DDW, 0.001%, 0.005%, 0.01%, 0.05% and 0.1% w/v Tx-100 in DDW. The mobile phase was allowed to migrate roughly 1 cm above the application point and plates were dried thoroughly prior to LA.

RESULTS AND DISCUSSION

Chromatographic separation

The mobility of the chromium species was investigated with DDW as a mobile phase and five surfactant concentrations ranging from 0.001% w/v to 0.1% w/v Tx-100. The range of concentrations studied was below, and above the critical micelle concentration (CMC) for Tx-100, which is 0.0155% w/v. It was found that the chromic ion ($Cr(H_2O)_6^{3+}$), which is hydrated in aqueous solutions, was irreversibly adsorbed on the silanols from the silica gel and remained at the point of application (Rf = 0) in all the mobile phases studied. The dichromate anion ($Cr_2O_7^{2-}$) was completely unretained and migrated with the aqueous mobile

phase (R_f = 1) in all cases. Although it is normally desired to have $0 < R_f < 1$ to minimize interferences, in this case any co-migrating cation can be resolved by mass spectrometry. The extreme R_f values also provide a very sharp and quick separation of the chromium species that cannot be resolved by mass spectrometry. Separation of the chromium species can therefore be achieved with just water as a mobile phase. However, since the presence of Tx-100 did not affect their sharp separation, it could be added to the sample to separate additional cations[4] without risk of interfering with the speciation of the chromium species. A typical spectrum is shown in Figure 3-1, where the Cr^{3+} peak is located at the point of application on the plate and the Cr^{6+} peak is located at the solvent front, roughly 12 mm above the point of application.

The characteristic signal profile observed for Cr^{3+} in Figure 3-1(A) is due to the fact that during spot application the analyte is pushed away from the center of the spot, resulting in a higher analyte concentration along the edges of the spot. As the laser scans a 300-µm wide trench across the retained circular analyte spot, the lower edge creates a sharp peak but as the laser moves further, the intensity of the signal diminishes due to the lower analyte concentration at the center of the spot and then rises again when the laser reaches the top edge of the spot. The unretained Cr^{6+} peaks exhibits a more Gaussian distribution, because during the initial stage of development, the mobile phase drags the

bottom edge of the analyte spot and merges it with its top edge, resulting in a single peak as illustrated in Figure 3-1(B).
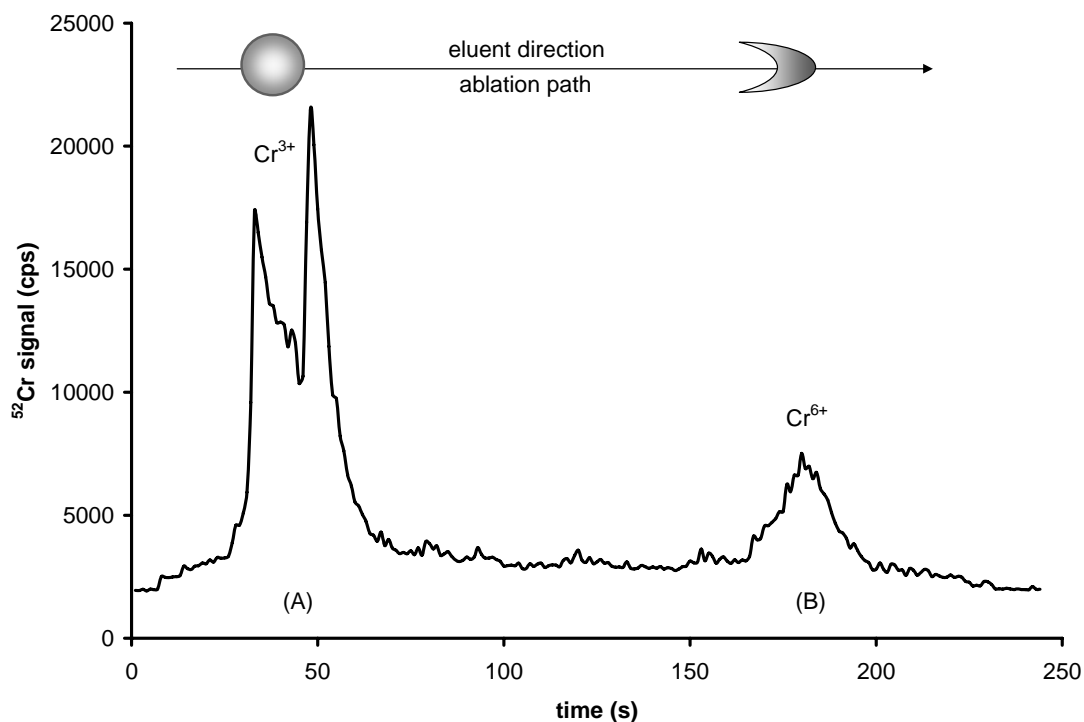
Figure 3-1. LA spectrum showing the typical signal profiles observed for (A) immobile Cr^{3+} and (B) mobile Cr^{6+}. This separation was obtained after development of the HPTLC plate with 0.1% w/v Tx-100 in DDW.

Pre-concentration capabilities

A commonly used method to improve detection limits in TLC involves reapplying the sample on the sorbent several times, in order to pre-concentrate the analyte. As illustrated in Figure 3-2, six repeated applications of a rhodium standard result in a 4.3 increase in analyte signal area. The increase is slightly

lower than expected due to some analyte spreading. Linear calibration ($R^2 >$ 0.99) has been obtained for Rh and Pb using this technique. Provided the plate is thoroughly dried between each application to avoid analyte spreading; this technique can be used to improve the detection limits achievable.
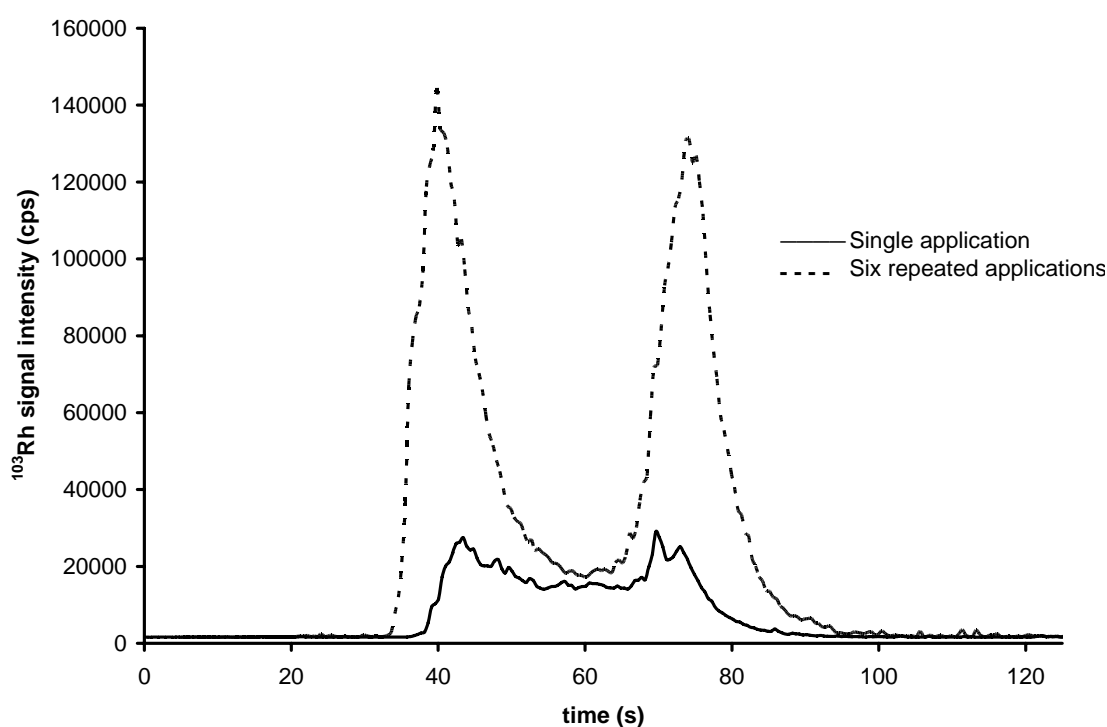
Figure 3-2. Analyte pre-concentration in thin layer chromatography

Silicon as an internal standard

It is often helpful to use internal standards (IS) in LA-ICP-MS to account for instrumental drift and variations in laser energy. However, the choice of an appropriate IS is complicated by the migration of the analytes in HPTLC.

Therefore, the IS should be contained within, or bound, to the adsorbent layer, making the ^{30}Si present in the silica gel stationary phase an ideal candidate. In commercially coated silica gel plates, it can be assumed that the sorbent layer is generally uniform in thickness and homogeneous so that the silicon signal is expected to be roughly constant throughout the plate. Most TLC plates contain a gypsum binder to increase the adhesion of the sorbent to the glass plate. However, gypsum is dissolved by water-based eluents making the Si signal uneven. The phenomenon is illustrated in Figure 3-3 where the Si signal is visibly lower at the bottom of the plate (left) and increases gradually towards the top of the plate (right) where the solvent front ends. Care should therefore be taken to choose plates containing a water resistant binder if Si is to be used as an internal standard.
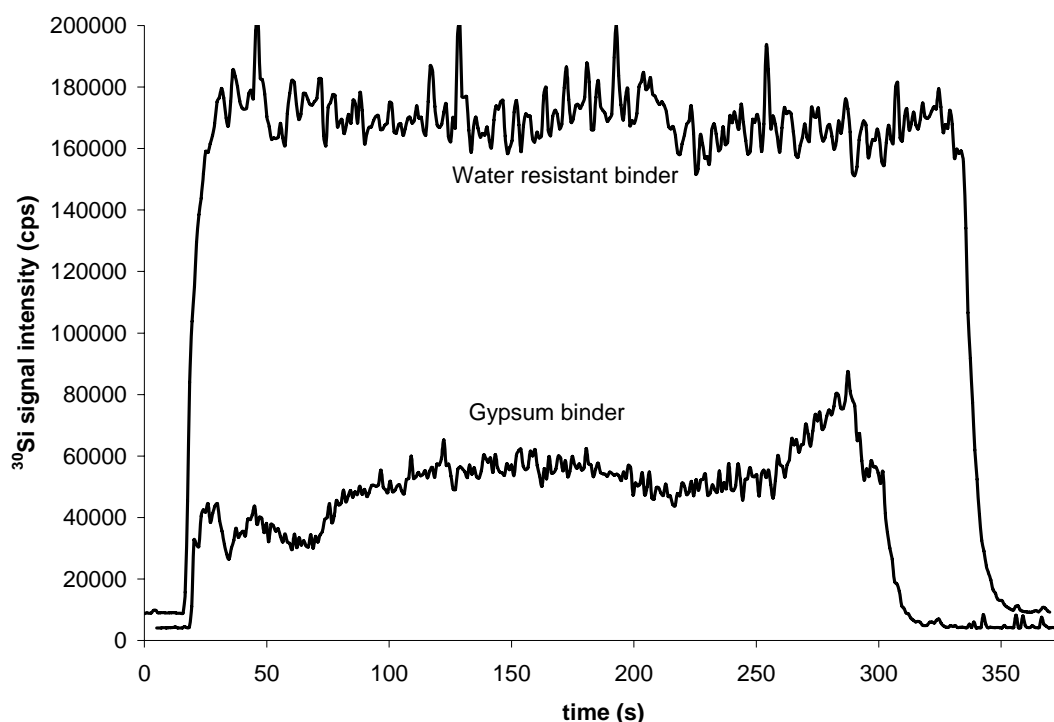
Figure 3-3. Dissolution of the silica gel on TLC plates with Gypsum binder compared to HPTLC plates with water resistant binder after development with an aqueous eluent (0.1% w/v Tx-100 in DDW).

As shown in Table 3-1, precision was improved by the use of silicon as an internal standard. However, the internal standardization procedure was most efficient in the case of the Cr^{3+} species due to its immobility on the sorbent stationary phase. The silicon signal from the stationary phase can be used to account for variations in laser energy, amount of material ablated from sample to sample and instrumental drift. However, the IS cannot compensate for

misalignment of the laser ablation path relative to the separation path through the TLC plate and subsequent analyte spot location. In the case of the immobile Cr^{3+}, the center of the spot was easier to locate and ablation was more consistent from replicate to replicate. For the mobile Cr^{6+} ion however, the longer migration distance increases the likelihood that the chromatographic path will have deviated from the expected vertical trajectory resulting in less analyte along the ablation path. This will result in a decrease in analyte signal while the amount of silicon vaporized will remain unaffected. Additional precision is lost because of the errors associated with manual positioning and application of samples on the sorbent layer which can lead to spot deformations. For both problems, applying the samples as horizontal bands using automated equipment would improve the precision achievable.

Table 3-1. Determination of chromium by LA-ICP-MS on HPTLC plates developed with 0.1% w/v Tx-100 in water.

	Slope (counts/µg)	R^2	Error bars[†]	Detection limit[‡]
Cr^{3+}	$2*10^7$	0.99	25-34%	0.4 ng or 0.9 µg/ml[*]
Cr^{3+}/Si		0.99	3-22%	
Cr^{6+}	$1*10^6$	0.90	17-41 %	6 ng or 11 µg/ml[*]
Cr^{6+}/Si		0.98	12-40%	

[†]Errors are reported at the 95% confidence level for 3-15 replicates at each of four concentrations used to construct the calibration curve.

[‡]The detection limit is calculated as $3\sigma_{blank}$.

[*]Based on a 0.5 µL sample.

Quantification by LA-ICP-MS

Good correlation between analyte signal intensity and concentration was obtained for both chromium species studied and calibration results are listed in Table 3-1. The detection limits listed in Table 3-1 indicate that only 4 µl of sample would be required to detect Cr^{3+} at natural levels while 60 µl would be needed for Cr^{6+}. However the method is sensitive enough to be used without pre-concentration to detect chromium in contaminated wastewaters. It can also be expected that a larger laser beam size/ spot area ratio could be useful in improving the detection limits.

CONCLUSIONS

This new separation and analysis technique has the potential for rapid on-site sampling of contaminated waters for chromium analysis. The rapidity of the procedure due to the radical differences in mobility of Cr^{3+} and Cr^{6+} combined with the ability of the ICP-MS to resolve any interferences caused by co-migrating species make it an easy operation to perform directly on site. The separated analytes can then be stored easily on the chromatographic plates before transport to the laboratory for further analysis by LA-ICP-MS, reducing potential errors associated with the reductions of Cr^{6+} to Cr^{3+}.

ACKNOWLEDGMENTS

REFERENCES

(1)   Hagendorfer, H.; Goessler, W. *Talanta* **2008**, *76*, 656-661.

(2)   Wolf, R. E.; Morrison, J. M.; Goldhaber, M. B. *Journal of Analytical Atomic Spectrometry* **2007**, *22*, 1051-1060.

(3)   Mohammad, A.; Sirwal, Y. H. *Acta Chromatographica* **2003**, *13*, 117-134.

(4)   Mohammad, A.; Iraqi, E.; Khan, I. A. *Journal of Chromatographic Science* **2002**, *40*, 162-169.

(5)   Gusev, A. I. *Fresenius' Journal of Analytical Chemistry* **2000**, *366*, 691-700.

(6)   Mowthorpe, S.; Clench, M. R.; Cricelius, A.; Richards, D. S.; Parr, V.; Tetler, L. W. *Rapid Communications in Mass Spectrometry* **1999**, *13*, 264-270.

(7)   Mehl, J. T.; Hercules, D. M. *Analytical Chemistry* **2000**, *72*, 68-73.

(8)   Dewey, C. R.; Finney, R. W. *Analytical Proceedings* **1990**, *27*, 125-127.

(9)   Resano, M.; Garcia Ruiz, E.; Mihucz, V. G.; Moricz, A. M.; Zaray, G.; Vanhaecke, F. *Journal of Analytical Atomic Spectrometry* **2007**, *22*, 1158-1162.

(10)   Bemben, K. J. Thesis (M.Sc.), McGill University, Montreal, **2006**.

Chapter 4 - Design and fabrication of centrifugal microfluidic solid phase extraction devices

ABSTRACT

In the previous chapter, Thin Layer Chromatography (TLC) is used to separate metal ions prior to direct laser sampling. However, TLC is a relatively slow technique as it relies only on capillary forces to drive the fluid flow. Faster separations can be achieved by forcing the mobile phase flow by centrifugal force. Chapters 5, 6 and 7 describe experiments done on centrifugal chromatographic devices. This chapter describes how a combination of small machined parts and adhesive layers can be used to manufacture these miniature centrifugal chromatographs. The evolution of the various designs tested is presented. Emphasis is put on packing the miniature chromatographic systems. Optimization of the Laser Ablation (LA) instrumental parameters for use in conjunction with these devices is presented in Appendix C and the set up and calibration of the motor used to spin the devices is described in Appendix E. Finally, the volumetric flow rate and the column efficiency of the miniature centrifugal chromatographic devices are modeled in Appendix F.

INTRODUCTION

Several microfabrication methods are commonly used for the manufacture of microfluidic systems, most of them based on photolithography, which was

originally developed for the microelectronic industry. The disadvantage of this method is that glass and silicon are more expensive than polymers, etching of silicon is time consuming and expensive, as the technique requires clean room facilities, and silicon wafers are fragile. Furthermore, silicon is optically opaque, making it an unattractive choice for on-device optical detection. Some of these disadvantages can be overcome by using silicon photolithography for the creation of molds for the casting of polymeric replicas instead. Poly(dimethylsiloxane) (PDMS) has the advantage as a material for device fabrication in that it is transparent down to 280 nm, an attractive feature for absorbance and fluorescence detection schemes. Duffy *et al.* developed a rapid prototyping method for the fabrication of microfluidic systems in PDMS using a combination of high-resolution printing and contact photolithography[1-3] as well as one based on conventional machining of poly(methylmethacrylate) (PMMA)[2], the combination of PMMA machined parts and PDMS molded replicas are used to create centrifugal microfluidic devices. However, a disadvantage of using PMMA as a substrate is that it is incompatible with many organic solvents and offers a poor resistance to weak acids, limiting the possible applications. Soft-lithographic techniques for the fabrication of microfluidic systems in PDMS have been described in a review by McDonald *et al.*[4] Polymer microfabrication technologies, such as hot embossing, injection molding, microthermoforming, casting,

lithography and laser ablation, are reviewed by Becker and Gärtner.[5] Lee *et al.*[6] also presented a series of fabrication techniques capable of prototyping or mass producing polymer-based microfluidic devices such as centrifugal microfluidic platforms. Laser Ablation (LA) micromachining can also be used to construct microfluidic devices in polymers[7] and has the advantage of being able to produce smaller feature sizes than conventional Computer Numerically Controlled (CNC) milling, with feature sizes down to the micrometer or tens of micrometer scale with ultra short laser pulses.[8] Micronics, Inc. developed a prototyping process based on laser cutting and lamination of thin layers of plastic.[9] In this technique, alternating regular cut-out laminate layers and layers with additional adhesive on both sides forms the microfluidic circuit. Bartholomeusz *et al.*[10] also used a thin-film based lamination technique, called xurography, that necessitates only the use of a cutting plotter traditionally used in the sign industry for cutting graphics in adhesive films. Using this technique, they successfully built a 3-D microfluidic structure consisting of seven layers of adhesive in less than 30 minutes. This technique is suitable for low aspect ratio flow features, such as channels, columns and vent lines, but it does not allow for deep reservoirs or reaction chambers. More versatile devices can be fabricated using a rapid prototyping technique based on a combination of thin film lamination[9] and xurography[10] developed by Kido *et al.*[11] Xurography is used to create patterns in thin adhesive

layers with conventional CNC milling of thicker polycarbonate layers to create deep reservoirs. This synergistic combination offers a maximum of flexibility in design and applications and is the method used here to fabricate centrifugal Solid Phase Extraction (SPE) microfluidic devices.

EXPERIMENTAL SECTION

Design and Conception

Several programs, listed in Table 4-1 allow multi-layered illustrations and facilitate the design of laminated devices. Structures are drawn as layers, inspected visually, and then the drawings are used to generate an intermediate machine-readable file such as Data eXchange Files (DXF).

Table 4-1. Instruments and design software

MANUFACTURER	MODEL, DESCRIPTION
Hardware	
T-Tech, Inc. (Norcross, GA)	*QuickCircuit 5000*
	XY milling table with a high speed spindle
Graphtec America, Inc., (Santa Ana, CA)	CE2000-60 and CE3000MK2-60
	24" wide cutter
	Programmable resolution: 10 µm, 25 µm
	Mechanical resolution: 5 µm
Desert Laminator, Inc. (Palm Springs, CA)	Sidewinder
	24" Hand cranked cold laminator
Drytac (Concord, ON)	Jet Mounter ML25
	25" hand crank cold laminator
Software	
SolidWorks Corp. (Concord, MA)	SolidWorks 2005
	3D Computer-Aided Design (CAD) software
Adobe Systems Inc. (San Jose, CA)	Adobe Illustrator 10
	Vector based computer drawing tool

Table 4-2. Supports, films and adhesives

MANUFACTURER	MODEL, DESCRIPTION
U-Tech Media Corp. (Taiwan, R.O.C)	CDs and DVDs Blank, Uncoated
CYRO Industries (Rockaway, NJ)	**Acrylite OP-1** 3.178 mm (1/8") thick PMMA sheets
MSC Industrial Supply Co. (Melville, NY)	**Extruded Clear Acrylic** 1.588 mm (1/16") thick PMMA Sheets
Prism Research Glass, Inc (Research Triangle Park, NC)	**Quartz discs** Custom cut, 120 mm O.D. x 15.1 mm I.D. x 1.588 mm (1/16") thick
FLEXcon (Spencer, MA)	**FLEXmount** DFM-050-Clear V-95 150 poly V-95 400 poly (double sided adhesive) **FLEXmount** DFM-200-Clear V-95 150 poly V-95 400 poly (double sided adhesive) **FLEXmark** PM 200 Clear, V-302ULP 90 PFW (Clear transfer tape)
R-Tape Corp. (South Plainfield, NJ)	Conform series 4076-RLA Transfer tape
Lofo High tech films GmbH (Weil am Rhein, Germany)	Pokalon OG 461GL Polycarbonate film (3 mil, 76.2 µm)
Coburn Graphics Inc. (Lakewood, NJ)	Claritex Polycarbonate film (3 mil, 76.2 µm)
Sigma-Aldrich Corp. (St. Louis, MO)	Nunc sealing tape T9571 Polyolefin material with pressure sensitive acrylate adhesive

To create a single thin channel using this lamination technique, a minimum of three layers are required. The first layer being the base, a second layer consisting of the cut-out features desired and a third layer to seal the device. Layers can be added as needed to create deeper structures and more complex designs. Smaller aspect ratio features are cut in a 50 or 100 μm thick adhesive film using a cutting plotter and higher aspect ratio features are milled into blank, uncoated, Compact Disks (CDs) and Digital Versatile Discs (DVDs) (Table 4-2), making sure to alternate polycarbonate disc layers with adhesive layers for bonding. The choice of using a CD or a DVD depends on the application, both supports (discs) are made of the same poly(carbonate) material, but CDs are twice the thickness (1.2 mm) of DVDs (0.6 mm), allowing the creation of deeper structures. Alternately, PMMA sheets (Table 4-2) machined in house to the dimensions of a CD/DVD and custom cut Quartz discs (Table 4-2) were used in applications that required optical transparency at lower wavelengths. A 7-layer microfluidic platform is illustrated in Figure 4-2 (individual layers) and Figure 4-2 (exploded view). All layers have an alignment hole. The base DVD in which an alignment hole has been milled towards the edge of the disc is shown in Figure 4-2(A). In Figure 4-2(B) the first adhesive layer containing cut-out reservoirs and a matching alignment hole is illustrated. Figure 4-2(C) shows a CD layer used to create deep reservoirs. A vent line coming up from the left side of the bottom

83

(waste) reservoir is milled on the CD but does not go completely through the material. The same is true for the circular pattern milled at the center of the CD to remove the protruding stacking ring. The two sample reservoirs are completely cut out of the disc so that their thickness will add to the adhesive thickness from the previous layer. In Figure 4-2(D), the 100 µm-thick adhesive layer containing the channel that will hold the 1 mm-wide chromatographic column, linking both reservoirs as illustrated. A 75 µm-thick polycarbonate film (Figure 4-2 (E)) seals all the channels and reservoirs, leaving only small access holes for filling and venting. An adhesive layer, with matching filling/vent holes as well as a viewing window over the location of the chromatographic column is added Figure 4-2(F)) to bond the device to the top cover. A DVD, Figure 4-2(G)) in which windows have been milled to allow access to the polycarbonate film covering the chromatographic column completes the assembly. The windows are necessary for experiments requiring future analysis by Laser Ablation.
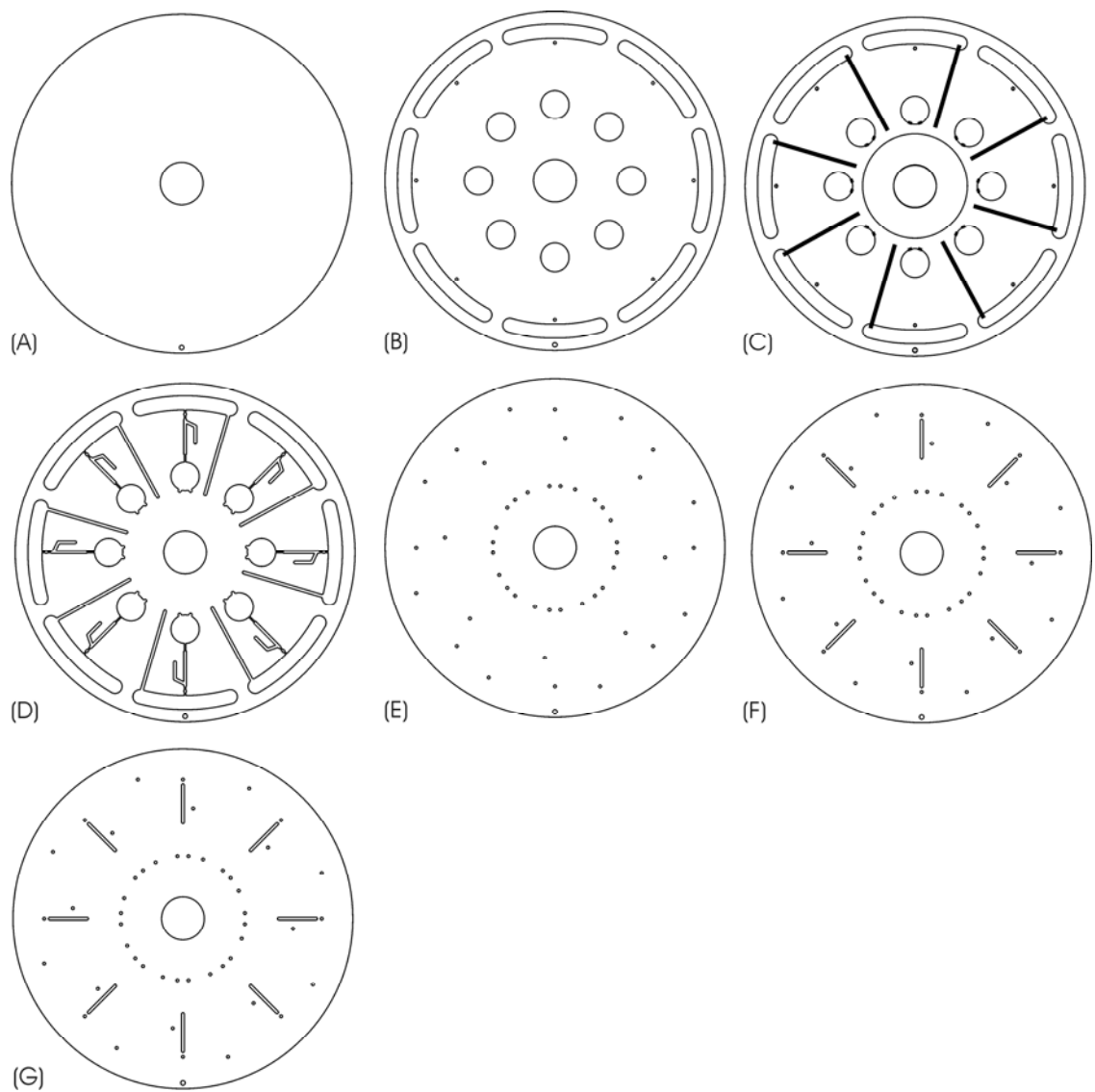
Figure 4-1. Model Minimax XII decomposed into layers. (A) DVD base layer. (B) Adhesive layer. (C) CD. (D) Adhesive layer. (E) Polycarbonate film. (F) Adhesive layer. (G) DVD top layer.
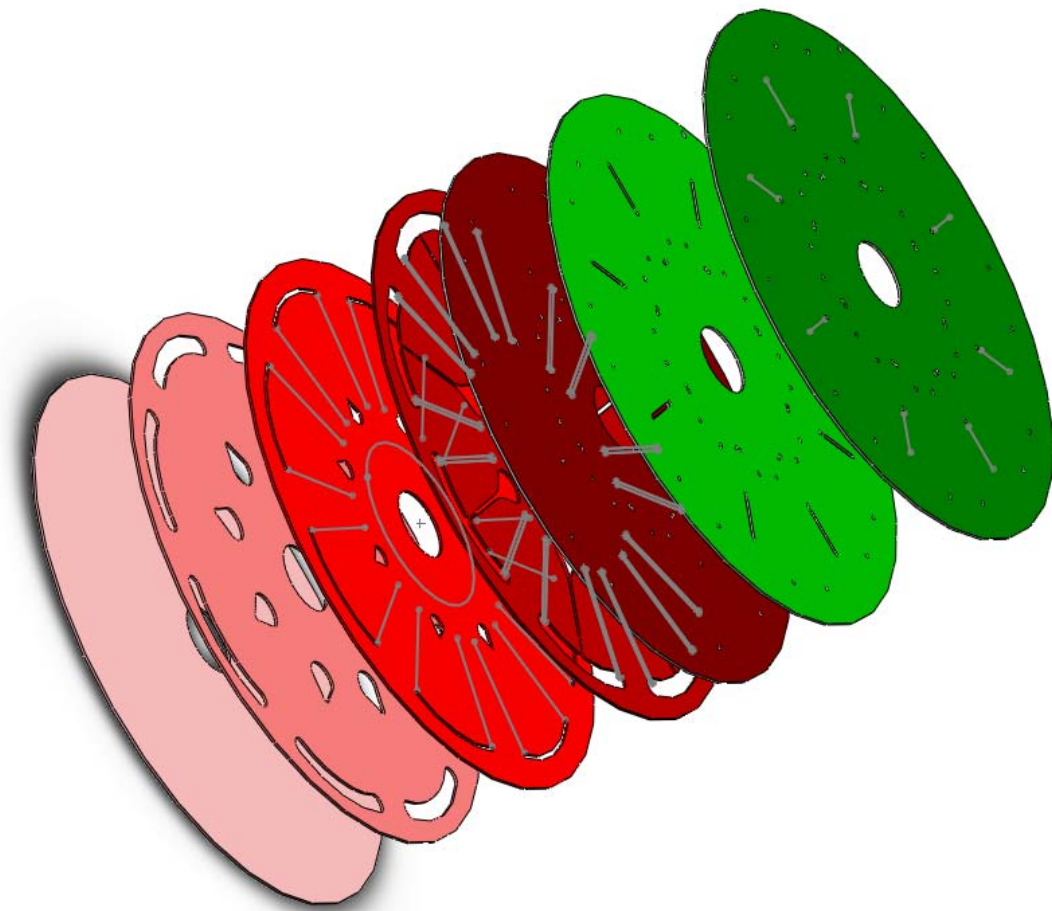
Figure 4-2. Exploded view of Model MINIMAX VI. (A) DVD base layer. (B) Adhesive layer. (C) CD. (D) Adhesive layer. (E) Polycarbonate film. (F) Adhesive layer. (G) DVD top layer.

Device Assembly

Each new layer can be aligned to the previous layers by using two alignment features on the discs. For a centrifugal device, the central hole of the disc can also be used as an alignment fixture. For unambiguous precise

alignment, a second alignment hole is required to ensure a good alignment of the layers. The alignment stage, illustrated in Figure 4-3(A), possesses the central alignment spindle as well as an alignment pin located towards the edge of the disc. Each layer of the drawing, as illustrated in Figure 4-2, and consequently each disk or adhesive layer created must also have an alignment hole.

A typical alignment procedure is illustrated in Figure 4-3. The first layer is the base of the device. Usually this is a DVD. These are convenient because they have no stacking ring, a feature that protrudes above the surface on the thicker CDs. The first layer disk, illustrated in Figure 4-3(B), is placed and properly aligned on the two alignment fixtures of the assembly stage. The second layer, Figure 4-3(C), is an adhesive layer. This layer serves two purposes. First, it provides the adhesive that will hold the first layer disk and the third layer disk together. The second function is that of forming channels, reservoirs, and other low aspect ratio structures. The adhesive layer illustrated in Figure 4-3(C) shows a 1 mm wide channel formed in an adhesive layer connecting two reservoirs.
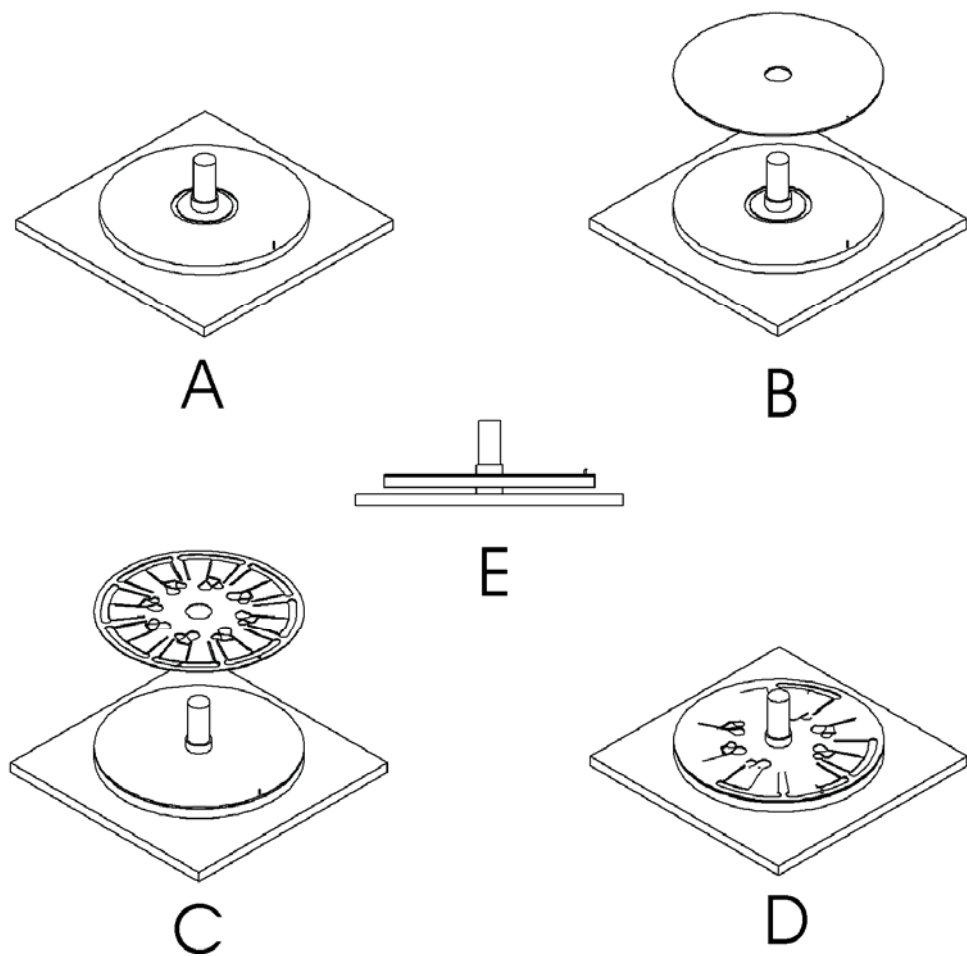
Figure 4-3. Device assembly. (A) Alignment stage. (B) Insertion and alignment of the base disc. (C) Insertion and alignment of a layer of adhesive. (D) Disc layer and first adhesive layer are assembled and aligned together, ready for a third adhesive or disc layer to be added. (E) Side view of the stage and assembly.

The adhesive (Table 4-2) is available as a 15 cm wide roll of double sided tape sandwiched between two release liners. Specifically, it consists of a clear polyester film (2 mil or 50.8 μm) coated on both sides with a clear permanent

high performance pressure sensitive acrylic adhesive (1 mil (25.4 μm) on each side) for pharmaceutical applications. The adhesive is backed on both sides with a smooth, clear silicone coated polyester liner referred to as the Top Release Liner (TRL) and the Bottom Release Liner (BRL). The TRL is thinner (1.5 mil (38.1 μm)) to allow the cutter blade to incise through the material easily. The BRL is thicker (4 mil (101.6 μm)) to provide adequate support and ease of manipulation. The adhesive, protected by the release liners, is friction fed into the cutting plotter. The cutting plotter (Table 4-2) uses a fine blade to cut a pattern that matches the structures cut with the CNC milling machine using the generated DXF files. The tension on the blade is adjusted so that the TRL and double-sided adhesive are cut completely while the BRL is, at most, lightly scored. The conventional techniques used in the sign industry are used to transfer the cut adhesive layer to the base CD, very much like a sign maker would transfer vinyl lettering onto the body of a promotional vehicle. The cut patterns, such as the center hole, alignment hole, any channels and reservoirs, are first weeded out. A large piece of transfer tape (Table 4-2) in which two holes have been cut out to avoid blocking the alignment holes is used to remove the adhesive from the BRL and transferring it to the base disc on the alignment stage (Figure 4-3(C)). A small hard rubber brayer is used to ensure a tight seal and remove any bubbles that might have been trapped between the base disc and

the adhesive layer. The ensemble is then pressed firmly using a larger hand crank laminator (Table 4-2) on which the pressure knobs are adjusted manually to provide adequate pressure. The transfer tape can then be peeled, removing the TRL as well and exposing the adhesive, which is solidly bonded to the base disc. The assembly can be transferred back to the alignment stage, Figure 4-3(D), where another adhesive layer or DVD/CD layer can be added.

Column Packing

The stationary phase material was introduced in the columns as methanol (ACS grade, EMD Chemicals, Gibbstown, NJ, USA) slurries using a micropipette. All slurries were carefully homogenized using a vortex mixer (Maxi-Mix, Barnstead International, Dubuque, IA, USA). The devices were tested by applying centrifugal force using either a bench top microcentrifuge modified to accept the centrifugal devices (model MiniMax, Thermo IEC, Waltham, MA, USA) or a device built in house and consisting of a permanent magnet type 90 V DC motor (Baldor Motor and Drives, Fort Smith, AZ, USA) driven manually with a motor drive (Penta KB Power, KBPC-240D, TechnoMotion, Montréal, QC, Canada) or digitally using a signal isolator (Penta KB Power, KBSI-240D, TechnoMotion, Montréal, QC, Canada). Two C_{18}-bonded silica gel brands were used as packing in the columns: Chromabond (60 Δ pore size, 45 μm mean

particle size, Macherey-Nagel, Düren, Germany) and Nucleosil (100 Δ pore size, 5 and 10 µm mean particle size, Macherey-Nagel, Düren, Germany).

RESULTS AND DISCUSSION

Column Restriction and Packing

Ideally, for long term storage and transport to the field for sampling, the columns should be pre-packed and ready to use. Conventional slurry-packing techniques for solid phase extraction columns require that a freshly packed column be kept in a container of mobile phase to avoid drying; otherwise the column must be re-poured. There are certain disadvantages in leaving the reservoirs and columns on the disc filled with methanol during transport to the field for sampling. There is a risk of damaging the adhesive holding the disc as no studies have been performed on its adhesion properties after weeks or even months of exposure to the solvent. Also, during transport, especially to a remote location, there is a high probability that the columns will be disturbed. If the discs are held in a vertical position, the columns which are inverted will have a tendency to flow back into the top reservoir, clogging the main channel and rendering the column unusable. For practical purposes, it is therefore preferable to dry the columns for storage and transport to the field. This should not affect the solid phase extraction procedure as it has been demonstrated that the incorporation of a drying step in the packing of columns by centrifugal force

allows the silica-based reverse phase packing material to be better accommodated inside the capillary column.[12] Prior to use, the column packing can be conditioned with a few bed volumes of solvent. During the solvation of the sorbent, the packing material "swells", resulting in a greater packing density.

One of the weaknesses of our rapid prototyping technique is the inability to cut small structures reproducibly with the cutting plotter or the CNC milling machine. Since the size of particles used for packing columns normally varies from 3 μm to 45 μm, this shortcoming became one of the greatest challenges in this project. The vinyl cutter was inadequate for cutting channels smaller than the size of the packing materials employed, like the weir illustrated in Figure 4-4(A), so other strategies had to be explored. To keep design simple and building time to a minimum, the accumulation of material in columns using a keystone effect, illustrated in Figure 4-4(B), as described by Penrose *et al.*[13] was investigated in the first generations of microfluidic devices built. The keystone effect occurs when a channel's size narrows significantly in order to force the accumulation of material even though the end of the channel is not physically blocked. Unlike a weir (Figure 4-4 (A)) where the opening is smaller than the particle size, this works even though the restriction width is larger than the diameter of the particles, because the entry to the restriction becomes blocked as all the particles try to rush through the restriction channel at the same time.
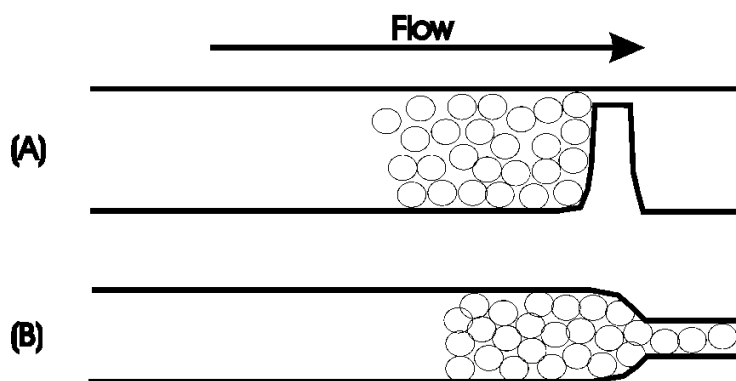
Figure 4-4. Column restrictions. (A) A weir smaller than the diameter of the particles supports the chromatographic bed. (B) The channel is tapered in order to create a keystone effect.

With our prototyping technique, there are three ways of significantly narrowing the channel size so that a restriction or a keystone effect will be created and successful packing will occur. The simplest method is to build the column in a single layer of adhesive and to cut a single line in the adhesive connecting the column to the waste reservoir as illustrated in Figure 4-5(A). In this configuration, the width of the restriction is equivalent to the thickness of the blade used and should restrict the flow of particles effectively. The second way is to use a juxtaposition of adhesive layers to create the restriction. As illustrated in Figure 4-5(B), a shorter channel cut into a 100 µm thick adhesive layer is superimposed to a longer channel cut into a 50 µm thick in order to create a 150 µm thick column and a 50 µm thick restriction. The third way is to gradually

decrease the width of the column as shown in Figure 4-5(C), where the width of the column decreases rapidly from 1000 μm to 250 μm.
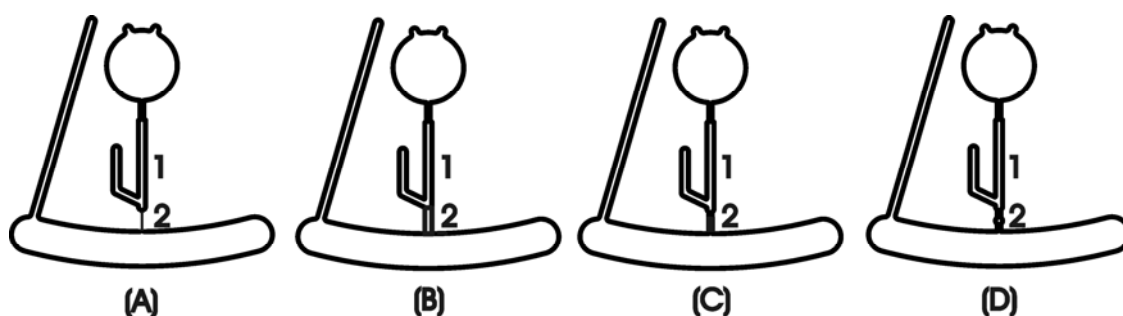
Figure 4-5. Column packing strategies. In all figures, 1 indicates the column, 2 indicates the restriction. (A) A single or multiple lines are cut to link the column to the waste reservoir. (B) Layers of adhesive are superimposed in order to create a change in the height of the channel, which goes from 150 μm deep at the column to 50 μm deep at the restriction. (C) The width of the channel is gradually reduced from 1000 μm to 250 μm. (D) A quartz wool plug is inserted at the bottom of the column to restrict the flow of particles.

The first method illustrated in Figure 4-5(A) was unsuccessful because the cutter blade did not manage to cut a clear path through the adhesive, resulting in blockages that prevented fluid flow. In the second method illustrated in Figure 4-5(B), a keystone effect was generated when 45 μm particles were used as packing material, but difficulties in aligning two adhesive layers on top of each

other resulted in irreproducible results as well as blockages and column bleeding. Problems arose also as the large 45 µm particles would stay stuck in the top reservoir as the diminution of the width of the reservoir combined with the decrease in height to form the column channel also acted as a restriction as pictured in Figure 4-6(A). With a lot of patience however, it was possible to pack columns with the 45 µm packing material as pictured in Figure 4-6(B).
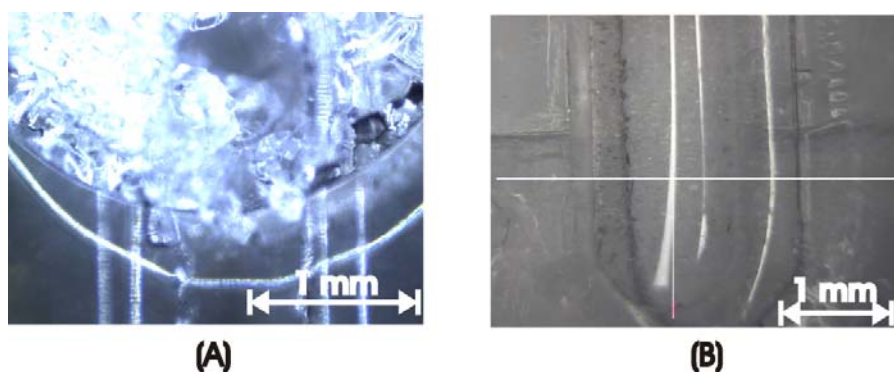
Figure 4-6. 45 µm packing. (A) A restriction is created at the junction between the sample reservoir and the column channel, hindering the packing of the column. (B) Successfully packed column.

The following attempts were performed with smaller, more uniform 5 µm packing material and using the third restriction method, illustrated Figure 4-5(C). In initial attempts, the columns were filled with slurry, sealed and left standing overnight to allow gravity packing and avoid bleeding (Figure 4-7). The absence of a physical barrier often resulted in column bleeding and even complete loss of

column as soon as column consolidation under centrifugal pressure was performed.
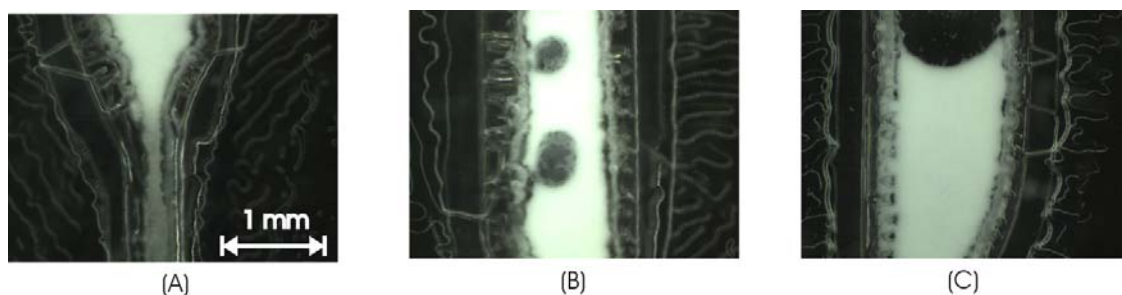
Figure 4-7. Gravity packing. (A) Keystone effect in the column restriction filled with 5 μm particles. (B) Holes in the packing before consolidation with mobile phase under centrifugal force. (C) Top of the column.

The third method was the most successful at creating a keystone effect and was used for several models (Figure 4-8- Minimax I through X). However, with the keystone effect, column packing remained difficult and rotational rates had to be kept low (1000-1200 RPM) to avoid column bleeding. Using this design, it often took several hours to perform all the steps of a solid phase extraction procedure on the centrifugal microfluidic devices. The problem was solved by forming a small quartz wool frit at the bottom of the column, in the restriction, as illustrated in Figure 4-5(D). This addition completely eliminated column bleeding problems and allowed spinning at higher rotational rates (up to 3000 RPM) which reduced the amount of time required for a complete solid

phase extraction procedure on the disc from several hours down to roughly 20 minutes.

Fluidic Network

Several configurations illustrated in Figure 4-8 were explored in order to obtain a successful device for analytical work.
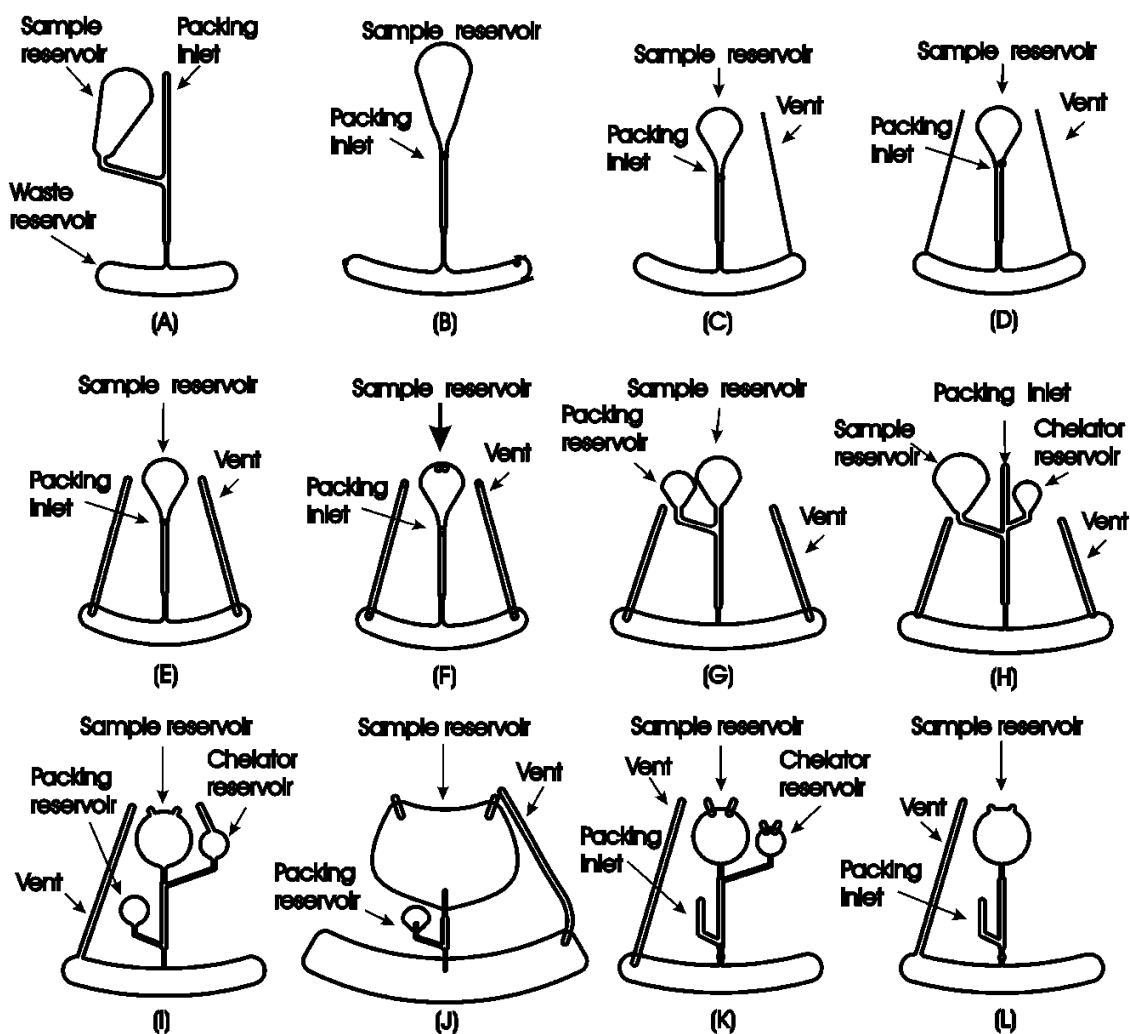
Figure 4-8. Minimax model evolution (A) Minimax I (B) Minimax II (C) Minimax III (D) Minimax IV (E) Minimax V (F) Minimax VI (G) Minimax VII (H) Minimax VIII (I) Minimax IX (J) Minimax X (K) Minimax XI (L) Minimax XII.

Minimax I

The first model built, Figure 4-8(A), was based loosely on the miniature centrifugal chromatograph developed by Penrose *et al.*[13] It was designed like an upward oriented fork, where the packing slurry, sample and mobile phase reservoirs are all located close to the center of the device and merged into a single column forming channel. The packing was introduced at the top of the long central channel in order to pack material in the first third of the channel, thereby forming the column. Attempts at packing columns this way were mildly successful as the channel was easily overfilled, resulting in blockage of the sample reservoir channel.

Minimax II - VI

To avoid overfilling the column, the following models, Figure 4-8(B)-(F) had a filling hole located at the top of the column channel, just below the sample reservoir. In this model, the top reservoir was located very close to the center of the disc, slightly overlapping with the stacking rings found on commercial DVDs. Unfortunately, this overlap created leakage. This could be used advantageously in other experiments where a distribution channel is required to fill all the top reservoirs of a device with the same solution in order to obtain replicates or performing multiple tests on a single sample.

The third model was made shorter to avoid the stacking rings. In order to improve flow, a vent line was also added, allowing the air inside the reservoir to escape as the waste reservoir is filled with mobile phase. Models IV and V improved the vent design, making them larger and deeper. In all of these models, blockage of the top reservoir with the packing slurry, pictured in Figure 4-9(A), was frequent so we concluded that although the vent design was good, improvement in the way of packing the columns was necessary. Minimax VI was the first model which included a polycarbonate window for laser ablation (i.e. models with a thin polycarbonate film ablation window require 7 layers, as illustrated in Figure 4-2, instead of 5). All subsequent designs featured the thin polycarbonate film ablation window.
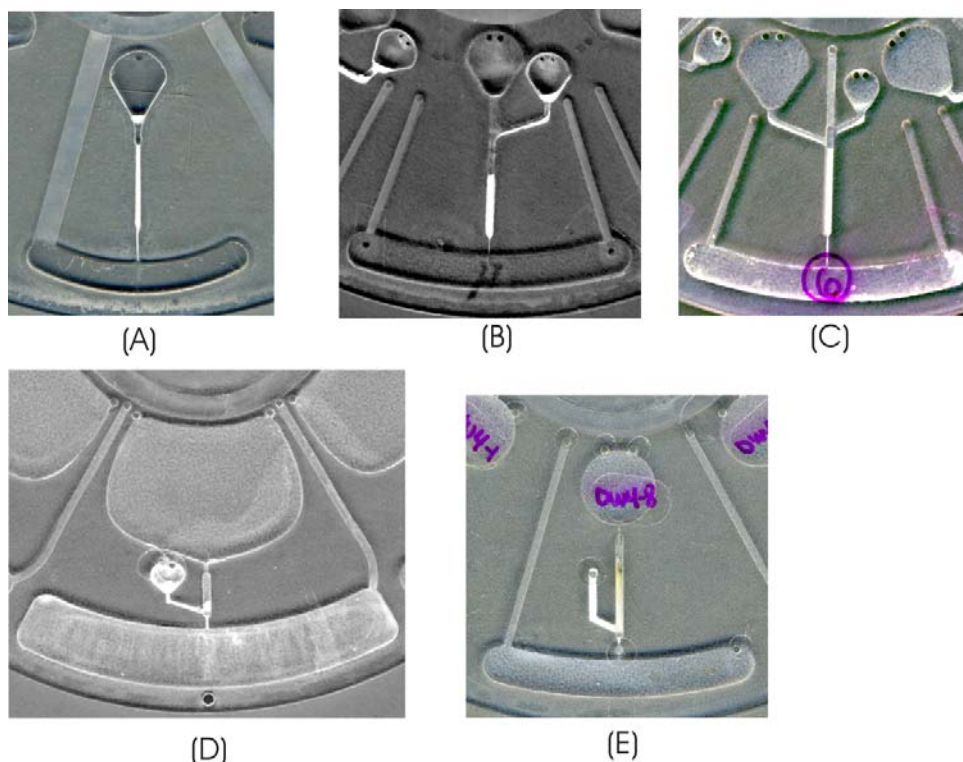
Figure 4-9. Packed columns. (A) Packing overflows in the sample reservoir when the packing slurry is inserted from the top of the column. (B) In models featuring a packing reservoir, a keystone effect is created at the junction between the packing reservoir and channel, resulting in blockage and difficulty in packing long columns. (C) The keystone effect in the sample reservoir was avoided by filling through a long, central, straight channel, but material filled neighbouring channels as well, resulting in blockages. (D) A column that is too short often resulted in packing overflow in the sample reservoir. (E) Packing is achieved by inserting a quartz wool plug at the bottom of the column. A chelated metal sample is trapped on the column, forming a green-yellow band.

Minimax VII-VIII

To avoid the problems of the proceeding models, a separate packing reservoir was added to model Minimax VII. This way, the sample reservoir remained free of packing. As pictured in Figure 4-9(B), although it is possible to pack columns using this type of fluidic network, material tended to accumulate in the packing reservoir making the packing of long columns difficult. Model Minimax VIII avoided this blockage problem by not having a reservoir, but rather by filling the slurry at the top of a long central channel. However, as pictured in Figure 4-9(C), packing the columns this way was unsuccessful because the packing material entered the sample and chelator channels as it reached their junctions.

Minimax IX-X

Model Minimax IX solved the slurry insertion problems. Starting with this model, the slurry is inserted at the bottom of the column. A combination of capillary forces and gentle pressure applied using the pipette forces the packing up the column channel and, if properly done, overflowing of the slurry into the top reservoir is avoided. A second model, Minimax X (also pictured in Figure 4-9(D)), features a larger sample reservoir capable of accommodating samples as big as 1 mL, but to make space on the disc for the large reservoir, the column length

had to be reduced significantly, making it difficult to form columns of an acceptable length for use without having packing overflow in the top reservoir.

Minimax XI-XII

Models Minimax XI and XII, pictured in Figure 4-9(E), present the most significant improvements through the line of Minimax models. Minimax XII was used for all the final experiments outlined in Chapters 6 and 7. The packing slurry is inserted at the bottom of the column, but this time through a straight channel rather than a reservoir, eliminating blockages. As discussed in Figure 4-5(D), the addition of a quartz wool plug greatly improved column packing by preventing column bleeding and allowing higher rotational rates and faster experiments. The layout of Minimax XII is detailed in Figure 4-10.
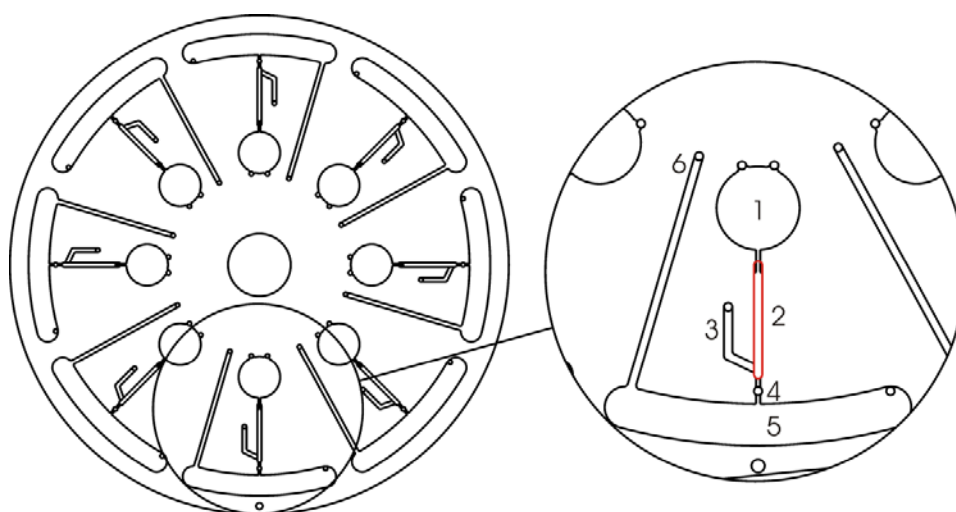
Figure 4-10. Centrifugal microfluidic device layout of Minimax XII (final successful design). Detailed view: (1) Sample reservoir 1.3 mm deep topped with two filling/vent holes. (2) 1 mm wide and 100 microns deep column. The red outlines the ablation polycarbonate window. (3) Packing inlet. (4) 250 μm wide and 100 microns deep restrictor channel with central 1 mm wide quartz wool plug. The quartz wool plug traverses all the layers of the device to rest on the base DVD. (5) 1.3 mm deep waste reservoir. (6) 500 μm deep vent line.

CONCLUSIONS

Using a rapid prototyping technique, miniature centrifugal chromatographic devices were built in-house, without the use of expensive fabrication or clean room facilities. Several fluidic networks were investigated in order to obtain an adequate device for SPE. The best design involved packing the column through a channel at the bottom of the column and retaining the column packing with a quartz wool frit.

REFERENCES

(1)   Duffy, D. C.; McDonald, J. C.; Schueller, O. J. A.; Whitesides, G. M. *Analytical Chemistry* **1998**, 70, 4974-4984.

(2)   Duffy, D. C.; Gillis, H. L.; Lin, J.; Sheppard, N. F., Jr.; Kellogg, G. J. *Analytical Chemistry* **1999**, 71, 4669-4678.

(3)   Duffy, D. C.; Schueller, O. J. A.; Brittain, S. T.; Whitesides, G. M. *Journal of Micromechanics and Microengineering* **1999**, 9, 211-217.

(4)   McDonald, J. C.; Duffy, D. C.; Anderson, J. R.; Chiu, D. T.; Wu, H.; Schueller, O. J. A.; Whitesides, G. M. *Electrophoresis* **2000**, 21, 27-40.

(5)   Becker, H.; Gärtner, C. *Analytical and Bioanalytical Chemistry* **2008**, 390, 89-111.

(6)   Lee, L. J.; Madou, M. J.; Koelling, K. W.; Daunert, S.; Lai, S.; Koh, C. G.; Juang, Y. J.; Lu, Y.; Yu, L. *Biomedical Microdevices* **2001**, 3, 339-351.

(7)   Waddell, E. A.; Locascio, L. E.; Kramer, G. W. *JALA - Journal of the Association for Laboratory Automation* **2002**, 7, 78-82.

(8)   Liu, X.; Du, D.; Mourou, G. *IEEE Journal of Quantum Electronics* **1997**, 33, 1706-1716.

(9)   Weigl, B. H.; Bardell, R.; Schulte, T.; Battrell, F.; Hayenga, J. *Biomedical Microdevices* **2001**, 3, 267-274.

(10) Bartholomeusz, D. A.; Boutte, R. W.; Andrade, J. D. *Journal of Microelectronic Systems* **2005**, 14, 1364-1374.

(11) Kido, H.; Zoval, J.; Madou, M. ECS *Transactions* **2006**, 4, 101-105.

(12) Maloney, T. D.; Colon, L. A. *Electrophoresis* **1999**, 20, 2360-2365.

(13) Penrose, A.; Myers, P.; Bartle, K.; McCrossen, S. *Analyst* **2004**, 129, 704-709.

Chapter 5 - Miniature centrifugal chromatographic devices for the pre-concentration and determination of lead in aqueous samples

ABSTRACT

Chapter 4 presented the evolution of the various designs envisioned in the process of creating a miniature centrifugal chromatographic device. This chapter presents the results of the testing of these various intermediate designs for single element determination. This is the first example of in-column analysis using a miniature centrifugal chromatographic device coupled to an Inductively Coupled Plasma Mass Spectrometer (ICP-MS) by Laser Ablation (LA). The devices were tested by adsorbing lead-8-hydroxyquinoline complexes onto C_{18}-bonded silica gel miniature columns on the centrifugal chromatographic discs. Analogous to the work presented in Chapter 3, where chromium species are sampled directly onto High Performance Thin Layer Chromatographic (HPTLC) plates, the lead chelates were sampled directly on the stationary phase material by LA-ICP-MS. Extraction results for several of the designs shown in Chapter 4 are presented and different extraction methodologies are evaluated.

Some of this work has previously been published in the microTAS 2007 Conference Proceedings:

Lafleur, J. P.; Salin, E. D. *Proceedings of mTAS 2007, Eleventh International Conference on Miniaturized Systems for Chemistry and Life Sciences* **2007**, *2*, 1441-1443.

The optimization of the LA instrumental parameters for use in conjunction with these devices is presented in Appendix C. The set up, calibration and digital control of the motor used to spin the devices are presented in Appendix E. Finally, the estimated volumetric flow rate and predicted column efficiency of the miniature centrifugal chromatographic devices are modeled in Appendix F.

INTRODUCTION

Taking advantage of its softness, high density, low melting point and ability to form alloys, humans have used lead for thousands of years and continue to find applications for this heavy metal today. Due to its widespread use and toxicity, lead is a significant environmental contaminant and governments have adopted various laws and regulations in order to regulate its use and release.[1] Health Canada has established a maximum acceptable concentration for lead in drinking water of 10 ppb. Lead is not very soluble in water, but leaching from old water pipes can lead to elevated levels in domestic supplies and is a concern in many cities with old water pipes, such as Montreal. Ongoing exposure to even very small amounts of lead can be harmful, especially in infants and young children, leading to brain and nervous system damage.[2] In fact, it is speculated that lead poisoning was a major factor in the decline of the Roman Empire.[3, 4] Lead was used by Romans to line aqueducts and in glazes on containers used for food and wine storage.[1] Since lead intake was correlated with social class, the high lead intake in the Roman Aristocracy could have resulted in mental incompetence as well as rapidly declining birth rates eventually leading to the fall of the Empire.[3] It is also believed that members of Sir John Franklin's ultimate expedition to the Northwest Passage in the mid-1840s died from lead poisoning. With poor prospects of obtaining food in the arctic, the crew had stocked up

provisions for three years, including 8000 tins.[5] Explanations of what might have

happened to the doomed expedition started to surface only in the 1980's when

an anthropologist found many skeletal remains from the crew, including one

perfectly preserved frozen corpse. Bone analysis revealed that the lead content

of the bones was 228 ppm compared to 22-36 ppm for Inuit remains found

nearby while the lead content in the hair of the perfectly preserved body reached

600 ppm in their terminal parts.[5] The technology for preparing canned meats had

just been patented in the early 19th century and the 8000 cans of supply brought

on board for survival were sealed with a solder of tin with a high lead content.

Lead poisoning from the contaminated meats weakened the crew[5] although the

coup de grâce may have actually been inflicted by botulism.[6] Lead poisoning can

also result in some surprising outcomes. The famous painter Francisco de Goya

painted a series of disturbing artworks titled "The Caprices" after supposedly

contracting lead poisoning from mixing the pigments for Lead White; although

several other possibilities exist to explain his illness.[7] Hair analysis reveals that

lead poisoning may have also contributed to the end-of-life symptoms and

deafness of another famous artist. Beethoven, who overindulged in wine in the

last decade of his life, may have contracted lead poisoning from lead added

illegally to cheap wines at the time in order to sweeten and refresh them.[8]

However, lead content in hair is not recognized as a reliable biomarker of lead

absorption so this evidence is not considered persuasive.[9] Nevertheless, it is evident that lead poisoning has had an impact on human health for thousands of years. At the peak of the Roman Empire, lead production was already 80 000 tons per year[3] and has continued to increase, especially during the industrial revolution. Until the 1990s, the burning of leaded gas in automobiles was the largest source of lead in the environment, but since the ban of lead as an anti-knock additive in gasoline, industrial releases now exceed automotive emissions.[1] Considering the ubiquity of lead in the environment, it is of great interest to continue developing rapid and reliable methods for lead analysis.

Solid Phase Extraction (SPE) is a chromatographic technique commonly used for pre-concentration and matrix removal in trace metal determinations. In this technique, 8-hydroxyquinoline (8-HQ) is added in excess to the aqueous sample to be analysed or bound, physically or chemically, to the sorbent material. 8-HQ is a bidentate monoprotic chelating agent which can form water soluble uncharged chelates with at least 60 elements.[10, 11] Metals are bound to 8-HQ through the ring nitrogen and phenolate oxygen. Since 8-HQ is an ampholyte, the chelation process is largely dependent on pH. In acidic solution, the oxinium ion is formed by protonation of the ring nitrogen while in basic solution, the phenol group loses its proton to form the oxinate ion. Since most divalent and trivalent elements react with the oxinate form of 8-HQ, extractions are generally carried

out in basic solutions. The advantage of using 8-HQ as a chelator in trace metal pre-concentration of drinking and seawater samples is its lack of affinity for alkaline and alkaline earth elements. Once the metal chelates are adsorbed and concentrated on top of an octadecyl silica (C_{18}) chromatographic bed, the non-chelated interfering species can easily be washed away with water. Conventional methods of analysis by ICP-MS require elution of the lead complexes from the column, often with an organic solvent such as methanol, before being introduced in the plasma by solution nebulization. Lead can form complexes with oxygen containing groups such as the residual silanols on the silica based sorbent. Since these interactions cannot be disrupted by a change in carrier polarity, sample losses can occur upon elution with an organic solvent such as methanol.[12] Moreover, when ICP is used as the analysis technique, organic solvents should be avoided as they generate strong turbulence in the ICP.[13] Our technique differs from the conventional procedure by eliminating the final elution step. To eliminate the elution step, direct analysis of the lead laden sorbent can be performed by LA-ICP-MS. Laser sampling of the material directly on the column rather then elution has several advantages. Nebulization inefficiencies are avoided and higher pre-concentration factors can potentially be achieved since dilution with the eluent is avoided. Problems such as incomplete recovery and contamination by reagents are reduced. Also, only the portions of the column containing the

111

analytes of interest need to be sampled, thereby reducing analysis time. This direct sampling is made possible by the implementation of the SPE columns on centrifugal microfluidic discs. The miniature columns offer an ideal surface for laser sampling. The platforms also reduce analysis time by allowing the processing of multiple samples in parallel and greatly reducing the volumes necessary to carry out an analysis.

This chapter presents the various designs and methodologies that have been tested to optimize the centrifugal microfluidic device for the extraction of lead in aqueous samples.

EXPERIMENTAL

Centrifugal microfluidic devices

The devices used were built using a rapid prototyping technique[14] which combines thin film lamination[15] and xurography[16] and is described in detail in Chapter 4. Reservoirs were created using conventional Computerized Numerically Controlled (CNC) milling of polycarbonate discs (120 mm diameter). The channels and vent lines were cut in 100 μm adhesive film with a cutting plotter. A 75 μm polycarbonate film was used to cover the top of the columns.

Solid Phase Extraction Procedure

The packing material (Nucleosil C_{18} silica, 100 Å pore size and 5 μm mean particle size, Macherey-Nagel, Düren, Germany) was introduced in the columns

as a methanol slurry. The packed bed was consolidated by applying centrifugal force with a 90 V DC motor with manual speed control. The packing was conditioned with 5 µl of methanol and then washed with 5 µl of acidified methanol (1% w/w concentrated HCl (Baker Instra-Analyzed, J.T.Baker, Phillipsburg, NJ, USA) in methanol) to remove contaminants. The column was then conditioned for the introduction of the aqueous sample by adding 5 µl of water (18 MΩ) adjusted to pH 9 with ammonium hydroxide (ACS Plus, Fisher Scientific, Pittsburgh, PA, USA). Unless otherwise indicated, 8-hydroxyquinoline (99+% purity, Sigma-Aldrich Canada Ltd., Oakville, ON, Canada) was added in excess to the lead standards (diluted single element reference solution, 1000 $\mu g \cdot L^{-1}$ in 2–5% HNO3, Fisher Scientific, Pittsburgh, PA, USA) and water blanks before adjusting their pH to 9 with ammonium hydroxide. The samples were then percolated through the column at 1000 – 2000 RPM (20-1000 µl aliquots). The columns were stored in a desiccator prior to LA-ICP-MS analysis.

LA-ICP-MS Analysis

The laser ablation system (LSX-200, CETAC technologies, Omaha, NE, USA) operating parameters were optimised for the analysis of chromatographic material (Appendix D). The vaporized samples were carried by an argon stream to an ICP-MS system (Perkin-Elmer SCIEX Elan 6000, SCIEX, Concord, ON, Canada) at a flow rate of 1 $L \cdot min^{-1}$.

RESULTS AND DISCUSSION

The extraction procedure is illustrated in Figure 5-1(A). Figure 5-1 shows a magnified picture of a packed microchannel before (B) and after (C) ablation. The corresponding LA-ICP-MS transient scans are shown in Figure 5-2. In Figure 5-2(A), the laser is used to selectively vaporize the thin polycarbonate film covering the column and the chromatographic bed (see Chapter 4 for details on the disc layers).   No silicon signal, the major stationary phase constituent, is observed during this ablation scan. During the second superimposed LA scan across the length of the microchannel, the laser is now vaporizing the stationary phase, as exemplified by the relatively large silicon signal observed in Figure 5-2(B). A signal is observed for the trapped lead during this second ablation scan.

(A)   (B)   (C)
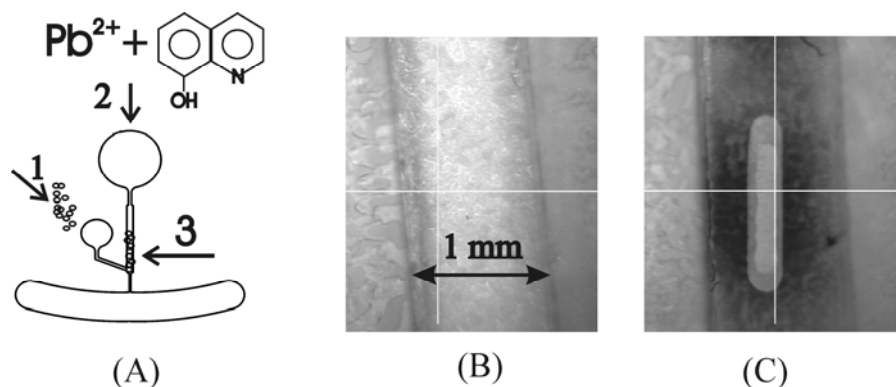
Figure 5-1. (A) Solid phase extraction procedure. (1) Column packing (2) Adsorption of the chelated sample. (3) Direct laser ablation of the sample. (B) A packed microchannel. (C) The same channel after ablation of the polycarbonate window to expose the packing.
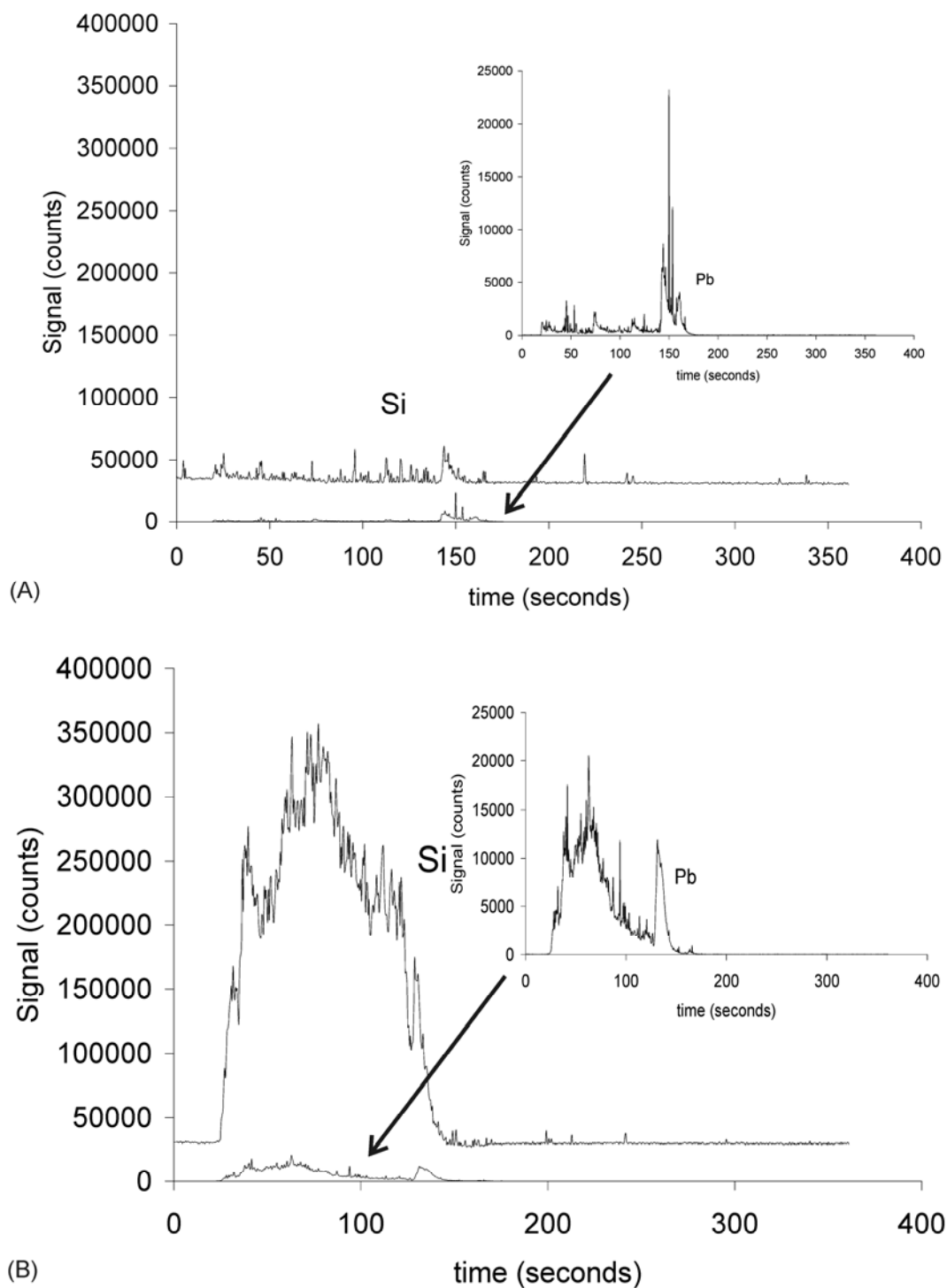
Figure 5-2. LA-ICP-MS spectra. (A) Only the polycarbonate window is vaporized.

(B) During the second ablation scan, the chromatographic material is vaporized.

DYNAMIC IMMOBILIZATION OF 8-HQ ON THE STATIONARY PHASE (MINIMAX VIII)

For the pre-concentration of trace metals from water samples, the technique used has been the object of several investigations[17-20] and in which a metal chelator (8-hydroxyquinoline, 8-HQ) is added in excess to the sample. At least 2-3 fold excess is necessary to ensure complete chelation.[21] After complexation, the sample is simply percolated through the SPE column to extract the metal chelates. However, if the difference in selectivity of the sorbent between the free chelating agent and the metal chelate complex is not sufficient, the sorbent will absorb free ligand in addition to the metal chelate complex during the pre-concentration step.[12] A potential inconvenience, especially for very small columns, is that the sorbent could get overloaded before all the metal complexes are adsorbed, resulting in sample losses. An additional inconvenience arises from our new analysis technique in which samples are vaporized directly from the column rather than eluted. In our modified technique, a great excess of chelator could result in band spreading in the "laser chromatogram" as some sites on the chromatographic bed are occupied only by the free ligand. In order to verify this hypothesis, a different methodology which involves the direct immobilization of 8-HQ on the stationary phase material prior to sample extraction was tested. In this technique, the column was flushed with an excess of 8-HQ to dynamically

immobilize the chelator on the sorbent material. The coating of the column was followed by column conditioning with pH 9 DDW and finally the sample, adjusted to pH 9. During percolation, the metal ions in the sample come into intimate contact with a relatively high concentration of 8-HQ on the sorbent. However, the contact time is relatively short, so that the rate of chelate formation must therefore be relatively rapid.[21]

Transient ablation scans for both methods are compared in Figure 5-3. The Si signal corresponds to the length of the column as it is the major component of the stationary phase material. LA starts at the top of the column (left side of the plot) down to the bottom of the column (right side of plot). As illustrated in Figure 5-3(A), when the chelator is added in excess to the sample, the Pb LA-ICP-MS signal is maximal in the top half of the column, which indicates that the sample effectively gets adsorbed on top of the column. However, as illustrated in Figure 5-3(B), when the chelator is added directly to the stationary phase prior to extraction, the Pb signal is low and spread over the entire length of the column. A potential cause of this spreading is the too short interaction time between the chelator on the column and the sample as it flows down the column. Poor chelation ensues and the lead gets spread out over the entire length of the column and probably even gets washed out. Another possibility is that the physically bound chelating agent has been flushed out of the sorbent during

sample percolation, a common drawback of this technique.[13] The use of a new sorbent containing the appropriate chelating group or of a functionalized sorbent on which the chelating group is chemically bound would probably solve this problem. Another possible source of error when using this second technique is that the pH of the water sample is adjusted without the presence of the chelator. The problem is that metals are most soluble in acidic solutions and that the addition of ammonium hydroxide prior to the addition of the oxine could result in precipitation and incomplete extraction. The soundest way to avoid precipitation is to add the oxine solution to the metal solution, then adjust the pH and finally to extract.[10] It was concluded from these experiments that adding the chelator directly to the sample gives better results and is the preferred technique for all subsequent experiments.
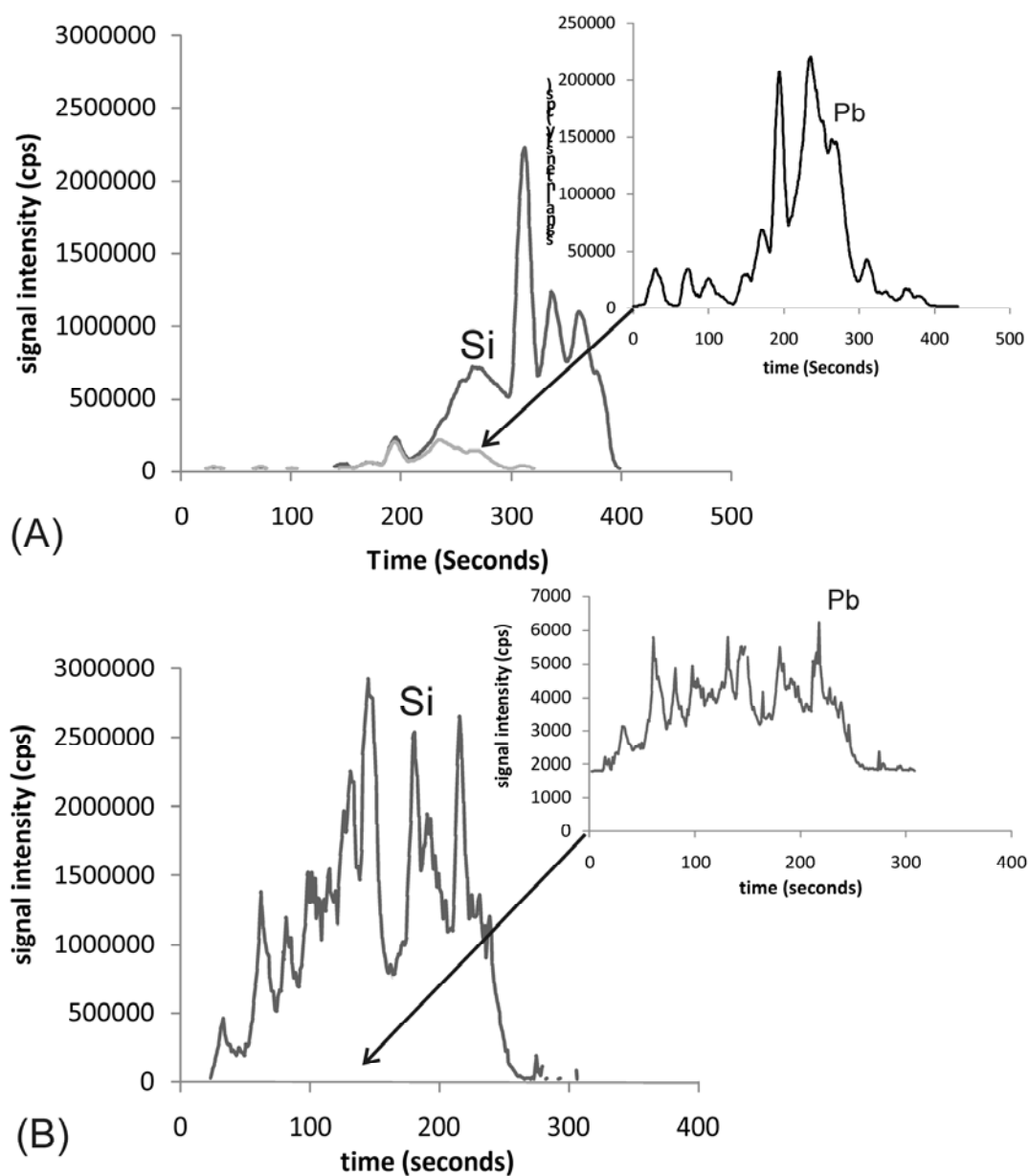
Figure 5-3. Comparison of the LA-ICP-MS transient signals obtained with two SPE methods: (A) The chelator is added directly to the sample. (B) The chelator is dynamically immobilized on the stationary phase prior to sample extraction.

First extraction results obtained using the conventional method (Minimax IX)

Preliminary results (Figure 5-4) show that the Pb signal increases with increasing Pb trapped on the column, with precision ranging from 31-42% (3 replicates) and a limit of detection (3 sigma) of 3 ng or 30 ng·mL^{-1} based on a 100 µL sample. The low precision could certainly be improved with an internal standard, but the columns are not uniform enough to use the silicon present in the stationary phase as an internal standard. In this model, the columns are still retained only through a keystone effect (Chapter 4) and good column quality is difficult to obtain as seen in Figure 5-2 and Figure 5-3, where the silicon signals are very uneven along the length of the columns. Other internal standardization solutions are investigated in Chapter 6.
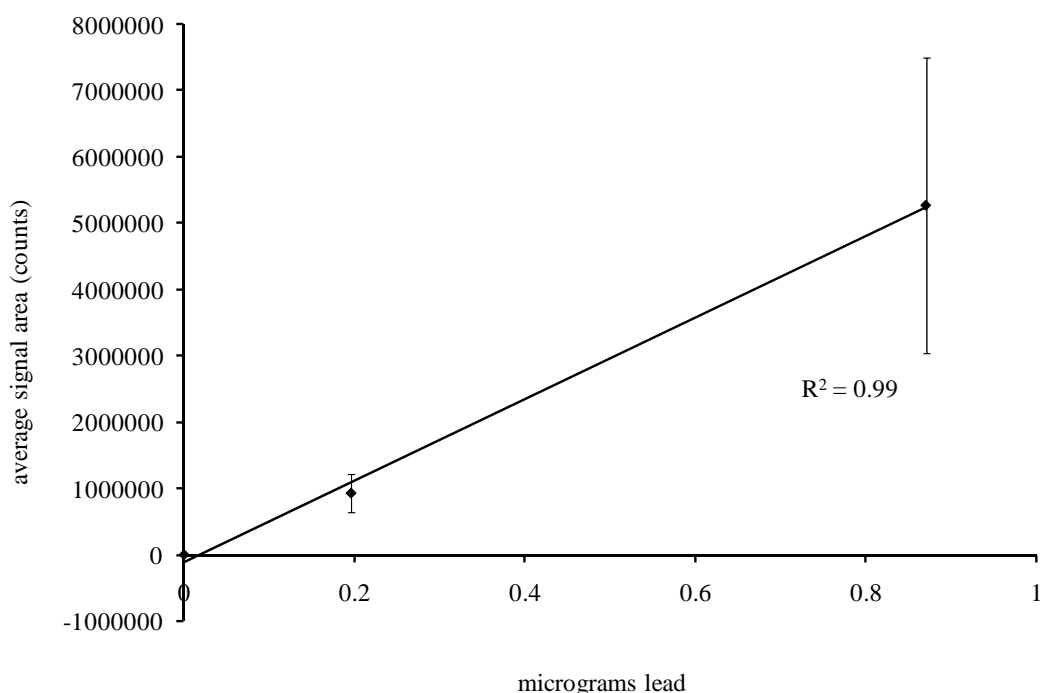
Figure 5-4. Determination of Lead-8-Hydroxyquinolate adsorbed on C_{18}-bonded silica microcolumns (model Minimax IX) by LA-ICP-MS.

Attempts at using larger reservoirs (Minimax X)

In order to improve the detection limits achievable, devices with reservoirs capable of accommodating samples as large as 1 mL were created. Unfortunately, as mentioned in Chapter 4, the size of the reservoir could only be accommodated by a reduction in column length. Aside from being more difficult to pack, the smaller columns proved much less stable than the conventional columns and they frequently bled or even washed out completely upon the addition of the 1 mL sample. Again, these columns were only retained by a

keystone effect. Very slow rotational speeds were used to avoid column loss (maximum 1000 RPM), resulting in extremely long extraction times. Several hours were required to extract each sample, and a total of almost two weeks was necessary to run all standards and replicates shown in Figure 5-5. An estimate of the volumetric flow rate for this device can be found in Appendix F. Due to the poor quality of the columns, no improvements in detection limits were found with this model, with an LOD (3σ) of 90 ng mL^{-1}.
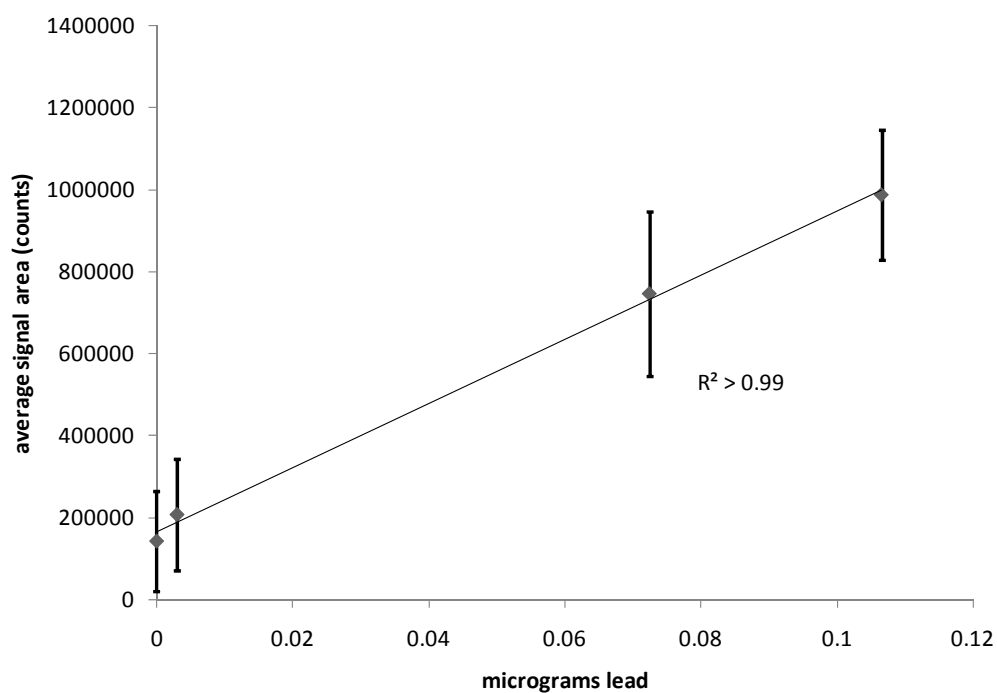
Figure 5-5. LA-ICP-MS calibration results for the extraction of lead using (large) 1 mL samples.

CONCLUSIONS

It was demonstrated that LA-ICP-MS can be used to retrieve lead trapped on miniature centrifugal chromatographic columns without elution of the sample. Results show that it is preferable to add the chelator in excess to the sample prior to extraction than attempt to minimize band broadening by coating the chelator directly on the sorbent material. Results presented in this Chapter show relatively poor detection limits and precision, partly caused by the lack of an appropriate internal standard and the poor column quality when the keystone effect is used to retain the columns. In the next chapter, column quality and speed of analysis are greatly improved by the introduction of the quartz wool frit. The external addition of internal standards and multi-element capabilities are also investigated.

REFERENCES

(1)   Environement_Canada; The Green Lane, Environment Canada's World Wide Web site, http://www.atl.ec.gc.ca/epb/envfacts/lead.html, 2002.

(2)   Health_Canada; Minister of Health, http://www.hc-sc.gc.ca/hl-vs/iyh-vsv/environ/lead-plomb-eng.php: Ottawa, 2008.

(3)   Woolley, D. E. *Neurotoxicology* **1984**, 5, 353-362.

(4)   Nriagu, J. O. *New England Journal of Medicine* **1983**, 308, 660-663.

(5)   Bayliss, R. *Journal of the Royal Society of Medicine* **2002**, 95, 151-153.

(6)   Horowitz, B. Z. *Journal of Toxicology - Clinical Toxicology* **2003**, 41, 841-847.

(7)   Ravin, J. G.; Ravin, T. B. *Survey of Ophthalmology* **1999**, 44, 163-170.

(8)   Mai, F. M. *The journal of the Royal College of Physicians of Edinburgh* **2006**, 36, 258-263.

(9)   Eisinger, J. *Toxicological and Environmental Chemistry* **2008**, 90, 1-5.

(10)   Sandell, E. B.; Onishi, H. *Photometric determination of traces of metals : general aspects*; Wiley: New York, 1978 pp. 422-425.

(11)   Minczewski, J.; Chwastowska, J.; Dybczyński , R. *Separation and preconcentration methods in inorganic trace analysis*; Halsted Press: New York, 1982, p. 197.

(12) Lancaster, H. L.; Marshall, G. D.; Gonzalo, E. R.; Ruzicka, J.; Christian, G. D. *Analyst* (Cambridge, United Kingdom) **1994**, 119, 1459-1465.

(13) Camel, V. *Spectrochimica Acta - Part B Atomic Spectroscopy* **2003**, 58, 1177-1233.

(14) Kido, H.; Zoval, J.; Madou, M. *ECS Transactions* **2006**, 4, 101-105.

(15) Weigl, B. H.; Bardell, R.; Schulte, T.; Battrell, F.; Hayenga, J. *Biomedical Microdevices* **2001**, 3, 267-274.

(16) Bartholomeusz, D. A.; Boutte, R. W.; Andrade, J. D. *Journal of Microelectronic Systems* **2005**, 14, 1364-1374.

(17) Sturgeon, R. E.; Berman, S. S.; Willie, S. N. *Talanta* **1982**, 29, 167-171.

(18) Skinner, C. D.; Salin, E. D. *Journal of Analytical Atomic Spectrometry* **2003**, 18, 495-500.

(19) Otero-Romaní, J.; Moreda-Piñeiro, A.; Bermejo-Barrera, A.; Bermejo-Barrera, P. *Analytica Chimica Acta* **2005**, 536, 213-218.

(20) Lam, R.; Salin, E. D. *Canadian Journal of Chemistry* **2008**, 86, 586-589.

(21) Fritz, J. S. *Analytical Solid Phase Extraction*; Wiley-VCH: New York, 1999.

Chapter 6 - Pre-concentration of trace metals on centrifugal microfluidic discs with direct determination by Laser Ablation Inductively Coupled Plasma Mass Spectrometry

Chapters 4 and 5 presented the design, construction and testing of several centrifugal microfluidic devices coupled to a Laser Ablation Inductively Coupled Plasma Mass Spectrometer (LA-ICP-MS) for the pre-concentration and determination of a single element in aqueous samples. This chapter presents the multi-elemental determination results obtained with the final, optimal, device designed. The results presented in this chapter were published as:

Lafleur, J.P. and Salin, E.D. *Journal of Analytical Atomic Spectrometry* **2009**, 24(11), 1511 – 1516.

Additional information on instrumental parameter optimization, motor calibration and control, flow modeling and Van Deemter plots can be found in Appendices C, E and F respectively. All calibration curves for this chapter can be found in Appendix G.

ABSTRACT

Solid Phase Extraction (SPE) is commonly used for pre-concentration and matrix removal in trace metal determinations. This paper presents a novel centrifugal microfluidic device for field sampling and on-site pre-concentration of water samples. Metal-8-hydroxyquinoline complexes are adsorbed onto miniature C_{18}-bonded silica gel columns on centrifugal microfluidic discs. Laser Ablation (LA) is used to directly vaporize the analytes from the column, instead of eluting the pre-concentrated analytes for introduction in an Inductively Coupled Plasma Mass Spectrometer (ICP-MS) by conventional solution nebulization. Absolute detection limits ranging between 0.1 and 12 ng were obtained for Ni, Cu, V, Pb and Co in drinking water Certified Reference Materials (CRMs). These centrifugal devices require only 1 - 600 µL samples and necessitate no more than a simple motor to actuate fluid flow. The discs can be used to perform multiple extractions simultaneously as well as allowing the easy storage of samples before transport to the laboratory for LA-ICP-MS analysis.

INTRODUCTION

Solid Phase Extraction

Sample preparation is often an essential part of the measurement process, especially in environmental analyses as many samples are not found in a form or at a concentration suitable for direct introduction into analytical

instruments. Sample preparation represents almost 60% of an analyst's time and contributes about 30% to the error in the global analysis of a sample.[1] Consequently, it is desirable that sample preparation methods be developed which are rapid, provide high sample throughput, minimize sample losses by reducing sample manipulation steps, are easily automated and limit the use of noxious organic solvents. As an example, it is often necessary in the analysis of drinking water and seawater, where analyte concentrations are very low, to pre-concentrate the samples. Seawater also poses additional problems, as its saline composition can be a source of matrix and spectral interferences.

Solid Phase Extraction (SPE) is commonly used for pre-concentration and matrix removal in trace metal determinations. In this reversed phase liquid chromatographic technique described originally by Sturgeon *et al.*[2], neutral metal-8-hydroxyquinoline (8-HQ) complexes are adsorbed on hydrophobic C_{18}-bonded silica gel. Alkali, alkaline earth and other matrix components, which are not chelated, are eluted from the SPE column during a subsequent washing step. Conventional methods of analysis by Inductively Coupled Plasma Mass Spectrometry (ICP-MS) require elution of the pre-concentrated metal complexes from the column, by changing the carrier polarity from water in the sample to methanol.[2] Typically, a 500 – 1000 mL sample will be eluted with approximately 5 - 10 mL of methanol, resulting in enrichment factors of 50 to 200. The use of

methanol as an eluent has various disadvantages. Organic solvents can negatively affect ICP performance, so the elution step generally has to be followed by an evaporation step and subsequent dilution to 10 mL with 1% $^v/_v$ nitric acid, increasing risks of sample losses and contamination, as well as the time required for an analysis. Another disadvantage is that residual silanol sites on the silica based sorbent material provide another binding pathway for the analytes. Lancaster *et al.*[3] showed that this secondary binding could result in as much as 60% analyte uptake through interactions which can only be disrupted by a change in carrier pH rather than polarity. Therefore, considerable losses can be incurred when eluting the analytes with methanol. Other groups[4, 5] have used 2.0 M nitric acid to directly elute the concentrated metal-8-HQ complexes, so that the methanol evaporation step can be avoided.

The error associated with the elution process can be circumvented by directly sampling the pre-concentrated analytes on the stationary phase. The number of sample manipulation steps is reduced, minimizing sample losses and contamination as well as analysis time, while reducing the use of organic solvents which are detrimental to health and the environment. Several direct sampling methods have been reported for the analysis of organic compounds. The direct determination of ethylbenzene by Raman spectroscopy through the quartz wall of an SPE cartridge has recently been reported.[6] The analysis of pre-

concentrated biological fluids after elution of the analytes onto the membrane which seals an SPE cartridge has also been investigated by Desorption Electrospray Ionization (DESI) mass spectrometry.[7] In elemental analysis, the direct sampling of analytes from Thin Layer Chromatography (TLC) plates by Laser Ablation (LA) ICP-MS has been demonstrated.[8, 9] TLC is a relatively slow separation technique as it relies only on capillary forces. Faster separations can be achieved by forcing the mobile phase flow by centrifugal force.

Centrifugal Chromatography and Miniaturization

The use of centrifugal force to drive the mobile phase flow in paper chromatography was the object of an extensive review by Deyl *et al.* in 1964.[10] The method has since then been applied to TLC and preparative centrifugal thin layer chromatographs are now commercially available with such devices as the Chromatotron (Harrison Research, Palo Alto, CA) and the CycloGraph (Analtech, Newark, DE). Centrifugal chromatography has a very high potential for miniaturization and the processing of multiple samples in parallel. For analytical purposes, up to 72 samples can be applied on centrifugal TLC platforms for simultaneous separation.[11] Microfluidic devices that use centrifugal force to drive the flow of liquids have certain advantages over the more conventional electrokinetic pumping that is dependent on pH and ionic strength. A flow of liquid accelerated by centrifugal force is relatively insensitive to these

physicochemical properties and careful design of the channels allows one to work in a wide range of flow rates. Microfluidic devices that rely on centrifugal pressure to force the flow of liquids are commonly referred to as "CD-like" or "Lab on a CD" microfluidic platforms and have been the object of recent reviews.[12, 13] A device combining centrifugal chromatography with microfluidic functions has been developed previously but only used for the separation of colored dyes.[14] The application of microfluidic systems in environmental analysis has attracted considerable attention and has been the object of a recent review.[15] Several groups have reported the successful interfacing of microfluidic capillary electrophoresis with ICP-MS through the use of micro-flow nebulizers and volatile species generation.[16-21] We have reported recently a novel technique for the direct interfacing of microfluidic devices to ICP-MS through Laser Ablation.[22] We report here an investigation of the applicability of this method to the determination of V, Pb, Ni, Cu and Co in drinking water samples. As well as reducing the sample manipulation steps, this technique reduces the sample volumes necessary for an analysis by as much as four orders of magnitude, allows the processing of multiple samples in parallel, provides for the preservation of samples during transport to the laboratory after field sampling and has a high potential for automation.

EXPERIMENTAL SECTION

Standards and reagents

An acidified methanol solution was made from 1 mL of concentrated HCl (Baker Instra-Analyzed, J.T.Baker, Phillipsburg, NJ, USA) in 125 mL of methanol. A 2% NH_4OH solution was prepared from concentrated NH_4OH (ACS Plus, Fisher Scientific, Pittsburgh, PA, USA) diluted with distilled deionized water (DDW, 18 MΩ, Millipore Co., Bedford, MA, USA) and used to prepare pH 9 DDW. A 10% $^w/_v$ solution of 8-hydroxyquinoline (99+% purity, Sigma-Aldrich Canada Ltd., Oakville, ON, Canada) in methanol was prepared fresh on the day of extraction. Vanadium, calcium, bismuth and indium single element standard solutions (1000 µg·L^{-1} in 2–5% HNO_3) as well as the Drinking Water Certified Reference Materials (Enviromat High, EP-H-2 and Low EP-L-2) and the multi-element standard (PlasmaCal Trace Metal I) were obtained from SCP Science (Baie d'Urfé, Qc, Canada). Lead, nickel and copper single element reference solutions (1000 µg·L^{-1} in 2–5% HNO3) were obtained from Fisher Scientific (Pittsburgh, PA, USA). An Artificial Drinking Water sample was prepared containing 0.424 ppm V, 0.187 ppm Cu, 0.182 ppm Ni, 0.236 ppm Pb and 11.77 ppm Ca using single element standard solutions. Octadecylsilane silica gel (Nucleosil C$_{18}$ silica, 100 Å pore size and 10 µm mean particle size) was obtained from Macherey-Nagel (Düren, Germany). All sample and reagent containers

were conditioned in 10% HNO_3 (diluted in DDW from trace-metal grade concentrated HNO_3, Fisher Scientific, Pittsburgh, PA, USA) for at least 24 hours.

Device Fabrication

Devices were fabricated using a rapid prototyping technique based on a combination of thin film lamination[23] and xurography[24] developed by Kido *et al.*[25] High aspect ratio features such as reservoirs were created using conventional Computerized Numerically Controlled (CNC) milling (QuickCircuit 5000, T-Tech, Inc. Norcross, GA) of polycarbonate discs (Blank uncoated CDs and DVDs, 120 mm diameter, 1.2 and 0.6 mm thickness respectively, U-Tech Media Corp., Taiwan). DVDs were normally used as end pieces while CDs, which are thicker, were used in middle layers where deep reservoirs were required. Low aspect ratio features such as channels and vent lines were cut in 100 µm thick adhesive film (FLEXmount DFM-200-Clear V-95 150 poly V-95 400 poly, FLEXcon, Spencer, MA, USA) with a cutting plotter (CE300MK2-60, Graphtec America, Inc., Santa Ana, CA, USA). A 75 µm thick polycarbonate film (Claritex, Coburn Graphics Inc., Lakewood, NJ, USA) was used to cover the top of the columns. All layers were carefully aligned and pressed firmly together using a hand cranked cold laminator (Jet Mounter ML25, Drytac, Concord, ON, Canada) to ensure a good seal. The centrifugal device, which consists of a laminate of 7 layers, is illustrated in Figure 6-1. During sample storage, all vent and fill holes were sealed

with microplate sealing tape (Nunc sealing tape T9571, Sigma-Aldrich Corp., St

Louis, MO, USA) to avoid contamination.
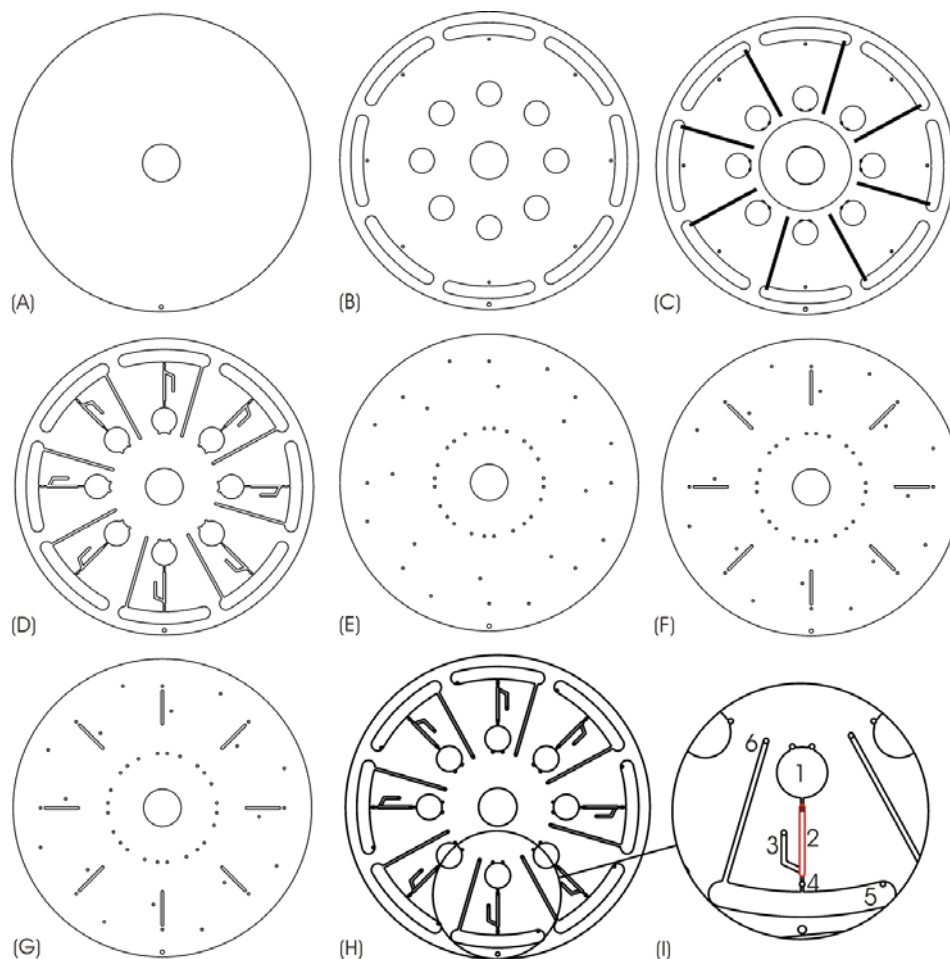
Figure 6-1. Device component layers. (A) DVD base (bottom of assembly). (B)

Adhesive layer. (C) CD layer. (D) Adhesive layer. (E) Thin polycarbonate film. (F)

Adhesive layer. (G) DVD in which windows have been milled to allow access to

the polycarbonate film covering the SPE column. (H) Complete assembly. (I)

Detailed view of the assembly. (1) Sample reservoir (2) Packed microcolumn with

superimposed window (3) Packing channel. (4) Quartz wool column frit. (5)

Waste reservoir. (6) Vent.

Column Packing

The sorbent material was introduced in the columns as methanol slurries using a micropipette. All slurries were carefully homogenized using a vortex mixer (Maxi-Mix, Barnstead International, Dubuque, IA, USA). Column consolidation was achieved by applying centrifugal force (1700 RPM) using a device built in-house and consisting of a permanent magnet type 90V DC motor (Baldor Motor and Drives, Fort Smith, AR, USA) driven manually with a motor drive (Penta KB Power, KBPC-240D, TechnoMotion, Montréal, QC, Canada) or digitally using a signal isolator (Penta KB Power, KBSI-240D, TechnoMotion, Montréal, QC, Canada).

Solid Phase Extraction

The blanks and samples (10 mL) were prepared for the extraction by adding the chelator (10 µL of 10% 8-HQ in methanol) and their pH were adjusted to 9 with small additions of 2% NH_4OH solution. Prior to the extraction, the packing was conditioned with 10 µL of methanol to allow resolvation of the sorbent. The column was then washed with acidified methanol (10 µL) to remove contaminants followed by methanol (10 µL). The column was conditioned for the introduction of the aqueous sample by slowly changing the mobile phase carrier from methanol to pH 9 DDW. The samples (consisting in one 300 µL aliquot of the 10 mL prepared sample) were then percolated through the column at

1500 RPM. Finally, the columns were washed with 10 µL DDW adjusted to pH 9 to remove concomitants and stored in a desiccator until analysis.

Analytical Methodology

All calibration curves were obtained using the method of standard additions. The 10 mL samples were spiked with 10 µL, 15 µL, 20 µL (and 25 µL for EP-H-2) of multi-element standard (100 ppm Co, Cu, Ni, Pb and 250 ppm V). A 10 µL spike of internal standard (In and Bi, 500 ppm each) was also added to the artificial drinking water standards. Aliquots were run through 4 to 8 different SPE columns each in order to obtain replicates. The blanks were treated in the same way as the samples. After extraction, the discs containing the EP-L-2 extracts and the artificial drinking water extracts were stored for 9 weeks prior to LA-ICP-MS analysis.

Spectroscopic Analysis

A Q-switched Nd:YAG laser, frequency quadrupled at 266 nm LA system (LSX-200, CETAC technologies, Omaha, NE, USA) coupled to a Perkin-Elmer Elan 6000 ICP-MS system (SCIEX, Concord, ON, Canada) were used. The eight SPE units were cut out from the discs using a high speed rotary tool (Dremel tool, Robert Bosch Tool Corporation, Mount Prospect, IL) to allow their insertion in the laser ablation cell. The ICP-MS operating parameters were optimized using the standard procedure for solution nebulization. The LA system was operated in the

single line scan mode, in which the sample holder moved horizontally at a constant speed while the laser was firing repetitively. The laser defocus (50 μm), energy level (10 on a scale of 1 - 20), pulse repetition rate (10 Hz) and scanning speed (100 μm s^{-1}) were optimized on 150 μm thick HPTLC plates (Hard Layer Silica Gel GHL Uniplates, Analtech, Newark, DE, USA) as well as on prepared columns.

RESULTS AND DISCUSSION

Sampling, Extraction and Storage

The miniature centrifugal SPE devices were tested with 300 μL samples, a three to four order of magnitude reduction in sample size compared to conventional SPE procedures which use 500 to 1000 mL samples. As illustrated in Figure 6-1, each centrifugal disc could accommodate a total of 8 SPE units, so multiple extractions could be performed simultaneously. Both the reduction in sample size and the processing of multiple samples in parallel reduced the time required for the SPE procedure to about 20 minutes per disc (8 extractions). Another advantage of the extraction device lies in the fact that the extraction could be performed directly on-site with a device analogous to a portable compact disc drive. The extracted samples stored on one disc are much easier to carry back to a laboratory than the eight 1000 mL containers that would be required in the conventional SPE procedure. Sample losses through adsorption

on the container walls is also avoided as the analytes are extracted and stored on the sorbent immediately after sampling. To simulate on-site extraction and the waiting period before transport to the laboratory, the EP-L-2 CRM (**Error! Reference source not found.**) and Artificial Drinking Water sample (**Error! Reference source not found.**) were extracted and stored on the centrifugal SPE discs for 9 weeks prior to LA-ICP-MS analysis with no negative impact on the analysis results.

Laser sampling

An SPE unit ready for LA is shown in Figure 6-2(A). The metal chelates form a visible green band on top of the sorbent material after spinning the samples.
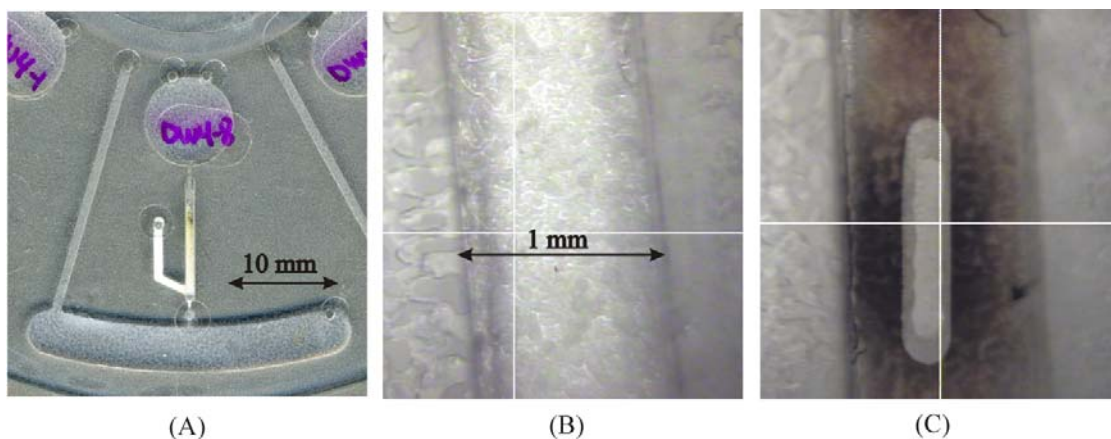
Figure 6-2. (A) Metal-8-Hydroxyquinolates form a thin green band as they are adsorbed on top of the solid phase extraction column. (B) Magnified Packed micro-channel (C) The same channel after laser ablation of the polycarbonate window to expose the sorbent material.

Since the column is covered only by a thin polycarbonate film, the LA system can be used first to directly vaporize the film to expose the sorbent and then to directly sample the trapped metals. Figure 6-2(B) shows the magnified intact column, prior to ablation and Figure 6-2(C) shows the column after the polycarbonate film has been vaporized, revealing the white stationary phase. The corresponding LA-ICP-MS transient signals are shown in Figure 6-3(A)-(D). As well as removing the polycarbonate film, the first LA pass is also useful to remove any dust particle or impurities that could have accumulated on the surface of the column during field sampling and storage. In Figure 6-3(A) and (B), no signal is observed as the polycarbonate film is vaporized but the column remains intact. At the laser power setting used, three consecutive, superimposed ablation scans are necessary to completely remove the polycarbonate film and reach the column material. As illustrated in Figure 6-3(C) and (D), once the laser reaches the column material, the silicon signal from the sorbent material appears in the ICP-MS spectrum as well as the signals for the analytes trapped on top of the column. Complete ablation of the column requires three additional superimposed LA scans (ablations four to six). On the seventh ablation, the silicon signal intensity drops back to baseline indicating that the laser has ablated completely through the column. For data analysis, the sum of the signal areas for the fourth, fifth and sixth ablation was used. Even though the laser is used to vaporize material over

the total length and thickness of the column, widthwise, only about a third (300µm spot size vs. 1000 µm wide column) of the column is sampled as illustrated in Figure 6-2(C). Since only a portion of the column material is ablated, somewhat higher detection limits are expected than if the complete width of the column had been ablated. This could be achieved by using a larger beam, performing additional laser ablation scans or reducing the width of the column. Precision would also be expected to improve if the column was ablated completely as the analyte is not homogeneously distributed on the column as illustrated by the non-uniform green analyte band pictured in Figure 6-2(A).
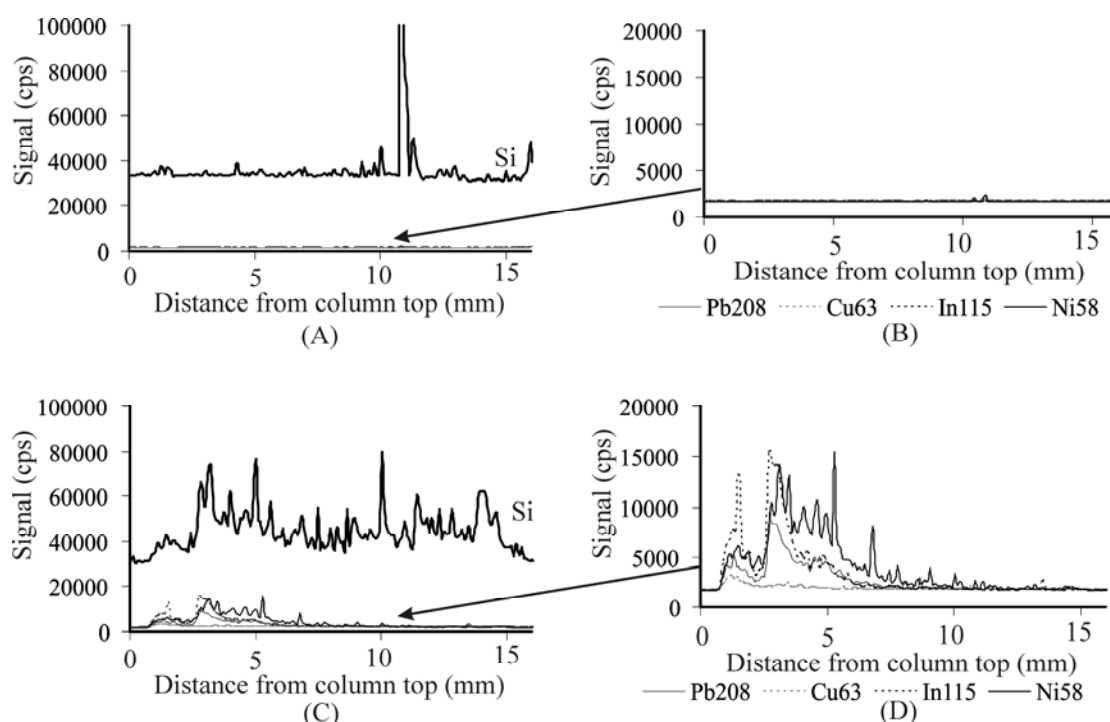
Figure 6-3. LA-ICP-MS transient signals. First ablation scan, only the polycarbonate window is vaporized, so that no signal is observed for either the silicon from the stationary phase (A) or the trapped analytes (B). On subsequent ablation scans, the chromatographic sorbent is vaporized, and a silicon signal is recorded as the laser scans along the length of the column (C). The magnified trace in (D) (ordinate axis) clearly shows that the analytes are trapped on the upper half of the column (left of plot).

Quantification by LA-ICP-MS

Good correlation between analyte signal intensity and concentration was obtained for all the species studied as presented in Table 6-1 and Table 6-2. For

the low concentration EP-L-2 CRM, linear calibration curves were obtained as illustrated in Table 6-1, but analyte concentrations were below the limit of quantitation for this method, although above the detection limit. Since this is a pre-concentration method, the size of the sample can be adjusted depending on the limit of detection of an analyte of interest and the concentrations expected for the type of sample. As expected, detection limits are higher than for conventional solid phase extraction. Table 6-3 compares the detection limits and precision obtained for conventional solution nebulization of pure standards (as specified by the manufacturer) with results obtained using SPE in conjunction with Electrothermal Vaporization - Atomic Absorption Spectrometry (ETV-AAS), Inductively Coupled Plasma - Atomic Emission Spectrometry (ICP-AES) Direct Sample Insertion (DSI) – ICP – AES and Induction Heating (IH) – ETV- ICP – AES. For example, Otero-Romani *et al.*[5] obtained detection limits one order of magnitude lower for Cu, Ni, Pb and V pre-concentrated from commercial C_{18} cartridges working with seawater sample volumes of 100 mL a volume 300 times larger than that used in the present experiment. None the less, this method is sensitive enough to be used as a rapid screening technique and could eliminate the need to transport larger volumes of sample back from the field.

Table 6-1. Pre-concentration of trace metals from drinking water on a centrifugal microfluidic disc

	Certified value tolerance interval (ppm)	Estimated concentration (ppm)[a]	R^2	Replicates standard deviation	LOD[b] (ppb)	LOD[c] (ng)	EPA MCL[d] (ppb)	min sample size[e] (µl)
Low concentration drinking water CRM (EP-L-2)								
^{63}Cu	0.014 - 0.019	*below LOQ[f]*	0.95	6-28 %	15	4	1300	3
^{59}Co	0.008 - 0.012	*below LOQ*	0.98	10-24 %	39	12	-	-
^{58}Ni	0.017 - 0.023	*below LOQ*	0.96	7-19 %	14	4	100	41
^{51}V	0.010 - 0.017	*below LOQ*	0.92	6-29 %	49	11	N/A[g]	-
^{208}Pb	0.000 - 0.010	*below LOQ*	0.996	9-16 %	31	9	15	624
High concentration drinking water CRM (EP-H-2)								
^{51}V	0.32 - 0.47	0.35($\pm$ 0.10)	0.98	17-20 %	2	0.5	N/A[g]	-
^{208}Pb	0.22 - 0.30	0.12($\pm$ 0.03)	0.96	17-33 %	1	0.3	15	76
^{58}Ni	0.28 - 0.40	0.11($\pm$ 0.01)	0.99	26-52 %	0.3	0.1	-	-
^{63}Cu	0.16 - 0.24	0.12($\pm$ 0.08)	0.99	12-28 %	2	0.6	1300	1

[a]Experimental variance is expressed in parentheses. [b]Limit of detection (3σ). [c]Absolute LOD (3σ) based on 300 µL sample [d]Maximum Contaminant Level established by the USEPA.[27] [e]Minimum sample volume required to detect a contaminant at its MCL as established by the EPA. [f]Limit of Quantitation (10σ) [g]Figures on the EPA Drinking Water Contaminant Candidate List.[28]

Difficulties arise in the quantification of high concentration samples because the uncharged metal chelates are very slightly soluble in water. In the EP-H-2 CRM, which contains a large quantity of metals that can form divalent

and trivalent chelates with 8-HQ, it proved impossible to add 8-HQ in excess to guarantee the formation of the metal chelates. For all the extractions, we used an 8-HQ concentration of 7×10^{-4} M, which is similar to the concentration used in other pre-concentration studies reported in the literature.[4, 5, 26] Experiments with higher 8-HQ concentrations were unsuccessful. Dark green particles could be seen floating in solution when the 8-HQ concentration was doubled and at concentrations one order of magnitude greater, a white precipitate forms instantly as the solution pH is adjusted to promote the formation of the neutral chelates. This means that with a concentration of 7×10^{-4} M the ratio of 8-HQ/metal in EP-H-2 is around 3 after the addition of three 10 μL spikes of multi-element standard solution, far from the 100x excess normally preferred for this type of extraction. This low ratio is probably the cause of the quasi systematic underestimation of concentrations in EP-H-2 as listed in Table 6-1. The limit of linearity was reached at the third spike, which corresponded to 0.5 ppm V and 0.2 ppm Pb, Cu, and Ni, after which calibration curves started to negatively deviate from linearity. A comparative study was performed to contrast the magnitude of the signals obtained for lead when extracted from pure aqueous standards with results obtained for the lead extracted from EP-H-2. The calibration curves obtained for both set of standards had similar slopes (10^6 counts / μg Pb), but the signal area obtained for the extraction of the pure lead standards was consistently

approximately 3 times higher than for the EP-H-2 standards. These results indicate that due to the limited amount of 8-HQ available compared to the quantity of analytes in solution in the more concentrated samples, only a portion of the available lead was chelated and subsequently extracted. This solubility issue results in the underestimation of the concentration of metals in very contaminated waters. This problem could be circumvented by the use of another form of 8-HQ, derivatized to increase its solubility, or by the direct immobilization of the chelator on the stationary phase. An artificial high concentration drinking water standard was prepared in which only five elements were present (V, Cu, Ni, Pb and Ca added as matrix specie) in order to increase the 8-HQ/metal ratio to 10 after the addition of three 10 µL multi-element spikes. The results listed in Table 6-2 show an increased recovery for the artificial sample containing fewer analytes.

Internal Standards

The precision and accuracy of any LA experiment is a concern due to the potential for variability in the ablation and transport processes. It is therefore often necessary to use internal standards in LA-ICP-MS. It has been demonstrated[9] that, when ablating chromatographic stationary phases, the silicon present in the sorbent material could be effectively used to improve precision and linearity. However, for this method to be useful, the sorbent material has to be

generally homogeneous and uniform in thickness. As illustrated in **Error! Reference source not found.**(C), the columns manually packed by centrifugal action are not uniform enough for such a purpose. Selection of appropriate internal

Table 6-2. Artificial high concentration drinking water

	Concentration (ppm)	Estimated Concentration (ppm) [a]	R^2	Replicates standard deviation
^{51}V	0.424	0.23($\pm$ 0.19)	0.79	9-38%
^{63}Cu	0.187	0.14($\pm$ 0.07)	0.87	8-35%
^{58}Ni	0.182	0.17($\pm$ 0.03)	0.98	22-39%
^{208}Pb	0.236	-	0.02	16-26%
$^{40}Ca^b$	11.77	-	-	-
$^{51}V/^{115}In$	0.424	0.41($\pm$ 0.07)	0.98	14-32%
$^{208}Pb/^{209}Bi$	0.236	0.08($\pm$ 0.02)	0.98	18-47%

[a]Experimental variance is expressed in parentheses. [b]Calcium was added as concomitant specie to mimic a real sample.

standards is complicated in this technique as the optimal extraction pH varies for different elements. A heavy element, Bi, and a mid-mass element, In, were selected as potential internal standards because they are not likely to be present in a drinking water sample and were absent from the CRMs under study. Furthermore, their chelation pH range with 8-HQ coincides with those of the other

elements under study.[29, 30]   Results shown in Table 6-2 illustrate that internal

standards improve the results for V and Pb. In could be used to both improve the

linearity and the accuracy of the determination when used as an internal

standard for V. In the same determination, the correlation factor for Pb calibration

increased from a mere 0.02 to 0.98 when another heavy element, Bi was used as

an internal standard. However, precision did not improve when an internal

standard was used.

Table 6-3. Comparison of the analytical performance of different water analysis
techniques

Method	Sample volume (mL)	Sample type	Elements analysed	Detection limit range (ppb)	% RSD
Solution nebulization	5	Pure standards	Multi- element	0.001 – 0.01	< 2 %
SPE – ETV –AAS[2]	500	Seawater	Cd, Zn, Cu, Mn, Fe, Ni, Co, Pb	N/A	4 – 25 %
SPE – ICP –AES[4]	500	Seawater	Mn, Cd, Cu, Zn, V, Ni, Pb, Fe	0.02 - 10	0.2 – 7%
SPE – ICP – AES[5]	100	Seawater	Al, Cd, Cu, Fe, Mn, Ni, Pb, Sn, V, Zn	0.001 - 2	0.7 – 8 %
SPE – DSI – ICP – AES[26]	100	Pure standards	Cd, Cu, Fe, Pb, Mn, Zn	0.008 – 0.06	8 – 10 %
SPE – IH – ETV[31]	20	Pure standards	Cd, Pb, Zn	15 - 150	N/A
Current method	0.001 – 0.6	Drinking water	Ni, Cu, V, Pb, Co	0.3 - 49	6 – 52%

CONCLUSIONS

This work demonstrates the potential applicability of novel method for the rapid sample preparation of water samples for LA-ICP-MS analysis on disposable, mass producible microfluidic polymeric devices. The device requires sample volumes which are up to four orders of magnitude smaller than those collected for the conventional SPE-ICP-MS method with an increase in detection limit of only one order of magnitude. Each compact disc shaped extraction device can be used to extract up to eight samples or replicates simultaneously in approximately 20 minutes. Columns can be prepared and sealed prior to field sampling to ease on-site manipulations. The devices also provide a small and convenient container for long term storage of the dry extracts before transport to the laboratory for direct LA-ICP-MS analysis.

ACKNOWLEDGMENT

148

REFERENCES

(1) Papadoyannis, I. N.; Samanidou, V. F. In *Encyclopedia of chromatography*; Cazes, J., Ed.; CRC: Boca Raton, Fl, 2004, pp 250-266.

(2) Sturgeon, R. E.; Berman, S. S.; Willie, S. N. *Talanta* **1982**, *29*, 167-171.

(3) Lancaster, H. L.; Marshall, G. D.; Gonzalo, E. R.; Ruzicka, J.; Christian, G. D. *Analyst (Cambridge, United Kingdom)* **1994**, *119*, 1459-1465.

(4) Abbasse, G.; Ouddane, B.; Fischer, J. C. *Journal of Analytical Atomic Spectrometry* **2002**, *17*, 1354-1358.

(5) Otero-Romaní, J.; Moreda-Piñeiro, A.; Bermejo-Barrera, A.; Bermejo-Barrera, P. *Analytica Chimica Acta* **2005**, *536*, 213-218.

(6) Niemelä, P. *Applied Spectroscopy* **2008**, *62*, 1378-1383.

(7) Dénes, J.; Katona, M.; Hosszu, A.; Czuczy, N.; Takats, Z. *Analytical Chemistry* **2009**, *81*, 1669-1675.

(8) Resano, M.; Garcia Ruiz, E.; Mihucz, V. G.; Moricz, A. M.; Zaray, G.; Vanhaecke, F. *Journal of Analytical Atomic Spectrometry* **2007**, *22*, 1158-1162.

(9) Lafleur, J. P.; Salin, E. D. *Analytical Chemistry* **2008**, *80*, 6821-6823.

(10) Deyl, Z.; Rosmus, J.; Pavlicek, M. *Chromatographic reviews* **1964**, *6*, 19-52.

(11) Nyiredy, S. *Journal of Chromatography A* **2003**, *1000*, 985-999.

149

(12) Madou, M.; Zoval, J.; Jia, G.; Kido, H.; Kim, J.; Kim, N. In *Annual Review of Biomedical Engineering*, 2006; Vol. 8, pp 601-628.

(13) Haeberle, S.; Zengerle, R. *Lab on a chip* **2007**, *7*, 1094-1110.

(14) Penrose, A.; Myers, P.; Bartle, K.; McCrossen, S. *Analyst* **2004**, *129*, 704-709.

(15) Li, H.-F.; Lin, J.-M. *Analytical and Bioanalytical Chemistry* **2009**, *393*, 555-567.

(16) Alvarez-Llamas, G.; Fernandez De La Campa, M. R.; Sanz-Medel, A. *Analytica Chimica Acta* **2005**, *546*, 236-243.

(17) Alvarez-Llamas, G.; Fernandez De LaCampa, M. D. R.; Sanz-Medel, A. *TrAC - Trends in Analytical Chemistry* **2005**, *24*, 28-36.

(18) Hui, A. Y. N.; Wang, G.; Lin, B.; Chan, W. T. *Journal of Analytical Atomic Spectrometry* **2006**, *21*, 134-140.

(19) Pearson, G.; Greenway, G. *Journal of Analytical Atomic Spectrometry* **2007**, *22*, 657-662.

(20) Song, Q. J.; Greenway, G. M.; McCreedy, T. *Journal of Analytical Atomic Spectrometry* **2003**, *18*, 1-3.

(21) Song, Q. J.; Greenway, G. M.; McCreedy, T. *Journal of Analytical Atomic Spectrometry* **2004**, *19*, 883-887.

(22) Lafleur, J. P.; Salin, E. D. *Proceedings of mTAS 2007, Eleventh International Conference on Miniaturized Systems for Chemistry and Life Sciences* **2007**, *2*, 1441-1443.

(23) Weigl, B. H.; Bardell, R.; Schulte, T.; Battrell, F.; Hayenga, J. *Biomedical Microdevices* **2001**, *3*, 267-274.

(24) Bartholomeusz, D. A.; Boutte, R. W.; Andrade, J. D. *Journal of Microelectronic Systems* **2005**, *14*, 1364-1374.

(25) Kido, H.; Zoval, J.; Madou, M. *ECS Transactions* **2006**, *4*, 101-105.

(26) Skinner, C. D.; Salin, E. D. *Journal of Analytical Atomic Spectrometry* **2003**, *18*, 495-500.

(27) *U.S. Environmental Protaction Agency, Drinking Water Contaminants, http://www.epa.gov/safewater/contaminants/index.html,* **2003**.

(28) *U.S. Environmental Protection Agency, Drinking Water Contaminant Candidate List and Regulatory Determinations, http://www.epa.gov/safewater/ccl/ccl2.html,* **2005**.

(29) Minczewski, J.; Chwastowska, J.; Dybczyński , R. *Separation and preconcentration methods in inorganic trace analysis*; Halsted Press: New York, 1982, p. 197.

(30) Sandell, E. B.; Onishi, H. *Photometric determination of traces of metals : general aspects*; Wiley: New York, 1978 pp. 422-425.

(31) Lam, R.; Salin, E. D. *Canadian Journal of Chemistry* **2008**, *86*, 586-589.

Chapter 7 - Miniaturised centrifugal chromatographic platforms for in-field sampling, pre-concentration and spectrometric detection of organic pollutants in aqueous samples

In the previous chapters, a novel device which miniaturizes the Solid Phase Extraction (SPE) process for trace metal analysis was presented. In the method as described in Chapters 5 and 6, dry extracts are stored on the disc devices and brought back to the laboratory for Laser Ablation Inductively Coupled Plasma Mass Spectrometry (LA-ICP-MS) analysis. Although it is much more convenient to bring back to the laboratory eight samples extracted on a disc the size of a regular music compact disc rather than eight 1 L jugs filled with water samples, the transport or shipment of the discs results in delayed analysis results. The possibility of obtaining analysis results directly in the field would greatly ease the monitoring of aquatic pollutants. This can be accomplished by directly coupling the miniature centrifugal chromatographic devices to absorption and emission spectrometers. The extraction can be performed in the field using a simple motor platform in which a light source and detector have been integrated, very similarly to a portable compact disc reader. Fluorescence and absorbance measurements can be obtained directly from an analyte trapped on the column after extraction for the rapid on-site screening of pollutants.

This Chapter presents the direct in-column measurements of the test fluorophore fluorescein and the polycyclic aromatic hydrocarbon anthracene. The results presented in this chapter were published as:

Lafleur, J. P.; Rackov, A. A.; McAuley, S.; Salin, E. D. *Talanta* 2009 (*Manuscript reference number: TAL-D-09-01648R01641*).

Theoretical calculations, additional figures and circuit schematics can be found in Appendix H.

ABSTRACT

Great variations in pollutant concentrations are observed in the environment and pre-concentration is often required to detect trace contaminants in water samples. This paper presents a novel solid phase-extraction device integrated onto a centrifugal microfluidic platform for rapid on-site pre-concentration and screening of organic contaminants in aqueous samples. In-column fluorescence and absorbance measurements are obtained directly from an analyte trapped on the top of a solid phase extraction microcolumn. Results are presented for the representative fluorophore fluorescein and the polycyclic aromatic hydrocarbon anthracene. An absolute detection limit of 20 ng was obtained for anthracene using a simple light emitting diode for fluorescence excitation. One of the main advantages of this device is that only a simple motor is needed to induce liquid flow, making simultaneous on-site extraction and measurement of multiple samples easy while minimizing sample losses and contamination.

INTRODUCTION

Many toxic or potentially harmful pollutants are released into the environment every day as a direct consequence of human activity. Polycyclic Aromatic Hydrocarbons (PAHs), which are widespread by-products of incomplete combustion, are an example of organic pollutants ubiquitous in the environment.

Their presence in our environment predates the industrial era due to such natural causes as forest fires and volcanic eruptions. Their concentrations have increased dramatically as a consequence of the burning of fossil fuels, resulting in increased contamination of water resources. Many PAHs are toxic to aquatic life and several have carcinogenic properties. Anthracene is one of the 16 PAHs selected by the US Environmental Protection Agency (EPA) as priority pollutants.[1]

New analytical tools that can rapidly screen organic pollutants with minimal sample handling are required in order to assess and monitor their fate and impact. A recent review by Li and Lin[2] demonstrates the growing interest in applying microfluidic technologies to environmental analysis. Microfluidic systems are a tool of choice for the analysis of pollutants in the environment because several steps of a chemical analysis can be performed rapidly and directly on the microfluidic platforms. Sample transportation to the laboratory becomes unnecessary, minimizing analysis time, sample losses and contamination.

Microfluidic devices that use centrifugal force to drive the flow of liquids have recently been developed for environmental analyses. LaCroix-Fralish *et al.*[3] recently developed a micro analytical system for the detection of nitrite and Cr(VI) to demonstrate the potential of centrifugal microfluidic systems for on-site (field) analysis of water samples. Lafleur *et al.*[4] also recently introduced a miniature

centrifugal Solid Phase Extraction (SPE) device for the rapid determination of trace metals in water by Laser Ablation (LA) Inductively Coupled Plasma Mass Spectrometry (ICP-MS).

SPE is one of the most commonly used sample preparation techniques for the extraction and pre-concentration of analytes in environmental samples.[5] Since the concentration of PAHs can range from less than 1 ppt in pure groundwater to greater than 1 ppm in heavily contaminated sewage, extraction and pre-concentration are often necessary.[6] PAHs can be extracted by SPE using a reversed phase C_{18} stationary phase column followed by elution with a toluene-methanol mixture.[7] The collected eluate is then analyzed using the appropriate method. However, fluorescence and absorbance measurements could be performed directly on the sorbent material. This has the advantage of reducing the number of sample preparation steps, thereby minimizing risks of sample loss and contamination and reducing analysis time. The elimination of the elution steps also reduces the use of organic solvents which are detrimental to health and the environment.

Several methods have been reported for the direct optical analysis of organic compounds pre-concentrated on stationary phases. In 1984, Guthrie and Jorgenson[8] proposed that a sizable sensitivity advantage could be gained by detecting analyte fluorescence directly on the stationary phase (*in-column*) in

open-tubular capillary liquid chromatography. This increased sensitivity arises from the minimization of dilution effects. Using perylene as a representative fluorophore, they obtained a detection limit of 10 pg. Walbroehl and Jorgenson[9] extended the method to non-fluorescing compounds by designing a UV absorption detector specifically for open tubular capillary electrophoresis, obtaining detection limits of 15 pg for isoquinoline and 250 pg for lysozyme. Carr and Harris[10] obtained detection limits as low as 0.17 parts per trillion for the in-situ detection of the PAH pyrene in 0.96 mm i.d. quartz tubes filled with C_{18} silica by laser fluorescence spectroscopy. More recently, the direct determination of ethylbenzene by Raman spectroscopy directly through the quartz wall of an SPE cartridge has been reported.[11] Laser induced fluorescence (LIF) measurements can also be performed directly on solid phase microextraction fibres (SPME) after 1 to 140 hours exposure allowing determination of PAHs (as total PAH-34) with a detection limit of 2 ng/mL.[12] Methods have also been developed for the direct spectrophotometric detection of benzenic pollutants on polydimethylsiloxane (PDMS) sorbents.[13]

According to Lamotte *et al.*,[13] direct determination methods cannot be expected to give results as precise as those given by chromatographic methods, but they may have valuable applications, particularly for on-site pollution monitoring. We present here a method for obtaining analysis results directly in

the field. Fluorescein and anthracene are extracted and pre-concentrated from water samples on miniature SPE devices where absorbance and fluorescence measurements are performed directly on the sorbent material.

EXPERIMENTAL

Standards and reagents

Octadecylsilane silica gel (Nucleosil C_{18} silica, 100 Å pore size and 10 μm mean particle size) was obtained from Macherey-Nagel (Düren, Germany). Fluorescein [Fluka, Ronkonkoma, NY, USA) was prepared in pH 9.8 buffer. Anthracene (200 μg/mL, 1 mL ampoules in methanol, Supelco, Bellefonte, PA, USA) was prepared in 0.05% Triton X-100 (TX-100, AccusSpec, Baie D'Urfé, QC, Canada). TX-100 was prepared with distilled deionised water (DDW, 18 MΩ, Millipore Co., Bedford, MA, USA).

Device Fabrication

Devices were fabricated using a rapid prototyping technique based on a combination of thin film lamination[14] and xurography[15] developed by Kido *et al.*[16] High aspect ratio features such as reservoirs were created using conventional Computerized Numerically Controlled (CNC) milling (QuickCircuit 5000, T-Tech, Inc. Norcross, GA) of polycarbonate discs (PC) (Blank uncoated CDs and DVDs, 120 mm diameter, 1.2 and 0.6 mm thickness respectively, U-Tech Media Corp., Taiwan) or poly(methylmethacrylate) (PMMA) discs (6.35 mm thick sheets cut to

120 mm diameter discs, Acrylite OP-1, Cyro Industries, Rockaway, NJ, USA). Low aspect ratio features such as channels and vent lines were cut in 100 μm thick adhesive film (FLEXmount DFM-200-Clear V-95 150 poly V-95 400 poly, FLEXcon, Spencer, MA, USA) with a cutting plotter (CE3000MK2-60, Graphtec America, Inc., Santa Ana, CA, USA). Quartz discs (120 mm diameter, Prism Research Glass, Raleigh, NC, USA) were used as top layers in experiments requiring UV excitation. All layers were carefully aligned and pressed firmly together using a hand crank cold laminator (Jet Mounter ML25, Drytac, Concord, ON, Canada). For the fluorescein determination, the centrifugal devices were constructed entirely out of PMMA. For the anthracene determination, the base of the device was made of polycarbonate while the top layer of the device was made out of quartz to ensure maximum transmission in the UV region of the spectrum. The device is illustrated schematically in Figure 7-1.
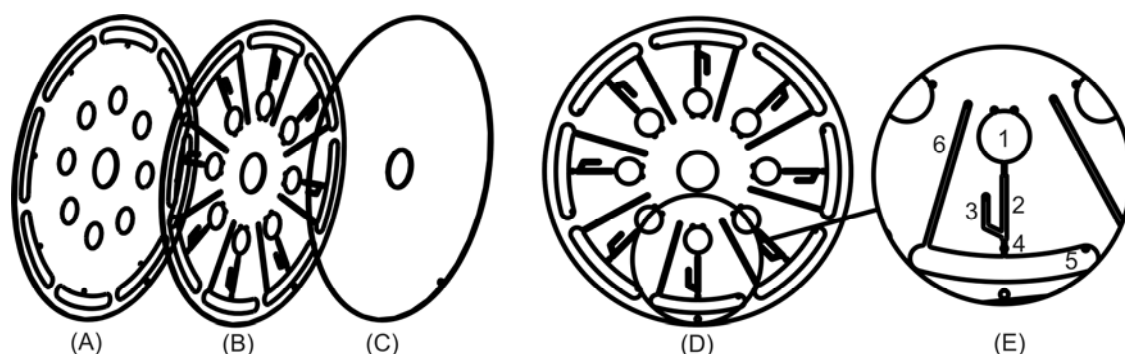
Figure 7-1. (left) Device component layers: (A) PMMA or PC base (the reservoirs are not milled completely through the material). (B) Adhesive layer. (C) Quartz or PMMA top layer. (Right) Device layout: (D) Assembly. (E) Detailed view of the extraction unit: (1) Sample reservoir. (2) Extraction column. (3) Packing channel. (4) Quartz wool frit. (5) Waste reservoir. (6) vent.

Column Packing

The sorbent material was introduced in the columns as a methanol slurry using a micropipette. The column volumes ranged between 1 and 1.5 μL. All slurries were carefully homogenized using a vortex mixer (Maxi-Mix, Barnstead International, Dubuque, IA, USA). Column consolidation was achieved by applying centrifugal force (2000 RPM) using a device built in-house consisting of a permanent magnet type 90 V DC motor (Baldor Motor and Drives, Fort Smith, AR, USA) driven with a motor drive (Penta KB Power, KBPC-240D, TechnoMotion, Montréal, Qc, Canada).

Solid Phase Extraction

Prior to the extraction, the packing was conditioned with 10 μL of methanol to allow resolvation of the sorbent. The column was conditioned for the introduction of the aqueous sample by slowly changing the mobile phase carrier from methanol to pH 9.8 buffer (fluorescein) or 0.05% TX-100 (anthracene). The samples (10 μL aliquots, 4 - 9 ppm fluorescein or 140 μL aliquots, 100 - 300 ppb anthracene) were percolated through the columns at 1800 RPM.

All calibration curves were obtained using the method of external standards with three to five calibration standards for each calibration curve. Replicates were obtained by running 5-8 aliquots of the same sample on different SPE columns. Each column was used only once and contained sufficient packing material to ensure that the maximum loading capacity was not reached.

Spectroscopic Analysis

The discs were mounted on a stage built in-house which allowed scanning along the length of the columns at intervals of 1 mm. Alternately, the discs were mounted on a motorized translation stage (MTS-50 with TDC001 controller, Thorlabs, Newton, NJ, USA) to provide higher resolution scanning of the column. A 600 μm diameter UV-Vis optical fibre (QP600-2-SR, Ocean Optics, Dunedin, FL, USA) was used to illuminate the column with a deuterium tungsten halogen light source (DT mini, Ocean Optics, Dunedin, FL, USA). Alternately, A UV Light

Emitting Diode (255 nm ± 10 nm LED, Seoul semiconductors, Roithner Lasertechnik Gmbh, Vienna, Austria) equipped with a ball lens was used to illuminate the column directly without a fibre optic. Fluorescent light was collected on the front face of the microfluidic device with a 600 µm diameter UV-Vis optical fibre and recorded with a photomultiplier tube (PMT, H5784-04, Hamamatsu, Bridgewater, NJ, USA) equipped with a 320 nm or 400 nm longpass filter. Absorbance was measured simultaneously by placing a third 600 µm diameter UV-Vis optical fibre directly facing the illumination fibre optic, behind the SPE column. Transmission was recorded with a diode array spectrophotometer (USB 4000, Ocean Optics, Dunedin, FL, USA). The detection system layout is illustrated in Figure 7-2.

For the recovery studies, the content of the waste reservoirs were collected after sample extraction/pre-concentration and analysed with a Fluormax-2 spectrofluorometer (Horiba Jobin Yvon, Edison, NJ, USA).
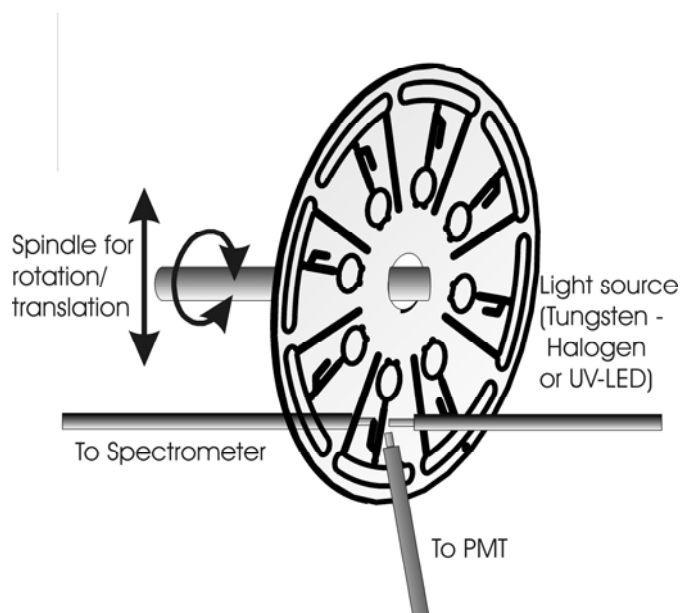
Figure 7-2. Optical detection configuration used for fluorescence and absorbance measurements.

RESULTS AND DISCUSSION

Two practical problems are encountered when analysing PAHs. The first is the low solubility of PAHs in water. The second problem is the adsorption losses encountered during storage. For these reasons, Certified Reference Materials (CRMs) are not available for PAHs in water.[17] Hertz *et al.*[18] showed that adsorption losses in 1 ppb PAH solutions could reach 80% after 4 hours of stirring in a glass container. Solubility is often increased by the addition of organic modifiers to the solvent. Ratios ranging from 2:98 to 0.3:99.7 acetonitrile-water can be used during pre-concentration.[19,20] Alternatively, it has been

demonstrated that non-ionic surfactants (such as Brij-35) at concentrations greater than the critical micelle concentration can be used to both increase the solubility and diminish the loss of PAH by adsorption on polymeric material.[21] Guha *et al.*[22] also showed that PAH solubility could be enhanced in micellar solutions of TX-100 and that solubility increased with surfactant concentration. In this study, we have used the non-ionic surfactant TX-100 to increase anthracene solubility in water and to reduce the losses by adsorption on the polymeric disc material. A longpass filter was used to reduce the broad emission peak of Triton X-100 centered at 300 nm.

Simultaneous front face fluorimetry and absorbance measurements were obtained for fluorescein using the optical set-up illustrated in Figure 7-2 while only fluorescence was monitored for anthracene. The experimental procedure is illustrated schematically in Figure 7-3(A) for fluorescein. The resulting extracted fluorescein is visible to the naked eye as a bright yellow slug concentrated on the top of the column pictured in Figure 7-3(B). The resulting fluorescein fluorescence signal recorded along the length of the column is shown in Figure 7-4(A). The signal is markedly higher at the top of the column, where the fluorescein is concentrated. The fluorescein absorbance signal recorded along the length of the column is shown in Figure 7-4(B), again exhibiting a marked

increase in absorbance at the top of the column, where the fluorescein is concentrated.

Recovery studies showed a 98% trapping efficiency when a 300 ppb anthracene sample is percolated through the miniature SPE column. As shown in Figure 7-3(B), some of the analyte travels along the walls of the column. This is due to some inhomogeneities in the packing along the column walls.
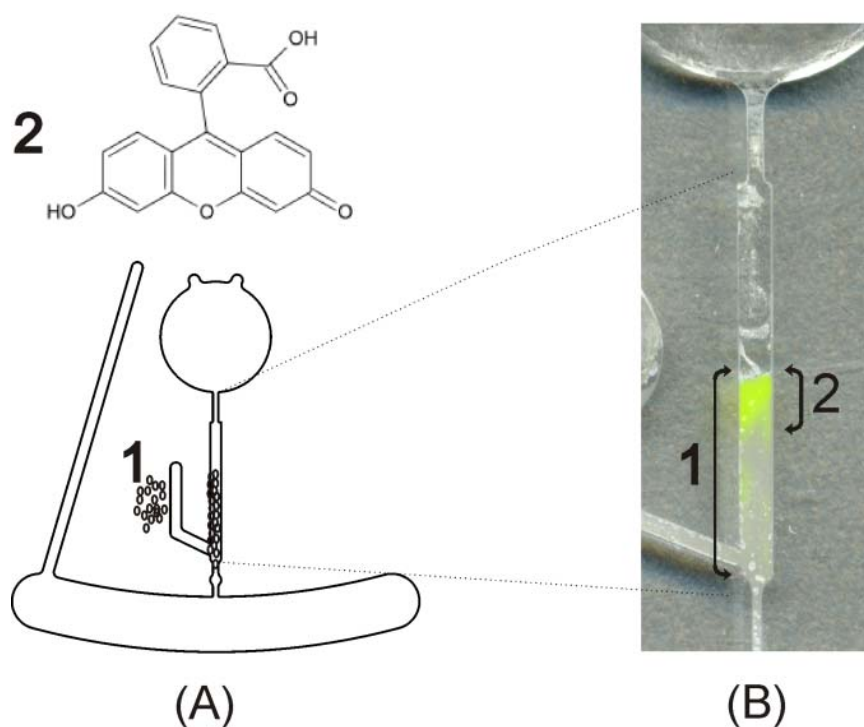
Figure 7-3. (A) Simplified experimental procedure: (1) the column is packed with C$_{18}$ functionalized silica gel and (2) fluorescein is added to the column. (B) Fluorescein trapped on a centrifugal solid phase extraction unit: (1) Packed column. (2) Fluorescein.
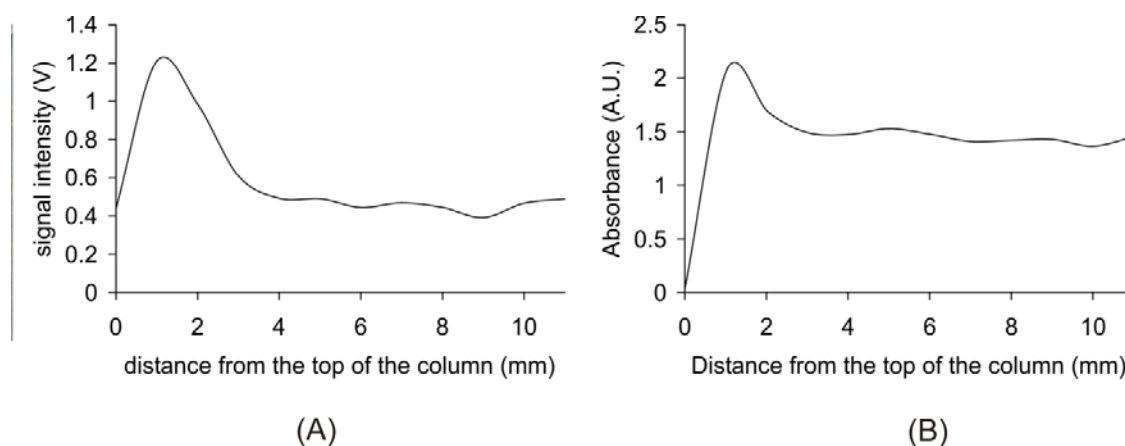
Figure 7-4. (A) Fluorescein fluorescence with halogen lamp excitation recorded with a PMT equipped with a 400 nm longpass filter. (B) Fluorescein absorbance with halogen lamp excitation recorded at 494.13 nm with a photodiode array spectrometer.

Calibration results are listed in Table 7-1. Although it is expected that fluorescence would result in a lower limit of detection than absorbance, the autofluorescence of PMMA, affected the precision of the fluorescein fluorescence measurements due to high blank fluorescence. This is a common drawback with using polymeric materials in spectrometric analyses.

Table 7-1. Calibration results for the direct determination of organic molecules trapped on a miniature centrifugal SPE platform.

	Fluorescein		Anthracene
	Absorbance	*Fluorescence*	*Fluorescence*
R^2	0.99 [a]	0.99 [a]	0.94 [b]
Least square equation	y = 13.2x – 0.03	y = 13.8x +0.03	y = 0.014x – 0,20
Precision	19-26 % [c]	13 - 35 % [c]	7 – 15 % [d]
Limit of detection [c,d]	5 mg·L^{-1} (50 ng)	5 mg·L^{-1} (50 ng)	1 mg·L^{-1} (20 ng)
Limit of linearity[d]	9 mg·L^{-1} (0.09 µg)	9 mg·L^{-1} (0.09 µg)	140 µg·L^{-1} (20 ng)

[a] N = 4 standards. [b] N = 3 standards. [c] M = 5 - 7 replicates. [d] M = 3 - 7 replicates [c] LOD calculated as 3 x standard deviation of the blank. [d]Absolute mass detection limits and limits of linearity are expressed in parentheses for 10 µL and 140 µL samples of fluorescein and anthracene, respectively."

For anthracene, an in-column fluorescence detection limit of 140 µg·L^{-1} (absolute LOD of 20 ng for a 140 µL sample) was obtained. The system behaves as predicted by a theoretical model with a detection limit only one order of magnitude greater than calculated for the ideal model [23]. Although this technique obviously cannot compete in sensitivity and selectivity with conventional SPE

used in conjunction with chromatographic separation, it should find its use for the rapid monitoring of some pollutants. Label free deep-UV fluorescence detection in microfluidic devices is the object of considerable interest as demonstrated by a 2009 review by Schulze and Belder.[24] UV-LEDs provide relatively good sensitivity, as demonstrated above, but their power is too low to provide excellent detection limits for the analysis of PAHs. The UV-LED used for the determination of anthracene above has a maximal 0.150 mW power output. A laser source, which can emit monochromatic light with a high intensity could be used to increase the linear range of the method and lower the detection limits achievable. For example, Kuijt *et al.*[25] used the light from a quadrupled Nd-YAG NanoUV laser emitting at 266 nm with an average power of 5.4 mW to detect PAHs in capillary Electrophoresis with 2-6 ppb detection limits. Using this more powerful light source, detection limits should be reduced by a factor of approximately 40, matching those obtained by Kuijt *et al.*[25] More powerful lasers are available but may not be suitable for field work.

As for selectivity issues, many PAHs have very distinctive fluorescent bands and multivariate calibration techniques can be used in the cases of overlapping spectra. Vilchez *et al.*[26] developed an auxiliary equation system in which the overlapping fluorescence contribution of the PAHs benzo[a]pyrene, benzo[a]anthracene and pyrene could be obtained, allowing their determination

by Synchronous Solid-phase spectrofluorimetry. Algarra *et al.*[27] have also shown that it is possible to determine several PAHs by synchronous direct fluorescence analysis and by front-face fluorimetry on a sorbent using partial least square analysis.[20] Also, in a more sophisticated design, separations should be possible on the SPE column after pre-concentration by addition of an appropriate amount of eluent. In this case, analytes would be separated physically on the column, without being eluted and scanning along the column would allow the quantification of the analytes.

CONCLUSIONS

It has been demonstrated that organic molecules, such as fluorescein and the PAH anthracene, can be trapped on miniature centrifugal chromatographic devices for rapid on-site extraction and detection. Fluorescence and absorbance measurements can be carried out directly and simultaneously on the sorbent material for rapid screening. The system performed as predicted by a theoretical model. The precision and sensitivity cannot compete with laboratory based methods of analysis, but the method has potential for the rapid on-site screening of contaminants.

AKNOWLEDGMENTS

REFERENCES

(1)   *U.S.   Environmental   Protection   Agency,
        http://www.epa.gov/waterscience/methods/pollutants.htm* 2008.

(2)   Li, H.-F.; Lin, J.-M. *Analytical and Bioanalytical Chemistry* 2009, *393*, 555-
        567.

(3)   LaCroix-Fralish, A.; Clare, J.; Skinner, C. D.; Salin, E. D. *Talanta* 2009, *80*,
        670-675.

(4)   Lafleur, J. P.; Salin, E. D. *Journal of Analytical Atomic Spectrometry* 2009,
        24, 1511-1516

(5)   Gilbert-López, B.; García-Reyes, J. F.; Molina-Díaz, A. *Talanta* 2009, *79*,
        109-128.

(6)   Smith, S. R.; Tanaka, J.; Futoma, D. J.; Smith, T. E.; Leenheer, J. A.;
        Thurman, E. M.; Malcolm, R. *Critical Reviews in Analytical Chemistry*
        1981, *10*, 375 - 425.

(7)   Patnaik, P. In *Handbook of environmental analysis : chemical pollutants in
        air, water, soil, and solid wastes*; CRC/Lewis Publishers: Boca Raton,
        1997, pp 167.

(8)   Guthrie, E. J.; Jorgenson, J. W. *Analytical Chemistry* 1984, *56*, 483-486.

(9)   Walbroehl, Y.; Jorgenson, J. W. *Journal of Chromatography A* 1984, *315*,
        135-143.

(10)   Carr, J. W.; Harris, J. M. *Analytical Chemistry* 1988, *60*, 698-702.

(11)   Niemelä, P. *Applied Spectroscopy* 2008, *62*, 1378-1383.

(12)   Hawthorne, S. B.; St Germain, R. W.; Azzolina, N. A. *Environmental
        Science and Technology* 2008, *42*, 8021-8026.

(13)   Lamotte, M.; Fornier De Violet, P.; Garrigues, P.; Hardy, M. *Analytical and
        Bioanalytical Chemistry* 2002, *372*, 169-173.

(14)   Weigl, B. H.; Bardell, R.; Schulte, T.; Battrell, F.; Hayenga, J. *Biomedical
        Microdevices* 2001, *3*, 267-274.

(15)   Bartholomeusz, D. A.; Boutte, R. W.; Andrade, J. D. *Journal of Microelectronic Systems* **2005**, *14*, 1364-1374.

(16)   Kido, H.; Zoval, J.; Madou, M. *ECS Transactions* **2006**, *4*, 101-105.

(17)   Bercaru, O.; Ricci, M.; Ulberth, F.; Brunori, C.; Morabito, R.; Ipolyi, I.; Sahuquillo, A.; Rosenberg, E. *TRAC Trends in Analytical Chemistry* **2009**, *28*, 1073-1081.

(18)   Hertz, H. S.; May, W. E.; Wise, S. A.; Chesler, S. N. *Analytical Chemistry* **2008**, *50*, 428A-434A.

(19)   Lim, L. W.; Okouchi, Y.; Takeuchi, T. *Talanta* **2007**, *72*, 1600-1608.

(20)   Algarra, M.; Jimenez, V.; Fornier de Violet, P.; Lamotte, M. *Analytical and Bioanalytical Chemistry* **2005**, *382*, 1103-1110.

(21)   Brouwer, E. R.; Hermans, A. N. J.; Lingeman, H.; Brinkman, U. A. T. *Journal of Chromatography A* **1994**, *669*, 45-57.

(22)   Guha, S.; Jaffe, P. R.; Peters, C. A. *Environmental Science & Technology* **1998**, *32*, 930-935.

(23)   Lafleur, J. P. Ph.D. Thesis, McGill University, Montreal, 2009, pp. 150-185.

(24)   Schulze, P.; Belder, D. *Analytical and Bioanalytical Chemistry* **2009**, *393*, 515-525.

(25)   Kuijt, J.; Garcia-Ruiz, C.; Stroomberg, G. J.; Marina, M. L.; Ariese, F.; Brinkman, U. A. T.; Gooijer, C. *Journal of Chromatography A* **2001**, *907*, 291-299.

(26)   Vilchez, J. L.; Del Olmo, M.; Avidad, R.; Capitan-Vallvey, L. F. *Analyst* **1994**, *119*, 1211-1214.

(27)   Algarra, M.; Radin, C.; Fornier De Violet, P.; Lamotte, M.; Garrigues, P.; Hardy, M.; Gillard, R. *Journal of Fluorescence* **2000**, *10*, 355-359.

Chapter 8 - Conclusions and suggestions for future work

Several hybrid analytical techniques for environmental analysis were developed. All the techniques investigated share the following advantages:

- They reduce the number of steps required for an analysis, minimizing the potential of contamination and sample losses.

- They avoid, or minimise, the use of organic solvents which are noxious to health and the environment.

- They require only micro amounts of sample, facilitating automation and the processing of multiple samples in parallel.

- They reduce the time required to complete an analysis, from sampling to determination.

In Chapter 2, it was demonstrated that the IH-ETV can be coupled to an ICP-MS to rapidly determine mercury concentrations in single human hair strands. The results obtained suggest that IH-ETV-ICP-MS could possibly be used for routine hair analysis for mercury. Further work[1] has demonstrated that the IH-ETV-ICP-MS was also suitable for the direct determination of As, Cd, Cu, Hg, Pb and Zn in sub-milligram amounts of solid hair material. Additional work[2] demonstrated that the IH-ETV could also be coupled to atomic absorption and fluorescence spectrometers for in-field monitoring. However, further work is required to explore how the excellent temperature control offered by the IH-ETV

(demonstrated in Appendix A) can be used to perform thermal speciation of species such as mercury and methylmercury, increasing the versatility of the technique.

In Chapter 3, a new separation and analysis technique was reported in which LA-ICP-MS is directly coupled to HPTLC for chromium speciation analysis. This hybrid technique allows the rapid separation and determination of chromium species in microlitre volumes of contaminated water samples. Although results have shown that precision could be improved by the use of the silicon present in the stationary phase as an internal standard, some avenues still need to be explored in order to improve the results achievable. The application of the samples as horizontal bands using automated equipment and an increase in the laser beam size to spot area ratio could potentially be used to improve precision and detection limits, respectively, for this method.

Centrifugal microfluidic solid phase extraction devices for the pre-concentration of metal chelates (Chapters 5 and 6) and PAHs (Chapter 7) were initially developed in Chapter 4. Although the rapid prototyping technique presented in Chapter 4 is attractive because it does not use expensive fabrication or clean room facilities, it is obvious that several difficulties encountered could have been avoided by using techniques which allow a better control over the dimensions of the channels created. Not only could smaller

restriction channels have been created to retain the packing inside the column more effectively, but precisely ordered stationary phase coated etched micropillars[3] could have replaced the traditional HPLC packing in the columns. With higher quality columns, the versatility of the technique could be extended to include actual separations. The centrifugal microfluidic devices created were interfaced to LA-ICP-MS (Chapters 5 and 6), fluorescence (Chapter 7) and absorption spectrometry (Chapter 7). The results obtained for the pre-concentration of metal chelates in Chapters 5 and 6 are promising. As well as reducing the size of the sample required for an analysis by several orders of magnitude and allowing the processing of multiple samples in parallel, the device can be used as a small and convenient container for the storage of multiple samples prior to transport to the laboratory for direct LA-ICP-MS analysis. When coupled to molecular absorbance or fluorescence in Chapter 7, the hybrid technique can be used to obtain analysis results directly in the field. Although it can be estimated that the detection limit achievable could be improved by using a more powerful light source, such as a laser, this still needs to be demonstrated through experimentation. The precision of the centrifugal microfluidic devices, used in conjunction with either LA-ICP-MS or molecular absorbance and fluorescence could greatly benefit from having a better control of the size of the features designed on the microfluidic devices.

REFERENCES

(1)   Lam, R.; Salin, E. D. *Journal of Analytical Atomic Spectrometry* **2007**, *22*, 1430-1433.

(2)   Duford, D. A.; Lafleur, J. P.; Lam, R.; Skinner, C. D.; Salin, E. D. *Journal of Analytical Atomic Spectrometry* **2007**, *22*, 326-329.

(3)   Mery, E.; Ricoul, F.; Sarrut, N.; Constantin, O.; Delapierre, G.; Garin, J.; Vinet, F. *Sensors and Actuators, B: Chemical* **2008**, *134*, 438-446.

Appendix A - Optimization of the Inductively Heated – Electrothermal Vaporizer (IH-ETV) for hair analysis

This appendix presents the work that led to the publication of the article reproduced in Chapter 2. The temperature calibration of the IH-ETV is described as well as the initial cup design and preliminary results on thermal speciation.

INTRODUCTION

When power is applied to the IH-ETV, the alternating current in the work coil sets up an electro-magnetic field, inducing Eddy currents that heat the cup without any physical contact. The graphite cup inserted at the center of the induction coil is illustrated in Figure A-1. The temperature of the graphite cup is controlled by varying the applied power with a variable transformer. The temperature of the graphite cup is assumed to be the temperature of the sample. Since methylmercury is known to be more volatile (boiling point: 92 °C) than in its inorganic form (boiling point: 357 °C), a precise temperature profile of the IH-ETV could potentially be used to thermally speciate mercury. Methylmercury can bioaccumulate and is much more detrimental to health than inorganic mercury.
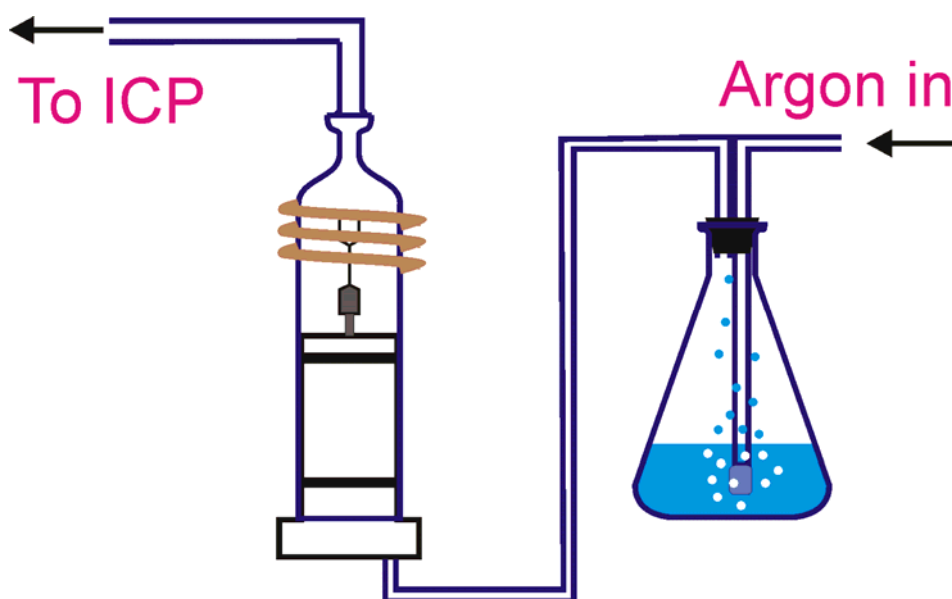
Figure A-1. Induction Heating-Electrothermal Vaporizer

EXPERIMENTAL

Graphite cups

In the initial experiments, the cup-shaped graphite probes illustrated in Figure A-2 were machined in-house from 3/8-inch diameter graphite rod stock (HLM grade, SGL carbon group, Speer Canada Inc., St-Laurent, QC, Canada) using high-speed tools on a benchtop lathe (Emco Compact 5, Emco Maier, Columbus, OH, USA). In later experiments, commercially available graphite cups along with boiler caps were used (type S-16 and BC-1, Bay Carbon Inc., Bay City, MI, USA).

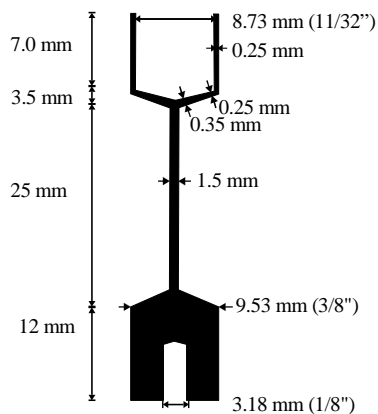Figure A-2. Dimensions of the graphite cup machined in-house

Temperature calibration

The temperature of the machined graphite cups corresponding to different voltage settings on the variable transformer has been calibrated with a K-type infrared thermocouple (Omega IRt/c series model OS37-CF-K, Omega Engineering, Laval, QC, Canada) equipped with a 6.0 mm aperture. The IR thermocouple was protected from humidity by wrapping it in a thin film of polyethylene that does not absorb infrared radiation (Glad Cling Wrap, Clorox Company of Canada, Toronto, ON, Canada). Prior to its use, the IR thermocouple was calibrated on a piece of graphite heated to various temperatures on a hot plate. The "real" temperature of the graphite block was measured by a type K thermocouple brought in contact with the graphite through thermally conductive cement (Omegabond 700, Omega Engineering, Laval, QC, Canada).

Once the linearity and stability of the system had been established with the infrared thermocouple, the temperature of commercial graphite cups and their boiler caps was determined using temperature indicating pellets and lacquers (PLT-0231, PLT-0575, PLT-1200, LAQ-225G and LAQ-1000G, Omega Engineering, Laval, QC, Canada).

Detectors

Results from the machined electrodes were obtained with a Perkin-Elmer SCIEX Elan 5000 ICP-MS system (SCIEX, Concord, ON, Canada). Results from the commercial electrodes with boiler caps were obtained with a Perkin-Elmer SCIEX Elan 6000 ICP-MS system (SCIEX, Concord, ON, Canada). The samples were transported to the detector by an argon gas stream flowing at 500 ml$\cdot$min^{-1} through PTFE tubing. Typical operating values were used for the other parameters of the ICP-MS.

RESULTS AND DISCUSSION

Temperature calibration

The IH-ETV was calibrated for temperatures between 100 and 750 °C. As seen from Figure A-3, the temperature of the graphite cups is directly proportional to the applied power (variac setting). Figure A-4 reveals that, in

most cases, it takes roughly 20 seconds to reach a steady temperature which

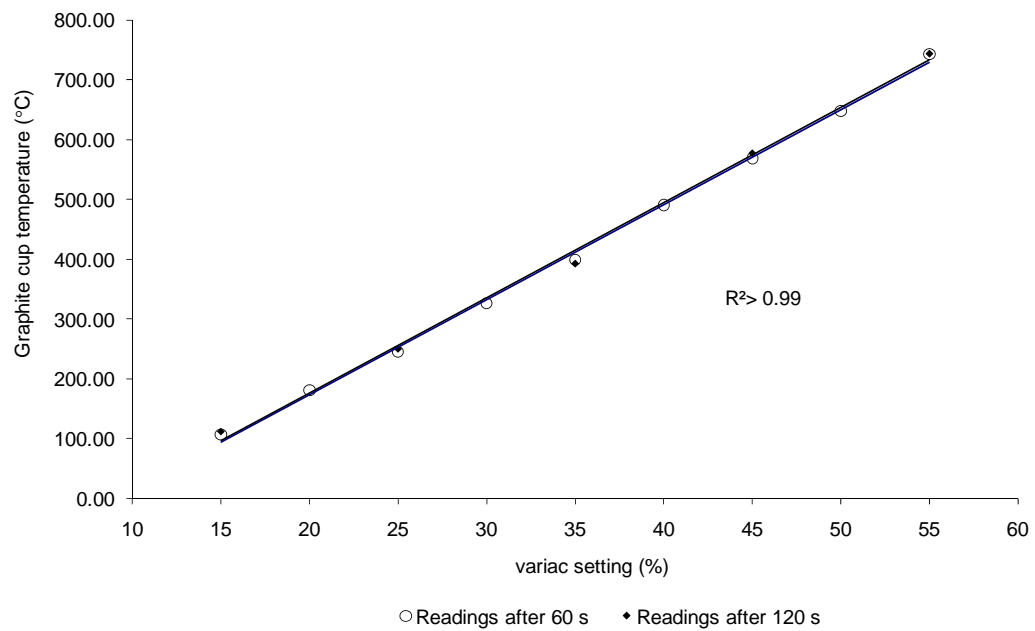then remains constant (+/- 3 % maximum over 2 minutes).

Figure A-3. Temperature calibration of the IH-ETV (readings recorded 60 and
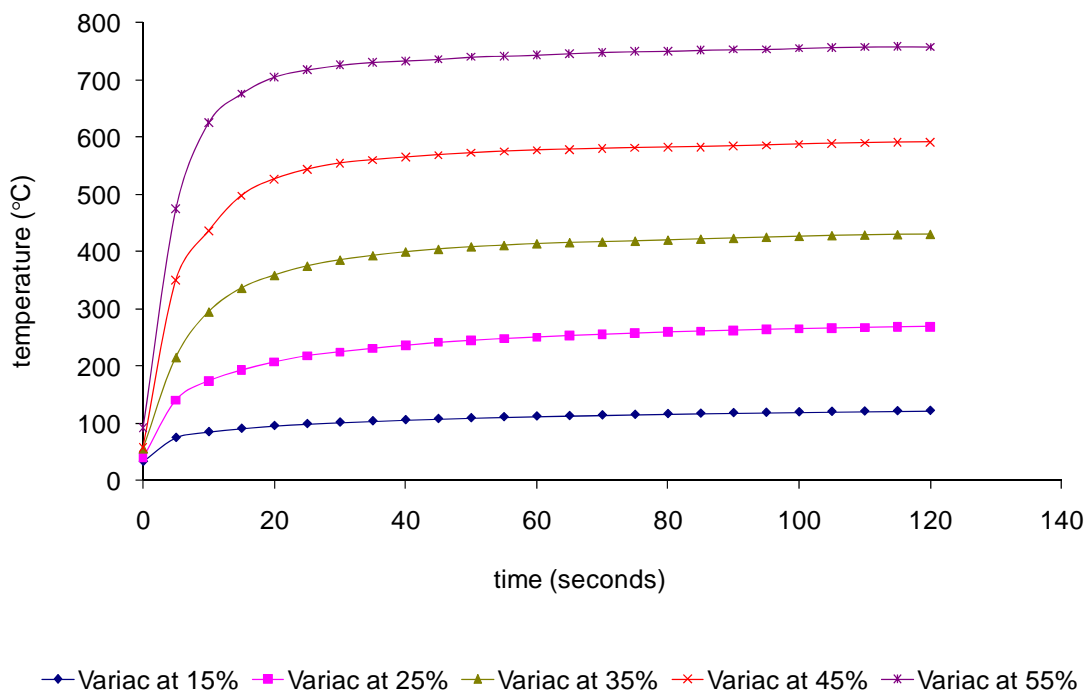
120 seconds after applying power)

Figure A-4. Time dependence of the graphite cup temperature for various final temperature settings

Cup Design

The preliminary experiments for this study were performed using graphite electrodes machined in-house, as illustrated in Figure A-2. This cup gave poor reproducibility for both types of sample, strands and powders. Both samples tended to escape from the cup before being vaporized, leading to poor results. In the case of the hair strands, intact hair strands were often found lying, intact, at the bottom of the quartz chamber after power was applied. For the powdered sample, most trials resulted in a dousing of the plasma due to the large amount

of unvaporized material swept out of the cup by the argon carrier gas. When the plasma did not extinguish, very broad transient profiles were observed (up to 100 seconds).

In later experiments, commercial electrodes with a boiler cap were used. A boiler cap is a graphite cover that fits over the sample cup, preventing unvaporized sample from escaping the cup when carrier gas and heating is applied. A small hole at the top of the cap allows the vaporized sample to exit.
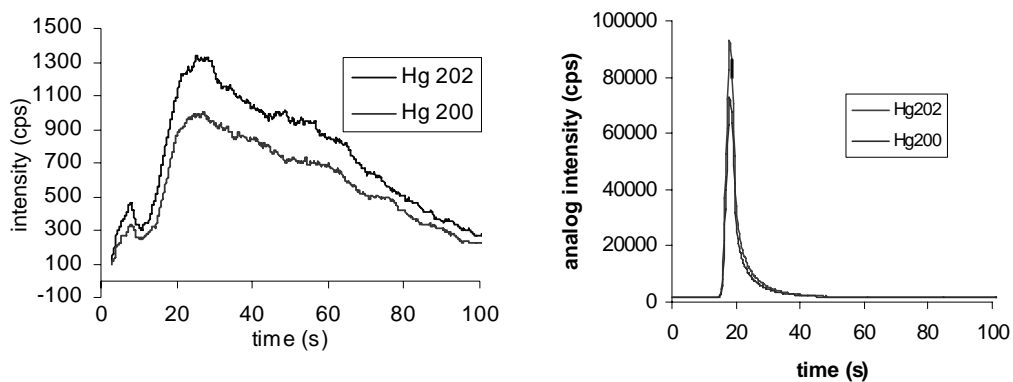
Figure A-5. Left: Powdered CRM signal profile vaporized from a cup with no boiler cap (Acquired by Josiane Lafleur). Right: Powdered CRM signal profile vaporized from a cup with a boiler cap (Acquired by Rebecca Lam).

As seen in Figure A-5, the addition of a boiler cap resulted in much narrower and sharper signal profiles. Good precision (< 4%) was achievable with the boiler caps.

Thermal Speciation

Experiments with temperature programming, shown in Figure A-6, shows that some mercury is released at temperatures lower than the boiling point of inorganic mercury. This indicates that some other, more volatile form of mercury, such as methylmercury, may be present in the sample. The temperature is set higher than the actual boiling points of the compounds to compensate for the fact that the IH-ETV requires some time to reach its set temperature. At a vaporization temperature of 195°C, a temperature well below the 357°C boiling point of inorganic mercury, some mercury is vaporized as shown in Figure A-6. This could only come from some other, more volatile, form of mercury, such as methylmercury which boils at 92°C. When the temperature is increased to 830°C, all the remaining mercury is released, resulting in the large signal observed in Figure A-6. No calibration was attempted because of the lack of data on the amount of methylmercury present in the hair strands analyzed.
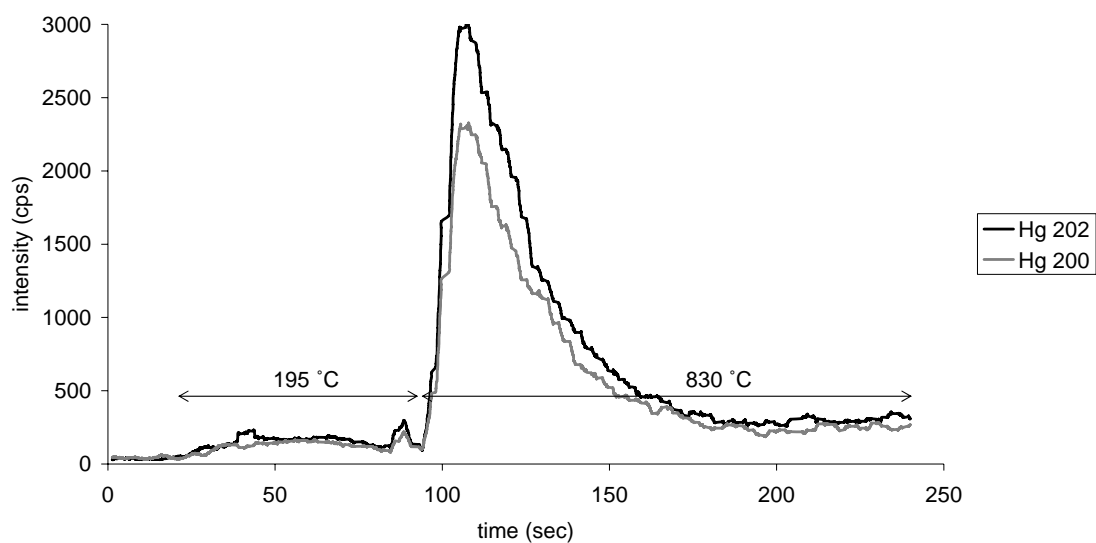
Figure A-6. IH-ETV temperature programming

CONCLUSIONS

We have demonstrated that the temperature of the graphite probe varies linearly with applied power and that this feature could be used to vaporize mercury in solid samples.

Appendix B - Determination of mercury with an Inductively Heated-Electrothermal Vaporizer coupled to an atomic absorption spectrophotometer

In Chapter 2 it was demonstrated that the Inductively Heated – Electrothermal Vaporizer (IH-ETV) could be used for direct analysis of mercury in human hair strands when combined with Inductively Coupled Plasma – Mass Spectrometry (ICP-MS) detection. The primary disadvantage of using IH-ETV-ICP-MS for mercury analysis is its costly and bulky detection system. To overcome this problem, we investigated the use of the IH-ETV as a sample introduction device for Atomic Absorption Spectrometry (AAS). The AAS offers the potential for a much more compact and less expensive instrument which could easily be made field portable. In this Appendix, we demonstrate that the IH-ETV effluent can be successfully used as an input for a Cold Vapour type AAS system which does not have the atomization capability of an ICP. It was found that this new hybrid system provides nanogram detection limits for mercury and that signal flicker (sample introduction imprecision) limited its signal-to-noise ratio.
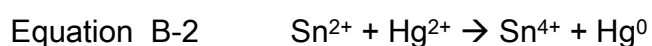
INTRODUCTION

Atomic absorption spectrometry is based on the absorption of radiation by neutral, ground state atoms produced by an atomizer. The Beer-Lambert law gives the linear relationship between concentration (c) and absorbance (A):

Equation B-1 $A = \varepsilon bc$

Where ε is the molar absorptivity and c the pathlength through the sample. The Beer-Lambert law is a limiting law, so that the direct relationship does not hold true for all concentration ranges and at all absorbance wavelengths. In solutions, deviations can occur at high concentrations where interactions between molecules can cause changes in charge distributions. The matrix can also cause such changes as well as shifts in equilibrium. Also, strict adherence to Beer-Lambert law is observed only for true monochromatic radiation.

Two types of atomizers are conventionally used to provide the atomic vapour, flame atomizers and electrothermal atomizers. Electrothermal atomizers generally provide two orders of magnitude better detection limits than flame atomizers due to the longer residence time of the analyte in the optical path and to the relatively small dilution of the atomic vapour by the atomizer gas. However, for mercury, the cold vapour generation technique is usually favoured. Mercuric

ions in solution are reduced by $SnCl_2$, to form metallic mercury, which has a considerable vapour pressure at room temperature. A carrier gas transports the mercury vapour to an absorption cell for detection.

Equation B-2 $\qquad Sn^{2+} + Hg^{2+} \rightarrow Sn^{4+} + Hg^0$

The IH-ETV is proposed as a sample introduction device for AAS. A mercury standard deposited inside a graphite cup is inserted at the center of the IH-ETV induction coil. The atomic vapour is produced when the alternating current in the induction coil sets up an electromagnetic field, producing eddy currents that heat the cup without any physical contacts. The atomic vapour produced is then transported to a long path absorption cell by an argon stream for detection.

EXPERIMENTAL

IH-ETV sample introduction system

The IH-ETV system used in this experiment is described in detail in Appendix A.

Mercury vapour atomic absorption detector

The detection system was built in-house inside a plywood box and is schematically illustrated in Figure B-1. The equipment consisted of a 20 cm

glass cell equipped with two quartz windows. Ultra-smooth inner surface tubing (Tygon® 3350 Sanitary Silicone tubing, Saint-Gobain Performance Plastics, Paris, France) was fitted on both sides of the cell to provide Hg/Ar circulation. A quartz lens with a 6.5 cm focal length collected the light from a mercury pen lamp (Mercury Pen-Ray Lamp equipped with a Model PS-1 power supply, UVP, Upland, CA, USA) and collimated it so it traversed the cell. On the other side of the cell, a second quartz lens collected the light and focused it on a 25 mm^2 UV-enhanced silicone photodiode (NT 54-037, Edmund Industrial Optics, NJ, USA) equipped with a 254 nm filter. The lenses were aligned in such a way that all radiation passing through the cell was parallel, resulting in uniform pathlengths. All lens mounts and cell mounts were affixed inside the box to avoid any movement of the parts. The box was equipped with a double cover and all holes and cracks were sealed. Due to the high temperature attained by the mercury pen lamp, holes were drilled in the source compartment to avoid overheating.
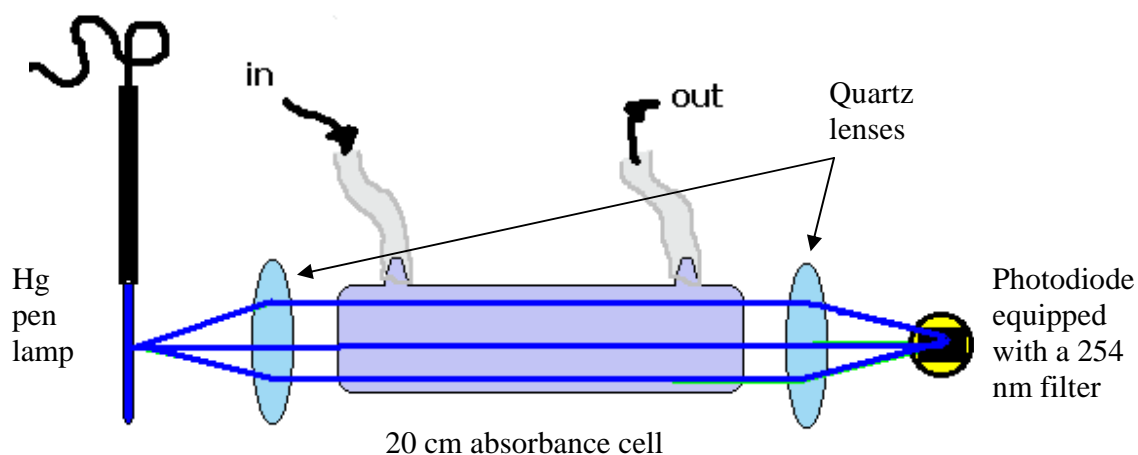
Figure B-1. Layout of the mercury vapour atomic absorption system.

The silicone photodiode detector was used in unbiased mode and the circuit schematic is shown in Figure B-2. A load resistance (R) of 220 KΩ was used to ensure that its value would be much smaller than the value of the shunt resistance of the photodiode (30 MΩ). A 1.0 µF capacitor (C) was added in parallel to the load resistance to provide a low pass filter with a time constant (τ = RC) of 0.22 seconds, and a response time (τ = 5RC) of 1.1 seconds. This is reasonable considering that the smallest signal observed lasted approximately 7 seconds, so that τ is never greater than one tenth of the time duration of the transient signal.
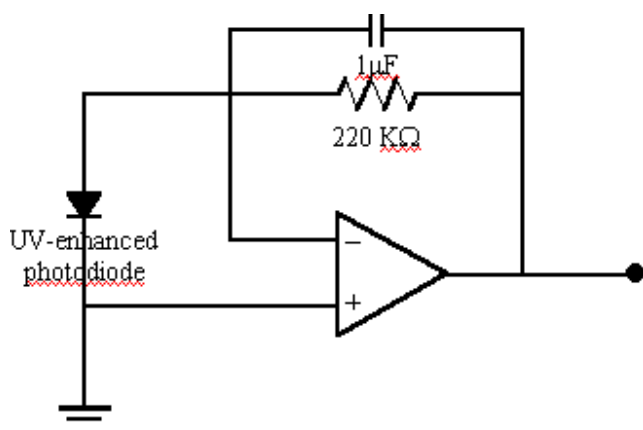
Figure B-2. Unbiased photodiode circuit.

The transient signals were recorded as voltages using a strip chart recorder (Fisher Recordall series 5000, Model B5217-5I, Houston Instruments, Houston, Texas, USA) or with a digital multimeter (Fluke 10, John Fluke Mfg. Co., Everett, WA, USA).

Standards and reagents

Standard solutions were prepared by consecutive dilutions of an Hg stock solution, (PlasmaCal, SPC Science, Champlain, NY, USA) with 1% trace metal grade nitric acid (TraceSelect, Fluka Chemica, Buchs, Switzerland) in 18 MΩ distilled deionized water (Milli-Q water system, Millipore Corp., Bedford, MA, USA). All standards were stored in polypropylene containers (Nalgene, USA) that had been preconditioned with 10 % trace metal grade nitric acid for a period of 24 h and rinsed with distilled deionized water.

191

RESULTS AND DISCUSSION

Dark signal measurement and light leakage

The dark signal of the detector was measured, to determine if noise in the electronics was likely to be a problem. The dark signal was measured with the room lights on and off in order to determine if room light leakage occurred. In Figure B-3, a slight voltage drift is observed when the signal is measured immediately after the detector has been turned ON. However, the signal stabilized after approximately 5 minutes, after which the readout resolution of the digital multimeter is too low to distinguish any change in the signal. From the same figure it is also observed that the presence of the room lights does not affect the signal measured. The quantization uncertainty is due to the finite resolution of the multimeter and can be estimated by:

Equation B-3 $\sigma_q = 0.29q$

Where q is the quantization level readout resolution.

$\sigma_q = 0.29q = 0.29 * 0.001 \text{ volt} = 0.00029 \text{ volts} \sim 0.3 \text{ mV}$

Since no noise was seen in the readout signal, measurements are limited by the readout resolution, $\sigma_q = q/2 = 0.0005$ V. The detector was left on for the entire duration of the experiment to avoid the initial signal drift observed.
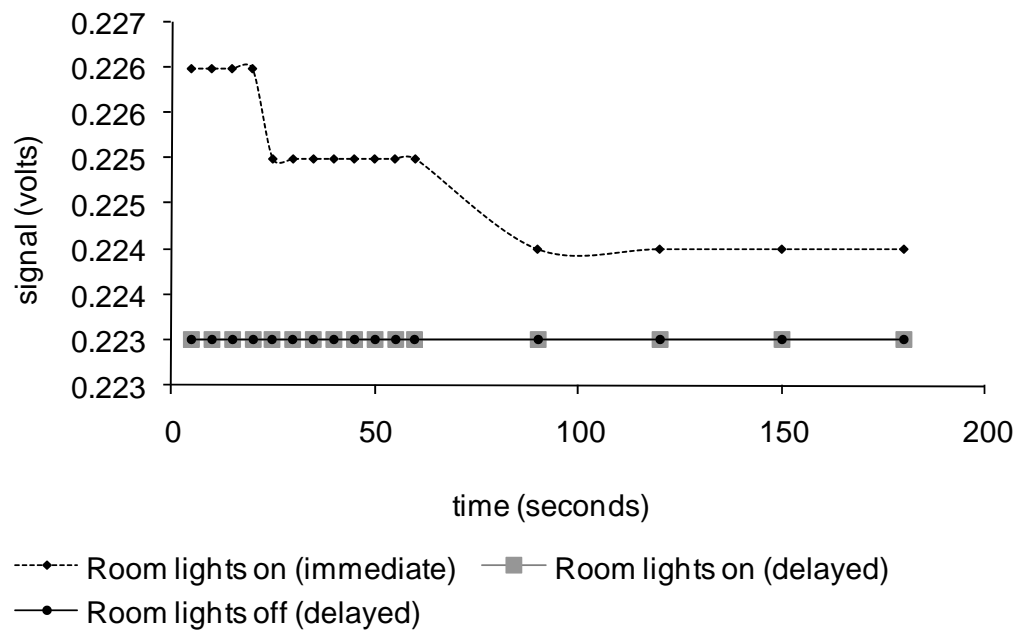

Figure B-3. Stability of the photodiode dark signal immediately after being turned on and after a 5 minutes warm-up period (delayed).

Noise in the blank

It was observed that when an empty cup is inserted in the induction coil of the IH-ETV and power is applied for 60 seconds to obtain a cup temperature of approximately 750°C, a shift in the baseline occurs as seen in the strip chart trace in Figure B-4. As mentioned earlier, a water mist was used to prevent

193

arcing in the IH-ETV. A water mist entering the absorbance cell can lead to false absorbance signals due to scattering. This effect was not visible when the power was off, but as soon as gases were heated in the combustion chamber of the IH-ETV, the light intensity dropped, probably due to the hot gas expansion. A possible solution to this problem would be the use of drying tubes right after the atomizer, before the entrance of the atomic vapor in the absorbance cell to remove water. The standard deviation of this blank signal was estimated using a digital multimeter, recording 10 different voltage values over a 50 s period. The average blank signal was found to be 0.4681 V with a 0.0007 V standard deviation.
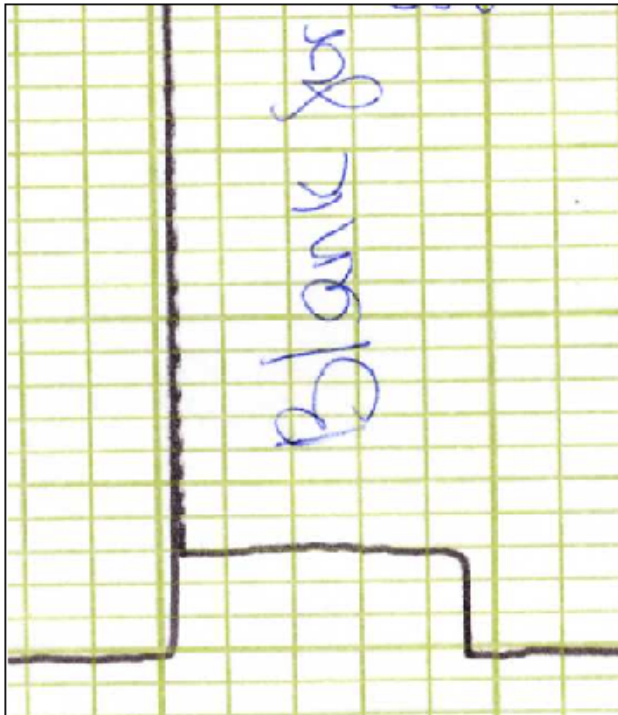
Figure B-4. Blank signal for which the standard deviation was recorded using a voltmeter (note: the sharp peak on the left of the blank signal is due to some electronic artefacts and was observed in all measurements)

Two series of 10 blank measurements were also recorded under two different sets of conditions. In the first set, the power was applied for 10 seconds, 10 consecutive times, with approximately 30 seconds of interval between the firings. In the second set, the cup was moved horizontally and vertically in between the firings to see if changes in the cup position would affect the recorded blank signal.

195

It was found that the error at the 95% confidence level (t = 2.26) increases from 2% with an unmoved cup to 3% when the cup is moved. An ANOVA test showed that the variance between the two series of measurements was greater than the variability within each series (F = 162.2 and $F_{critical}$ = 4.41). Effectively, the average blank signal was (14.8 ± 0.3) mm for the unmoved cup, and (12.0 ± 0.4) mm for the moved cup. A t-test showed that the two means are significantly different at the 95% confidence interval. The pooled variance of the two data sets is given by:

Equation B-4 $$S_{12} = \sqrt{\frac{(N_1 - 1)S_1^2 + (N_{21} - 1)S_2^2}{N_1 + N_2 - 2}}$$

Where S_1 and S_2 are the standard deviations of each data set and N the number of replicate measurements.

$$S_{12} = \sqrt{\frac{(10-1)0.497^2 + (10-1)0.486^2}{10+10-2}} = 0.492\,V$$

The estimated standard deviation in the difference between the two means, S_D is given by:

196

Equation B-5
$$S_D = S_{12}\sqrt{\frac{1}{N_1} + \frac{1}{N_2}}$$

$$S_D = 0.492\sqrt{\frac{1}{10} + \frac{1}{10}} = 0.220V$$

at the 95% confidence level, for ($N_1 + N_2 - 2$) degrees of freedom,

Equation B-6
$$tS_D = 2.10 \times 0.220 = 0.462V$$

Finally, the difference between the two means,

Equation B-7
$$\Delta x = \left| \overline{x_1} - \overline{x_2} \right|$$

$$\Delta x = \left| 12.0 - 14.8 \right| = 2.8\,V$$

Since $\Delta x > tS_D$, the difference is significant at the 95% confidence level.

More experiments are desired to find the source of this phenomenon. It would have been desirable to perform the same experiment, but with mercury inside the cup to see how cup position affects mercury volatilization, but this was not attempted since it is impossible with the actual setup to introduce mercury inside the cup without moving it. Not only must the cup position affect the precision of the signal, but also the placement of the sample inside the cup.

These imprecisions could be reduced by the addition of an autosampler and automation of the cup insertion at the center of the induction coil.

Instrument detection limit for mercury

In order to determine the instrument detection limit for mercury, 10 µl of three different mercury standards (0.97, 5.18 and 9.72 ppm Hg) were vaporized at 750°C. The power was applied for 60 seconds to ensure complete vaporization and cleaning of the cup. A sample transient signal is shown in Figure B-5. Four to six replicate measurements were obtained at each concentration. The height of the signals was used. Areas could be used instead of heights if the data was to be digitally acquired. This could possibly improve linearity, since the peaks are asymmetric, but precision in the peak area can be worse than for peak heights due to degradation of the signal to noise ratio for measuring points in the wings of the atomization profile. Calibration results are shown in Figure B-6.
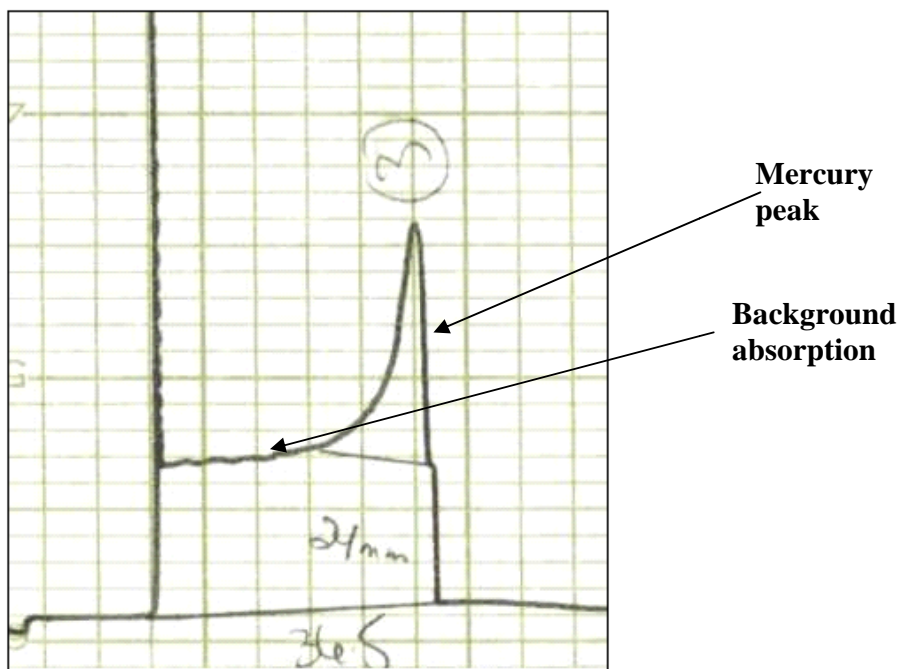
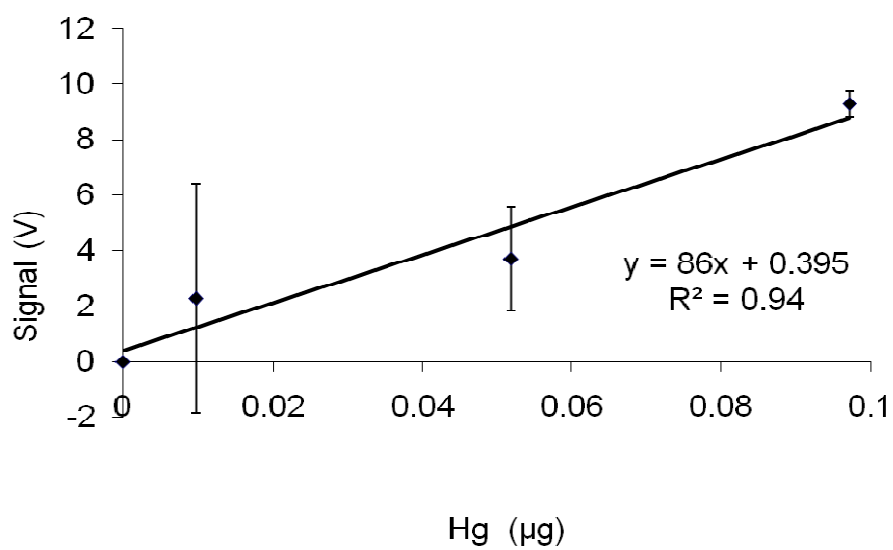Figure B-5. Sample transient signal obtained for 10 µl of a 10 ppm Hg standard

Figure B-6. Calibration curve obtained for the IH-ETV/ Hg vapour atomic absorption spectrophotometer

The detection limit was calculated as:

Equation B-8 $LOD = k*S_{bk} / m$

Where k is set to be 3 for 98.3 % confidence, S_{bk} is the standard deviation of the blank determined above, and m is the slope of the calibration curve.

$$LOD = 3 * 0.000138 \ / \ 77.973 = 0.0028 \ \mu g = 3 \ ng$$

The range of concentration studied in this experiment was not large enough to evaluate the limit of linearity of the method. In general, in absorption measurements, linear ranges are relatively small, often less than two orders of magnitude. At high concentrations of analyte, calibration curves usually exhibit negative deviations from linearity due to limitations to Beer's law. In this case, a low-pressure mercury pen lamp was used, so the width of the emission line should be narrow enough compared to the absorption peak. However, it was noticed that the mercury pen lamp became quite hot, so Doppler broadening is possible. A problem usually occurs when the radiation source is not narrow enough, so that it encompasses a spectral region where the absorber exhibits a large change in its molar absorptivity coefficient.

Signal-to-noise ratio characterization

It has been shown above that the dark noise was insignificant compared to the blank noise. Even though it was shown that position of the cup did not have much effect on the standard deviation of the blank signal, it is expected that variability in the cup position and sample position inside the cup itself could result in the instrument being limited by signal flicker noise (atomizer transmission noise). The signal-to-noise ratio plot in Figure B-7 confirms this hypothesis. The signal-to-noise ratio is highest at the lowest concentration due to the high light level, and levels off at higher concentration due to flicker noise.

Equation B-9 $\qquad$ $S/N = A_T/\sigma_T$

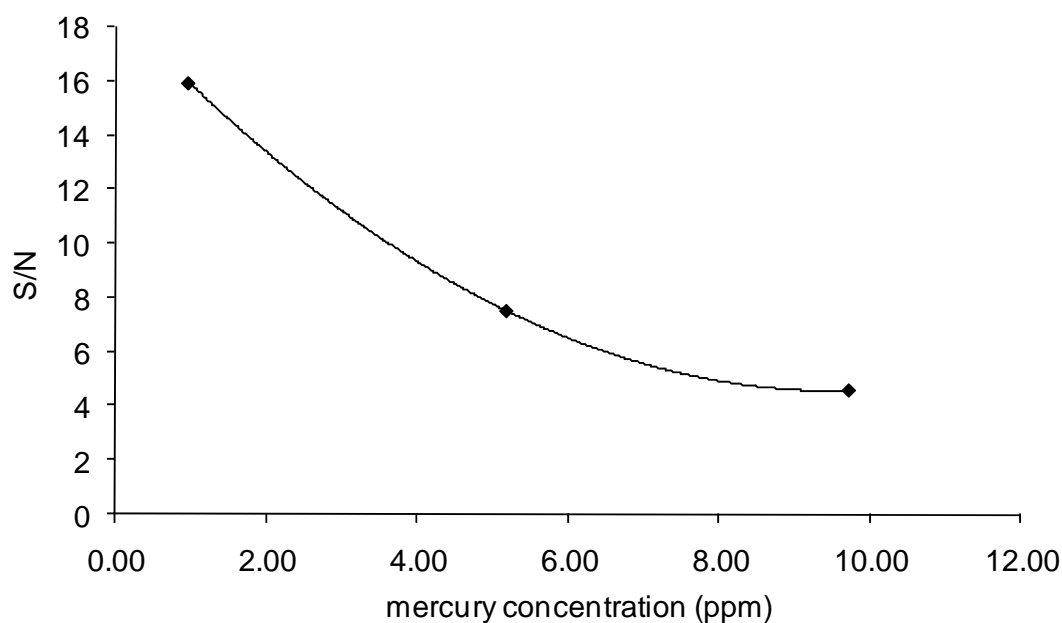where A_T is the total signal and σ_T its standard deviation.

Figure B-7. Dependence of the total signal-to-noise ratio on mercury concentration

Other sources of noise

It was observed that the intensity of the light emitted by the mercury pen lamp drifted slightly over the entire course of the experiments, but it is not expected to be a problem since the signals are measured from the baseline. It would however be very easy to correct for an eventual problem associated with this drift by splitting the incident beam in space or in time.

Another possible source of error observed was the degradation of the sample cup. In Figure B-8, we can easily see that pieces of carbon are literally missing from the cup. The apparition of a brown coloration on the inlet tubing to

the detector cell accompanied this deterioration. The degradation of the cup could be the cause of possible inferences due to background scattering. Possible causes could be the poor quality of the graphite used, as well as oxygen impurity in the argon stream. A possible solution would be to pyrolytically coat the cups to ensure a longer lifetime as well as using higher quality graphite and higher purity argon. A possible positive side effect to the degradation of the cup, however, would be enhanced transport efficiency. The soot particles can provide condensation nuclei for the atomic mercury vapour, facilitating its transport to the detector.

Figure B-8. Used (left) and new (right) graphite cups.

CONCLUSIONS

It has been demonstrated here that the IH-ETV can be used as a sample introduction device for Atomic Absorption Spectrometry. A system using the IH-ETV and gold amalgamation trapping in tandem with either a commercial atomic fluorescence spectrometry or a commercial atomic absorption spectrometry (AAS) with background correction detection was later developed by David Duford *et al.*[1] Using these techniques, detection limits of 0.1 ng or 160 ng g^{-1} and 0.08 ng or 130 ng g^{-1} (based on a 0.6 mg sample) of Hg were achieved for AFS and AAS respectively.

REFERENCES

(1)   Duford, D. A.; Lafleur, J. P.; Lam, R.; Skinner, C. D.; Salin, E. D. *Journal of Analytical Atomic Spectrometry* **2007**, *22*, 326-329.

Appendix C - Optimization of the LSX-200 laser ablation System for

the analysis of silica gel thin layer chromatography plates, high

performance thin layer chromatography plates and microfluidic solid

phase extraction columns

The laser ablation system operating parameters need to be optimized in order to provide the high sensitivity and stability required for analysis. This appendix presents here the methodology used to optimize the Laser Ablation (LA) system settings for the direct analysis of the Thin Layer Chromatographic plates (TLC) and High Performance Thin Layer Chromatographic plates (HPTLC) discussed in Chapter 3 and the microfluidic Solid Phase Extraction Columns (μ-SPE) discussed in Chapters 5 and 6.

LASER ABLATION SYSTEM

A Q-switched Nd:YAG laser, frequency quadrupled to 266 nm laser ablation system was used (LSX-200, CETAC technologies, Omaha, NE, USA). The specifications of this ablation system include a flat-top laser beam energy profile, with 6 mJ/pulse and 1 % precision. A schematic representation of the LA system is shown in Figure C-1.
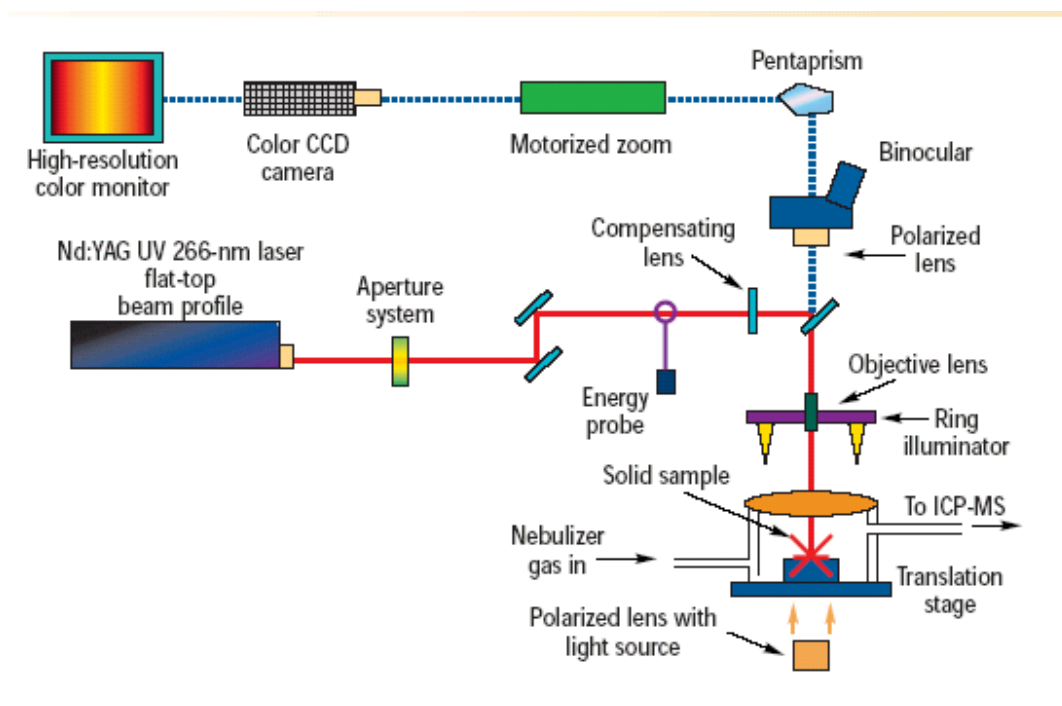
Figure C-1. Optical layout of the laser ablation system (CETAC Technologies, Omaha, NE, USA).

DETECTOR

The analysis was performed on a PE-Sciex Elan 6000 Inductively Coupled Plasma – Mass Spectrometer (ICP-MS) with a cross-flow nebulizer and a Scott-type spray chamber. The nebulizer gas flow rate and ion lens voltage were determined using the standard daily optimization procedure outlined by the manufacturer. The Auto Lens function was turned on, and the ion lens voltage was optimized for the whole mass range using ^{9}Be, ^{115}In, and ^{27}Co signals. The operating conditions and operational parameters are outlined in Table C-1.

Table   C-1. ICP-MS operating parameters.

Operational parameters	
RF power	1000 W
Sampling and skimmer cones	Nickel
Plasma gas flow rate	15 L min^{-1} Ar
Auxiliary gas flow rate	1.2 L min^{-1} Ar
Carrier gas flow rate	0.925 L min^{-1} Ar
Signal measuring parameters	
Detector mode	Analog
Acquisition mode	Peak hopping
Sweeps per reading	1
Readings per replicate	Adjusted so that the total analysis time was ~ 2 minutes
Replicates	1
Dwell time	333 ms per isotope
Isotopes measured	^{30}Si, ^{28}Si

LASER PARAMETER OPTIMIZATION

Analysis of a surface by LA-ICP-MS can be performed in two different ways. The single point method allows the user to move to a pre-selected location, fire a laser burst, then move to another location and fire again (up to 20 different points). When this method was used, the spots were ablated at ten different locations and the results shown represent an average of these ten points along with its 95% confidence interval.
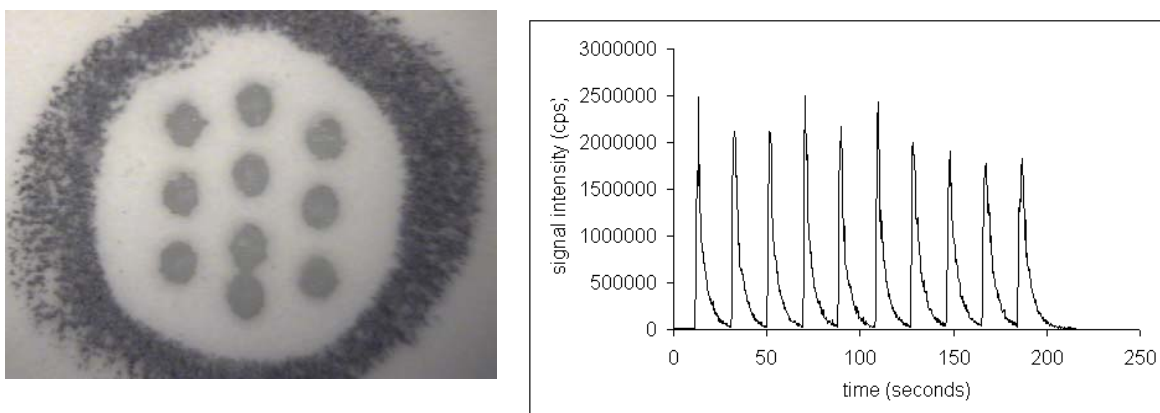
208

Figure C-2. Left: Ten 300 μm ablation points on a 1 μL solution spot. Right: Resulting ^{30}Si signal profile.

A second way of analysing a surface by LA-ICP-MS is to use a single line scan mode. In this method, the sample cell moves horizontally at a constant speed while the laser is firing continuously.

Figure C-3. Left: Single line scan (~4000 μm distance) of a silica gel TLC plate. Right: Resulting ^{30}Si signal profile.

TLC OPTIMIZATION

The laser operating parameters were optimized for the ablation of TLC plates (Silica gel 60F, 250 µm thickness, Silicycle, Quebec City, QC, Canada).

LASER DEFOCUS OPTIMIZATION

Keeping all parameters constant (Table C-2), the laser focus was varied in order to find optimal settings for the ablation of silica gel TLC plates. The importance of adjusting the laser defocus is illustrated by the magnified pictures of laser craters formed in a TLC plate at different settings shown in Figure C-4. When the laser is focused directly on the surface of the TLC, a small non-uniform crater is formed. As the laser is defocused, the ablation crater becomes larger and more uniform, and when the defocus is too extreme, the crater becomes quite shallow as not enough energy is focused on the surface of the TLC.
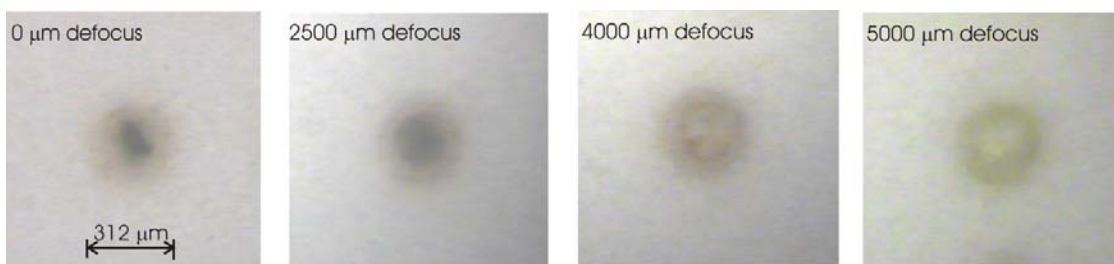
Figure C-4. Effect of varying the laser defocus on the ablation crater shape.

Table   C-2. Laser settings used during the defocus optimization.

Parameter	Setting
Energy level	8
Pulse repetition rate	20 Hz
Burst count	40
Shots	40
Spot size	300 µm

The results shown in Figure   C-5 represent the average and 95% confidence interval for ten consecutive ablations. Results show that the signal intensity increases as the laser defocus is increased from 0 to 2000 µm after which point it stabilizes. The signal-to-noise ratio plot, shown Figure   C-6, does not show a clear trend, but confirms the selection of the 2000 µm defocus as the optimal setting.
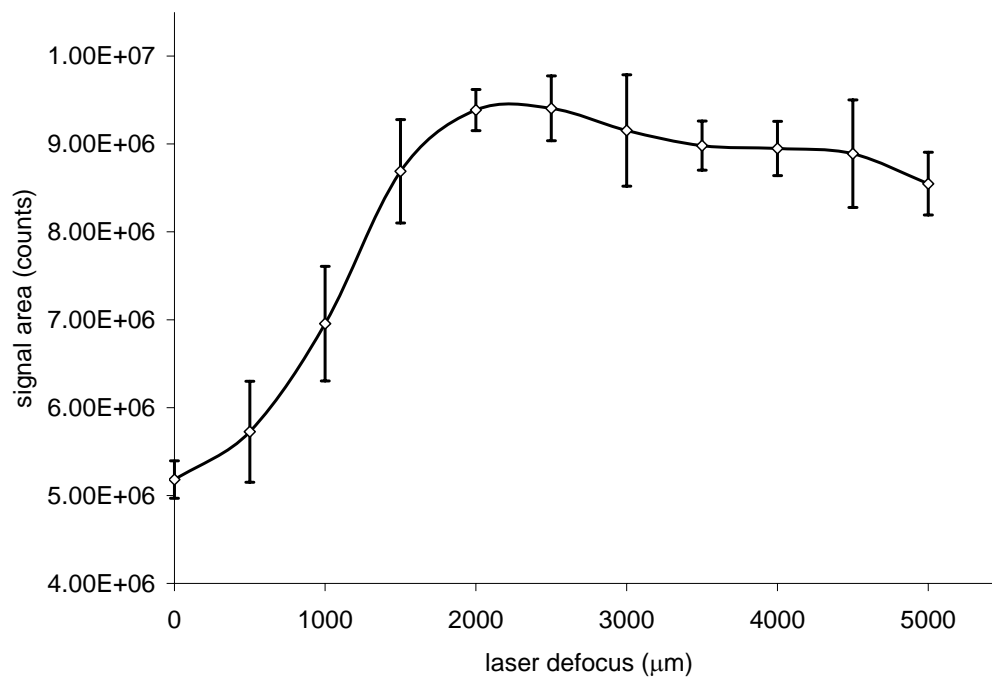
Figure C-5. Effect of varying the laser defocus on the ^{28}Si signal.
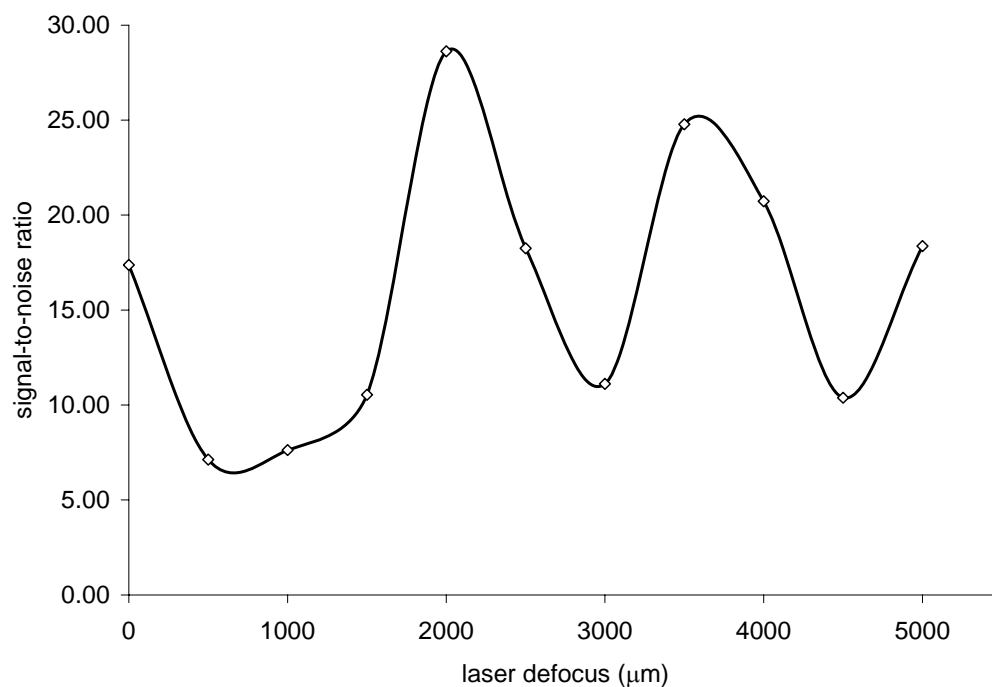
Figure C-6. Signal-to-noise ratio for ^{28}Si as the laser defocus is varied.

OPTIMIZATION OF THE PULSE REPETITION RATE

The pulse repetition rate is the number of laser pulses fired per second and is expressed in Hz. All laser operating parameters were kept constant, Table C-3, while the pulse repetition rate was varied. The experiment was repeated at two different energy levels settings, 10 and 15.

Table   C-3. Laser settings for the pulse repetition rate optimization.

Parameter	Setting
Laser defocus	2000 um
Energy level	10 / 15
Burst count	40
Spot size	300 µm

Figure   C-7 shows that, as expected, the signal increases as the pulse repetition rate is increased, but as shown in Figure   C-8, at both energy level settings tested (10 and 15), a pulse repletion rate of 10 Hz results in the highest signal to noise ratio (S/N = 25 at level 10 and 22 at level 15).
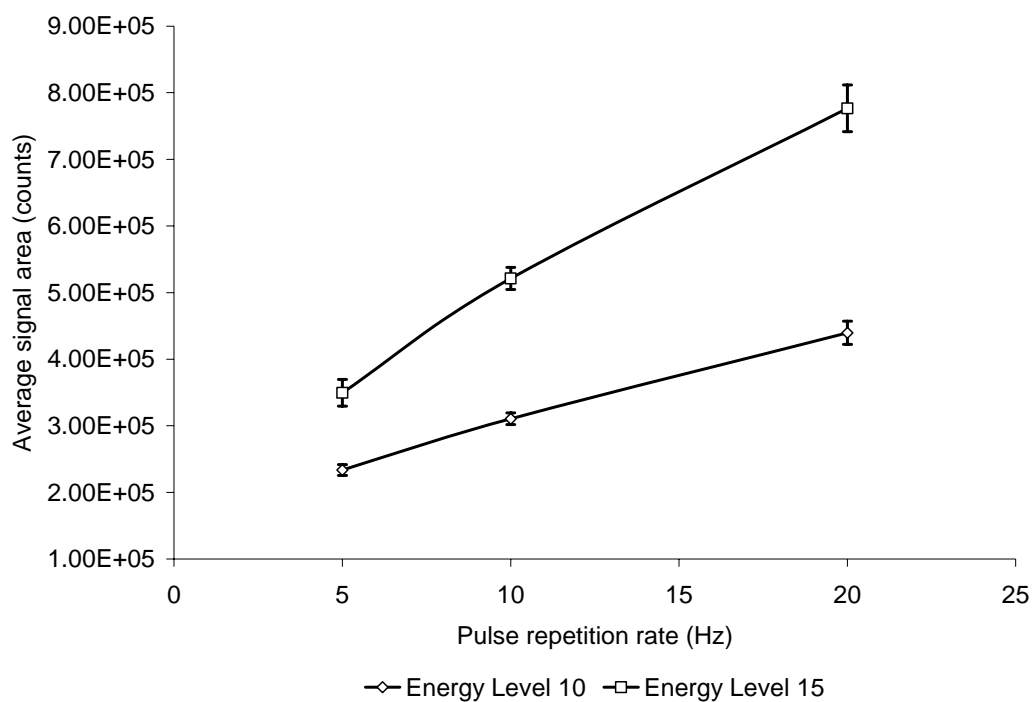
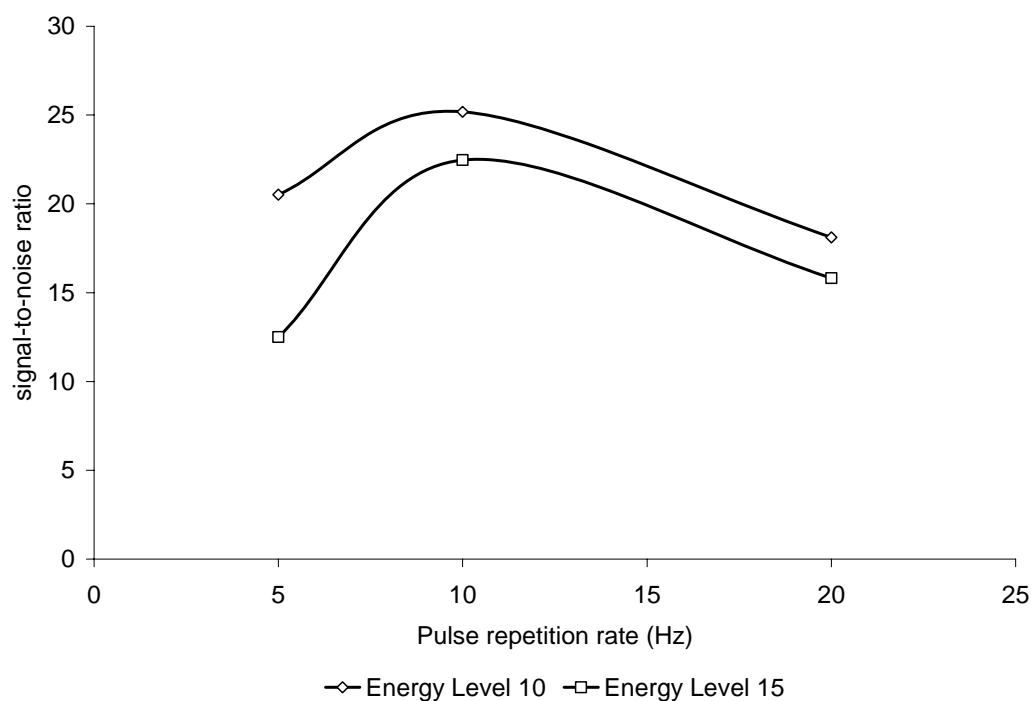Figure C-7. Effect of varying the pulse repetition rate on ^{30}Si signal.

Figure C-8. Signal-to-noise ratio of ^{30}Si as the pulse repetition rate is varied.

ENERGY LEVEL OPTIMIZATION

The laser energy output can be set by varying the energy level between 5 and 20. All laser operating parameters were kept constant, as listed in Table C-4, while the energy level was varied.

Table   C-4. Laser settings for the energy level optimization

Parameter	Setting
Laser defocus	2000 µm
Pulse repetition rate	10 Hz
Burst count	40
Shots	5
Spot size	300 µm

As expected, the average signal are for ^{30}Si increases as the energy setting is increased (Figure   C-9), but as revealed in Figure   C-10, the maximal signal-to-noise ratio is reached at a setting of 11.
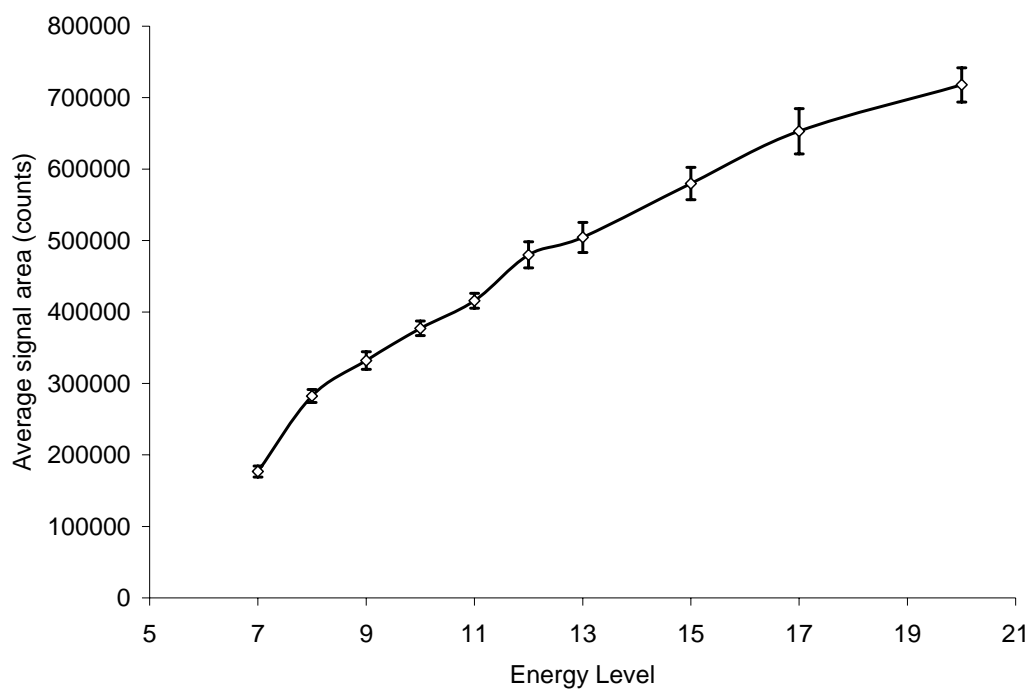
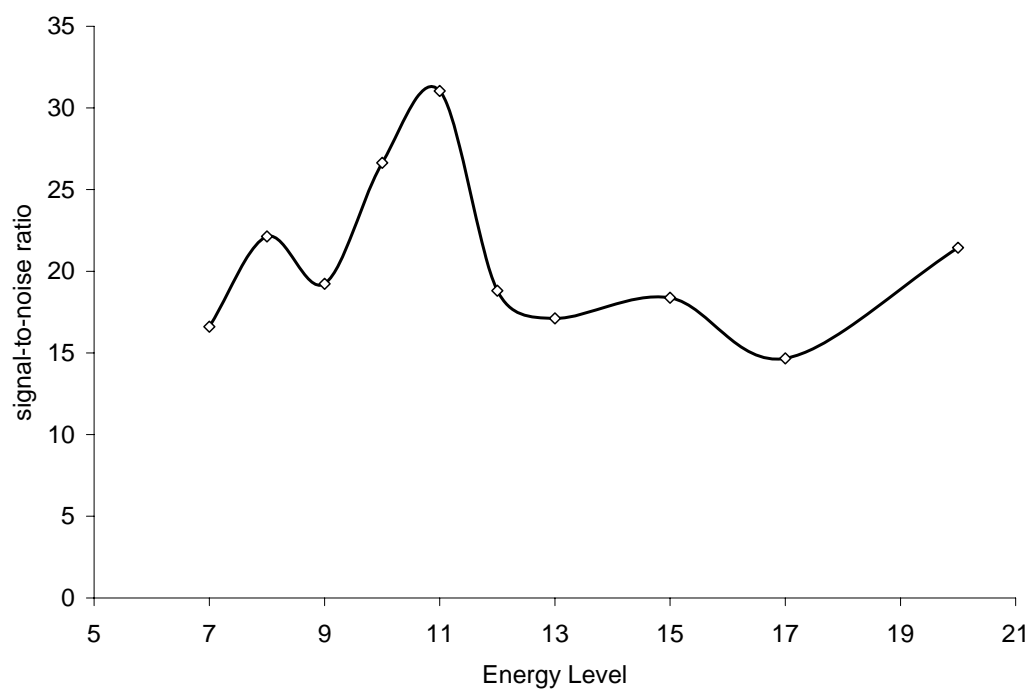Figure C-9. Effects of increased laser power on ^{30}Si signal.

Figure C-10. Signal-to-noise ratio plot for ^{30}Si as the energy is increased.

216

LASER SCAN RATE OPTIMIZATION

In single line scan mode, the laser scan speed has to be optimized to avoid uneven ablation. The laser scanning rate was increased from 25 µm s^{-1} to 300 µm s^{-1}. All other laser operating parameters were kept constant, as listed in Table C-5. As shown in Figure C-11, as the laser scan rate is increased, more material is ablated per unit time and the signal intensity increases. However, at very high scan rates, such as 300 µm s^{-1}, the translation stages moves so fast compared to the laser pulse repetition rate that the trench formed is very uneven, leaving un-ablated spots along the way. It is obvious that if one wishes to use very high scan rates, the pulse repetition rate would have to be readjusted. Nevertheless, as shown in Figure C-12, the signal-to-noise ratio varies very little with variations in laser scan rate.

Table C-5. Laser settings for the laser scan speed optimization.

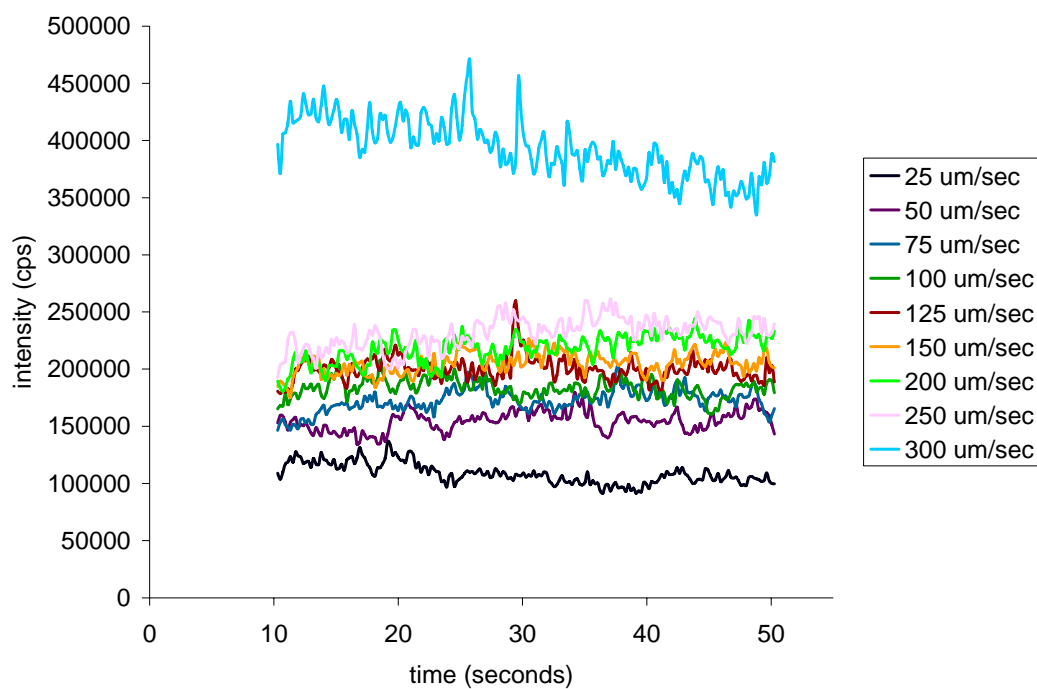| Parameter	Setting
Laser defocus	2000 µm
Pulse repetition rate	10 Hz
Energy Level	11
Spot size	300 µm

Figure C-11. Effect of increasing the laser scan rate on ^{30}Si signal.
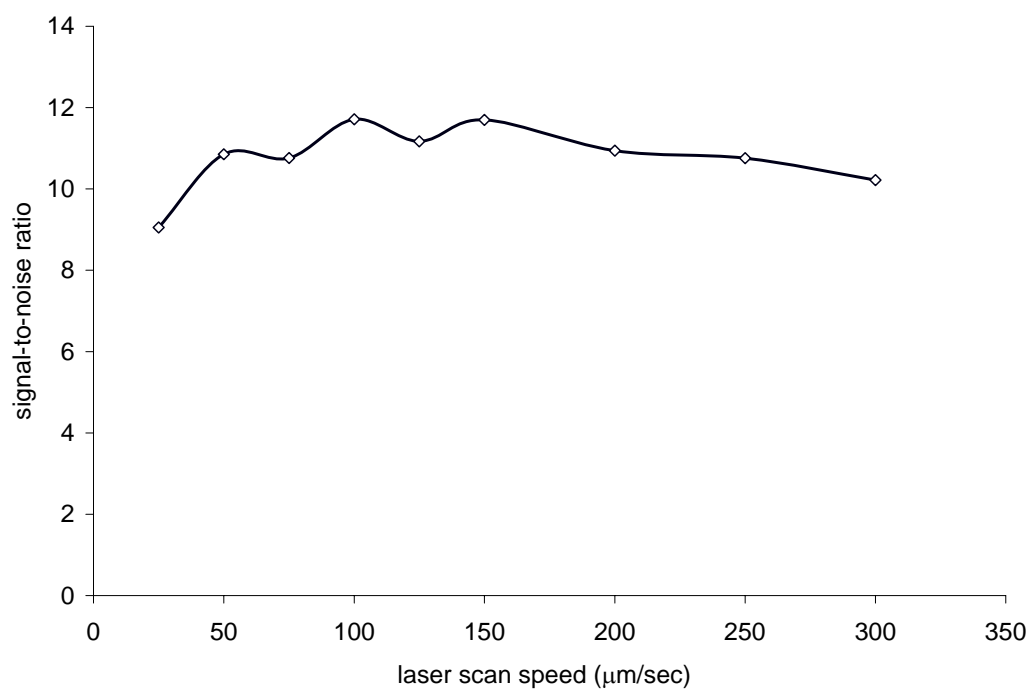

Figure C-12. Effect of increased scan speed on ^{30}Si signal-to-noise ratio.

OPTIMIZATION SUMMARY FOR TLC PLATES

The optimal laser ablation parameters determined for the ablation of TLC plates are listed in Table   C-6. These setting were used for all the experiments involving 250 μm thick silica gel TLC plates.

Table   C-6. Optimal laser operating parameters for the ablation of TLC plates.

Parameter	Setting
Laser defocus	2000 μm
Pulse repetition rate	10 Hz
Energy Level	11
Scan rate	100 μm s^{-1}
Spot size	300 μm

HPTLC OPTIMIZATION

Experiments were also performed with 150 μm thick silica gel plates (Hard Layer Silica Gel GHL Uniplates, Analtech, Newark, DE, USA). The optimization results for theses plates were also used for the laser ablation of the solid phase extraction columns (Chapters 4 and 5). Unlike the optimization for the TLC plates, single line scans, rather than single point mode, was used for the optimization as this is the type of ablation used in experimental conditions.

LASER ENERGY OPTIMIZATION

All laser operating parameters were kept constant, as listed in Table C-7, while the energy level was varied.

Table C-7. Laser parameter settings for the energy setting optimization.

Parameter	Setting
Laser defocus	700 µm
Pulse repetition rate	10 Hz
Scan rate	30 µm s^{-1}
Spot size	300 µm

The laser energy output can be set by varying the energy level between 5 and 20. A first 3-point rough optimization, as shown in Figure C-13, was performed to identify the range of energy levels of interest. A finer optimization was then performed in the region of the maxima of the first rough estimation. As shown in Figure C-14, the average signal for ^{29}Si and ^{30}Si increases as the energy setting is increased, but as revealed in Figure C-15, the maximal signal-to-noise ratio is reached at a setting of 9 or 11.
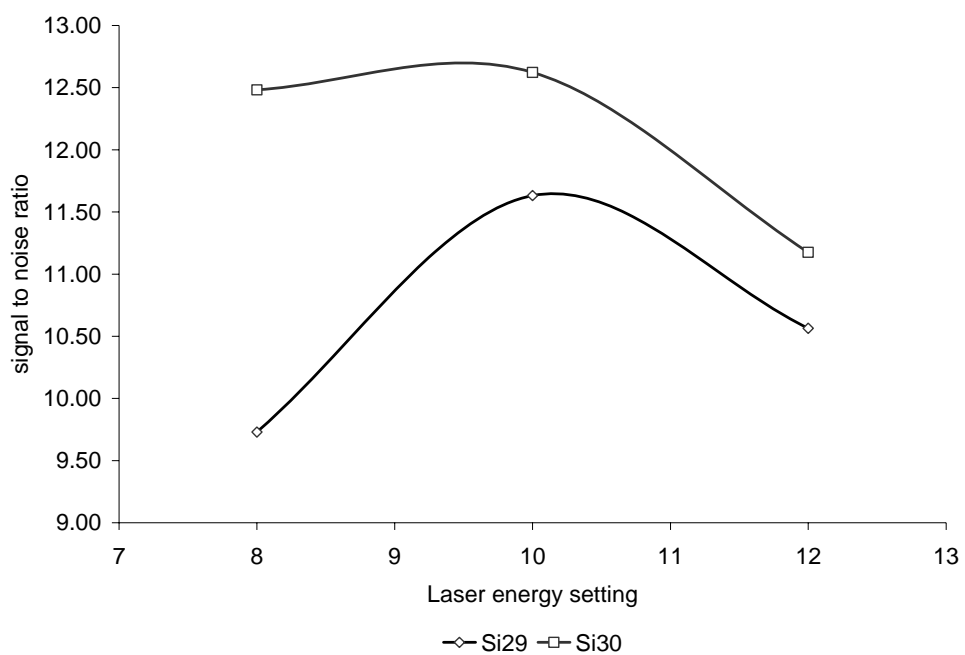
Figure C-13. Effect of varying the laser energy on Si signal-to-noise ratio (rough
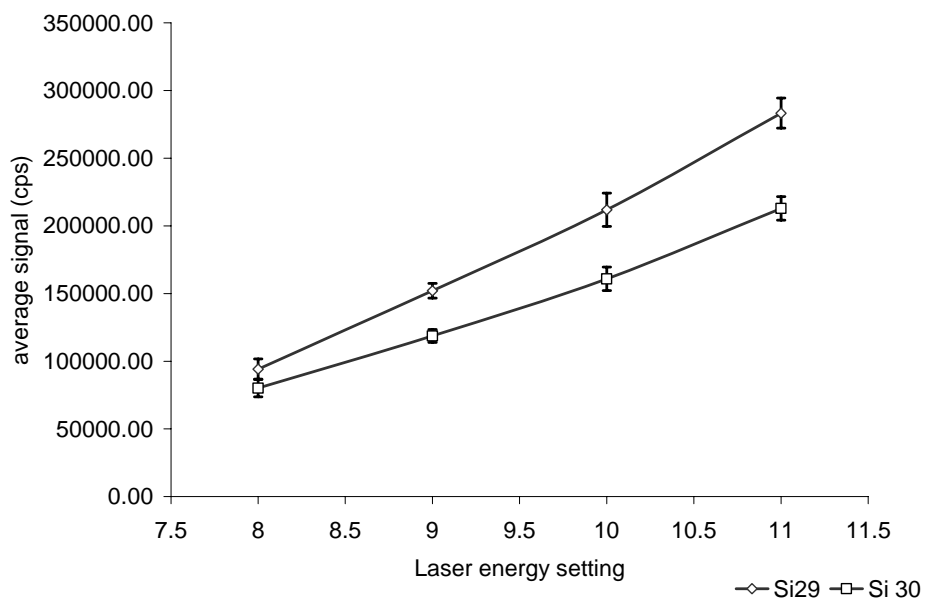
optimization).

Figure C-14. Effect of varying the laser energy on Si signal (fine adjustment).
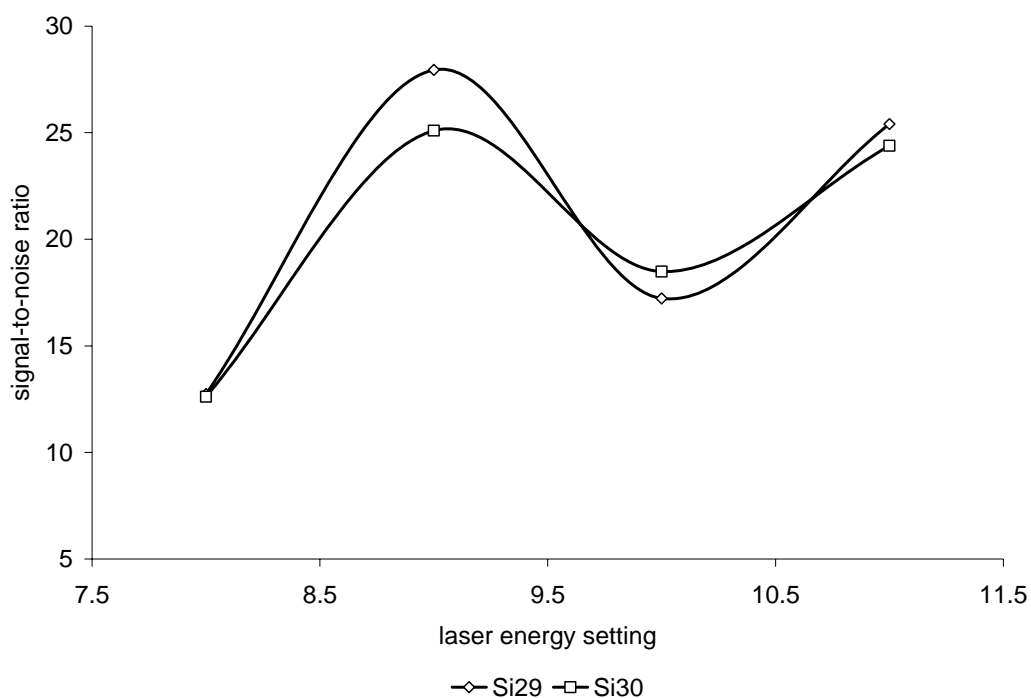
Figure C-15. Effect of varying the laser energy on Si signal-to-noise ratio (fine adjustment).

LASER SCAN RATE OPTIMIZATION

In the rough optimization, the laser scanning rate was increased from 10 μm s^{-1} to 150 μm s^{-1}. All other laser operating parameters were kept constant, as listed in Table C-8. As shown in Figure C-16, a higher signal-to-noise ratio is achieved at scan rates below 50 μm s^{-1}. As shown in Figure C-17, as the laser scan rate is increased, more material is ablated per unit time and the signal intensity increases. As shown in Figure C-18, the signal-to-noise ratio varies very little with variations in laser scan rate between 30 μm s^{-1} and 50 μm s^{-1}.

Table C-8. Laser parameter settings for the scan rate optimization

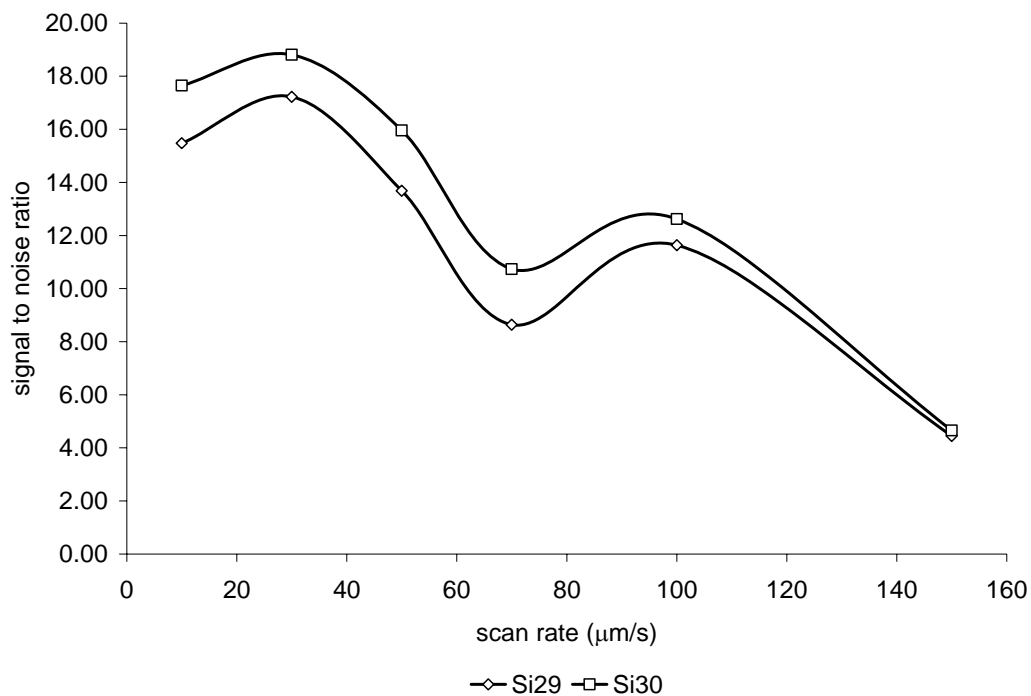| Parameter	Setting
Laser defocus	700 μm
Pulse repetition rate	10 Hz
Energy	10
Spot size	300 μm

Figure C-16. Effect of varying the laser scan rate on Si signal-to-noise ratio (rough optimization).
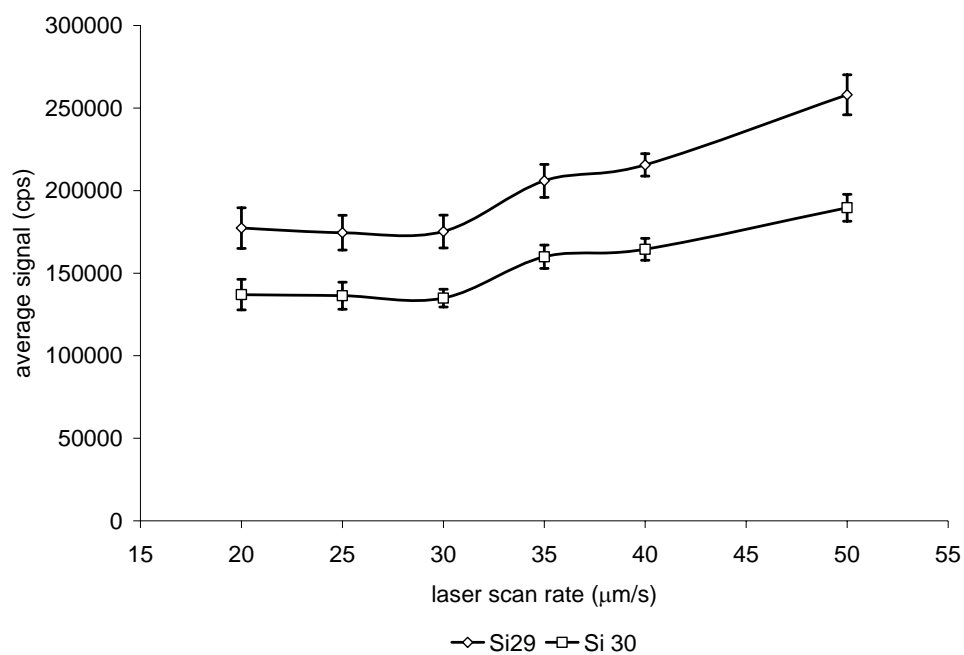
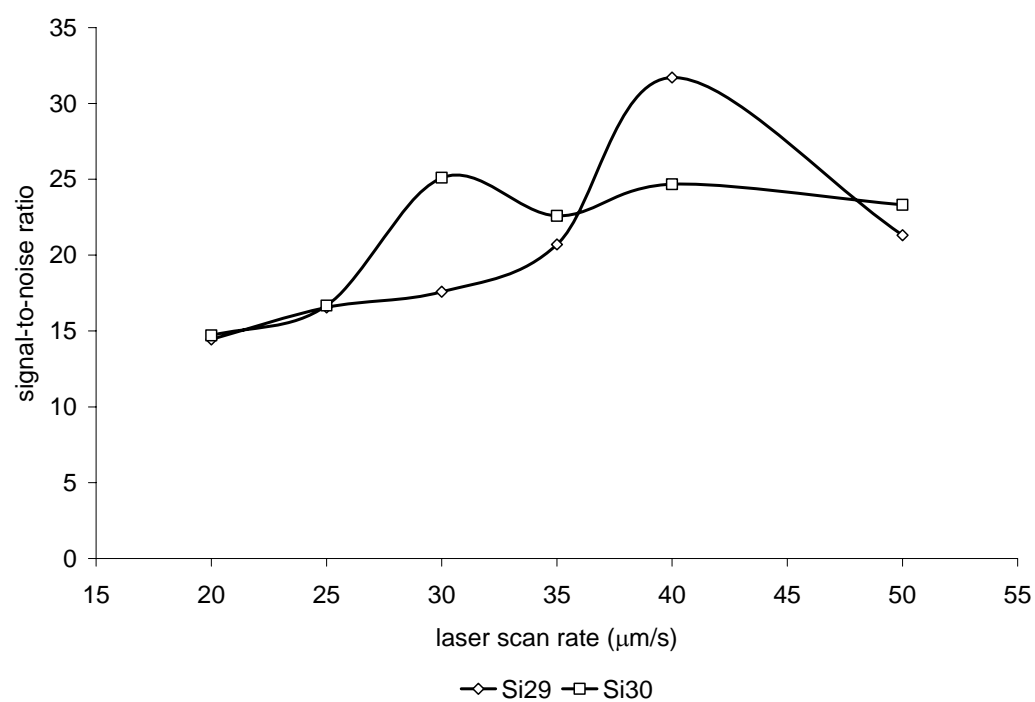Figure C-17. Effect of varying the laser scan rate on Si signal (fine optimization).

Figure C-18. Effect of varying the laser scan rate on Si signal-to-noise ratio (fine

optimization).

224

LASER DEFOCUS OPTIMIZATION

Keeping all parameters constant (Table C-9), the laser focus was varied in order to find its optimal settings for the ablation of silica gel HPTLC plates. The rough optimization (Figure C-19), shows a clear peak in signal-to-noise ratio around 700 µm defocus. However, Figure C-20 shows little variation in signal intensity as the defocus is increased from 0 to 1000 µm. The signal-to-noise ratio plot (Figure C-21) shows that there is little variation in sgnal-to-noise ratio between 50 and 600 µm defocus, after which a slight decrease is observed.

Table C-9. Laser parameter settings for the defocus optimization.

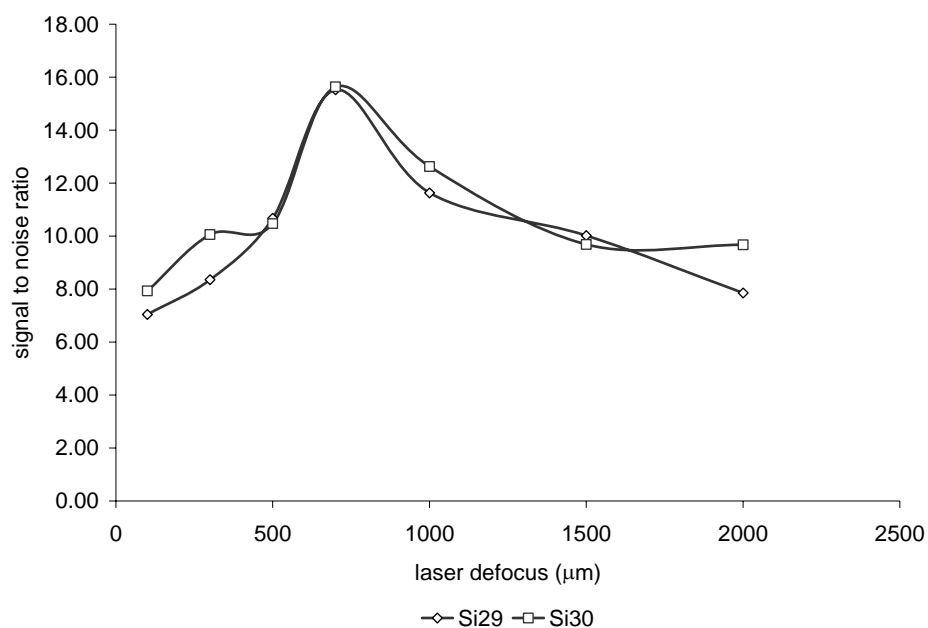| Parameter	Setting
Energy	10
Pulse repetition rate	10 Hz
Scan rate	30 µm s^{-1}
Spot size	300 µm

Figure C-19. Effect of varying the defocus on Si signal-to-noise ratio (rough optimization).
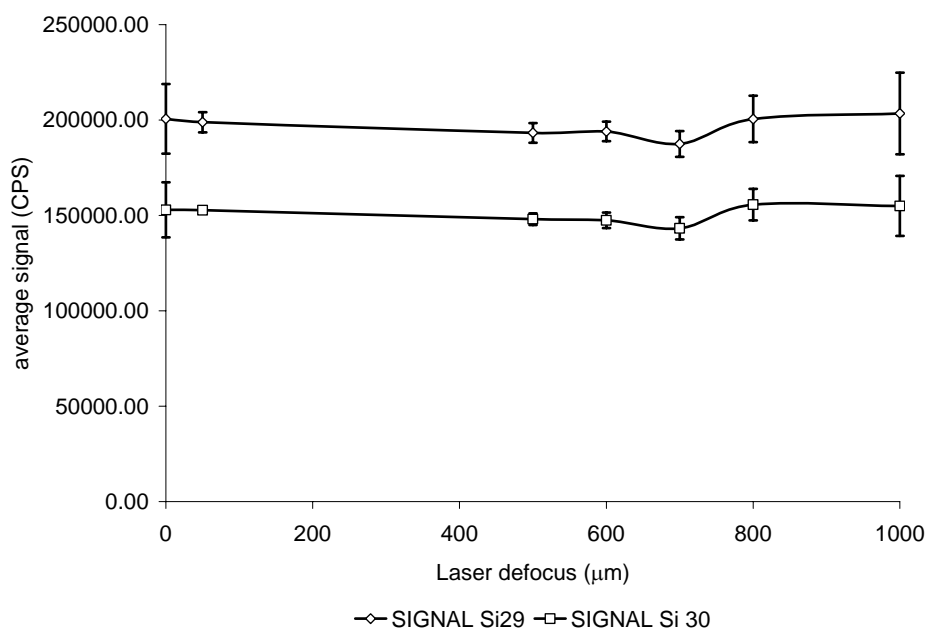

Figure C-20. Effect of varying the laser defocus on Si signal ratio (fine optimization).
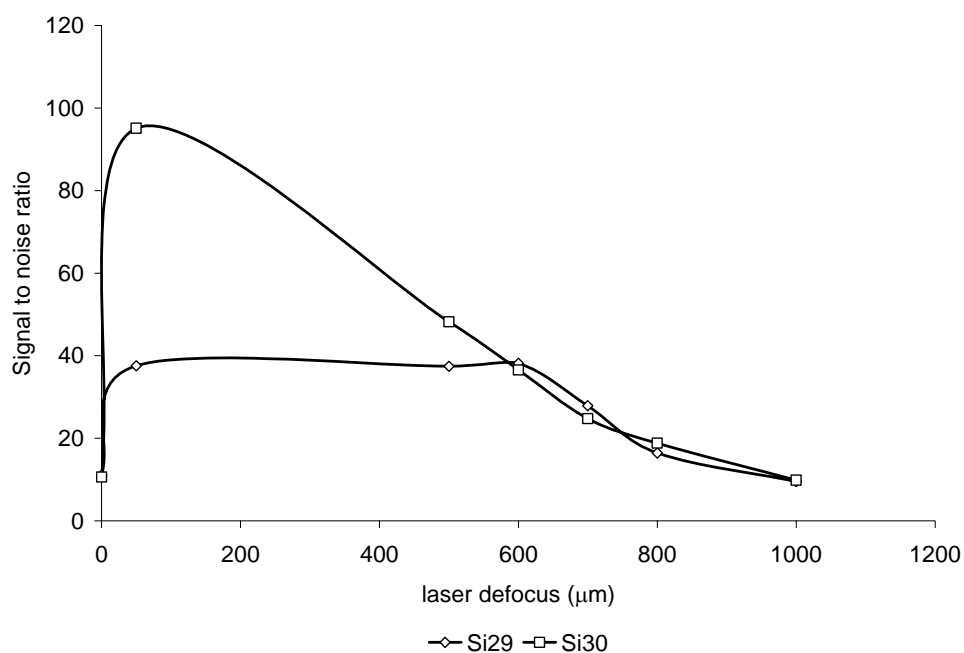
Figure C-21. Effect of varying the laser defocus on Si signal-to-noise ratio (fine optimization).

PULSE REPETITION RATE OPTIMIZATION

All laser operating parameters, listed in Table C-10 were kept constant while the pulse repetition rate was varied.

Table C-10. Laser settings for the pulse repetition rate optimization.

Parameter	Setting
Laser defocus	700 um
Energy level	10
Scan rate	30 µm S^{-1}
Spot size	300 µm

Figure C-22 shows that the signal-to-noise ratio is maximal at a pulse repetition rate of 5 and 10 Hz. Unfortunately, no finer adjustments are possible for the laser pulse repetition rate as these are the only settings available.
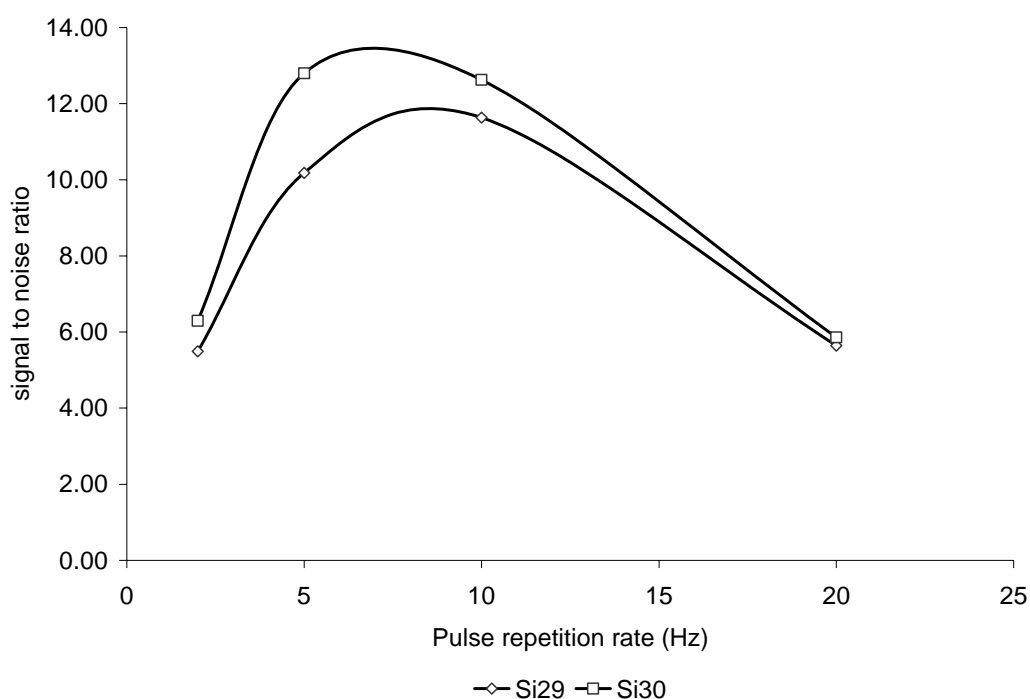

Figure C-22. Effect of varying the pulse repetition rate on Si signal-to-noise ratio.

SUMMARY OF OPTIMAL PARAMETERS FOR LA OF HPTLC PLATES

The optimal laser ablation parameters determined for the ablation of HPTLC plates are listed in **Error! Reference source not found.**. These setting were used for all the experiments involving 250 µm thick silica gel HPTLC plates

and were also use as a base for the ablation the solid-phase extraction columns described in Chapter 4, 5 and 6.

Table C-11. Optimal laser operating parameters for the ablation of HTLC plates.

Parameter	Setting
Laser defocus	50-600 µm
Pulse repetition rate	5-10 Hz
Energy Level	9-11
Scan rate	30-50 µm s^{-1}
Spot size	300 µm

MINIMAX OPTIMIZATION

The optimal laser operating parameters determined for the ablation of HPTLC plates were used as a starting point to determine optimal conditions for the ablation of the solid phase extraction columns on miniature centrifugal chromatographic discs presented in Chapters 4, 5 and 6. The difficulty here lies in the necessity to remove the 75 µm – thick polycarbonate film covering the column before vaporizing the analytes for LA-ICP-MS analysis. Testing was performed on blank columns at low (Table   C-12) and high (Table   C-13) defocus. As seen in Figure   C-23(A), at 50 µm defocus, almost no column material is vaporized on the first laser pass, indicating that only the polycarbonate film is being vaporized. The laser reaches the column material on the following

passes, Figure C-23(B)-(F), as indicated by the silicon signal observed. At higher

defocus, some column material is visibly ablated during the first laser pass,

Figure C-24(A), but the signal seems visibly higher for the subsequent laser

passes, Figure C-24(B)-(E). Although the 500 µm defocus provided higher signal

intensities, the 50 µm defocus was chosen as a setting of choice because of its

clean removal of the polycarbonate film without damaging the column and

because higher defocus tended to damage the quartz window of the ablation cell.

Table   C-12. Parameters for the LA of Minimax XII at low defocus.

Parameter	Setting
Laser defocus	50 µm
Pulse repetition rate	10 Hz
Energy Level	10
Scan rate	30-50 µm s^{-1}
Spot size	300 µm

Figure C-23. Laser Ablation of Minimax VII at 50 μm defocus: (A) First pass. (B) Second pass. (C) Third pass. (D) Fourth pass. (E) Fifth pass. (F) Sixth pass.

Table C-13. Parameters for the LA of Minimax XII at high defocus

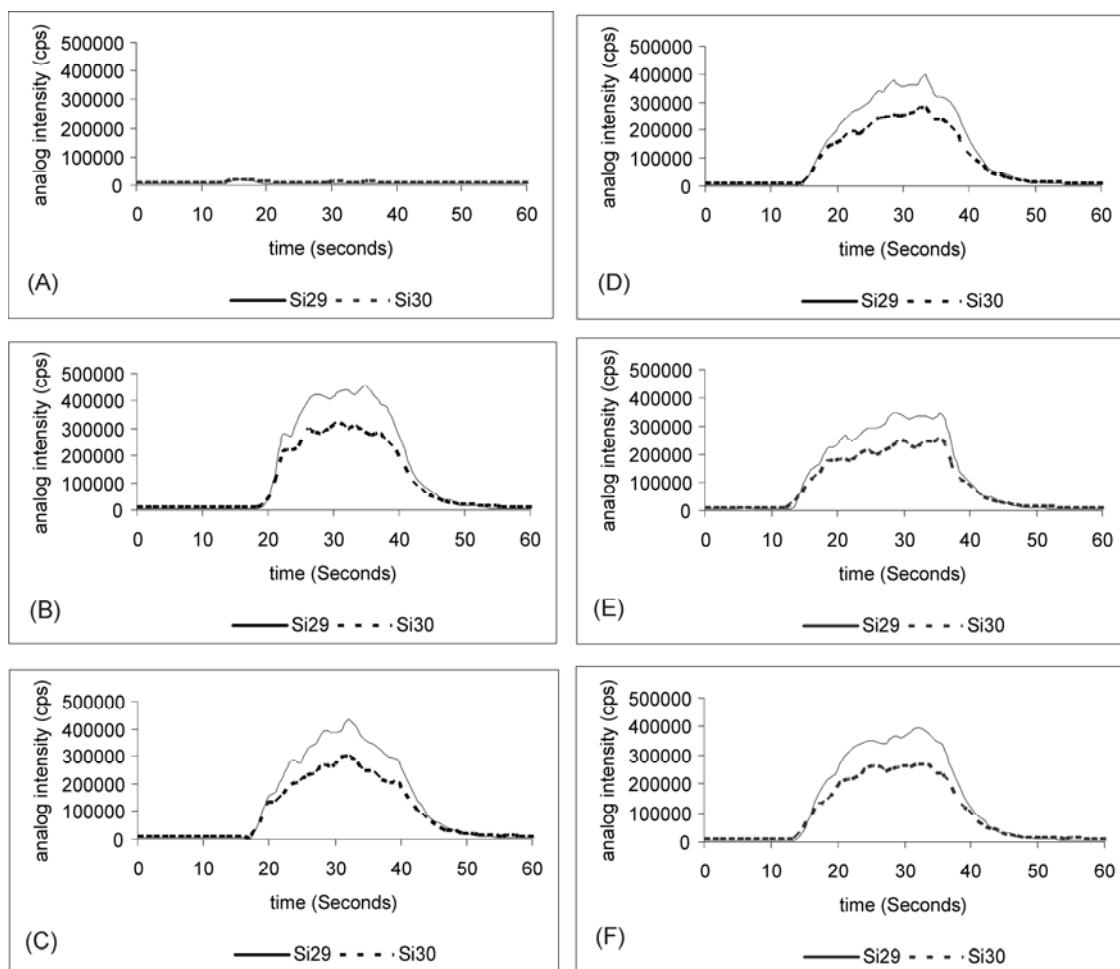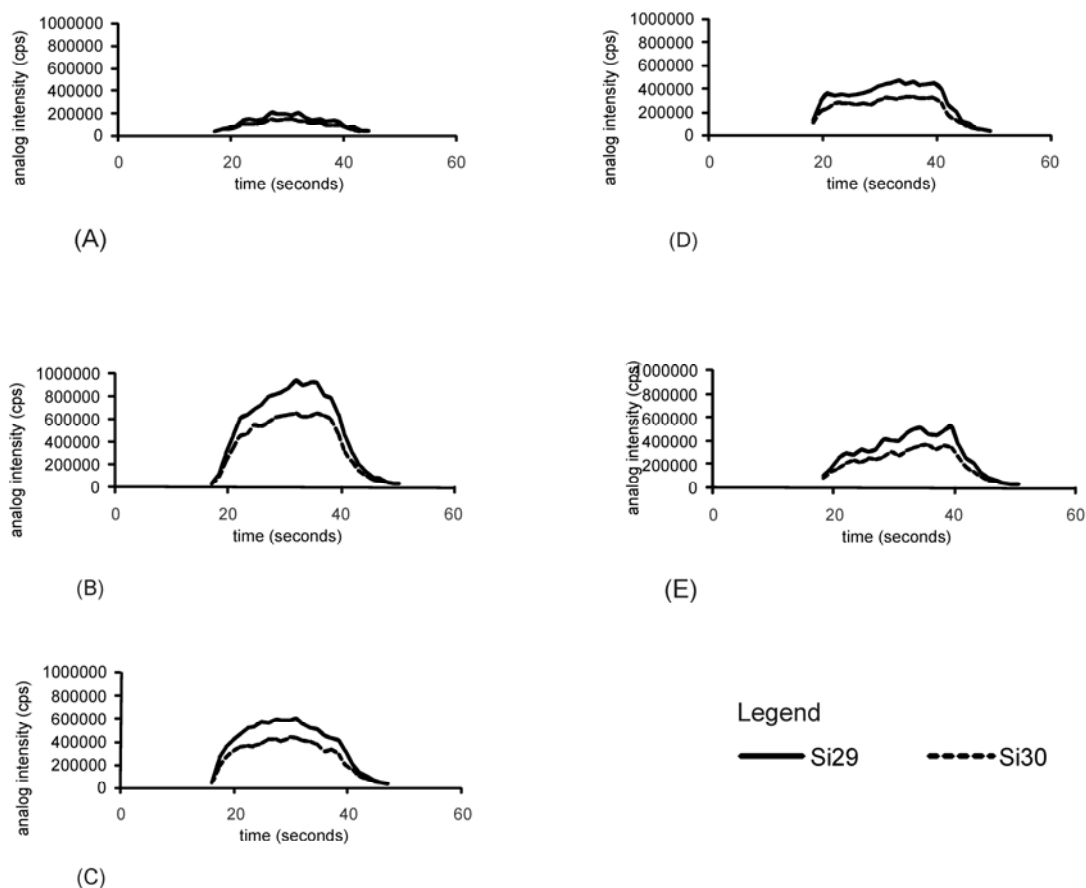| Parameter	Setting
Laser defocus	500 μm
Pulse repetition rate	10 Hz
Energy Level	10
Scan rate	30-50 μm s^{-1}
Spot size	300 μm

Figure C-24. Laser Ablation of Minimax VII at 500 μm defocus: (A) First pass. (B) Second pass. (C) Third pass. (D) Fourth pass. (E) Fifth pass.

Figure C-25 offers a magnified view of the columns after two super-imposed laser ablation scans at 50 and 500 μm defocus. At both settings, the white column material is exposed after the two ablation scans.
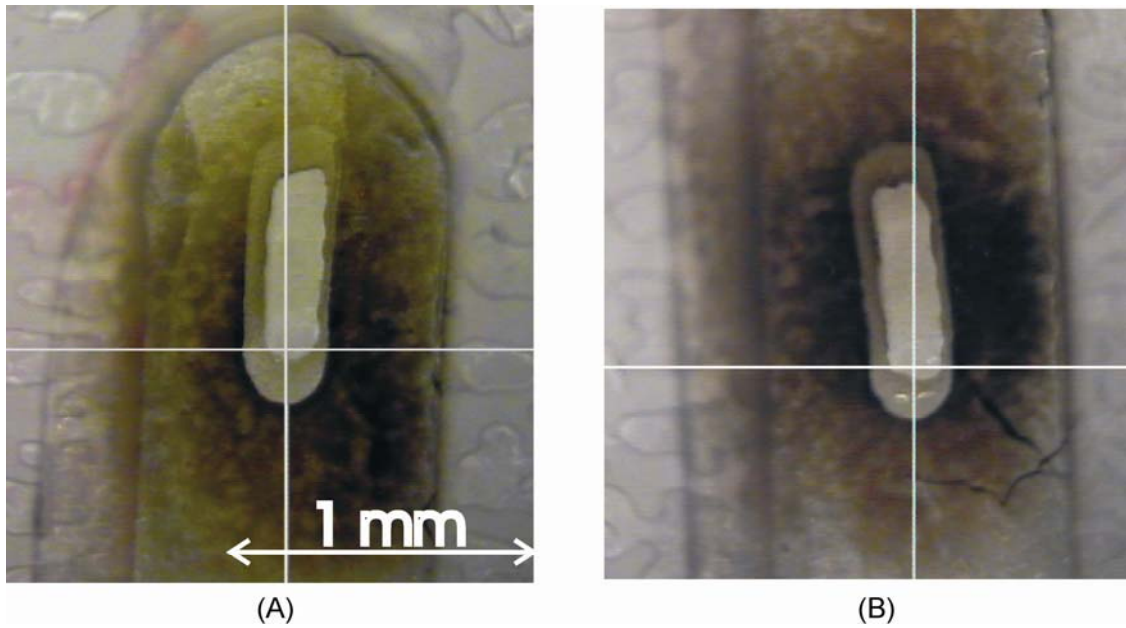
Figure C-25. Removal of the thin polycarbonate film covering the columns after two superimposed laser ablation scans. (A) 50 μm defocus. (B) 500 μm defocus.

Appendix D - Direct elemental analysis of thin layer chromatography plates (TLC) by laser ablation (LA) inductively coupled plasma mass spectrometry (ICP-MS)

Preliminary studies on the feasibility of using laser ablation (LA) ICP-MS to vaporize elemental species directly from chromatographic plates are presented here. Results of pre-concentration studies, internal standardization as well as separation of heavy metals by TLC-LA-ICP-MS are presented. The calibration curves for the data presented in Chapter 3 are also presented.

Experimental

LASER ABLATION SYSTEM

A Q-switched Nd:YAG laser, frequency quadrupled at 266 nm laser ablation system was used (LSX-200, CETAC technologies, Omaha, NE, USA). The laser ablation system operating parameters were optimized for the analysis of silica gel TLC plates in order to provide the high sensitivity and stability required for this type of analysis. Optimal laser operating parameters, determined in Appendix C, are listed in Table   D-1.

Table   D-1. CETAC LSX-200 optimal operating parameters.

Laser defocus	2000 μm
Energy level	11
Pulse repetition rate	10 Hz
Spot size	300 μm
Laser scan speed	100 μm s^{-1}
Burst count	40 (not optimized, mid value)

DETECTOR

The analysis was performed on a Perkin-Elmer SCIEX Elan 6000 ICP-MS system (SCIEX, Concord, ON, Canada). The carrier gas flow rate and ion lens voltage were determined using the standard daily optimization procedure. The Auto-Lens function was turned on, and the ions lens voltage was optimized for the whole mass range using ^{9}Be, ^{115}In and ^{27}Co signals. The operating conditions and experimental parameters are outlined in Table   D-2.

Table D-2. ICP-MS operating parameters.

Operational parameters	
RF power	1100 W
Sampling and skimmer cones	Nickel
Plasma gas flow rate	15 L min^{-1} Ar
Auxiliary gas flow rate	1.2 L min^{-1} Ar
Carrier gas flow rate	0.925 L min^{-1} Ar
Signal measuring parameters	
Detector mode	Analog
Acquisition mode	Peak hopping
Sweeps per reading	1
Readings per replicate	Adjusted so that the total analysis time was ~ 2 minutes
Replicates	1
Dwell time	50 ms per isotope
Isotopes measured	^{30}Si, ^{28}Si, ^{208}Pb, ^{103}Rh, ^{63}Cu

PREPARATION OF TLC PLATES

Commercially available silica gel TLC plates (Silica gel 60F, 250 µm, Silicycle, Quebec City, QC, Canada) were used for all analyses. Disposable 1 µl pipettes (Drummond microcaps, Drummond Scientific Company, Broomal, PA) were used to spot the aqueous standards on the sorbent stationary phase.

STANDARDS AND REAGENTS

Standard solutions were prepared by consecutive dilution of elemental stock solutions, (PlasmaCal, SPC Science, Champlain, NY, USA) with 1% trace

metal grade nitric acid (TraceSelect, Fluka Chemica, Buchs, Switzerland) in 18 MΩ distilled deionized water (Milli-Q water system, Millipore Corp., Bedford, MA, USA). All standards were stored in polypropylene containers (Nalgene, USA) that had been preconditioned with 10 % trace metal grade nitric acid for a period of 24 h and rinsed with distilled deionised water.

RESULTS AND DISCUSSION

Direct sampling of Copper by LA-ICP-MS on a TLC plate

Initial experiments were performed with the element copper. Preliminary results showed that an element spotted on a TLC plate could be effectively retrieved by LA-ICP-MS and that the signal varied linearly with concentration as shown in Figure D-1. In this series of experiments, the standard solutions were applied as 1 µL spots at the center of a pencil-marked 2.38 mm diameter circle. The spots were ablated at ten different locations within their centers using the single point laser ablation mode. It was also demonstrated that linearity could be improved using the silicon present in the stationary phase as an internal standard, but with no significant impact on precision, as illustrated in Figure D-2. However, these preliminary results were disappointing with a detection limit (3σ) for Cu of 5 ppm, much higher than the low ppb detection limits normally expected in ICP-MS analyses.
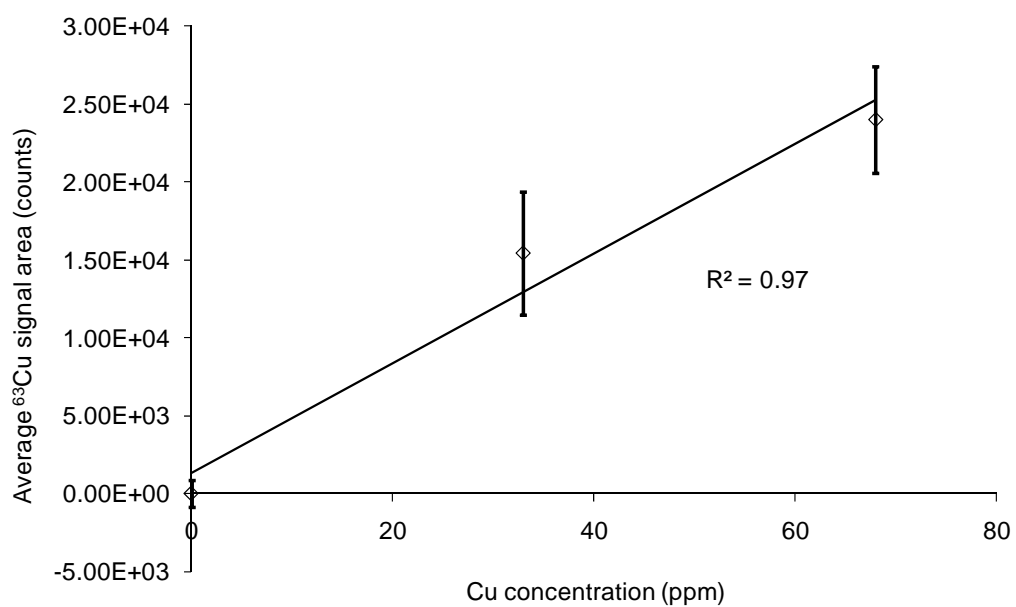
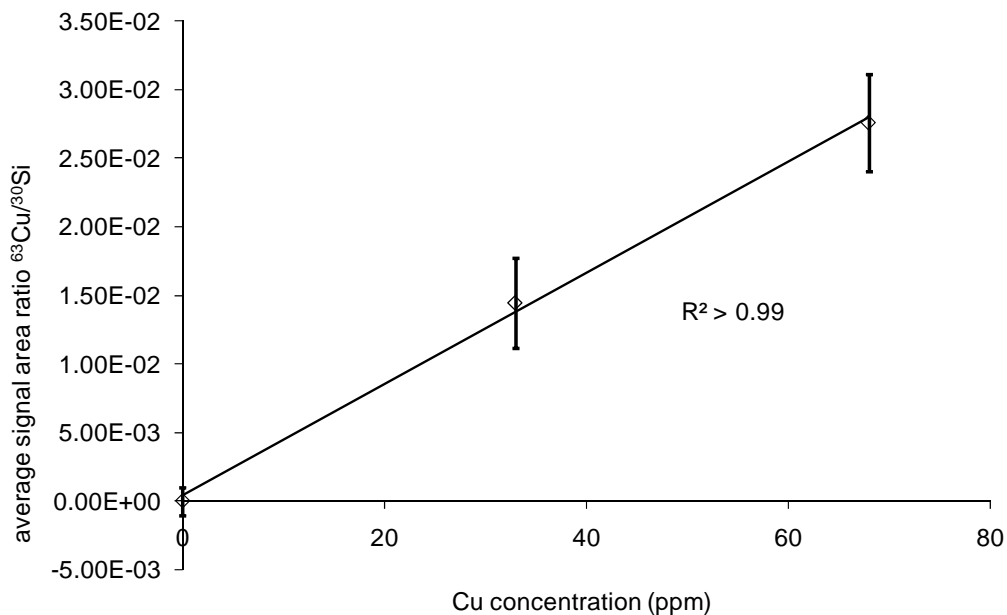Figure D-1. Direct Laser sampling of Copper spotted on a TLC plate.

Figure D-2. Use of the silicon present in the stationnary phase as an internal standard to improve linearity.

238

Pre-concentration studies

In an attempt to improve the detection limit achieved, a pre-concentration technique was tested. This technique consisted in repeating the sample spotting step at the same location on the TLC plate multiple times, allowing the plate to dry thoroughly in between each application. However, as illustrated in Figure D-3 and Figure D-4, three successive applications of the sample had little effect on the calibration curves for rhodium and lead and the detection limit remained in the low ppm range for both elements, or even increased slightly. As illustrated in Figure D-5, when the rhodium application is repeated five times, the detection limit remains in the low ppm range.
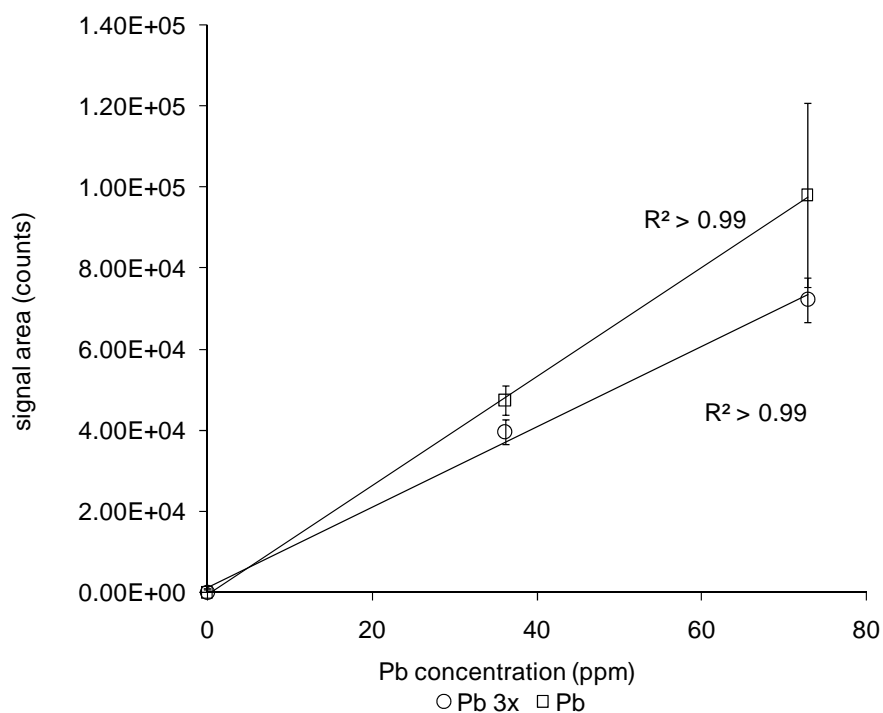
Figure D-3. Pre-concentration of lead on a TLC plate. (3x corresponds to 3 successive applications).
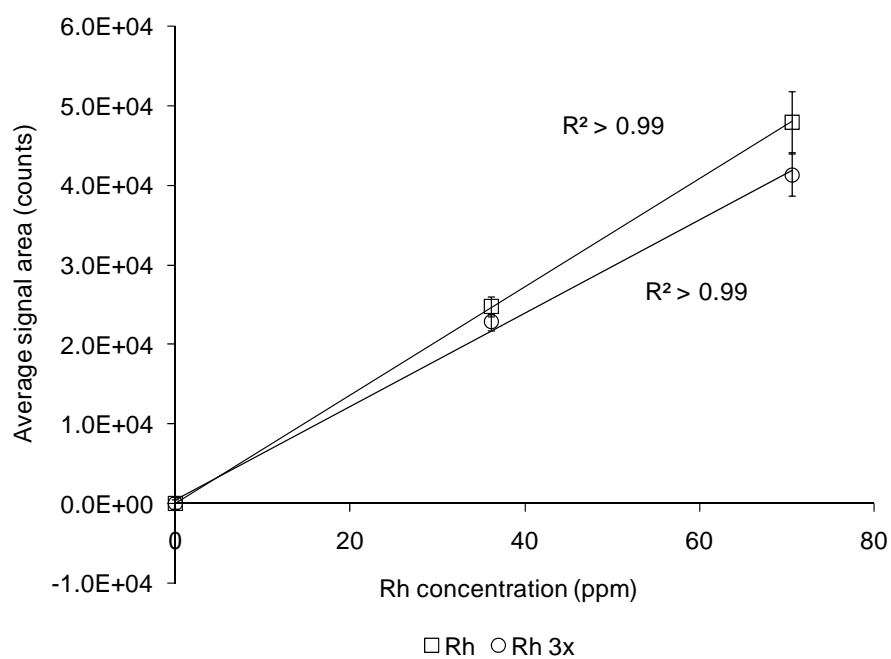

Figure D-4. Pre-concentration of rhodium on a TLC plate. (3x = 3 applications).
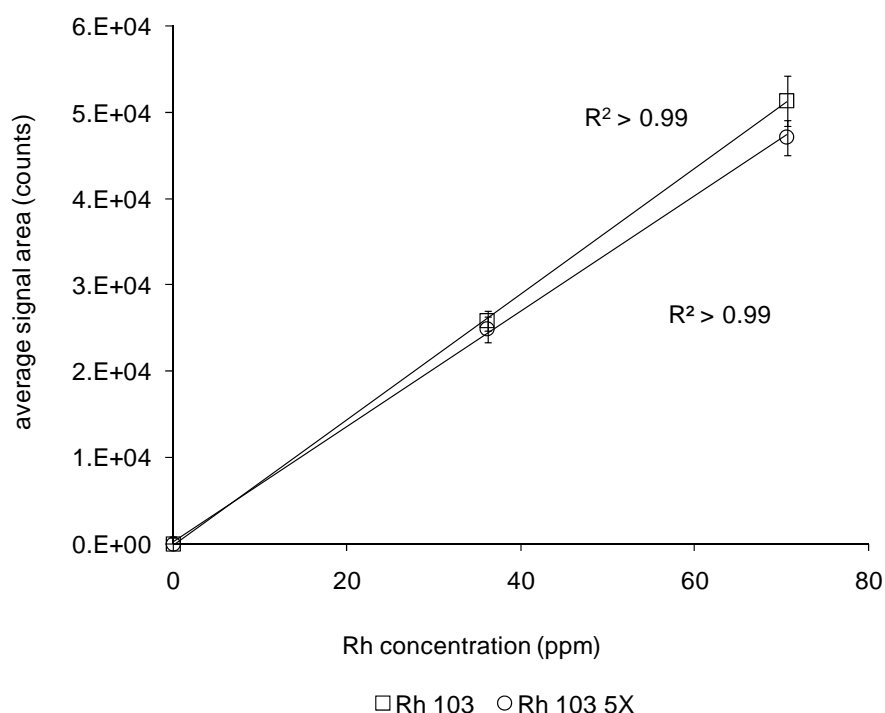
Figure D-5. Pre-concentration of rhodium on a TLC plate. For the data series marked 5x, the sample was reapplied five times on the same location.

Analysis of TLC plates using the single line scan ablation method

In this series of experiment, the standard solutions were applied as 1 µL spots at the center of a 2.38 mm pencil marked circle. The center of each circle was located visually and ablated across its center using the single line scan method. The total ablation length was roughly 4 mm. This time, the detection limit obtained for Rh was roughly an order of magnitude lower than with the previous method at 200 ppb. Moreover, it was possible to improve the detection limit further down to 100 ppb by repeating the application six times. The calibration

curves are shown in Figure D-6 where each point represents the average of three replicates. The comparative results obtained for the two methods are presented in Table D-3.

Table D-3. Detection limits obtained for Rhodium using two different methods.

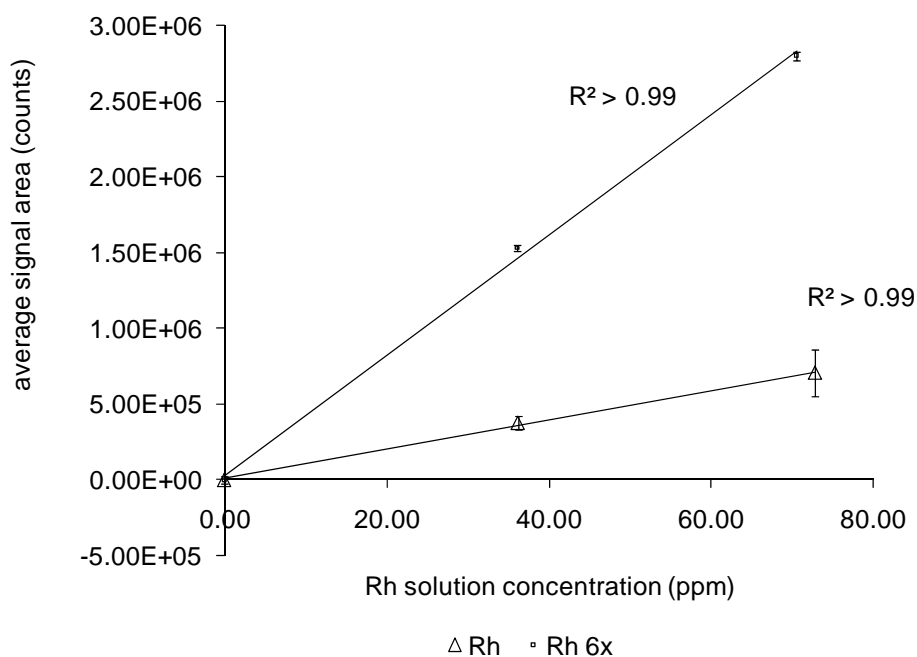| Method	Single application	Repeated applications
Single point	3 ppm	3 ppm†
Single line scan	0.2 ppm	0.1 ppm‡

†N=5, ‡ N=6

Figure D-6. Calibration curves obtained for Rh using the single line scan ablation method. The curve labelled 6X illustrates the effect of repeating the sample application six times at the same location on the plate.

It is possible to understand the increase in the slope of the calibration curve when using this method by studying the signal profiles obtained. In Figure D-7, a 3 mm wide Rh spot is ablated across its center using the single line scan method. The Rh signal increases as the laser reaches the edge of the spot, than lowers while ablating through the center of the spot and finally, rises again as the laser reaches the other edge of the spot. We can see that the center of the spots show a similar signal intensity for both the single spot application and the repeated application. However, there is a significant increase in concentration at the outer edges of the spot when the sample application is repeated six times as shown in Figure D-7. So if the single shots are ablated only at the center of the spot, it becomes impossible to notice the increase in concentration which is located primarily in the edges of the spots.
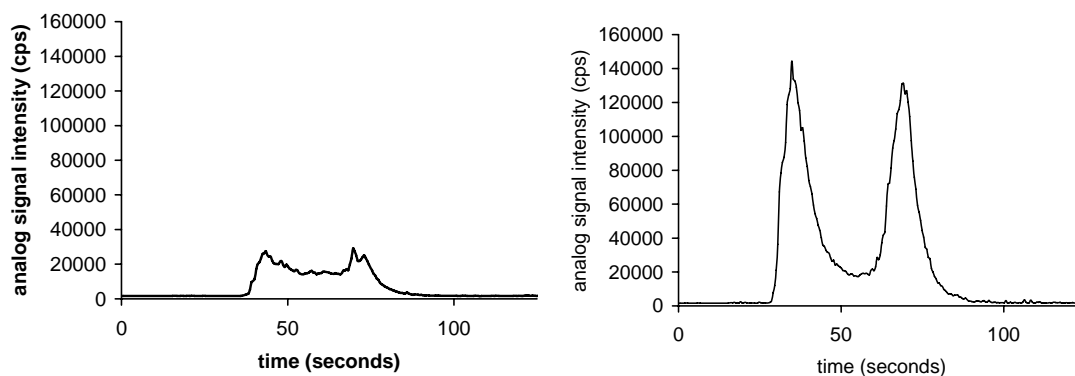
Figure D-7. Signal profile observed for: (Left) A 70 ppm 1 µL Rh spot and (Right) a 70 ppm 1 µL Rh spot that was re-applied six times at the same location on the TLC plate.

The particular sample distribution along the edges of the spot is due to the fact that during spot application, the solvent of the sample performs radial chromatography, pushing the analyte away from the center. This phenomenon is clearly illustrated in Figure D-8(A), where a significantly darker rim is visible on a red food color spot. The shape of the analyte spots will change as the lower edge of the spot will merge with its upper edge during migration as illustrated in Figure D-8(B).
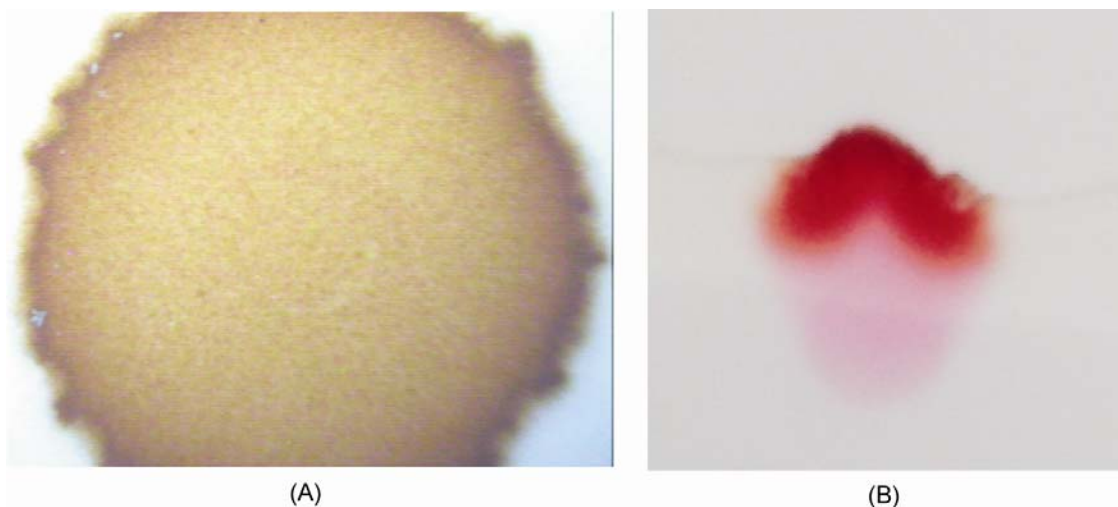
Figure D-8. (A) a 1 µL red food colour spot on a TLC plate. (B) A red food colour spot after migration on a TLC.

Separation of Cd, and Pb by TLC using Triton X-100 as a mobile phase

According to reports by Mohammad *et al.*[1] the non-ionic surfactant Triton X-100 (1% w/v) can be used as a mobile phase for the separation of heavy metal cations. For the separation of Cd^{2+} and Pb^{2+}, retardation factors of 0.87 and 0.00 are expected, respectively. As shown in Figure D-9, the Cd migrated with the solvent front as expected, only a small portion of the Pb remained at the application location, as illustrated by the characteristic double peak shape. A greater proportion of the Pb co-migrated with Cd, indicating that the Pb standard used must have been in at least two different chemical forms. Since the ICP-MS can resolve the co-migrating species by mass, this is not a problem in this case. However, the Si signal profile indicates that the stationary phase, retained by a

gypsum binder, gets dissolved by the water-based eluent, rendering the Si present in the stationary phase useless as an internal standard. As shown in Figure D-10, calibration curves are linear, but with very high imprecision (5-48% relative standard deviation) without an internal standard.
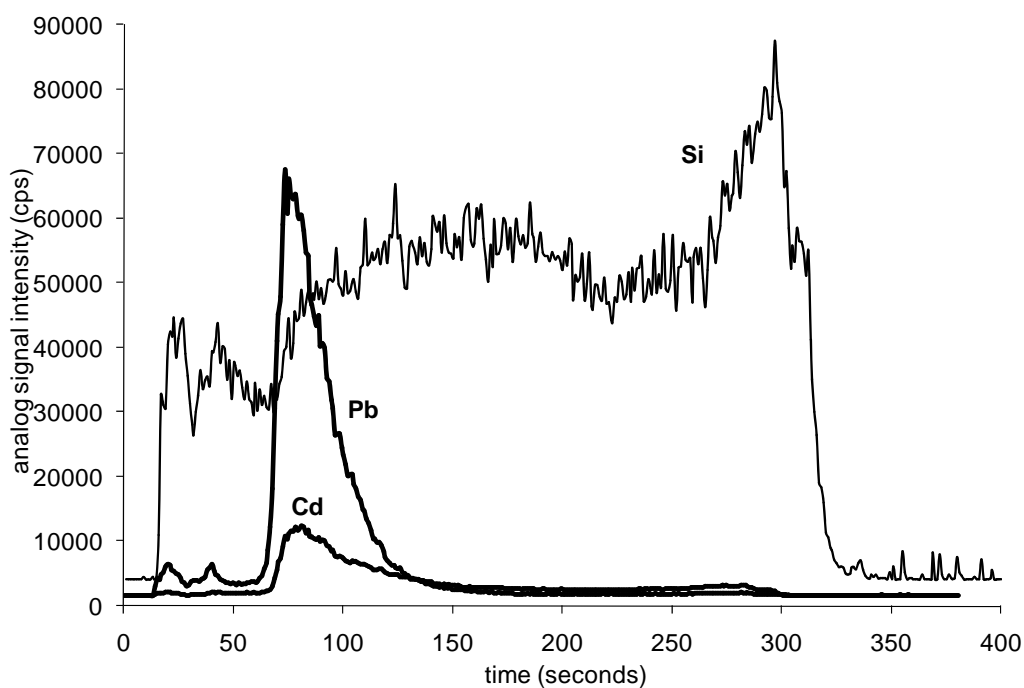

Figure D-9. Heavy metal migration from the bottom of the plate (left) to the top (right) with 1% Tx-100 eluent .
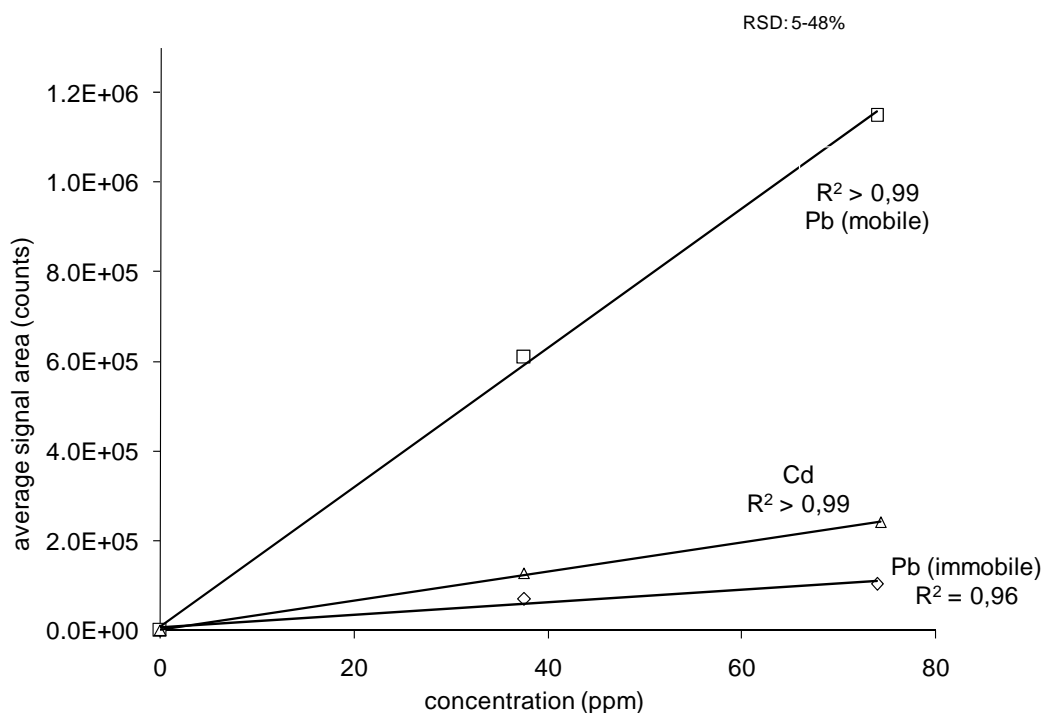
Figure D-10. Cd and Pb calibration curves obtained by TLC-LA-ICP-MS.

Speciation of Chromium

Reproducing experiments performed by Mohammad *et al.*,[2] it was expected that Cr^{3+} and Cr^{6+} could be separated by TLC with a methanol mobile phase with retardation factors of 0.05 and 0.34 respectively. However, no migration was observed when allowing the solvent to move over 10 cm. Since, as shown above, Triton X-100 can be used to separate heavy metal cations, this mobile phase was tested for chromium speciation. As seen in Figure D-11, with 1% Triton X-100 as eluent, the chromate ion $Cr_2O_7^{2-}$ (Cr^{6+}) migrates to form a broad peak while the hydrated chromic ion ($Cr(H_2O)_6^{3+}$ (Cr^{3+}) remains immobile.

Further experiments at different Triton X-100 concentrations showed that only water was sufficient to speciate chromium by normal phase TLC. As shown in Figure D-12, peak resolution was achieved by using High Performance Thin Layer Chromatography (HPTLC) plates instead of conventional TLC. Since the HPTLC plates contained a water resistant inorganic binder, instead of the gypsum found in the TLC plates, the flat Si signal shown in Figure D-12 could now be used as an internal standard. The following four calibration curves corresponds to the data presented in table format in Chapter 3. The improvement for the determination of Cr^{6+} was notable in Figure D-13 and Figure D-14, where both linearity and precision were improved when Si was used as an internal standard. In Figure D-15 and Figure D-16, the precision of the Cr^{3+} replicates also improved significantly when Si was used as an internal standard.
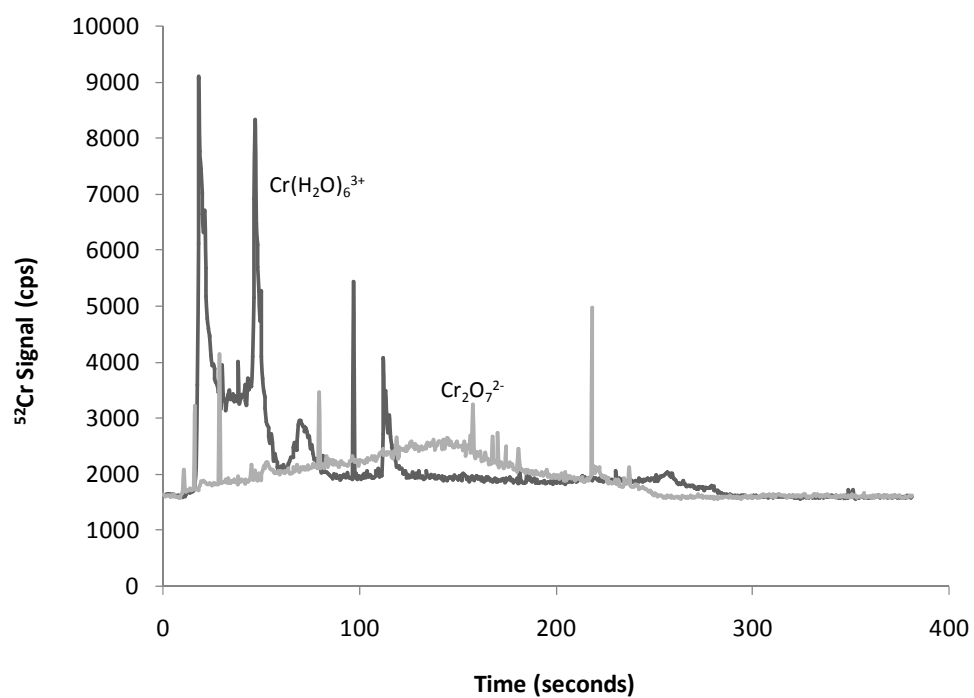
Figure D-11. Chromium speciation with a 1% Tx-100 mobile phase on a TLC plate.
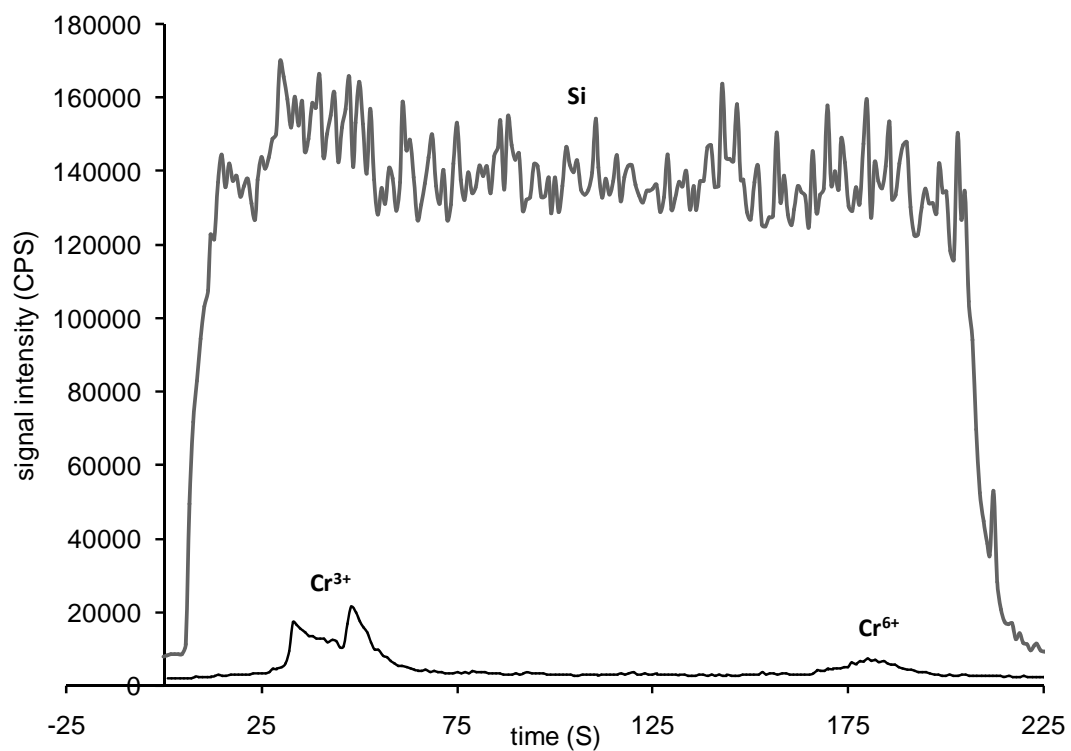
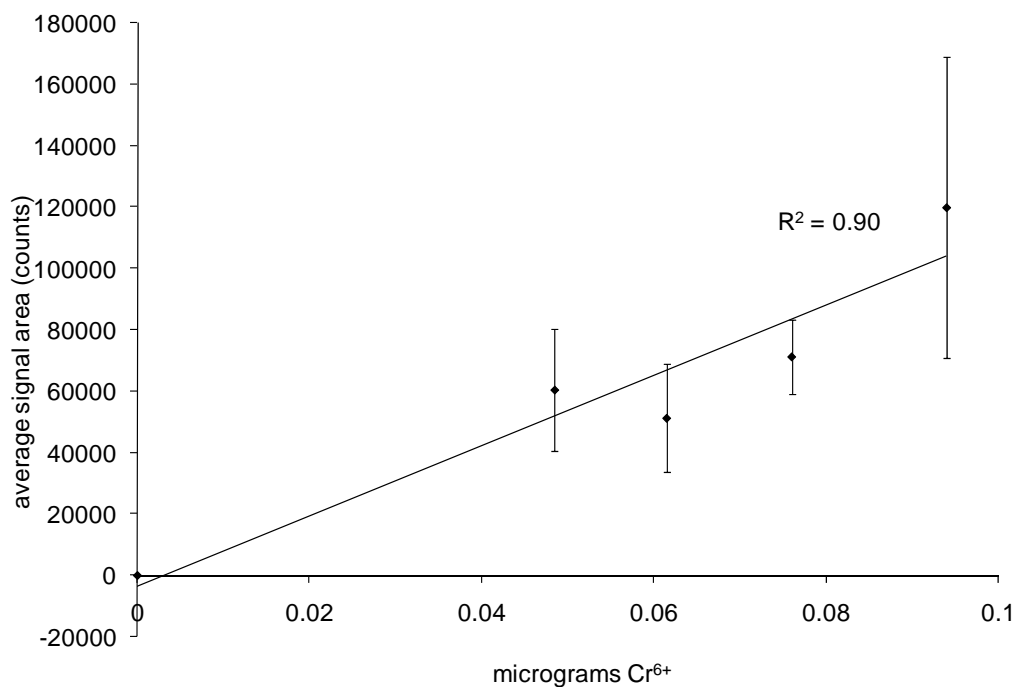Figure D-12. Chromium speciation with 0.1 % Triton X-100 on a HPTLC plate.

Figure D-13: Determination of Cr^{6+} by HPTLC-LA-ICP-MS.
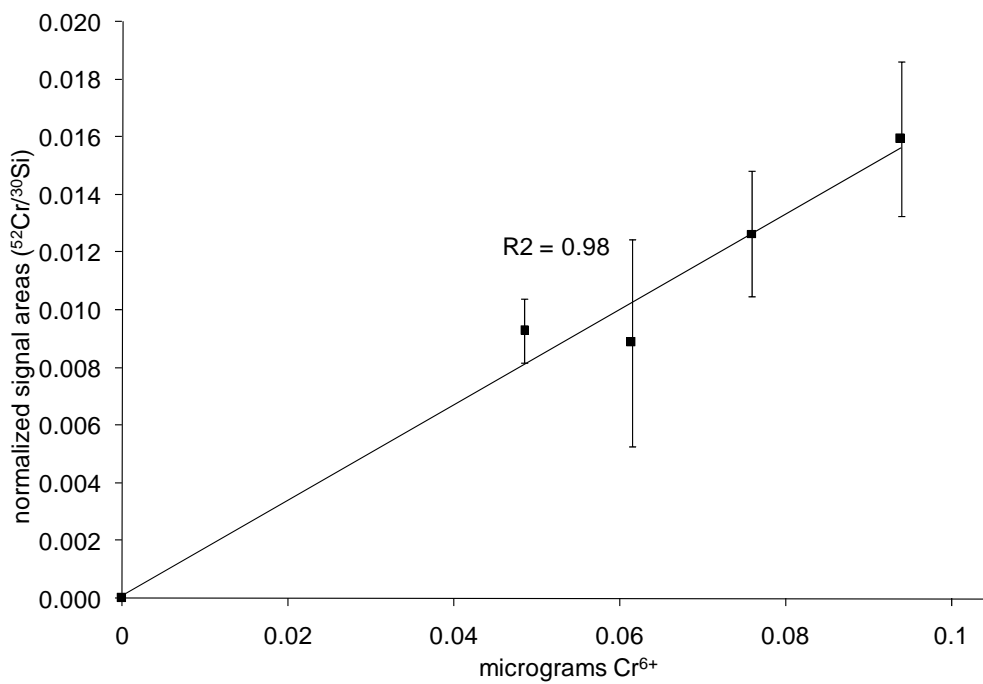
Figure D-14: Si as an internal standard in the determination of Cr^{6+}.
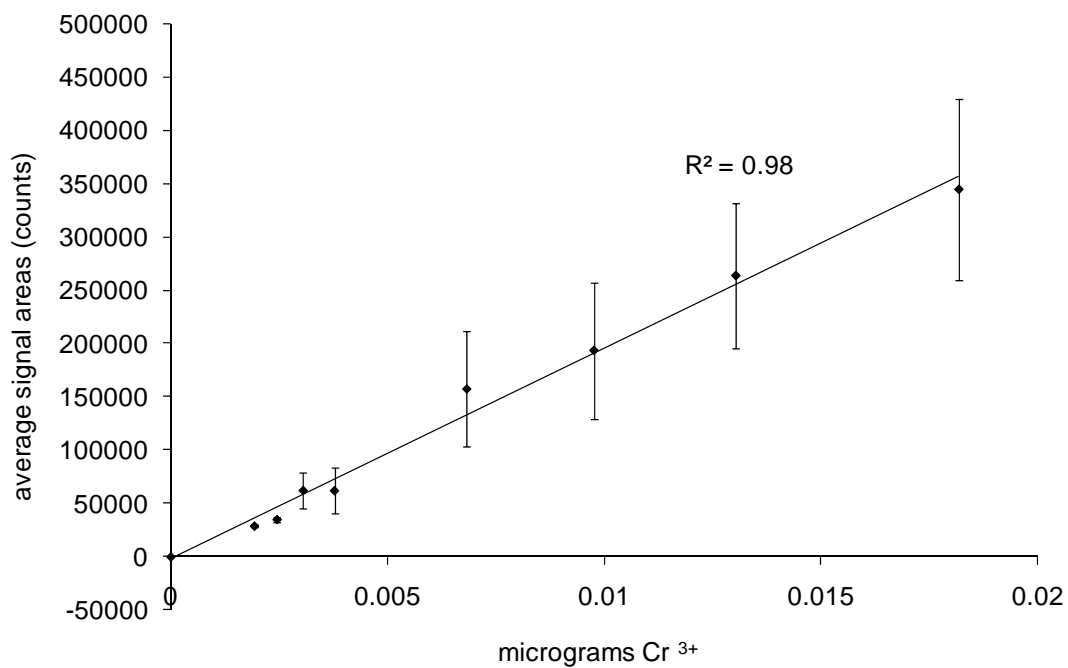
Figure D-15: Determination of Cr^{3+} by HPTLC-LA-ICP-MS.
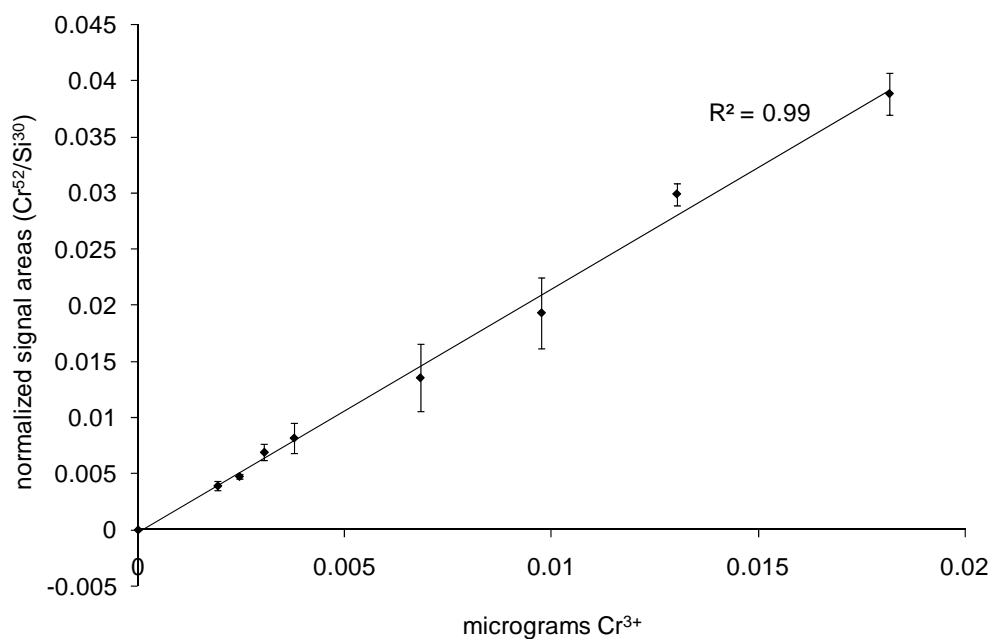
Figure D-16: Si as an internal standard in the determination of Cr^{3+}.

CONCLUSIONS

It has been demonstrated that elemental analytes can successfully be retrieved by laser ablation on a TLC plate. Detection limits are improved by ablating across a sample spot rather than at the centre of each spot with a single point method. It is also possible to improve detection limits by repeating the sample application at the same location on the TLC plate many times. The silicon present in the stationary phase material can be used, if required, as an internal standard to account for variability in laser energy.

REFERENCES

(1) Mohammad, A.; Iraqi, E.; Khan, I. A. *Journal of Chromatographic Science* **2002**, 40, 162-169.

(2) Mohammad, A.; Sirwal, Y. H. *Acta Chromatographica* **2003**, 13, 117-134.

Appendix E - Speed Monitoring and Digital Control of a DC Motor

The shaft speed calibration and digital control of the motor used for spinning the centrifugal microfluidic discs in Chapters 4, 5, 6 and 7.

MOTOR

The motor used was a permanent magnet type 90 V DC motor (Baldor Motor and Drives, Fort Smith, AR, USA). The motor can be driven in two ways. A motor drive (Penta KB Power, KBPC-240D, TechnoMotion, Montréal, QC, Canada) is used to control the motor speed manually. A signal isolator (Penta KB Power, KBSI-240D, TechnoMotion, Montréal, QC, Canada) can also be used to amplify and condition a DC voltage signal from an external source to drive the variable speed motor control with a voltage following input. The signal isolator therefore allows for digital control of the motor.

TACHOMETER DESIGN

A tachometer was built using an optical switch to measure the number of shaft rotations per minute (RPM). A microcontroller (Basic Stamp Model BS2SX, Parallax Inc, Rocklin, CA, USA) can be used to count the number of cycles (low-high-low or high-low-high) at one of its pins during a set period of time. The BS2SX stamp can respond to pulse widths as small as 1.66 µs, that is a square wave of 300 000 Hz, making it an appropriate tool for the range of speeds (0-3000 RPM or 0-50 Hz) to be monitored.

An encoder wheel consisting of a colorless, transparent plastic disk was fixed on the motor shaft. The encoder wheel was divided in four equal quarters, with alternating quarters covered with black electrical tape. The optical switch consisted of an emitter/detector pair placed on opposite sides of the rotating disk. The emitter was a green light emitting diode (LED), and the detector a simple photoresistor. As the disk rotates and alternately blocks the light, the presence or absence of the narrow light beam generated by the LED can be detected by the photoresistor. The circuit diagram is shown in Figure E-1. The voltage comparator needs to be adjusted in order to recognize when the light beam is blocked or facing a window. First, the voltage across the photoresistor is measured while the light beam is blocked (V_+ = 2.5 V), and then while the light beam is allowed to go through one of the windows (V_+ = 0.85 V). A voltage drop is observed when the photoresistor is exposed to light as the resistance diminishes and current starts flowing to ground. The voltage at the inverting input, which provides a reference voltage, is then adjusted using the potentiometer so its value is halfway between the two previous measurements (V_{ref} = 1.69 V). When the voltage at the non-inverting input is greater than the reference voltage, the voltage comparator's output is high. When the voltage at the non-inverting input is smaller than the reference voltage, the output of the voltage comparator is low.
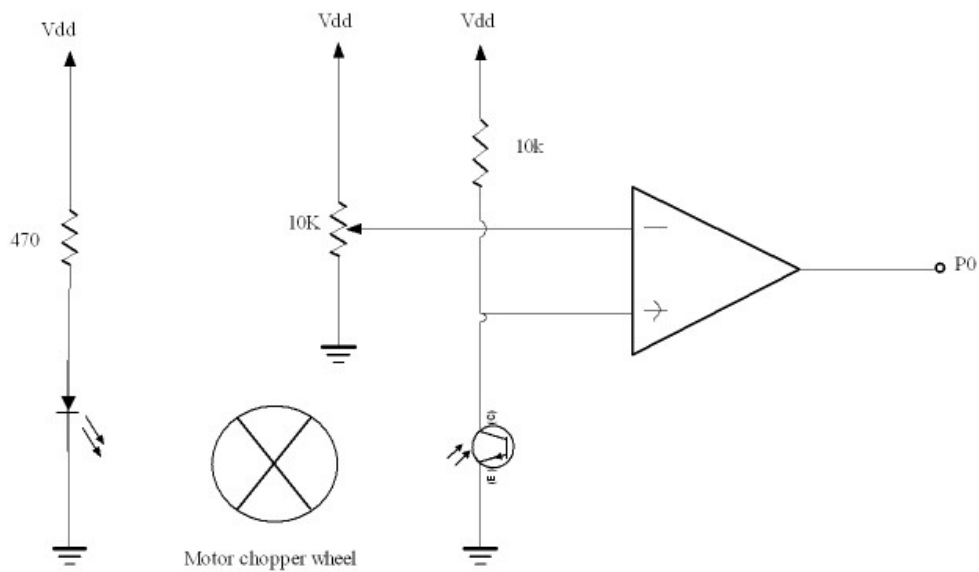
Figure E-1. Speed monitoring using a through-beam optical switch

An LCD screen (BPI-216, Scott Edwards Electronics Inc, Sierra Vista, AZ, USA) was used to display the number of counts that occurred at pin 0 during the set amount of time and to display the corresponding RPM. For example, when the adjustment knob of the motor drive is adjusted to 20, the LCD displays 555 RPM, a value that is reasonably close to the 690 RPM expected by multiplying the maximum speed of the motor, 3450 RPM, by 20%. The program was set up to count the number of pulses occurring at PIN 0 for 2 seconds to improve the stability of the readings. It is to be noted that increasing the number of cycles per

second can also increase the resolution. This is easily done by increasing the number of windows and alternating dark slices on the disk.

A retro-reflective optical switch was tested as well. In the previous configuration illustrated in Figure E-2 (left), the emitter/ detector pair was placed on either side of the chopper wheel. For the retro-reflective switch illustrated in Figure E-2 (right), both the emitter and detector were placed on the same side of the chopper wheel. The emitter consisted of an infrared transmitter (350-00017, Parallax Inc., Rocklin, CA, USA) and the detector was an infrared phototransistor (350-00018, Parallax Inc., Rocklin, CA, USA).   As described above for the through-beam optical switch, a voltage comparator was used to provide the pulses counted by the Basic Stamp. The encoder wheel consisted of a disk half of which was white the other half was black. When the emitter/detector pair faces the dark section of the disk, no light should be reflected, and the collector voltage should increase. When the pair faces the white segment of the disk, the infrared light beam is reflected back to the sensor, driving the infrared phototransistor towards saturation (ground). Even though this system should theoretically work, it proved impossible to obtain reasonable results with it. The speed displayed by the LCD screen was generally at least one order of magnitude higher than what was expected. Turning the room lights off did not improve the situation. The

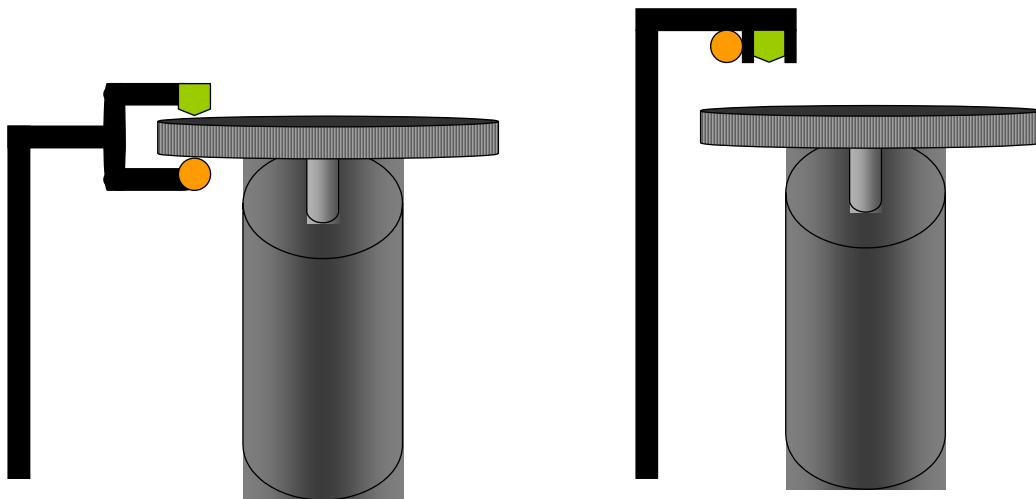proximity of many heat sources could potentially have been a problem (computers, stamp, students, etc.).

Figure E-2. Left: Beam-through optical switch. Right: Retro-reflective switch.

DIGITAL CONTROL OF THE DC MOTOR

A 12 bit serial digital to analog converter (DAC 8512FP-ND, Analog Devices, Norwood, MA, USA) was used to control the motor shaft rotation speed digitally. The first version of the circuit used a parallel digital to analog converter, but it required too many pins, so we quickly switched to serial. The DAC used has a range of 0-4.095 V with 1 mV for the least significant bit. An inverting amplifier with a gain of 2.44 is used to amplify the signal up to 10 V. Since the motor has a linear speed control with 0-10 V corresponding to 0-3450 RPM, and the minimum voltage provided would be 2.44 mV, this set up should provide us

with a 0.8 RPM/step resolution. In order to provide the necessary gain, a prototyping board with a built in power supply providing +/- 15 V was used. The grounds of the stamp and of the prototyping board were tied together. The circuit schematic is provided in Figure E-3. Two inverting amplifiers are used to provide a positive gain. The addition of a voltage follower proved necessary as the signal isolator was affecting the voltage produced by the digital to analog converter. Three pushbuttons were also added to the circuit. Messages and menus are displayed on the LCD screen, and the user can make his choice by pressing the appropriate button on the control panel. The program was designed so that a warning message is displayed on the LCD screen if the user tries to go above or below the voltage thresholds of the digital to analog converter. The user can also choose to control the motor manually or digitally. If he chooses digital control, the user pushes the appropriate pushbuttons ("+" and "-") to increase or decrease the rotation speed. The user can press the "*" to reset the speed to zero at any time. This allows the system to be very portable by eliminating the necessity of having a computer nearby.

Figure E-3. Circuit schematics for the digital control of the DC motor

Figure 4 illustrates the linearity of the speed response of the DC motor as a function of the voltage applied. The very high linearity indicates that it is not necessary to keep the speed-monitoring device (emitter/detector pair) in a permanent fashion. Figure E-4 reveals that the intercept of the digital calibration curve is non-zero. Effectively, it was noted that a minimum voltage of circa 850 mV is needed to drive the motor. The same phenomenon is observed when one tries to run the motor manually (Figure   E-5). This is not considered to be a

problem for future applications as it is not likely that a user would desire a rotation speed inferior to 60 RPM, the minimum obtainable.
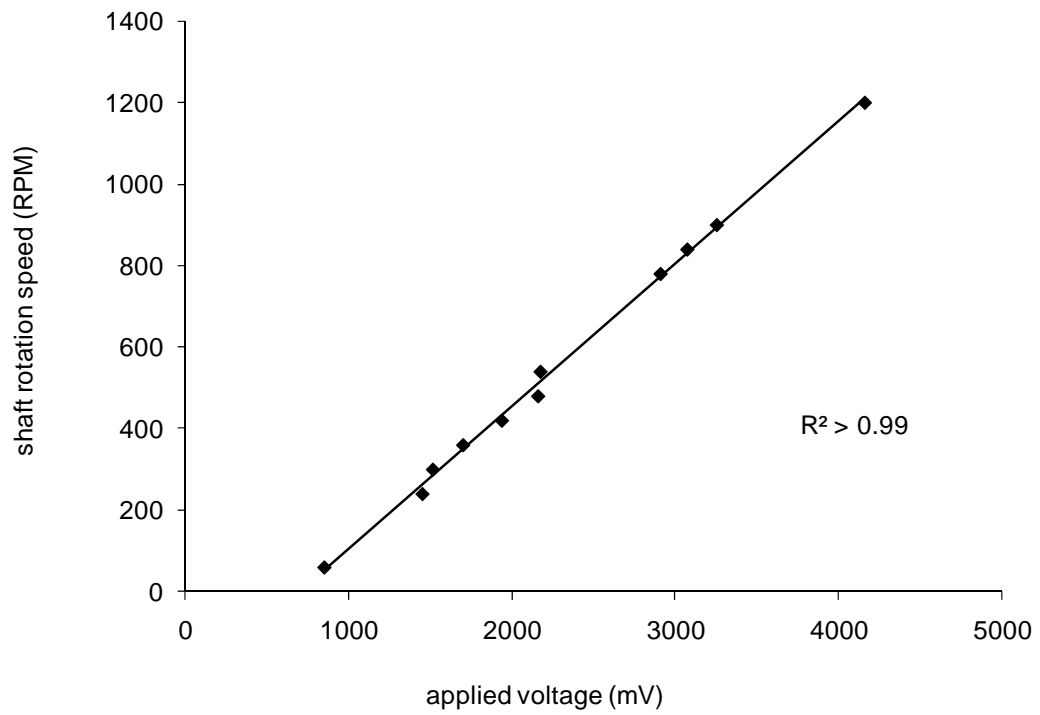

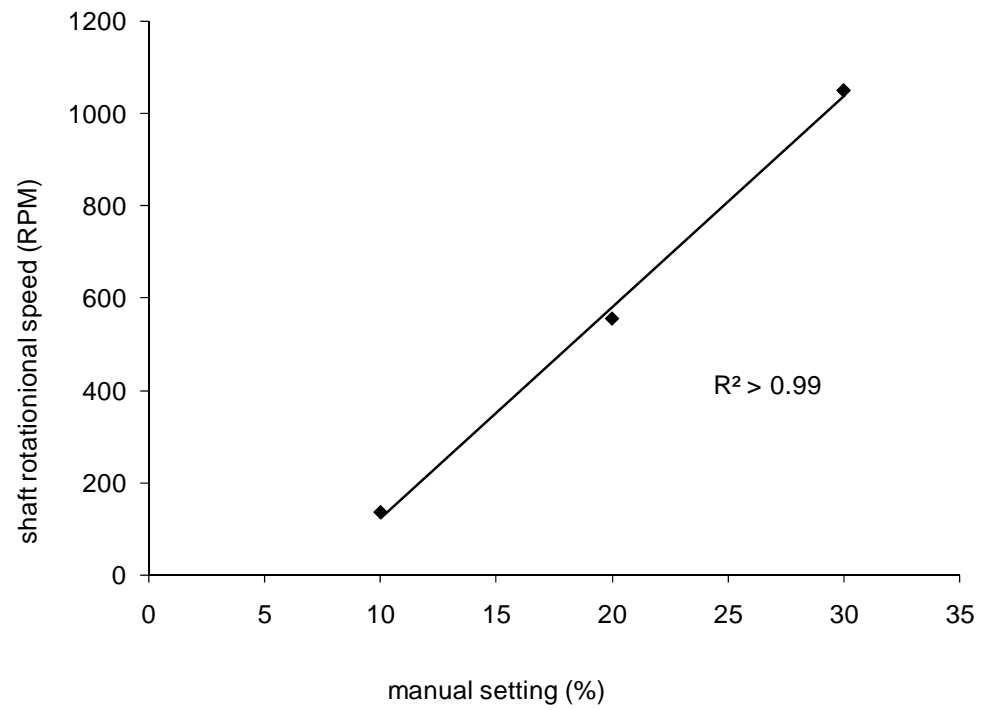Figure E-4. Digital control of the DC motor.

Figure E-5. Manual control of the DC motor.

PBASIC PROGRAM

```
' {$STAMP BS2sx}

' This program is used to monitor motor shaft speed with an optical switch

' and control digitally the speed of the Baldor motor with a Serial 12 bit DAC8512

'DECLARE ALL VARIABLES

  CS  CON 15      ' Chip select. Active low input

  CLK CON 14       ' Clock input for the internal serial input shift register

  SDI CON 13       ' Serial data input. Data on this pin is clocked into the internal

                    ' serial register on positive clock edges of the CLK pin, MSB

first

  LD  CON 11       ' Active low input which writes the serial register data into the

                    ' DAC register. Asynchronous input.

  CLR CON 12       ' Active low digital input that clears the DAC register to Zero,

                    ' setting the DAC to minimum scale. Asynchronous input


  n VAR Word       ' decimal value [0-4095] to be converted to an analog voltage


  LOW CLR          ' Clear DAC register to zero

  HIGH CLR         ' Initial setting

  HIGH LD          ' Initial settings
```

```
HIGH CS              ' Initial settings

n = 0                 ' Initial setting (0 volts)


Counts VAR Word        'Variable for result of count

RPM VAR Word           'Variable for calculated RPM

Counts=0                'Clear counts


N9600 CON $40F1         'Baudmode-9600 bps inverted

I CON 254               'Instruction prefix value

CLEAR CON 1             'LCD clear-screen instruction

LINE2 CON 192           'Address of 1st char of 2nd line

L1_C7 CON 135           'Address of line 1, character 7.

L2_C5 CON 197           'Address of line 2, character 5

L1_C4 CON 132           'Address of line 1, character 4.



'*******************************************************************

 ' First, offer to the user the choice to control the motor digitally or manually

SEROUT 1,n9600,[I,CLEAR]     ' Clear the LCD screen

 PAUSE 1

 SEROUT 1, n9600, ["+ for manual"]  'Print label
```

```
  SEROUT 1,n9600,[I,LINE2,"- for digital"]    'Move to line2 and print

MENU:

IF IN3=1 AND IN2=1 THEN MENU 'LOOP HERE UNTIL A BUTTON IS

PRESSED


 IF IN3=0 THEN MANUAL

 IF IN2=0 THEN AUTO


'*********************************************************************

' A LED and a phototransistor are facing each other

' Through a cardboard disk through which two holes have been carved

' so there should be two counts per revolution

' (two cycles, low-high-low per revolution)


MANUAL:

COUNT 0,5000, Counts          'Counts cycles on pin 0 for 2 second  (5000 *

400us)

RPM = Counts*15          'Scale to RPM


' Print out result to the LCD screen
```

```
SEROUT 1,n9600,[I,CLEAR]      ' Clear the LCD screen

PAUSE 1

SEROUT 1, n9600, ["count:"]  'Print label

SEROUT 1, n9600,[I, L1_C7]   'Move to line 1, character 7

SEROUT 1, n9600, [DEC Counts, "  "]     'Print value of counts followed by 2
spaces

SEROUT 1,n9600,[I,LINE2,"RPM:"]      'Move to line2 and print

SEROUT 1, n9600,[I, L2_C5]              'Move to line 2, character 5

SEROUT 1, n9600, [DEC RPM, "  "]      'Print value of RPM followed by 2 spaces


GOTO MANUAL

'********************************************************************

AUTO:

    SEROUT 1,n9600,[I,CLEAR]                          ' Clear the LCD screen

    PAUSE 1

    SEROUT 1, n9600, [" PRESS THE * "]

    SEROUT 1,n9600,[I,LINE2,"TO START/STOP"]    'Move to line2 and print


    START:
```

```
    IF IN4 = 1 THEN START                      'Loop here until star is

pressed


  LOOP:

  IF IN3 = 0 THEN INCREMENT

  IF IN2 = 0 THEN DECREMENT

  IF IN4 = 0 THEN RESET

  LOW  CS                                   ' Activate CS

  SHIFTOUT 13,14,MSBFIRST,[(n >>1)\12]       ' Send n to the stamp, most

significant

                                             ' bit first

  HIGH CS                                   ' Deactivate CS

  PULSOUT LD, 200                           ' Send a 400 usec load pulse


  COUNT 0,1225, Counts        'Counts cycles on pin 0 for 1/2 second  (1225 *

400us)

  RPM = Counts*60                          'Scale to RPM

  SEROUT 1,n9600,[I,CLEAR]                  ' Clear the LCD screen

  PAUSE 1

  SEROUT 1, n9600, ["mV:"]                  'Print label
```

```
SEROUT 1, n9600,[I, L1_C4]                      'Move to line 1, character 4

SEROUT 1, n9600, [DEC n, " * 2.44 "]            'Print value of volts

SEROUT 1,n9600,[I,LINE2,"RPM:"]                 'Move to line2 and print

SEROUT 1, n9600,[I, L2_C5]                       'Move to line 2, character 5

SEROUT 1, n9600, [DEC RPM, "  "]                'Print value of RPM followed by 2
spaces

GOTO LOOP


RESET:

n=0

GOTO LOOP


FASTER:

n=n+1

'PAUSE 20

GOTO LOOP


SLOWDOWN:

n=n-1

'PAUSE 20
```

```
        GOTO LOOP


    MESSAGE1:

     SEROUT 1,n9600,[I,CLEAR]                          ' Clear the LCD
screen

      PAUSE 1

      SEROUT 1, n9600, [" TOO FAST "]

      GOTO LOOP


    MESSAGE2:

     SEROUT 1,n9600,[I,CLEAR]                          ' Clear the LCD
screen

      PAUSE 1

      SEROUT 1, n9600, [" TOO SLOW "]

      GOTO LOOP


    INCREMENT:

    IF n >= 4095 THEN MESSAGE1

    IF n < 4095 THEN FASTER

    GOTO LOOP
```

DECREMENT:

IF n <= 0 THEN MESSAGE2

IF n >=1 THEN SLOWDOWN

GOTO LOOP

END   'Auto routine

'***

Appendix F - Flow modeling and column efficiency for centrifugal microfluidic packed columns

The theoretical models describing the expected fluid flow and column efficiency in the centrifugal microfluidics columns used and described throughout Chapters 4, 5, 6 and 7 are presented here. Part of this work was performed under the supervision of Prof. Cameron Skinner from Concordia University.

Liquid flow in packed microchannels achieved through centrifugally induced pressure

As introduced in Chapter 1, the fluid volumetric flow rate, Q, through packed microchannels on a centrifugal microfluidic device can be described by Equation F-1.

Equation F-1 $$Q = \left(\frac{(4R_{Hpached})^2 \rho \omega^2 \bar{r} \Delta r}{32 \eta L_{eff}} \right) hw\varepsilon$$

Where R$_{Hpacked}$ is the corrected hydraulic radius, as defined by Equation F-2:

Equation F-2 $$R_{Hpacked} = \frac{\varepsilon D_p}{6(1-\varepsilon)}$$

In which, ε is a porosity factor representing the fractional void volume in the column and D$_p$ is the diameter of the packing beads.

The quantities $\bar{r}$ and Δr represent the average distance of the liquid in the channels to the centre of the disk and the radial extent of the fluid, respectively and can be described by Equation F-3 and Equation F-4 respectively.

Equation F-3
$$\bar{r} = \frac{(r_1 + (r_0 - H))}{2}$$

Equation F-4
$$\Delta r = r_1 - (r_0 - H)$$

The quantities ρ and η are the mobile phase density and viscosity respectively, 80:20 methanol:water in this example. L_{eff} is the effective packed bed length as defined by Equation F-5, where a tortuosity factor, T, is introduced. The quantity ω is the angular velocity of the centrifugal microfluidic platform and h and w are the height and width of the column.

Equation F-5 L_{eff} = L x T

According to Equation F-3 and Equation F-4, the quantities $\bar{r}$ and Δr can be expressed in terms of r_0 and r_1, the inner and outer radii of the flowing liquid, and H, the head of the liquid being pumped through the microchannel. L is the length of the packed microchannel. Important dimensions are illustrated

schematically in Figure F-1 for model Minimax XII, the centrifugal microfluidic

device used in Chapters 6 and 7.
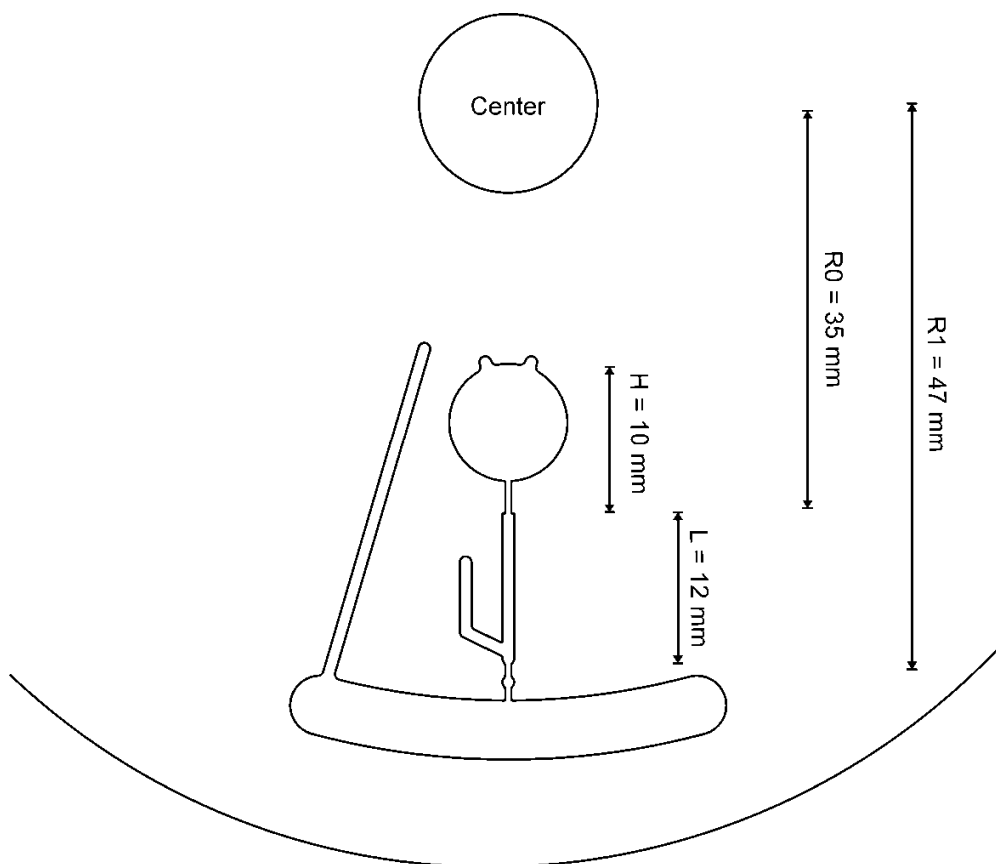
Figure F-1. Important dimensions of model Minimax XII.

The values necessary for the calculations of the volumetric flow rate are listed in

Table F-1.

Table F-1. Parameter values to calculate the volumetric flow rate in Minimax XII

Parameter	Value
H	1.0×10^{-02} m
R_0	3.5×10^{-02} m
R_1	4.7×10^{-02} m
$\bar{r}$	3.6×10^{-02} m
Δr	2.2×10^{-02} m
ε (estimated)[1]	0.46
D_p	1.00×10^{-05} m
R_h	$1.66_7 \times 10^{-06}$ m
ρ (80% methanol : water)[2]	842.6 Kg m^{-3}
η (80% methanol : water)[2]	$1,005 \times 10\text{-}03$ P (Kg m^{-1} s^{-1})
L	1.2×10^{-02} m
T (estimated)[1]	2
L_{eff}	2.40×10^{-02} m
w	1.00×10^{-03} m
h	1.00×10^{-04} m

Figure F-2 and Figure F-3 show the theoretical flow rates expected in Minimax XII's columns with 5 µm and 10 µm packing respectively. From these figures, it is obvious that the size of the packing has a large impact on the magnitude of the flow rate attainable in the centrifugal microfluidic devices. All models prior to Minimax XII used 5 µm packing, making extraction times very long, especially for Model Minimax X described in Chapter 5, which featured a 1000 µL sample reservoir. At the 1000 RPM rotational frequency used in this experiment, the calculated volumetric flow rate should be 0.3 µL min^{-1}, which

explains the two weeks it took to extract the samples. In model Minimax XII (Chapter 6 and 7), the particle diameter is increased from 5 µm to 10 µm and the rotational frequency to 1500 RPM, resulting in a theoretical volumetric flow rate of 3 µL min^{-1}. In practice, the flow rates observed were slightly higher than those calculated, perhaps due to shorter columns which were less tightly packed than estimated.
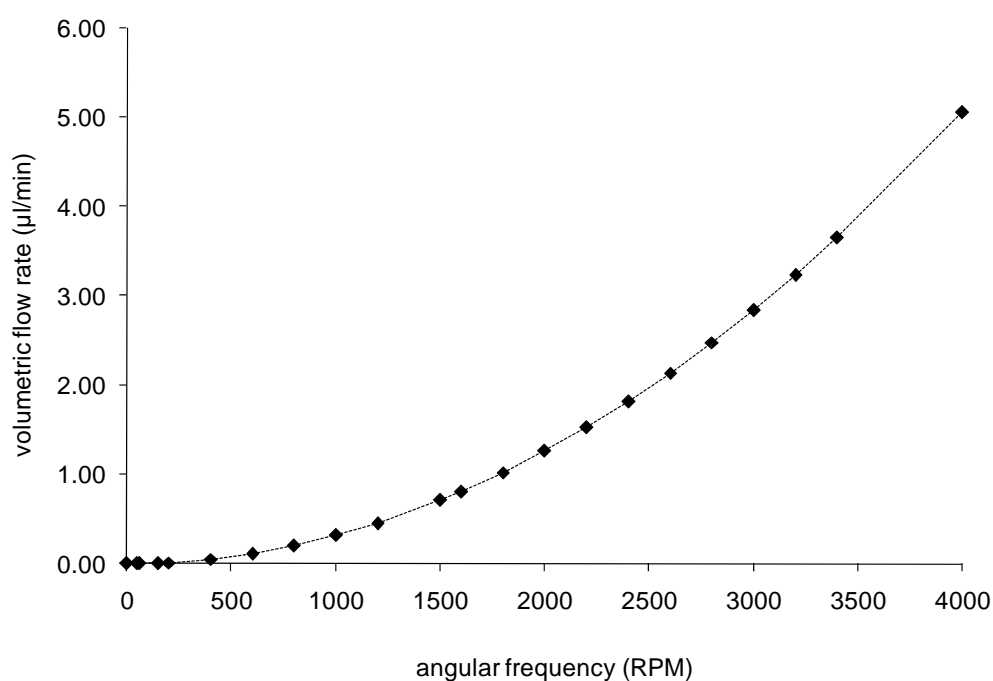

Figure F-2. Volumetric flow rate with 5 µm packing in Minimax XII's microchannels.
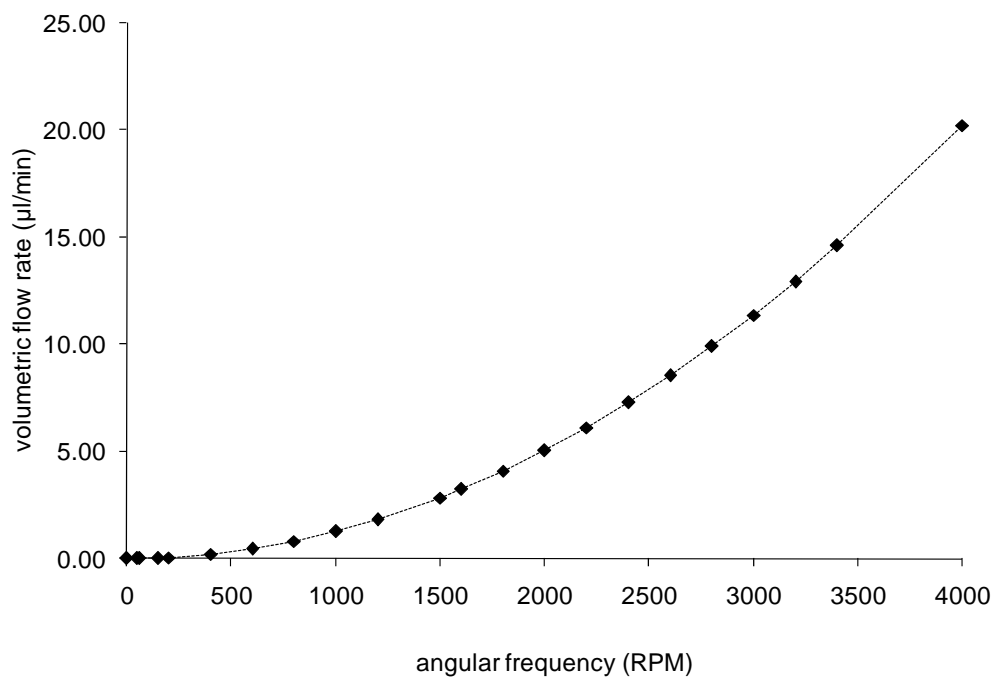
Figure   F-3. Volumetric flow rate with 10 µm packing in Minimax XII's microchannels.

COLUMN EFFICIENCY MODEL FOR THE MINIATURE CENTRIFUGAL CHROMATOGRAPHIC DEVICES

As described in Chapter 1, column efficiency can be described by the Van Deemter equation:

Equation F-6
$$H = A + \frac{B}{\upsilon} + C\upsilon$$

Where υ is the linear velocity of the mobile phase. A, B and C, are the coefficients for eddy diffusion, longitudinal diffusion and resistance to mass transfer, described by Equation F-7, Equation F-8 and Equation F-9 respectively.

Equation F-7
$$A = 2\lambda d_p$$

Where λ is the quality factor and d_p the diameter of the packing particles.

Equation F-8
$$B = 2\gamma D_M$$

Where γ is the obstruction factor and D_M the diffusion coefficient in the mobile phase.

Equation F-9
$$C = C_M + C_S = \left(\frac{1 + 6k' + 11k'^2}{24(1+k')^2} \frac{d_p^2}{D_M} + \frac{8k'}{\pi^2(1+k')^2} \frac{d_f^2}{D_s} \right)$$

Where k' is the capacity factor, D_f the thickness of the liquid coating on the stationary phase and D_s the diffusion coefficient in the stationary phase.

Using the values listed in Table F-1, the theoretical plate heights can be calculated for different mobile phase linear velocities. The results are shown in Figure F-4 for a molecule with a capacity factor, k', of 10. From these results, it can be estimated that the optimal column efficiency is achieved at a mobile phase velocity of 400 μm·s^{-1} with a minimum plate height of 24 μm (i.e. 417 plates for a 1 cm column).

Table F-1. Important variables for the estimation of the column efficiency in Minimax XII.

Variable/Constant	Value
D_M[†]	2000 μm^2·S^{-1}
D_S[†]	2000 μm^2·S^{-1}
k'	10
d_p	10 μm
d_f[‡]	2.70 x 10^{-02} μm
γ[*]	0.6
λ[*]	0.5

[†] From 1 to 4 E^{-05} cm^2 s^{-1} for solutes ranging from about 60-600 Da in molecular weights.[3]

[‡] 18 C-C bonds measuring roughly 15 Å each.

[*] For a well packed column.[4]
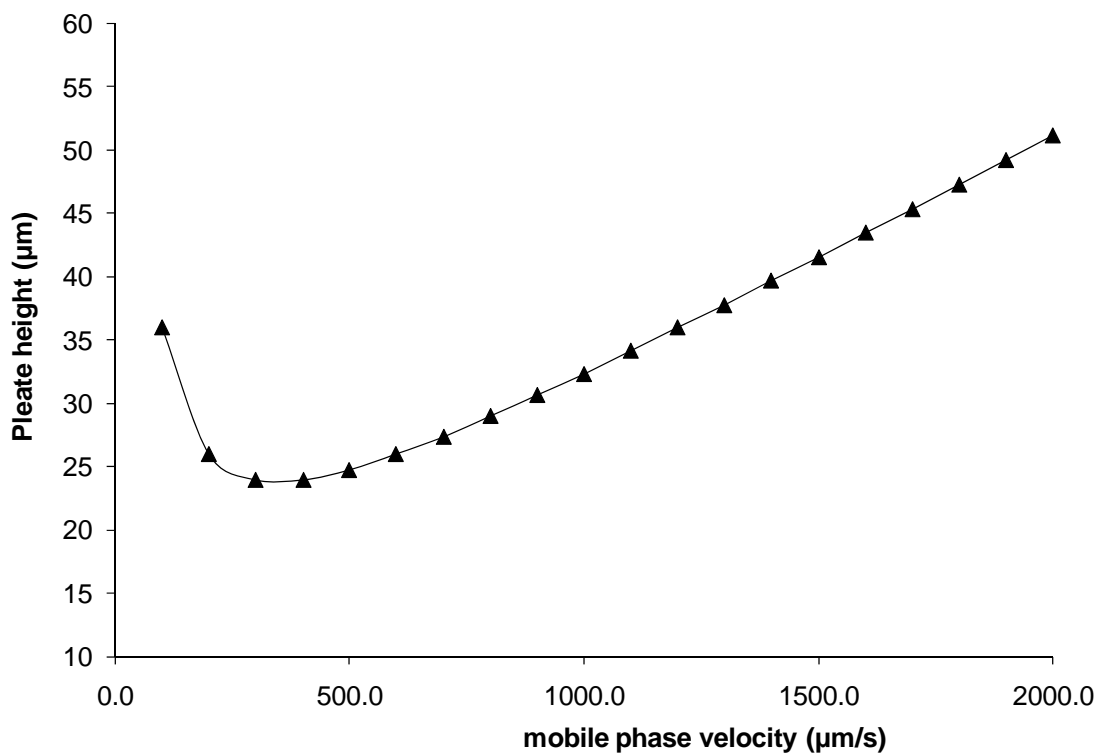
Figure F-4. Van Deemter plot for model Minimax XII when packed with 10 μm packing for a compound with a hypothetical k' of 10.

CONVERSION OF THE OPTIMAL MOBILE PHASE VELOCITY TO VOLUMETRIC FLOW RATE

Assuming that the column is composed of perfectly spherical particles uniformly packed and covered with a thin film of stationary phase material (SP), the volume of mobile phase (V_{MP}) in the column can be estimated using Equation F-10.

Equation F-10

$$V_{MP} = Volume\ inside\ column\ \times Fraction\ of\ space\ occupied\ by\ MP$$

$$Volume\ inside\ column = hwL$$

$$Fraction\ of\ space\ occupied\ by\ MP$$

$$= \frac{Volume\ occupied\ by\ MP}{Volume\ occupied\ by\ a\ box\ surrounding\ each\ sphere}$$

$$Fraction\ of\ space\ occupied\ by\ MP$$

$$= \frac{Volume\ of\ a\ box\ surrounding\ each\ particle - (volume\ of\ particle + volume\ of\ SP)}{volume\ of\ a\ box\ surrounding\ each\ sphere}$$

$$Fraction\ of\ space\ occupied\ by\ MP = \frac{d_p^3 - \left(\frac{4\pi\left(\frac{d_p}{2}\right)^3}{3} + volume\ SP\right)}{\left(d_p\right)^3}$$

$$Volume\ of\ SP = Volume\ SP\ /Unit\ area\ silica\ \times Surface\ area\ of\ one\ particle$$

$$Volume\ of\ SP = \frac{mass\ of\ SP/unit\ area\ silica}{density\ of\ SP} \times surface\ area\ of\ one\ particle$$

$$Volume\ of\ SP = \frac{SP\ MW * SP\ Surface\ density}{density\ of\ SP} \times surface\ area\ of\ one\ particle$$

$$Volume\ of\ SP\ = \frac{SP\ MW \times (Surface\ coverage \times silanol\ density)}{density\ of\ SP} \times 4\pi \left(\frac{d_p}{2}\right)^2$$

Fraction of space occupied by MP

$$= \frac{d_p^3 - \left(\frac{4\pi \left(\frac{d_p}{2}\right)^3}{3} + \left(\frac{SP\ MW \times (Surface\ coverage \times silanol\ density)}{density\ of\ SP} \times 4\pi \left(\frac{d_p}{2}\right)^2\right)\right)}{\left(d_p\right)^3}$$

Replacing the values for the 10 µm diameter silica octadecylsilane functionalized packing material used and typical values for the surface coverage and silanol density:[5]

Fraction of space occupied by MP

$$= \frac{(10\ \mu m)^3 - \left(\frac{4\pi \left(\frac{10\ \mu m}{2}\right)^3}{3} + \left(\frac{284.6\ g\ mol^{-1} \times (0.34 \times 8E^{-18}\ mol\ \mu m^{-2})}{7.95E^{-13}\ g\ \mu m^{-3}} \times 4\pi \left(\frac{10\ \mu m}{2}\right)^2\right)\right)}{(10\ \mu m)^3}$$

Fraction of space occupied by MP $= 0.48$

$$V_{MP} = hwl \ \times fraction\ of\ space\ occupied\ by\ MP$$
$$= 0.01\ cm \ \times \ 0.1\ cm \ \times 1.2\ cm \times \ 0.48 = 5.7E^{-4}\ cm^3$$

The corresponding volumetric flow rate at the optimal mobile phase velocity can be calculated using Equation F-11.

Equation F-11
$$Q = \frac{V_{MP}}{dead\ time} = \frac{V_{MP}}{L/v}$$

$$Q = \frac{5.7E^{-4}\ cm^3}{1.2\ cm/0.04\ cm\ s^{-1}} = 1.9E^{-5}\ cm^3 s^{-1} = 1.1\ \mu L\ min^{-1}$$

Therefore, the optimal flow rate for a molecule being separated on Minimax XII with a hypothetical k' of 10 would therefore be 1.1 µL min^{-1}, which corresponds to a rotational frequency of 950 RPM referring back to Figure F-3.

REFERENCES

(1)   Penrose, A.; Myers, P.; Bartle, K.; McCrossen, S. *Analyst* **2004**, *129*, 704-709.

(2)   Mikhail, S. Z.; Kimel, W. R. *Journal of Chemical & Engineering Data* **1961**, *6*, 533-537.

(3)   Scott, R. P. W. In *Liquid Chromatography Column Theory*; John Wiley and Sons: New York, 1992, pp 279.

(4)   Giddings, J. C. *Dynamics of Chromatography*; Marcel Decker: New York, 1965.

(5)   Snyder, L. R.; Kirkland, J. J.; Glajch, J. L. *Practical HPLC Method Development*; John Wiley and Sons: New York, 1997.

Appendix G - Supplementary figures for Chapter 6

Calibration curves are shown for the results described in Chapter 6.

LOW CONCENTRATION DRINKING WATER (EP-L-2) CRM

Calibration curves are shown below for the standard additions on the low concentration drinking water certified reference material (CRM) EP-L-2. The CRM was spiked three times with a multi-element reference solution and four to eight replicates were obtained at each concentration.
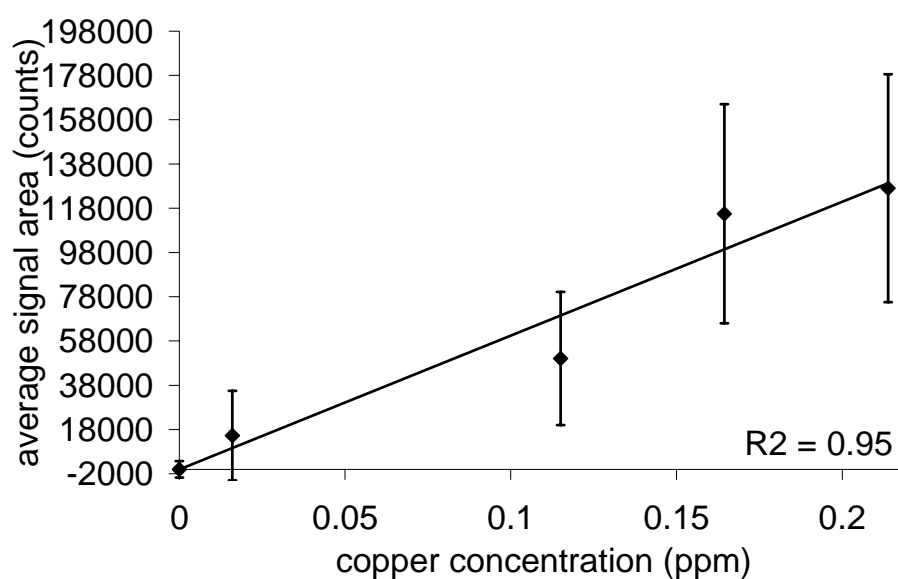
Figure G-1. Copper calibration curve obtained by spiking of EP-L-2 CRM.
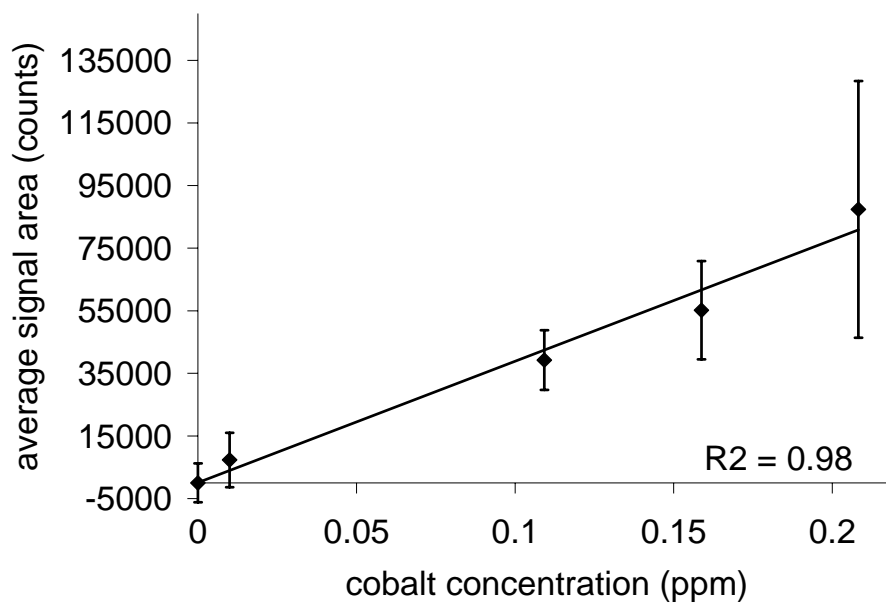
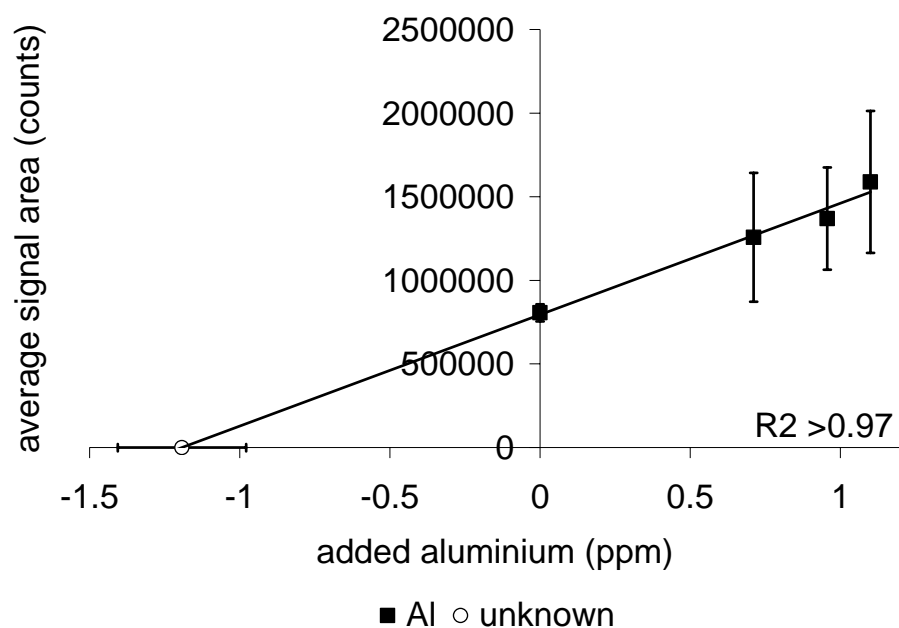Figure G-2. Cobalt calibration curve obtained by spiking of EP-L-2 CRM.
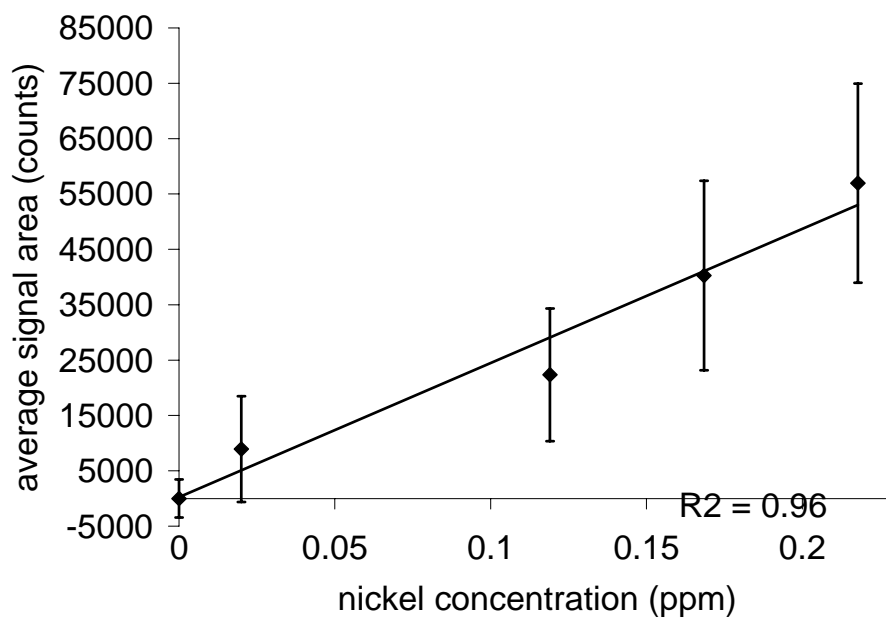
Figure G-3. Nickel calibration curve obtained by spiking of EP-L-2 CRM.
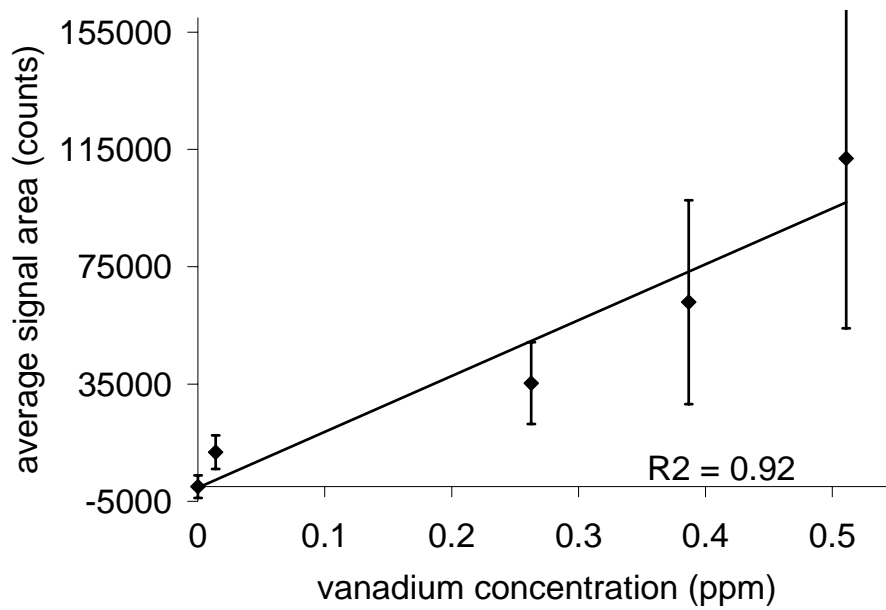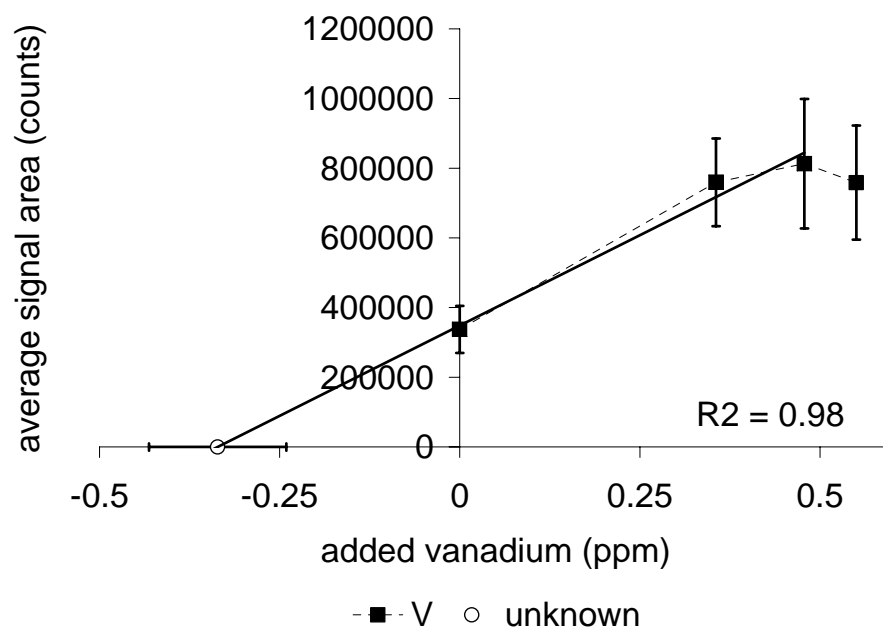
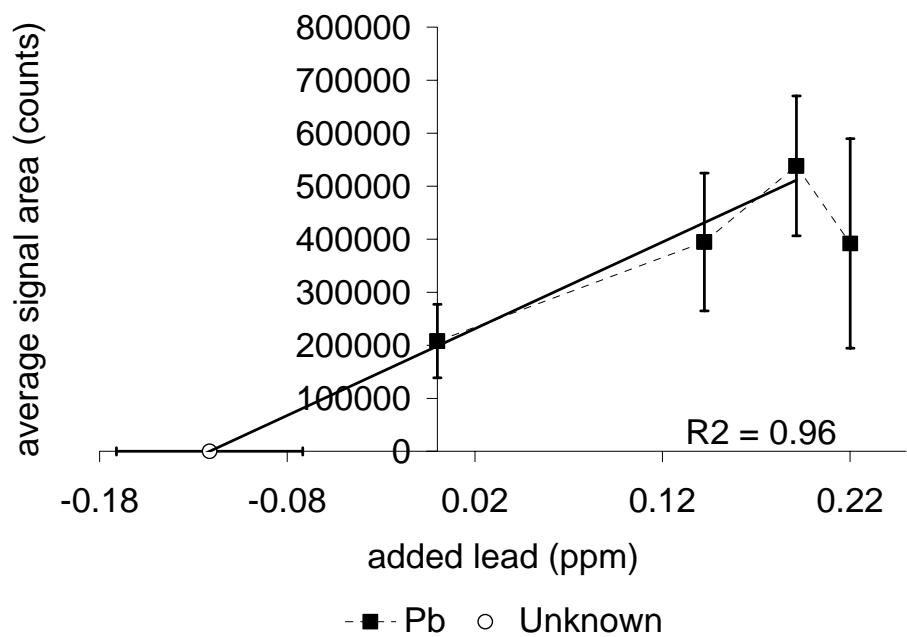Figure G-4. Vanadium calibration curve obtained by spiking of EP-L-2 CRM.
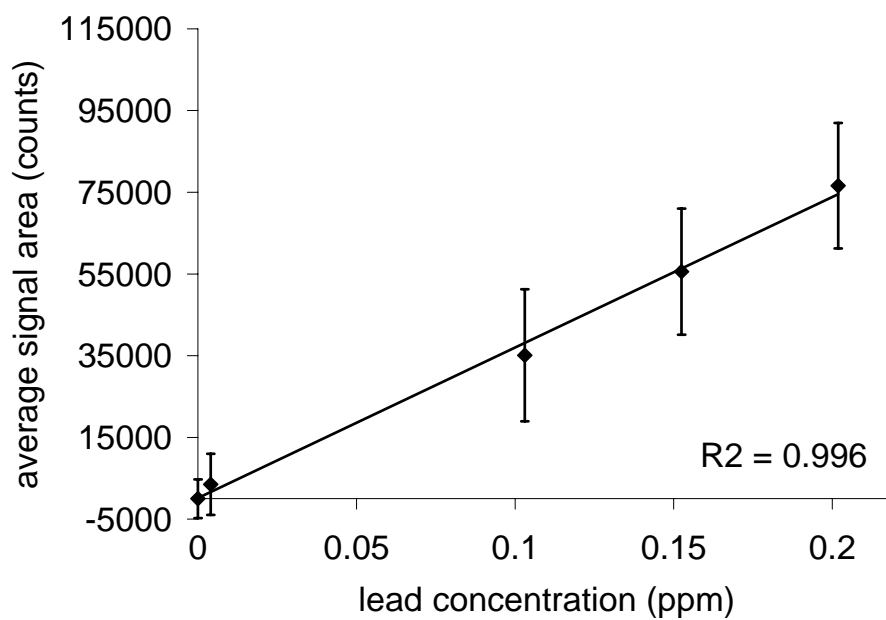
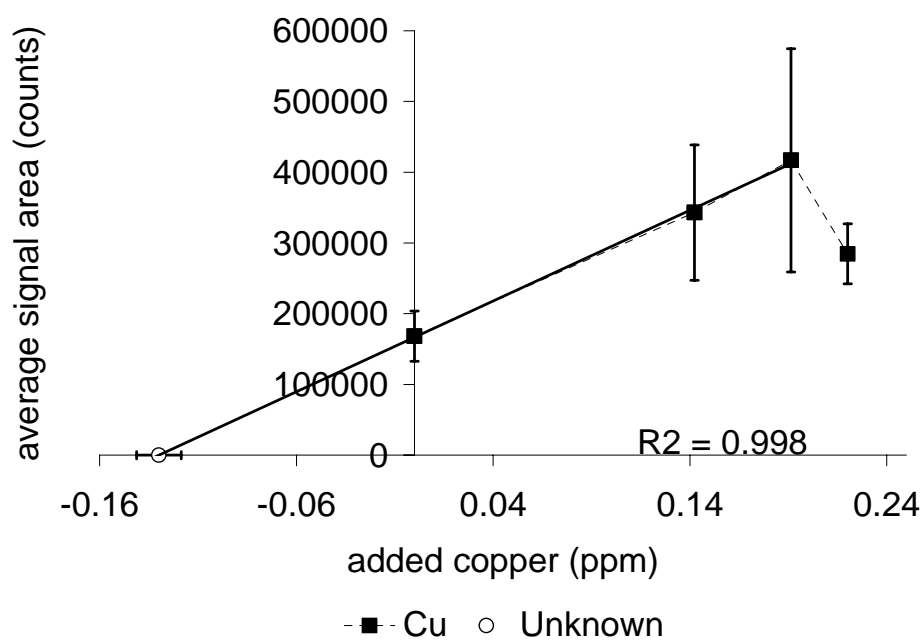Figure G-5. Lead calibration curve obtained by spiking of EP-L-2 CRM.

HIGH CONCENTRATION DRINKING WATER (EP-H-2) CRM

Calibration curves are shown below for the standard additions on the high concentration drinking water certified reference material (CRM) EP-H-2. The CRM was spiked three times with a multi-element reference solution and five to eight replicates were obtained at each concentration. The points labelled "unknown" in the plots represent the estimated concentration of the CRM as determined using the graphical method in standard additions. The calibration curve for Aluminium is shown but was not used due to the very high blanks obtained for this element, indicating impurities in the packing material. The curves for the other elements show the deviations from linearity encountered at the highest concentrations.

Figure G-6. Aluminium calibration curve obtained by spiking of EP-H-2 CRM.

Figure G-7. Vanadium calibration curve obtained by spiking of EP-H-2 CRM.

Figure G-8. Lead calibration curve obtained by spiking of EP-H-2 CRM.

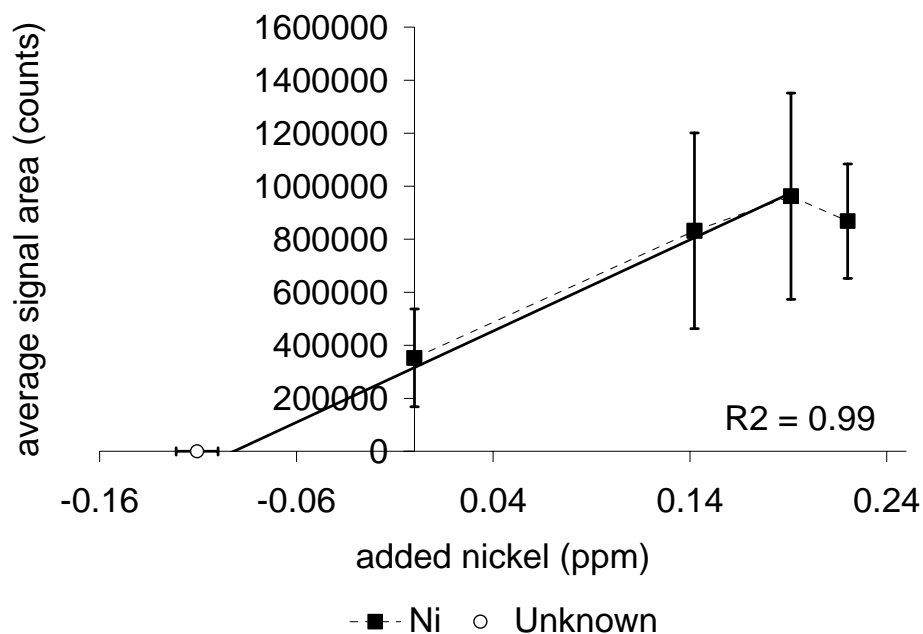Figure G-9. Copper calibration curve obtained by spiking of EP-H-2 CRM.

Figure G-10. Nickel calibration curve obtained by spiking of EP-H-2 CRM.

EXTRACTION OF CONTAMINATED VS. PURE STANDARDS

As described in the text, the spiking of the high concentration CRM EP-H-2 resulted in estimated concentrations lower than the actual concentrations. Figure G-11 compares the calibration curves obtained for lead extracted from EP-H-2 and from pure aqueous standards matrices. The signal areas obtained for the extraction of the pure standards is consistently approximately three times higher than for the EP-H-2 standards.
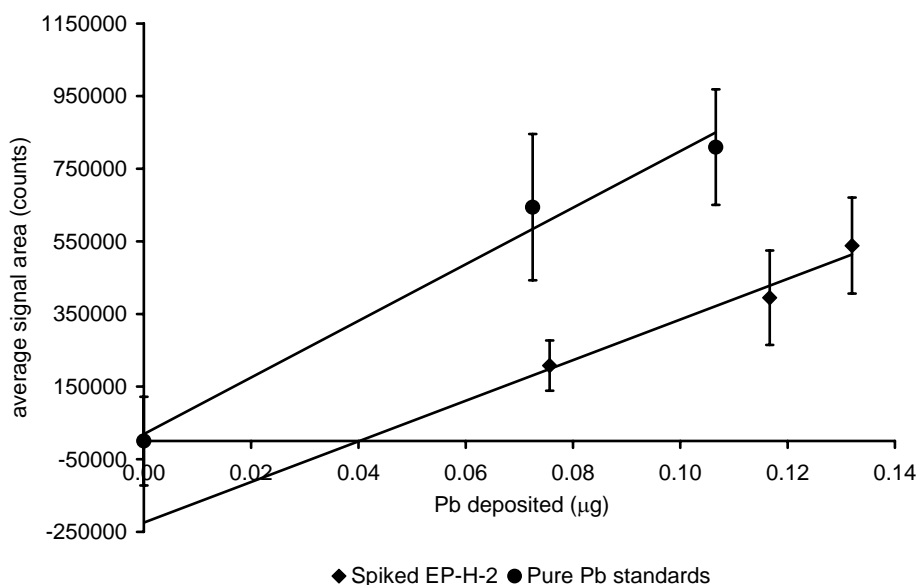
Figure G-11. Discrepancy in the lead signal intensity in pure standards and contaminated drinking water CRM (EP-H-2)

ARTIFICIAL HIGH CONCENTRATION DRINKING WATER

Calibration curves are shown below for the standard additions on the artificial high concentration drinking water. The artificial drinking water sample was spiked three times with a multi-element reference solution and four to eight replicates were obtained at each concentration. The points labelled "unknown" in the plots represent the estimated concentration of the artificial drinking water sample as determined using the graphical method in standard additions. The calibration curves after internal standardization are also shown for Vanadium and Lead.
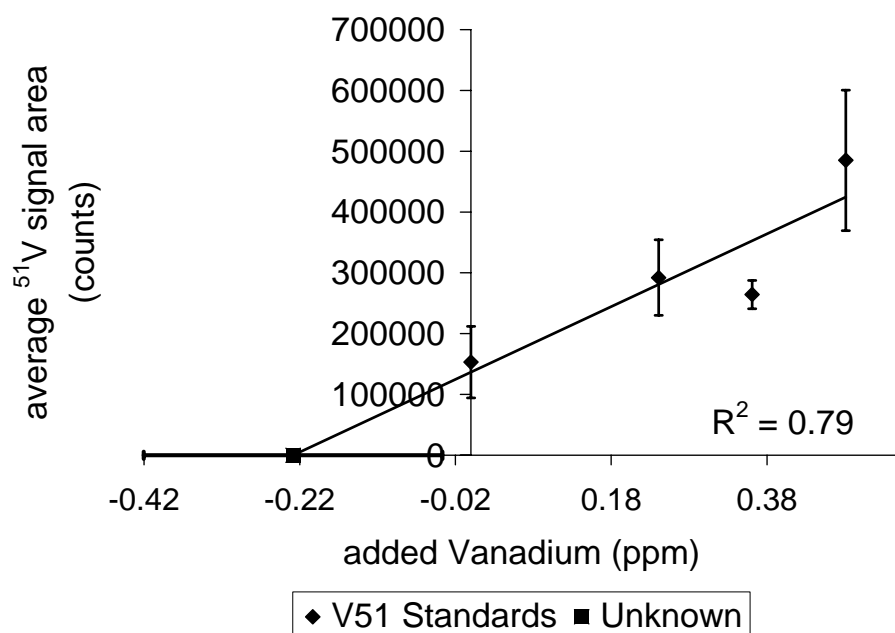
Figure G-12. Vanadium calibration curve obtained by spiking the artificial high concentration drinking water sample.
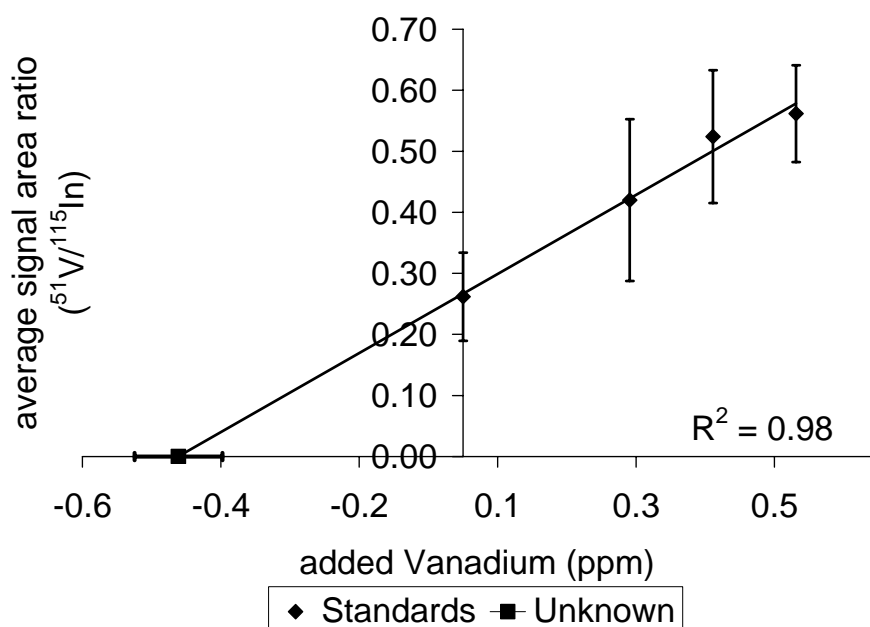

Figure G-13. Vanadium determination with Indium as an internal standard.
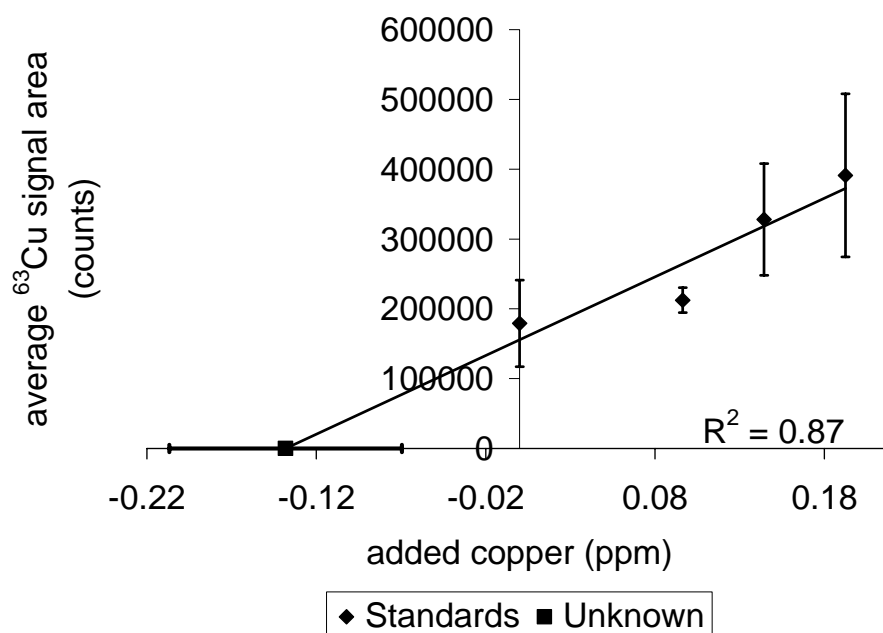
Figure   G-14. Copper calibration curve obtained by spiking the artificial high
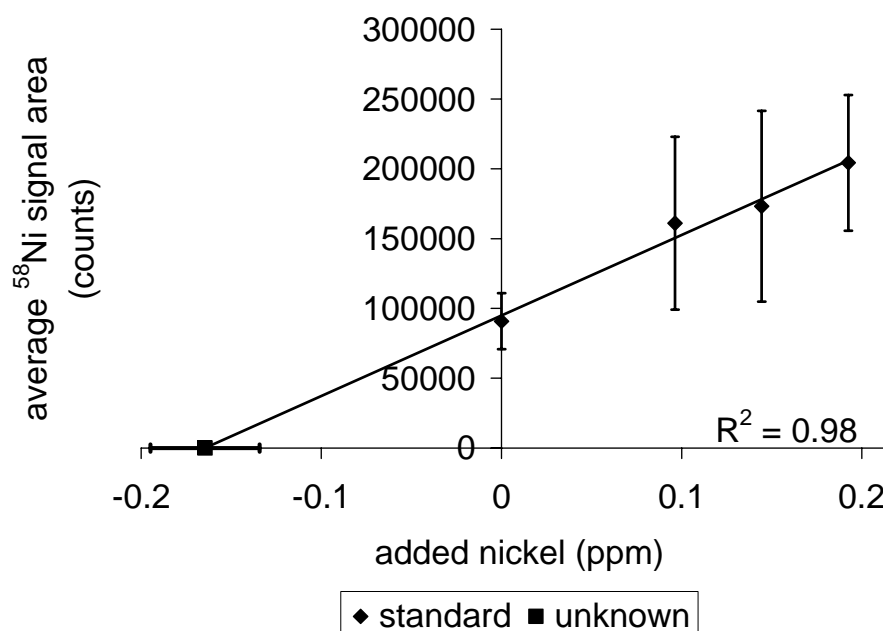
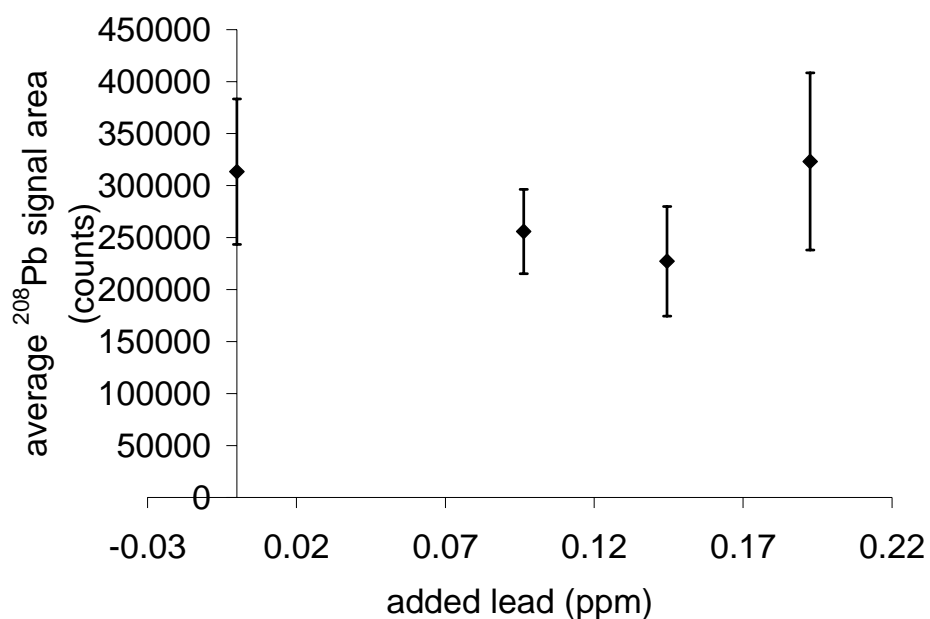concentration drinking water sample.

Figure G-15. Nickel determination.

Figure   G-16. Lead calibration curve obtained by spiking the artificial high
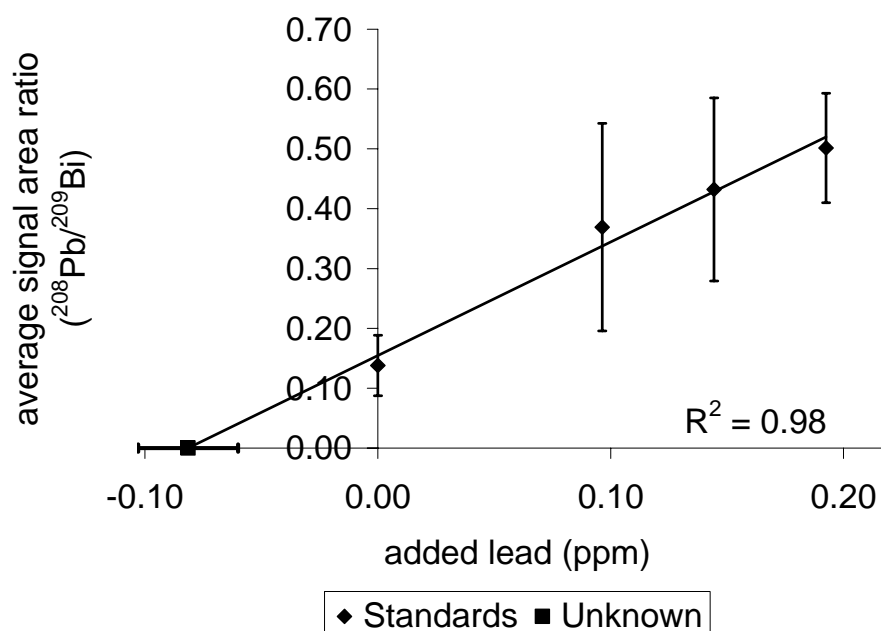
concentration drinking water sample.
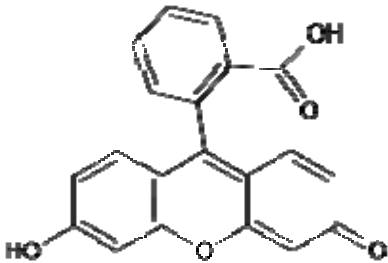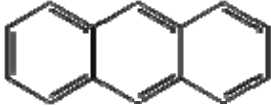

Figure G-17. Lead determination with bismuth as an internal standard.

Appendix H - Theoretical calculations, additional figures and circuit schematics for Chapter 7

CHOICE OF MATERIAL FOR OPTICAL APPLICATIONS

The properties of the two target molecules chosen for this study are listed in Table H-1. The choice of material to construct the polymeric microfluidic devices was dictated by the properties of the molecules studied.

Table H-1. Fluorescein and anthracene physical properties

Fluorescein	Anthracene
Excellent quantum yield (0.95)	Moderate quantum yield (0.36)[1]
Good water solubility (0.05 g/L)[1, 2]	Poor water solubility (0.000022 g/L)[2]
$\lambda_{excitation}$ 494 nm	$\lambda_{excitation}$ 252 nm
$\lambda_{emission}$ 518 nm	$\lambda_{emission}$ 380, 399, 425 nm

Polymethylmethacrylate (PMMA) and polycarbonate (PC) were chosen as materials for the construction of our centrifugal microfluidic devices due to their low cost and machinability. However, working with polymeric materials can have

several drawbacks when optical measurements are to be taken. As illustrated in Figure H-1, the transmittance of PC falls off sharply below 300 nm, making it unsuitable for the determination of anthracene. The transmission range can normally be extended by using PMMA, but care should be taken in the grade of material used. Initial experiments were performed with UV stabilized PMMA, which, as illustrated in Figure H-2, shows only a small transmission peak around 260 nm. However, for absorbance measurements, a special grade of PMMA, designed for improved light transmission in the ultraviolet region of the spectrum (transmittance provided in   Figure H-3) proved useful for absorbance measurements and was used for the fluorescein determination by absorbance spectrophotometry. Although it has better transparency the polycarbonate, PMMA exhibits auto-fluorescence as illustrated in Figure H-4 Figure H-4 Quartz was the only material capable of transmitting the light of the 255 nm UV LED used in the anthracene determination, so hybrid centrifugal devices, PC-Quartz, had to be used.
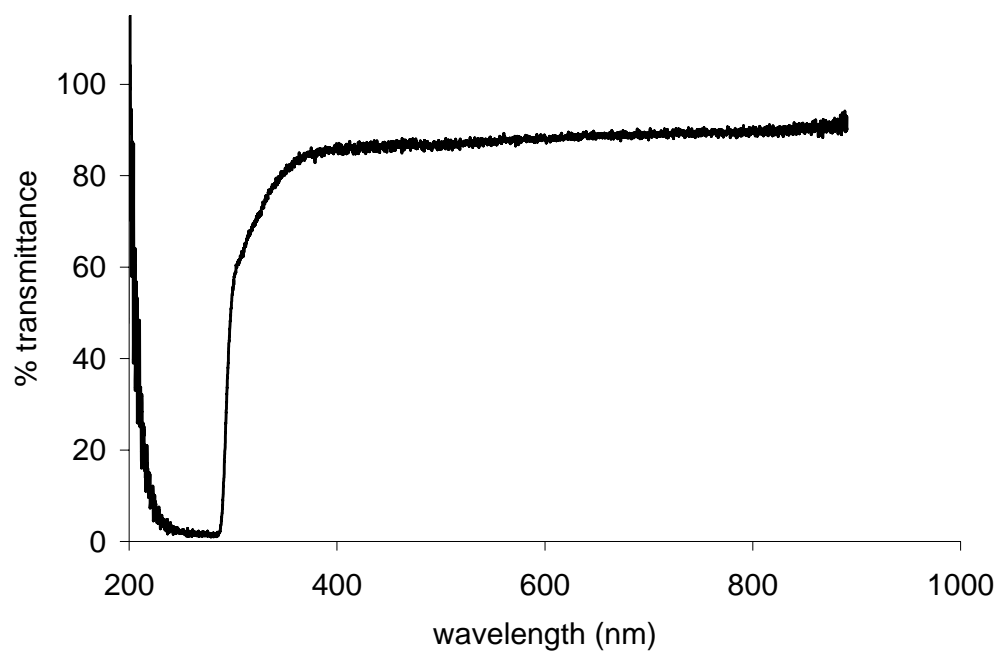
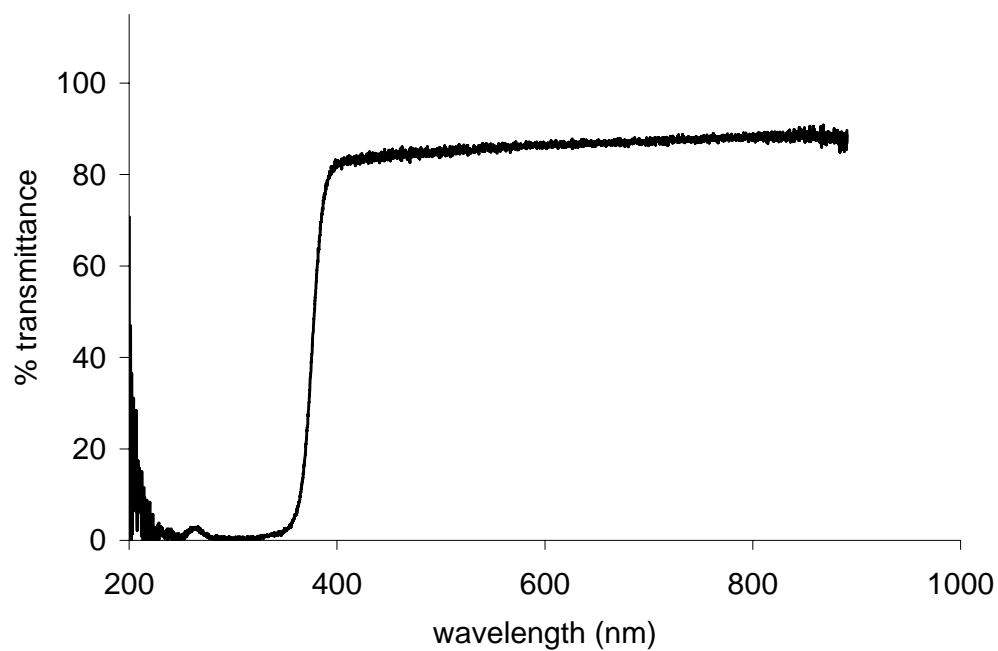Figure H-1. Transmission spectra of polycarbonate (Acquired by Scott McAuley)

Figure H-2. Transmission spectra of UV stabilized PMMA (Acquired by Scott McAuley)
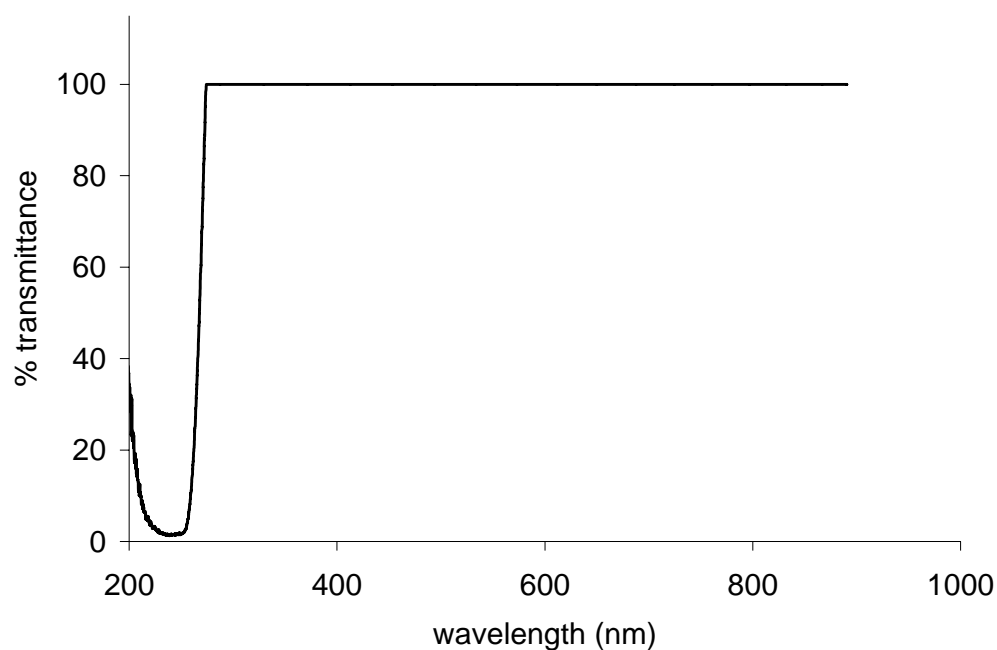
297

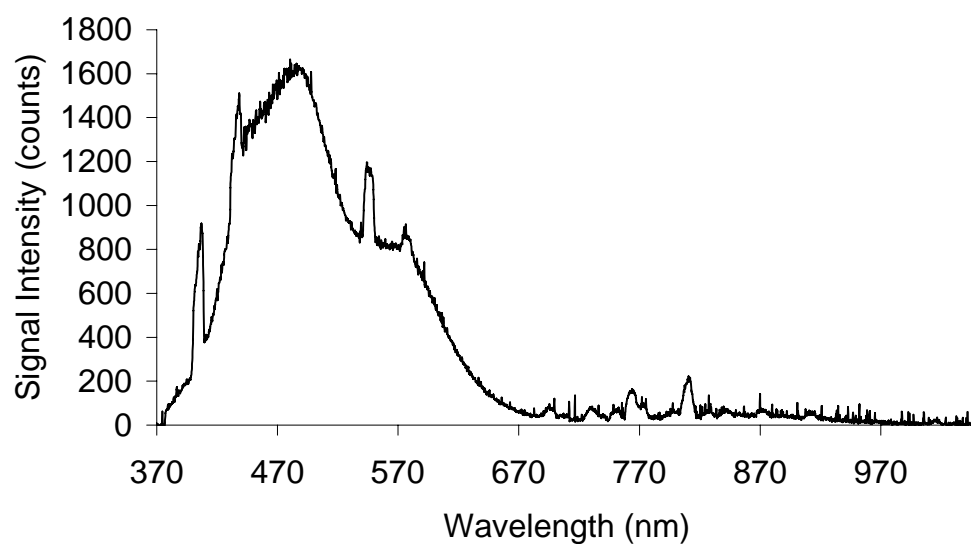Figure H-3. Transmission spectra of Acrylite OP-1 (Acquired by Scott McAuley).

Figure H-4. PMMA autofluorescence when excited with a mercury pen lamp equipped with a shortpass 254 nm filter.

Recovery studies

In order to determine the sorption efficiency of the miniature SPE columns, the contents of the waste reservoirs were collected after sample extraction/pre-concentration and analysed with a Fluormax-2 spectrofluorometer (Horiba Jobin Yvon, Edison, NJ, USA). The overlayed spectra of the blank, sample and waste are shown in Figure H-5. The large peak centered around 300 nm is due to the fluorescence of the Triton-X 100 surfactant. The characteristic fluorescence signal of anthracene is seen on the 300 ppb signal between 370 nm and 500 nm. Integration of the peaks in the 391-487 nm interval reveals that 98 % of the anthracene was adsorbed on the SPE column. The limit of detection of the method is 0,2 ppb and the concentration of anthracene in the waste is 7 ppb.
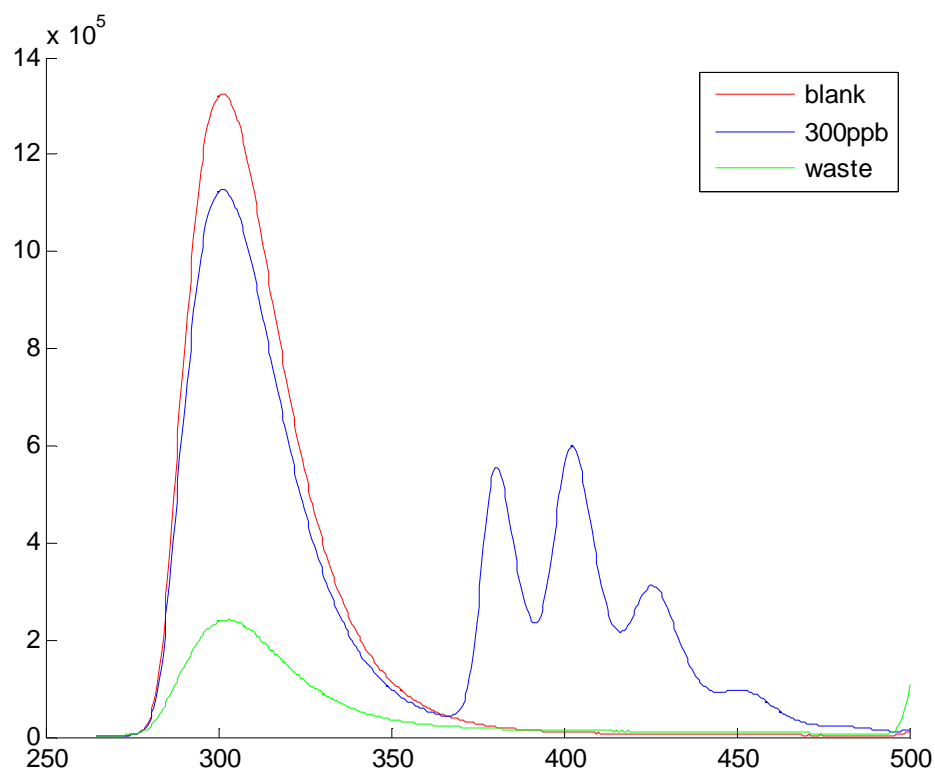
Figure H-5. Overlayed spectra of a Triton-X 100 blank, 300 ppb anthracene solutions and contents from the waste reservoir after extraction on the miniature SPE device.

Prediction of the expected limit of detection

Using theoretical equations and parameters listed in Table   H-2 we can model the expected detection limit for this system using the UV LED light source and PMT detector.

Due to the magnitude of the numbers, we list a large number of significant figures in the following calculations. However, these results are only good to one

significant figure. We can calculate the energy, E, of the photons emitted by the UV LED using Equation H-1.

Equation H-1 $\qquad E = h\nu = \dfrac{hc}{\lambda}$

Where h is Planck's constant, ν is the frequency of the photons electromagnetic wave, c is the speed of light and λ is the wavelength of the photon. The energy of a photon emitted by the UV LED at 256 nm is therefore:

$$E = \frac{6.626 \times 10^{-34} J\,s \times 299792458\, m\,s^{-1}}{256 \times 10^{-9}\, m} = 7.8 \times 10^{-19} J\,photon^{-1}$$

And the energy of the photons re-emitted by anthracene at 399 nm is $4.9 \times 10^{-19} J\,photon^{-1}$

Table   H-2. Theoretical parameters

Quantity	Value	Units
Anthracene properties		
Molecular weight	178.23	g mol^{-1}
Quantum efficiency (ϕ)	0.36 [3]	dimensionless
Molar Absorptivity (ε)	186 000 (at 256 nm)[4]	L mol^{-1} cm^{-1}
$\lambda_{excitation}$	256	nm
$\lambda_{emission}$	399	nm
PMT and UV LED characteristics		
PMT radiant sensitivity	30	V nW^{-1}
PMT ripple noise	2	mV
LED optical power output	150	μW
LED spot diameter	2	mm
Other important parameters		
Fibre optic acceptance angle (2θ)	25.4	degrees
Cell pathlength (b)	1	cm
Microcolumn pathlength (b)	0.01	cm
Microcolumn volume	0.001	cm^3

From the manufacturer's specification, we know that the power of the UV LED is 150 µW, we can therefore estimate how many photons are emitted per second.

$$\frac{0.00015 \, Js^{-1}}{7.8 \, x \, 10^{-19} \, J \, photon^{-1}} = 1.93312278 \times 10^{14} \, photons \, s^{-1}$$

The UV-Led created an approximately 1 mm diameter (r = 0.5 mm) focused output. Assuming that the sample is illuminated by a perfect cylinder of light, we can estimate the number of molecules in the volume encompassed by this light cylinder.

$$area \; illuminated \; = \; \pi \, r^2 \; = \; \pi(\, 0.05 \, cm)^2 \; = \; 0.0079 \, cm^2$$
$$Volume \; illuminated \; (cuvette) \; = \; 0.0079 \, cm^2 \; \times \; 1 \, cm \; = \; 7.9 \; \times 10^{-3} \, cm^3$$
$$Volume \; illuminated \; (microcolumn) \; = \; 0.0079 \, cm^2 \; \times \; 0.01 \, cm \; = \; 7.9 \; \times 10^{-5} \, cm^3$$

For a 100 ppb anthracene standard (5.61 x 10^{-7} M), we can estimate how many molecules are present in the illuminated volume. For comparison purposes, we treat the microfluidic device in three different ways. In the first, we treat it as just a simple microfluidic cell, with no column, to see what type of detection limit are achievable with such a short pathlength. In the second approach, we add the extraction column, so that when a 140 µL sample is percolated through the columns, all the anthracene molecules present are extracted and distributed uniformly through the column. In the third approach, we add the pre-

concentration capability and assume that all the extracted anthracene molecules

are concentrated in the upper third of the column.

$$Molecules\ illuminated\ (cuvette) = \ 5.61\ x\ 10^{-10} mol\ cm^{-3}\ \times 6.023\ \times$$
$$10^{23}\ molecules\ mol^{-1} \times\ 0.0079\ cm^3 = 2.7\ \times 10\ ^{12}\ molecules$$
$$Molecules\ illuminated\ (microfluidic\ cell) = \ 5.61\ x\ 10^{-10} mol\ cm^{-3}\ \times$$
$$6.023\ \times 10^{23}\ molecules\ mol^{-1} \times\ 0.000079\ cm^3 = 2.7 \times 10\ ^{10}\ molecules$$

$$Amount\ deposited\ (extraction/preconcentration\ microcolumn)$$
$$= 100\ ng\ cm^{-3}\ \times 0.140\ cm^{-3} = 14\ ng$$
$$Number\ of\ molecules\ extracted\ (extraction/preconcentration\ microcolumn)$$
$$= (14\ \times 10^{-9} g\ \div 178.23\ g\ mol^{-1}) \times 6.023\ \times 10^{23}\ molecules\ mol^{-1}$$
$$= 4.73\ \times 10^{13}\ molecules$$

$$Molecules\ illuminated\ (extraction\ microcolumn) = \frac{4.73\ x\ 10^{13} molecules}{0.001\ cm^3}\ \times$$
$$0.000079\ cm^3 = 3.7 \times 10^{12}\ molecules$$
$$Molecules\ illuminated\ (preconcentration\ microcolumn) =$$
$$\frac{4.73\ x\ 10^{13} molecules}{0.001\ cm^3 \times \frac{1}{3}}\ \times 0.000079\ cm^3 = 1.1 \times 10\ ^{13}\ molecules$$

Assuming that one molecule absorbs only one photon and that no photons

are lost at the cell walls, we can estimate the numbers of photons absorbed per

second using the Beer-Lambert law.

Equation H-2 $A = \ \varepsilon bc$

Where A is the absorbance, ε is the molecular absorptivity and c is the number of absorbing molecules.

$A(cuvette) = 3.08 \times 10^{-19} \, L \, molecule^{-1} cm^{-1} \times 1 \, cm \times 2.7 \times 10^{12} \, molecules = 8.2 \times 10^{-7} \, A.U.$

$A(microfluidic \, cell) = 3.08 \times 10^{-19} \, L \, molecule^{-1} cm^{-1} \times 1 \, cm \times 2.7 \times 10^{10} \, molecules = 8.2 \times 10^{-11} \, A.U.$

$A(extraction \, microcolumn) = 3.08 \times 10^{-19} \, L \, molecule^{-1} cm^{-1} \times 1 \, cm \times 3.7 \times 10^{12} \, molecules = 1.2 \times 10^{-8} \, A.U.$

$A(preconcentration \, microcolumn) = 3.08 \times 10^{-19} \, L \, molecule^{-1} cm^{-1} \times 1 \, cm \times 1.1 \times 10^{13} \, molecules = 3.5 \times 10^{-8} \, A.U.$

Using **Error! Reference source not found.** we can determine the number of photons transmitted and thus, the number of photons absorbed.

Equation H-3 $\qquad A = -LogT = Log\dfrac{I}{I_0}$

Where, T is the transmittance, I is the transmitted radiant power and I_0 is the incident radiant power.

$I(cuvette) = 1.9 \times 10^{14} \, photons \, s^{-1} \times 10^{-8.2 \times 10^{-7}}$
$= 1.933118 \times 10^{14} \, photons \, transmitted \, s^{-1}$

$I(microfluidic \, cell) = 1.9 \times 10^{14} \, photons \, s^{-1} \times 10^{-8.2 \times 10^{-11}}$
$= 1.9331212275 \times 10^{14} \, photons \, transmitted \, s^{-1}$

$$I(extraction\ microcolumn) = 1.9 \times 10^{14}\ photons\ s^{-1} \times 10^{-1.2 \times 10^{-8}}$$
$$= 1.933121150 \times 10^{14}\ photons\ transmitted\ s^{-1}$$
$$I(preconcentration\ microcolumn) = 1.9 \times 10^{14}\ photons\ s^{-1} \times 10^{-3.5 \times 10^{-8}}$$
$$= 1.93312107 \times 10^{14}\ photons\ transmitted\ s^{-1}$$

Taking into account anthracene's quantum efficiency, we can calculate the number of photons absorbed which are going to be re-emitted as fluorescence.

$$Photons\ emitted\ = photons\ absorbed\ \times \phi$$

$Photons\ emitted\ (cuvette) = (1.9 \times 10^{14}\ photons\ s^{-1} - 1.933118 \times 10^{14} photons\ s^{-1}) \times 0.36 = 1.3 \times 10^{8}\ photons\ s^{-1}$

$Photons\ emitted\ (microfluidic\ cell) = (1.9 \times 10^{14}\ photons\ s^{-1} - 1.93312123 \times 10^{14}\ photons\ s^{-1}) \times 0.36 = 1.3 \times 10^{4}\ photons\ s^{-1}$

$Photons\ emitted\ (extraction\ microcolumn) = (1.9 \times 10^{14}\ photons\ s^{-1} - 1.93312118 \times 10^{14} photons\ s^{-1}) \times 0.36 = 1.8 \times 10^{6}\ photons\ s^{-1}$

$Photons\ emitted\ (preconcentration\ microcolumn) = (1.9 \times 10^{14}\ photons\ s^{-1} - 1.93312107 \times 10^{14} photons\ s^{-1}) \times 0.36 = 5.6 \times 10^{6}\ photons\ s^{-1}$

If we multiply the number of photons by their energy when emitted at 399 nm, we obtain the fluorescence radiant power in $J\ s^{-1}$ or W.

$Fluorescence\ radiant\ power\ at\ 399\ nm\ (cuvette) = 4.9\ J\ photons^{-1} \times 1.3 \times 10^{8} photons\ s^{-1} = 6.5 \times 10^{-11}\ W$

$Photons\ emitted\ (microfluidic\ cell) = 4.9\ J\ photons^{-1} \times 1.3 \times 10^{4} photons\ s^{-1} = 6.5 \times 10^{-15}\ W$

$Photons\ emitted\ (extraction\ microcolumn) = 4.9\ J\ photons^{-1} \times 1.8\ \times 10^{6}$

$photons\ s^{-1} = 9.1\ \times 10^{-13}\ W$

$Photons\ emitted\ (preconcentration\ microcolumn) = 4.9\ J\ photons^{-1} \times 5.6\ \times 10^{6}$

$photons = 2.8\ \times 10^{-12}\ W$

If we make the assumption that anthracene acts as a point source which radiates light equally in all directions, we can estimate the amount of light collected by the fibre optic. As illustrated in Figure H-6, the light collected by the fibre optic can be obtained by comparing the solid angle of its acceptance cone to the solid angle of a sphere (Ω = 4π sr for a sphere). For a cone, the solid angle is defined by Equation H-4.[5]
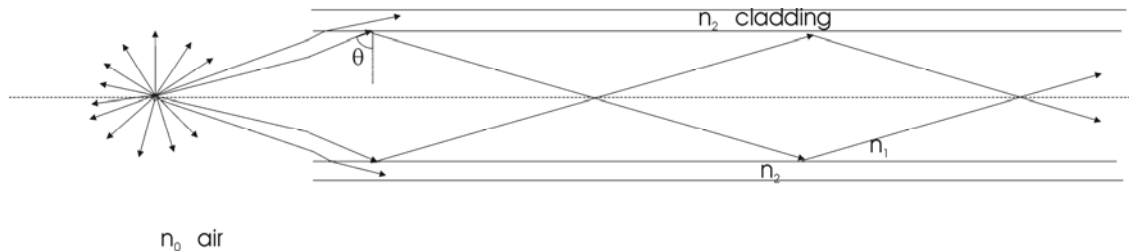

Figure H-6. Collection of the isotropic fluorescence emission of a point source by an optical fibre with acceptance angle 2θ.

Equation H-4 $\qquad \Omega = 2\pi(1 - cos\vartheta)$

Where θ is the half acceptance angle of the fibre optic. The cone's solid angle is therefore 1.97 sr and the fractional solid angle collected by the fibre optic is 0.16. Assuming that all the light collected by the fibre optic makes it to the PMT detector, we can estimate the voltage output of the PMT for a 100 ppb anthracene solution using its radiant sensitivity (as specified from the manufacturer).

$$PMT\ signal\ (cuvette) = (0.16\ \times 6.5\ \times 10^{-11}\ W)\ \times 30\ 10^9\ V\ W^{-1} = 0.3\ V$$

$$PMT\ signal\ (microfluidic\ cell) = (0.16\ \times\ 6.5\ \times 10^{-15}\ W)\ \times 30\ \times 10^9\ V\ W^{-1}$$
$$= 3\ \times 10^{-5}\ V$$

$$PMT\ signal\ (extraction\ microcolumn)$$
$$= (0.16\ \times 9.1\ \times 10^{-13}\ W\ )\times 30\ \times 10^9\ V\ W^{-1} = 4\ \times 10^{-3}\ V$$

$$PMT\ signal\ (preconcentration\ microcolumn)$$
$$= (0.16 \times 2.8\ \times 10^{-12}\ W\ )\times 30\ \times 10^9\ V\ W^{-1} = 1 \times 10^{-2}\ V$$

Calculating the slope from the above results and using the PMT ripple noise (as specified by the manufacturer) as the limiting noise, we can estimate the detection limit (3σ) of the system. Results are listed in Table H-3 alongside with the obtained experimental results for the same system.

Table H-3. Predicted and experimental detection limits obtained for anthracene

	Calculated (ppb)	Experimental
1 cm cuvette	2	3
0.01 cm microfluidic cell	20 000	N/A
0.01 cm extraction column†	100	N/A
0.01 cm pre-concentration column‡	50	140

†Anthracene is spread over the column length

‡Anthracene is concentrated in the top $\frac{1}{3}$ of the microcolumn

Experimentally, using the UV-LED and PMT detector, we obtained an in-column fluorescence detection limit of 140 ppb (absolute LOD of 20 ng for a 140 µL sample). This result is only one order of magnitude larger than the predicted result. It was expected that the experimental results would have higher detection limits than predicted due to column variability. The use of a motorised translation stage considerably improved the signal profile mapping, shown in Figure H-7, by allowing the acquisition of a data point every 0.1 mm instead of 1 mm. As seen in Figure H-8 the 300 ppb concentration (42 ng deposited) was out of the linear range for the method, most probably due to solubilization issues. This result is confirmed by fluorescence measurements of the same solutions made in conventional cuvettes (Figure H-8) showing negative deviations from linearity at the highest concentration.
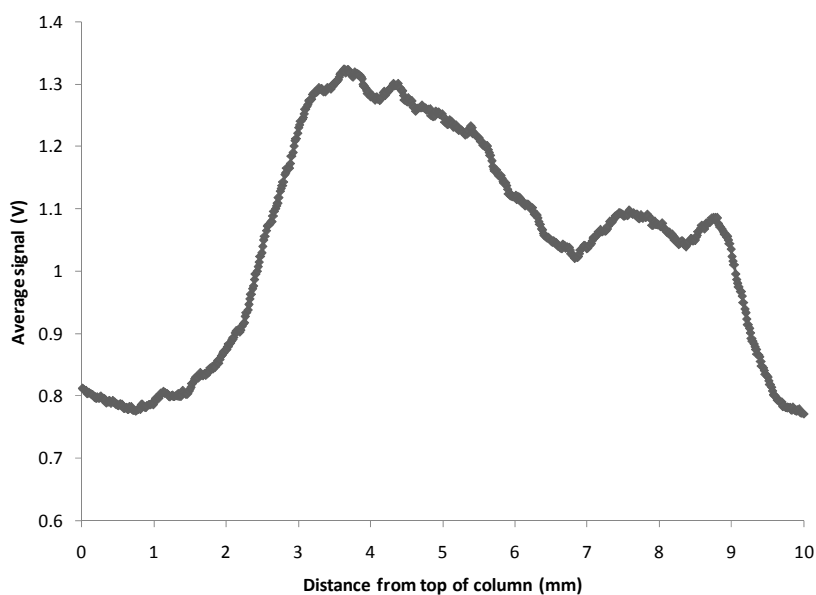
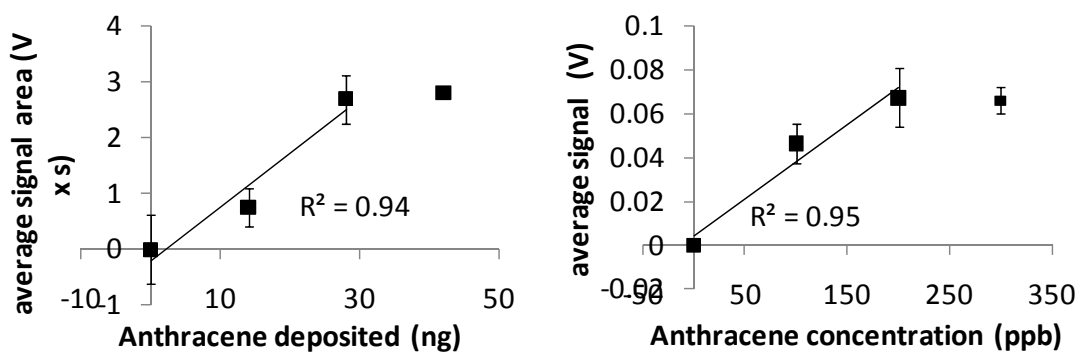Figure H-7. Anthracene *in-situ* fluorescence along the column

Figure H-8. Determination of anthracene by direct in-situ fluorescence in a microcolumn (left) and by regular fluorescence in a cuvette (right) with UV-LED excitation at 256 nm and recorded with a PMT equipped with a 320 nm longpass filter.

Circuit schematics

The circuit schematics for the UV Light Emitting Diode (UV LED) and the Photomultiplier Tube (PMT) power supply are illustrated in Figure H-9 and Figure H-10 respectively. These were assembled with the help of Richard Rossi from the Department of Chemistry's Electronic Shop.
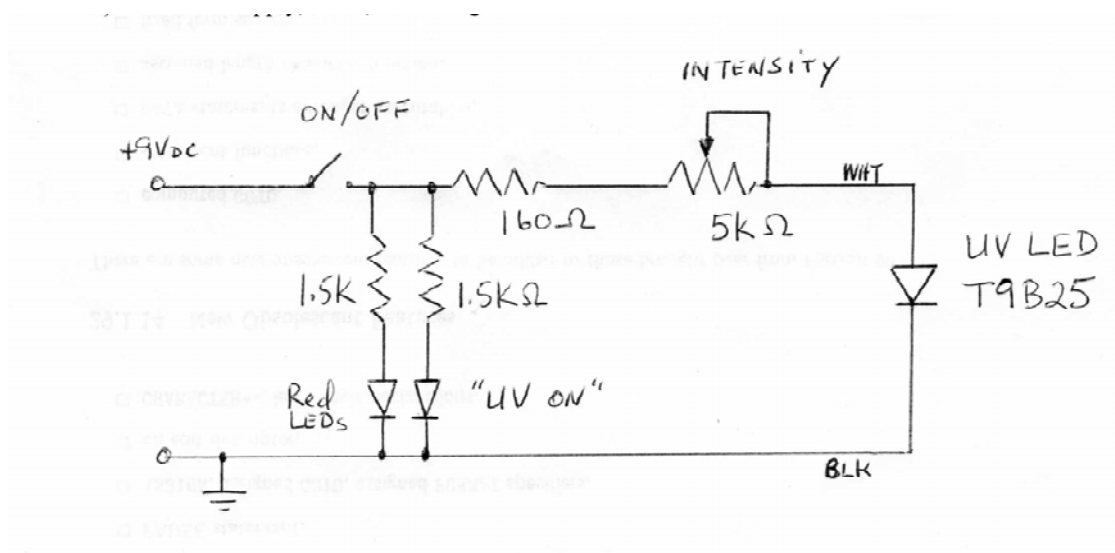

Figure H-9. Circuit diagram for the UV LED (T9B25, Seoul Semiconductors Co.) power supply.
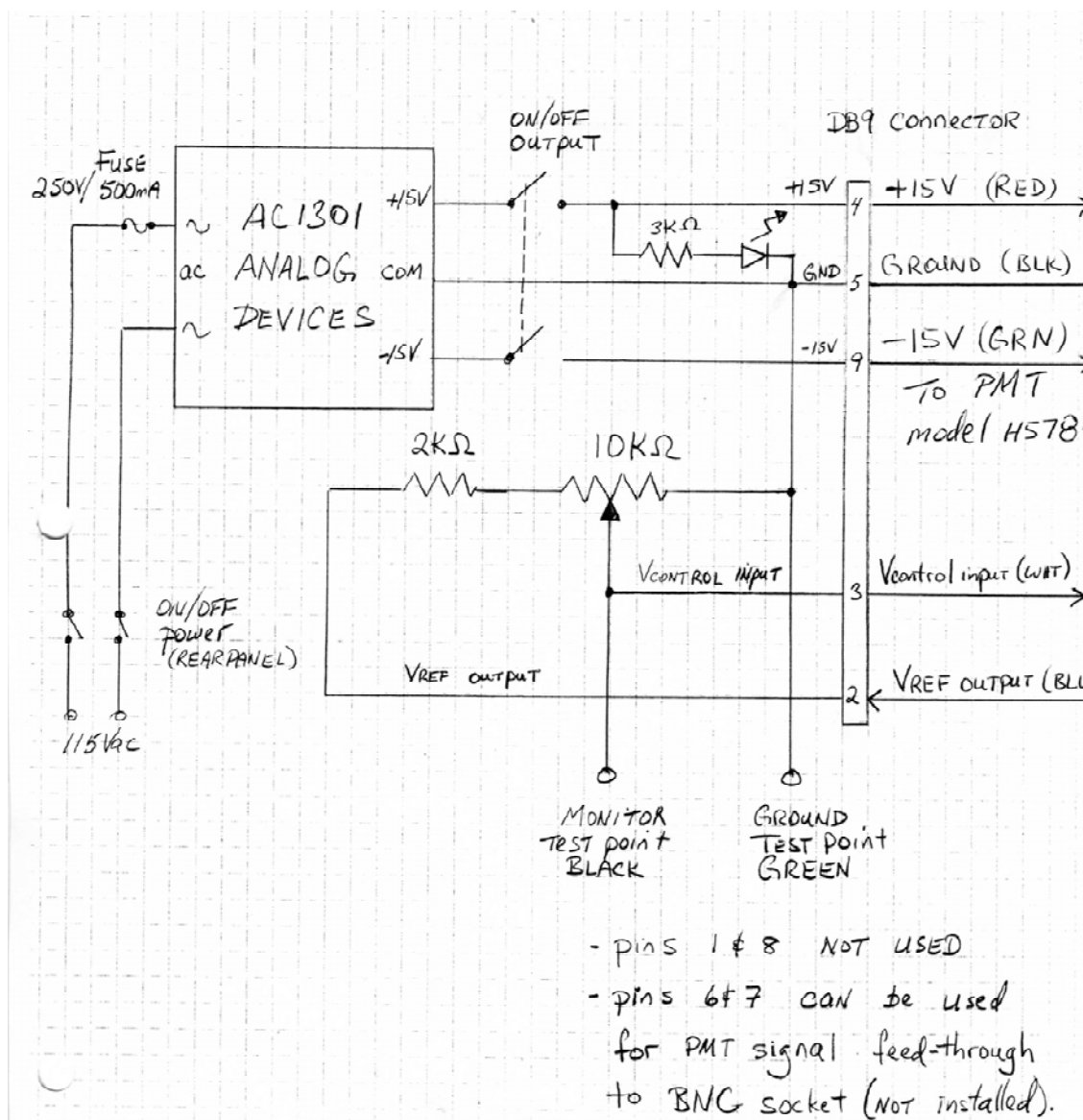
Figure H-10. Circuit diagram for connecting the PMT power supply (Hamamatsu H5784-04).

(1)   Berlman, I. B. *Handbook of fluorescence spectra of aromatic molecules*, 2 ed.; Academic Press: New York, 1971.

(2)   *CRC Handbook of Chemistry and Physics [electronic ressource]*, 89 ed.; CRC Press LLC: Boca Raton, FL, 2009.

(3)   Ware, W. R.; Baldwin, B. A. *The Journal of Chemical Physics* **1965**, *43*, 1194-1197.

(4)   Molnár-Perl, I., Ed. *Quantitation of Amino Acids and Amines by Chromatography* Elsevier Science: Burlington, MA, 2005.

(5)   Quimby, R. *Photonics and Lasers: An introduction*; John Wiley and Sons: New York, 2006.